

8-1-2010

## Dielectrophoretic characterization of particles and erythrocytes

Soumya Keshavamurthy Srivastava

Follow this and additional works at: <https://scholarsjunction.msstate.edu/td>

---

### Recommended Citation

Srivastava, Soumya Keshavamurthy, "Dielectrophoretic characterization of particles and erythrocytes" (2010). *Theses and Dissertations*. 1491.  
<https://scholarsjunction.msstate.edu/td/1491>

This Dissertation - Open Access is brought to you for free and open access by the Theses and Dissertations at Scholars Junction. It has been accepted for inclusion in Theses and Dissertations by an authorized administrator of Scholars Junction. For more information, please contact [scholcomm@msstate.libanswers.com](mailto:scholcomm@msstate.libanswers.com).

DIELECTROPHORETIC CHARACTERIZATION OF PARTICLES AND  
ERYTHROCYTES

By

Soumya Keshavamurthy Srivastava

A Dissertation  
Submitted to the Faculty of  
Mississippi State University  
in Partial Fulfillment of the Requirements  
for the Degree of Doctor of Philosophy  
in Chemical Engineering  
in the Department of Dave C. Swalm School of Chemical Engineering

Mississippi State, Mississippi

August 2010

Copyright 2010

By

Soumya Keshavamurthy Srivastava

DIELECTROPHORETIC CHARACTERIZATION OF PARTICLES AND  
ERYTHROCYTES

By

Soumya Keshavamurthy Srivastava

Approved:

---

Adrienne R. Minerick  
Associate Professor, Department of  
Chemical Engineering, Michigan  
Technological University  
(Director of Dissertation and Committee  
Participant)

---

Bill B. Elmore  
Interim Director and Hunter Henry Chair,  
Dave C. Swalm School of Chemical  
Engineering  
(Committee Member)

---

Keisha B. Walters  
Assistant Professor, Dave C. Swalm School  
of Chemical Engineering  
(Committee Member)

---

Jagdish P. Singh  
Research Professor, Institute for Clean  
Energy Technology  
(Committee Member)

---

Shane C. Burgess  
Associate Dean for Strategic Initiatives and  
Economic Development and Professor,  
College of Veterinary Medicine; Director  
Life Science and Biotechnology Inst.  
(Committee Member)

---

Rafael Hernandez  
Associate Professor, Dave C. Swalm School  
of Chemical Engineering  
(Graduate Coordinator)

---

Sarah Rajala  
Dean and Professor, Bagley College of  
Engineering

Name: Soumya Keshavamurthy Srivastava

Date of Degree: August 7, 2010

Institution: Mississippi State University

Major Field: Chemical Engineering

Major Professor: Dr. Adrienne R. Minerick

Title of Study: DIELECTROPHORETIC CHARACTERIZATION OF PARTICLES  
AND ERYTHROCYTES

Pages in Study: 279

Candidate for Degree of Doctor of Philosophy

Medical lab work, such as blood testing, will one day be near instantaneous and inexpensive via capabilities enabled by the fast growing world of microtechnology. In this research study, sorting and separation of different ABO blood types have been investigated by applying alternating and direct electric fields using dielectrophoresis in microdevices. Poly(dimethylsiloxane) (PDMS) microdevices, fabricated by standard photolithography techniques have been used. Embedded perpendicular platinum (Pt) electrodes to generate forces in AC dielectrophoresis were used to successfully distinguish positive ABO blood types, with O+ distinguishable from other blood types at >95% confidence. This is an important foundation for exploring DC dielectrophoretic sorting of blood types.

The expansion of red blood cell sorting employing direct current insulative dielectrophoresis (DC-iDEP) is novel. Here Pt electrodes were remotely situated in the inlet and outlet ports of the microdevice and an insulating obstacle generates the required dielectrophoretic force. The presence of ABO antigens on the red blood cell were found to affect the dielectrophoretic deflection around the insulating obstacle thus sorting cells

by type. To optimize the placement of insulating obstacle in the microchannel, COMSOL Multiphysics<sup>®</sup> simulations were performed. Microdevice dimensions were optimized by evaluating the behaviors of fluorescent polystyrene particles of three different sizes roughly corresponding to the three main components of blood: platelets (2-4  $\mu\text{m}$ ), erythrocytes (6-8  $\mu\text{m}$ ) and leukocytes (10-15  $\mu\text{m}$ ). This work provided the operating conditions for successfully performing size dependent blood cell insulator based DC dielectrophoresis in PDMS microdevices. In subsequent studies, the optimized microdevice geometry was then used for continuous separation of erythrocytes. The microdevice design enabled erythrocyte collection into specific channels based on the cell's deflection from the high field density region of the obstacle. The channel with the highest concentration of cells is indicative of the ABO blood type of the sample.

DC resistance measurement system for quantification of erythrocytes was developed with single PDMS microchannel system to be integrated with the DC-iDEP device developed in this research. This lab-on-a-chip technology application could be applied to emergency situations and natural calamities for accurate, fast, and portable blood typing with minimal error.

Key words: Microdevices, dielectrophoresis, insulating dielectrophoresis, human ABO blood system

## DEDICATION

This dissertation is dedicated to my parents, brother, and my husband for their continuous support and encouragement.

## ACKNOWLEDGEMENTS

First, I would like to thank my advisor Dr. Adrienne R. Minerick, without whom this dissertation could not have been written. Thanks to Dr. Minerick's high expectations and the way she always encouraged and challenged me throughout my academic program to reach high goals. She never accepted less than my best efforts and guided me to the right path through her expert advice. Her suggestions and advice have motivated and inspired me professionally and personally.

I am very appreciative of the funding of my graduate research stipend from the National Science Foundation through CBET CAREER grant #0644538.

I would like to express my gratitude to Dr. Blanca Lapizco-Encinas for her support and valuable advice towards my research. Meetings at National conferences and e-mail exchanges have benefited me in acquiring deeper knowledge in my research field.

I would also like to thank Dr. Shane Burgess, Dr. Keisha Walters, Dr. Jagdish Singh and Dr. Bill Elmore who serve as members of my examining committee. Many meetings with them contributed to my deeper understanding and knowledge. Several motivational discussions with Dr. Adrienne Minerick, Dr. Blanca Lapizco-Encinas, Dr. Keisha Walters, Dr. Hossein Toghiani, and Dr. Rebecca Toghiani have been very fruitful in my career. Professional guidance and perspective from Dr. Noel Schulz are gratefully acknowledged. I am grateful to Dr. David Wipf for donating electrometer and setting up LabVIEW for executing resistance measurement experiments. I would also like to thank Dr. Priscilla Hill for taking responsibility for our skeletal lab so that I could finish my



experiments when Dr. Minerick and the lab moved to Michigan Technological University.

I truly appreciate all my fellow members of the Medical microDevice Engineering Research Laboratory (M.D.-ERL), who always supported me and made this lab a great place to work. Several discussions I had with Ms. Kaela Leonard, Mr. Aytug Gencoglu and Ms. Chungja Yang resulted in improvements with my personal development and professional career. I would also like to express appreciation for the hard work of the undergraduate students who worked in the lab especially, Ms. Amanda Mixon, Mr. Eric Rutan, and Ms. Anell Pullen.

I wish to thank all the volunteers who donated blood for this research. The laboratory staff of the Longest Student Health Center was very helpful in drawing blood from volunteers. I would also like to thank Chemical Engineering Department staff, especially Ms. Sherre Denson and Ms. Sandra Shumaker, for their support in processing all my paperwork timely and answering all my questions related to administrative paperwork.

Special thanks to my friends for cheering me up whenever I felt down and giving me strength to follow my dreams.

Finally and most importantly, I would like to thank my family for their continued support, guidance, and constant love with special thanks to my parents and husband. My family has always been a great source of energy and motivation.

## TABLE OF CONTENTS

	Page
DEDICATION .....	ii
ACKNOWLEDGEMENTS .....	iii
LIST OF TABLES .....	x
LIST OF FIGURES .....	xii
CHAPTER	
I.    INTRODUCTION .....	1
1.1    Background .....	1
1.1.1    Cellular Diagnostics .....	2
1.1.2    Lab-on-a-chip / Microdevices .....	5
1.1.3    Microfluidics .....	12
1.1.4    Electrokinetics .....	13
1.1.4.1    Electrophoresis .....	15
1.1.4.2    Electro-osmosis .....	16
1.1.4.3    Dielectrophoresis .....	16
1.2    Motivation .....	17
1.3    Objective of the study .....	19
1.4    Outline of Dissertation .....	20
II.    MICRODEVICE MICROFABRICATION .....	21
2.1    Introduction .....	21
2.2    Fabrication techniques .....	21
2.2.1    Hard fabrication .....	22
2.2.2    Soft fabrication .....	22
2.3    Materials employed in soft fabrication .....	23
2.3.1    Poly(dimethylsiloxane) (PDMS) .....	26
2.4    Soft fabrication techniques .....	28
2.5    Fabrication of devices by rapid prototyping .....	31
2.5.1    Rapid prototyping .....	32
2.5.2    Replica molding .....	35
2.5.3    Polymeric device sealing .....	35

2.5.3.1	Surface modifications for PDMS.....	37
2.6	Summary .....	40
III.	DIELECTROPHORESIS .....	41
3.1	Introduction.....	41
3.2	Dielectrophoresis (DEP).....	41
3.2.1	Electrode geometry .....	46
3.2.2	Electrical signal considerations.....	46
3.3	Types of dielectrophoresis .....	48
3.3.1	Alternating Current Dielectrophoresis (AC-DEP).....	48
3.3.2	Direct Current Dielectrophoresis (DC-DEP).....	50
3.4	Manipulation of particles by dielectrophoresis.....	52
3.4.1	Dielectric properties of cells .....	55
3.5	Summary .....	57
IV.	HUMAN BLOOD SYSTEM.....	59
4.1	Introduction.....	59
4.2	Blood.....	59
4.2.1	Composition of blood .....	61
4.2.2	Erythrocytes .....	64
4.2.3	Challenges in blood sample preparation.....	67
4.3	Blood typing.....	68
4.3.1	ABO blood typing system.....	69
4.3.2	Other blood typing systems .....	74
4.4	Summary .....	75
V.	DIELECTROPHORETIC CHARACTERIZATION OF ERYTHROCYTES: POSITIVE ABO BLOOD TYPES.....	77
5.1	Introduction.....	77
5.2	Manipulation of red blood cells .....	78
5.3	Theory .....	80
5.3.1	Red blood cells (RBCs)/ erythrocytes.....	83
5.4	Materials and methods .....	85
5.4.1	Microdevice fabrication .....	85
5.4.2	Microsample preparation .....	86
5.4.3	Experimentation.....	87
5.4.4	Image analysis.....	90
5.4.5	Data analysis .....	90
5.5	Results and discussion .....	93
5.5.1	Total cell counts by wedge region .....	95
5.5.2	Average vertical movement .....	97
5.5.3	Mean fractional horizontal movement.....	102
5.5.4	Composite distance .....	106

5.6	Summary .....	108
VI.	DC INSULATOR-DIELECTROPHORETIC APPLICATIONS IN MICRODEVICE TECHNOLOGY: A REVIEW .....	112
6.1	Introduction.....	112
6.2	Microfluidic platform.....	113
6.3	Dielectrophoresis .....	115
6.4	DC dielectrophoresis: Theory .....	117
6.4.1	Insulating obstacle geometry .....	121
6.4.1.1	Single obstacle geometry .....	122
6.4.1.2	Multiple obstacle geometry.....	125
6.4.1.3	Channel variations .....	127
6.4.2	Comprehensive review of literature.....	129
6.4.3	Additional alternative dielectrophoretic schemes .....	139
6.5	Fabrication of insulator-based microdevices .....	141
6.6	Electric field characteristics .....	142
6.7	Performance characterization.....	144
6.7.1	Effect of medium pH .....	145
6.7.2	Effect of medium conductivity .....	146
6.7.3	Wall effects .....	147
6.7.4	Joule heating effects.....	147
6.8	Separation and trapping of biomolecules, bacteria, microparticles, and cells.....	148
6.8.1	DNA and proteins .....	149
6.8.2	Bacteria and virus .....	150
6.8.3	Polystyrene particles .....	153
6.8.4	Yeast cells and mammalian cells .....	157
6.9	Summary and conclusions .....	159
VII.	DC-INSULATOR DIELECTROPHORETIC SEPARATION OF FLUORESCENT POLYSTYRENE PARTICLES.....	163
7.1	Introduction.....	163
7.2	DC-iDEP in literature .....	164
7.3	Theoretical background .....	168
7.3.1	Particle motion .....	168
7.3.2	Particle pathlines.....	170
7.3.3	Mathematical model.....	171
7.4	Experimental methods .....	172
7.4.1	Device design and fabrication.....	173
7.4.2	Sample preparation .....	174
7.4.3	Operation.....	176
7.4.3.1	Electro-osmotic flow measurement .....	176
7.4.3.2	Polystyrene particle experiments .....	177
7.4.4	Image analysis.....	178

7.5	Results and discussion .....	180
7.5.1	Electro-osmotic flow measurement and baseline study .....	180
7.5.2	Polystyrene particle experiments .....	183
7.5.2.1	Size dependency.....	183
7.5.2.1.1	3.18 $\mu\text{m}$ particles.....	184
7.5.2.1.2	6.2 $\mu\text{m}$ particles.....	186
7.5.2.1.3	10 $\mu\text{m}$ particles.....	187
7.5.2.2	Electric field dependency.....	189
7.5.2.3	Medium conductivity dependency .....	192
7.5.3	2-channel system.....	194
7.6	Conclusions.....	196
VIII.	INSULATOR BASED DC DIELECTROPHORETIC BLOOD TYPING: HUMAN ABO SYSTEM .....	199
8.1	Introduction.....	199
8.2	Manipulation of bioparticles by DC-iDEP .....	200
8.3	Theory .....	205
8.3.1	Red blood cells / erythrocytes.....	208
8.4	Materials and methods .....	209
8.4.1	Experimentation.....	209
8.4.1.1	Device design and fabrication.....	210
8.4.1.2	Sample preparation .....	212
8.4.1.3	Operation protocol and experiment matrix .....	214
8.4.2	Video analysis.....	218
8.4.3	Data analysis .....	219
8.5	Results and discussion .....	222
8.5.1	Baseline study .....	222
8.5.2	Reproducibility Studies.....	223
8.5.3	Blood type dependency.....	225
8.5.4	Electric field dependency.....	228
8.5.5	Conductivity dependency.....	230
8.6	Conclusions.....	232
IX.	QUANTIFYING ERYTHROCYTES BY SOLUTION RESISTANCE MEASUREMENT .....	235
9.1	Introduction.....	235
9.2	Quantification techniques in literature.....	236
9.3	Theory involved in resistance measurement.....	238
9.4	Materials and methods .....	239
9.4.1	Experimentation.....	240
9.4.1.1	Device design and fabrication.....	240
9.4.1.2	Sample preparation .....	241
9.4.1.3	Operation.....	243
9.4.2	Data analysis .....	244

9.5	Results and discussion .....	246
9.5.1	Blood type dependency .....	246
9.5.2	Concentration dependency .....	248
9.5.3	Conductivity dependency.....	249
9.6	Conclusions.....	250
X.	CONCLUSIONS.....	252
10.1	Summary and key conclusions.....	252
10.2	Recommendations for future work .....	256
	REFERENCES .....	262

## LIST OF TABLES

TABLE		Page
4.1	Thirty blood typing systems classified by ISBT <sup>165</sup> .....	75
5.1	Percentage of cells remaining in the image field of view for all four positive blood types. The percentage of cells remaining in the image field of view is compiled for all four positive blood types. There is a steady decline in the total number of cells in the field of view as the experimental run time progresses.....	97
5.2	Linear trends of the vertical and horizontal movements for 4 positive blood types. The linear trends of the vertical and horizontal movements are shown for all the four positive blood types. The intercepts and slope are given along with the R <sup>2</sup> value. These data are compiled for the experimental run time of 0-60 s for vertical movement and 0-90 s for horizontal movement as 60 and 90 s were the time where best spatial separation of all the four blood types were achieved for vertical and horizontal movements respectively.....	100
5.3	Least significant difference multiple comparison results for vertical movement. Least significant difference multiple comparison results for average vertical movement are shown. The confidence level at which the vertical movement parameter is able to distinguish blood type is tallied.....	102
5.4	Least significant difference multiple comparison results for horizontal movement. Least significant difference multiple comparison results for horizontal movement is shown. The confidence level at which the horizontal movement parameter is able to distinguish blood type is tallied.....	105
6.1	Review of DC-iDEP research, including the media and particles used in those studies, insulating obstacle geometries, and applied electric fields. Estimates of the DEP force from COMSOL simulations and manual calculations, along with the COMSOL estimated relative DEP force, with the orders of magnitude difference between the highest and lowest DEP force within the system are also listed. The latter value is a measure of how effective a given obstacle is increasing the DEP force.....	131

7.1	Average conductivities of various dextrose added buffers with standard deviations and electrokinetic mobility with standard deviations for each buffer at 10.27 V/cm. The number $n$ represents the number of solutions averaged for calculating buffer conductivities. The values ranged between 20-850 mS/cm and do not show a mobility dependence on buffer conductivity. ....	175
8.1	Difference between AC and DC dielectrophoretic system .....	201
8.2	Average conductivity and pH values for the buffers prepared by adding D-Glucose.....	214
8.3	Ratios of the fraction of blood cells in channel 3 to the fraction of blood cells flowing into channel 4. All 8 blood types are distinguishable from each other. ....	227
9.1	Average values for initial and final resistances, change in resistance, and % change for each blood type in 1-1000 dilution in 5% D-glucose solutions (100 mS/cm). ....	247
9.2	Average values for initial and final resistances, change in resistance, and percent change for each concentration of A- blood type in 5% D-glucose solution. ....	248



## LIST OF FIGURES

FIGURE	Page
1.1 Steps involved in cellular diagnostics .....	5
1.2 Dimensional comparison of scale range with most familiar objects <sup>20</sup> (Published with permission from Michael Davidson, Florida State University).....	7
1.3 Lab-on-a-chip device, analysis and applications [Reproduced with permission] <sup>31</sup> .....	10
1.4 Electric double layer (EDL) representation of a negative charged particle experiencing electrokinetic phenomena. ....	14
1.5 Charged particle demonstrating electrophoresis in a bulk-liquid phase under an applied electric field. ....	15
1.6 Comparison of medical laboratory and future lab-on-a-chip device for blood testing purpose. ....	19
2.1 Chemical structure of poly(dimethylsiloxane) (PDMS). ....	26
2.2 Detailed protocol of rapid prototyping technique for fabricating PDMS microdevice from silicon wafer master [some individual pictures adapted from Google images <sup>61</sup> ].....	32
3.1 Chart showing the mammalian cell responses at frequency ranges applicable for dielectrophoresis <sup>95</sup> [Gascoyne, P. R. C.; Vykoukal, J., Particle separation by dielectrophoresis. Electrophoresis. 2002. 23. 1973-1983. Copyright Wiley-VCH Verlag GmbH & Co. KGaA. Reproduced with permission].....	44
3.2 Demonstration of AC-DEP where dark red represents the region of high electric field density and grey represents regions of lower electric field density. ....	50
3.3 DC-iDEP phenomena on a particle at the insulating obstacle region in a microdevice. ....	51

4.1	Composition of whole blood <sup>158</sup> [Reprinted with permission from Scott Potter]. [Copyright 2009].	61
4.2	Process of the blood cell production in the body from immature stem cells in the bone marrow <sup>159</sup> [permission provided for educational purpose].	62
4.3	SEM image of all the three cells (RBC, WBC and platelets) in human blood [Reprinted from ABC Science, Australia] <sup>161</sup> [Permission provided for educational purposes].	64
4.4	(a) Detailed view of a red blood cell membrane <sup>163</sup> [permission provided for educational purposes], (b) SEM close-up view of red blood cell, and (c) 16X microscope image of red blood cells.	66
4.5	Schematic of red blood cell membrane with blood group antigens fixed on it <sup>156</sup> [permission provided for educational purposes].	69
4.6	A, B and O antigen structure in the ABO blood typing system <sup>167</sup> [permission provided for educational purposes].	70
4.7	ABO blood typing system with antigens and antibodies representing A, B, AB and O groups <sup>159</sup> [permission provided for educational purposes].	71
4.8	Blood type distribution in U.S. [Image adapted from Stanford Medical center] <sup>169</sup>	72
5.1	Experimental set-up illustrating the custom microdevice mounted on an inverted microscope. Microdevice electrodes are connected directly to an AC waveform generator. Sample inlet port is used to introduce dilute blood suspensions. Erythrocytes responses in the dielectrophoretic field are recorded digitally with a high resolution CCD camera and stored for subsequent image analysis.	86
5.2	Untouched images of erythrocyte distributions in a dielectrophoretic field after 120 seconds of field application at 1 MHz for (a) A+ blood type, (b) B+ blood type, (c) AB+ blood type and (d) O+ blood type cells. The tip protruding into the bottom of the images is the electrode where field density is the highest and the horizontal dark region at the top of each image is the electrode where density is lowest. Red blood cells are aligned along field lines between the electrodes. The illustrates the difference in orientation of each of the positive ABO blood types studied after 120 seconds in a 1MHz, 0.025 Vpp/ $\mu\text{m}$ AC electric field.	88

5.3	Simulations of the electric field in the microdevice were performed in COMSOL Multiphysics. The geometry of the electrode does not affect the separation of erythrocytes (compare Figs. A and B) whereas the distance between the high field density region and low field density region electrodes plays a vital role (compare Figs. C and D) in determining optimal separation of cells. Dark represents high field density regions while light represents low field density regions. ....89	89
5.4	Wedge region construct for (X, Y) position tracking in MATLAB. The space between high field density and low field density electrode was broken into regions approximating the shape of the electric field. These wedge lines are calculated via an algorithm and cell movement is then tracked up or down each wedge region (vertical movement) as well as across wedge regions (horizontal movement). ....92	92
5.5	Comparison of the dielectrophoretic response of O+ blood type at times 5 (a, b), 60 (c, d), and 120 seconds (e, f) and their corresponding MATLAB representations (b, d, and f) within the wedge regions respectively. As demonstrated, the images and mapped (X, Y) cell position data from MATLAB are in good agreement. ....95	95
5.6	MATLAB output for the dielectrophoretic response analysis for O+ after 120 seconds of field application corresponding to the MATLAB representation in Figure 5.4 (f). Figure 5.5 (a) shows the horizontal spacing of total number of cells in each wedge region from L to R. Significant lateral movement of cells from midfield is suggestive of negative dielectrophoresis. In Figure 5.5 (b) vertical distance along the wedges was scaled from 0 to 1 with 0 located near the high field density electrode and 1 near the low field density electrode. ....96	96
5.7	Vertical movement is calculated according to Equation 5.8 and is shown as a function of experimental run time up to 60 s. Points are shown for A+, B+, AB+, and O+ blood types and standard error is represented for each point. In all cases, average cell position starts near 0.5 (halfway between electrodes). O+ hovers near 0.5 while all other blood types deviate towards the low field density electrode. The best separation achieved for all the four blood types was around 60 s. All the blood types converge back after 60 s as shown in Table 5.1. Trend lines are not shown in the figure but are compiled in Table 5.2 for the experimental run time of 0-90 s. ....99	99

5.8	Movement in the horizontal dimension is calculated via equation 5.9. Data points for A+, B+, AB+, and O+ blood types are plotted and corresponding standard errors shown. For all four blood types, initial cell position is near 0.5, which is halfway between midfield and the far left or far right of the image. Movement with time is away from midfield in all cases. From the figure, the best separation was achieved at 90 s for all four blood types. All the blood types converge back after 90 s as shown in Table 5.1. Trend line data is again compiled in Table 5.2 for the experimental run time of 0-90 s.....	103
5.9	Composite distance combining horizontal and vertical movement figures via the distance formula in equation 5.10. Distance increases with time away from image center for A+, B+, AB+, and O+ blood types. From the figure, A+, B+, and AB+ movements cease to appreciably change after approximately 90 s due to the loss of cells from the analysis area as shown in Table 5.1.....	107
6.1	Electric field lines around the rectangular obstacle, darker regions represent high field density regions, as generated by COMSOL simulations. ....	122
6.2	Electric field lines and contours of the field strength near the oil droplet. A particle in the high-field region is exposed to a negative DEP force. The darker region has stronger electrical field. <sup>120</sup> [Barbulovic-Nad I, Xuan X, Lee JSH, Li D (2006) Dc-dielectrophoretic separation of microparticles using an oil droplet obstacle. Lab on a Chip 6:274-279] – Reproduced by permission of The Royal Society of Chemistry.....	124
6.3	Schematic of a microfluidic DEP trap. (A) A metallic DEP trap made of micro fabricated wire(s) on a substrate. The wire(s) may be either free-floating or connected to a voltage source. (B) An electrodeless DEP trap made of dielectric constrictions. The solid lines are electric field lines $E$ . (C) A scanning electron micrograph of an electrodeless DEP device consisted of a constriction array etched in quartz. The constrictions are 1 $\mu\text{m}$ wide and 1.25 $\mu\text{m}$ deep. The whole chip measures 1 $\times$ 1 cm. The double-headed arrows show the applied electric field direction $z$ . [Reprinted from Biophysical Journal, 83, Chia-Fu Chou, Jonas O. Tegenfeldt, Olgica Bakajin, Shirley S. Chan, Edward C. Cox, Nicholas Darnton, Thomas Duke, and Robert H. Austin, Electrodeless dielectrophoresis of single- and double-stranded DNA, 2170-2179, Copyright 2002 with permission from Elsevier] <sup>128</sup> .....	126
6.4	Schematic diagram of the dielectrophoretic separation in a circular microchannel. Reproduced with permission <sup>215</sup> . ....	129

6.5	Models and boundary conditions used for the finite element calculations: (a) the classic DEP configuration and (b) the feDEP configuration <sup>203</sup> [Golan S, Elata D, Orenstein M, Dinnar U (2006) Floating electrode dielectrophoresis. <i>Electrophoresis</i> 27:4919-4926. Copyright Wiley-VCH Verlag GmbH & Co. KGaA. 2006 Reproduced with permission].	140
6.6	Photograph of the PDMS-insulating microstructure for concentrating of particles. Electric field strength increases gradually from regions 4-1. DEP trapping begins at region 2. “With kind permission from Springer Science + Business Media: Chen D, Du H, Tay CY (2010) Rapid concentration of nanoparticles with dc dielectrophoresis in focused electric fields. <i>Nanoscale Research Letters</i> 5:55-60, copyright 2009” <sup>138</sup> .	156
7.1	(a) A particle at the insulating obstacle due to electric field $\vec{E}$ , experiences electrophoretic force ‘ $F_{EP}$ ’ (negligible in this research due to particle size), electro-osmotic force ‘ $F_{EO}$ ’ from the fluid, and the dielectrophoretic force ‘ $F_{DEP}$ ’ (b) Rectangular obstacle geometry enlarged from (c) at the point highlighted bifurcating into four channels (c) Master on Silicon wafer showing device design of 1.46 cm in length compared to the size of a penny.	174
7.2	Raw images from 3.18 $\mu\text{m}$ particle experiments added by Maximum Intensity Projection (MIP) in AxioVision 4.6.3 software. Intensity profiles (shown in red lines) are drawn across each outlet channel at three different positions. Particles quantified by comparing relative profile intensity across each channel.	179
7.3	Electro-osmotic mobility of plasma-oxidation (in bold numbers), UV-Ozone, IPA washed glass slide and no treatment (native PDMS channels) sealing methods. Comparison of literature reported values from Ren X <sup>239</sup> , Ross D. <sup>242</sup> and Coltro W.K.T. <sup>241</sup> groups are included for plasma sealed and native PDMS channels for PBS buffer. Our EOF results are much greater in magnitude at lower applied fields and the average EOF value for plasma sealed device was $(40 \pm 2.3) \times 10^{-4} \text{ cm}^2/\text{Vs}$ at 10.3 V/cm.	182
7.4	Operating window for size dependency experiments at different buffer conductivity (50-850 mS/cm) and electric field strength (6.85-136 V/cm). Blue area is the safe operating zone for experiments, whereas in the red area heavy salt precipitation occurred at the inlet thus blocking the channels.	183

7.5	(a) Raw images of 3.18 $\mu\text{m}$ particle trajectories combined by MIP program at 50, 450 and 600 mS/cm and 17.12 V/cm. (b) Particle trajectories obtained for 3.18 $\mu\text{m}$ particles at 17.12 V/cm, 50, 450 and 600 mS/cm. Channels 3 and 4 are preferred at 17.12 V/cm. (c) Deflection of 3.18 $\mu\text{m}$ particles at 17.12 V/cm over a range of buffer conductivities. Channel 3 was the slightly preferred channel for all the buffer conductivities.....	185
7.6	(a) Raw images of 6.2 $\mu\text{m}$ particle trajectories combined by MIP program at 600 mS/cm and 17.12 V/cm. (b) Particle trajectories obtained for 6.2 $\mu\text{m}$ particles at 17.12 V/cm and 600 mS/cm. Channel 4 is preferred at 17.12 V/cm and lower conductivities. (c) Deflection of 3.18 $\mu\text{m}$ particles at 17.12 V/cm over a range of buffer conductivities. Channel 4 was preferred for all the buffer conductivities.....	187
7.7	(a) Raw images of 10 $\mu\text{m}$ particle trajectories combined by MIP program at 450 mS/cm, 17.12 V/cm. (b) Simulated particle trajectories obtained for 10 $\mu\text{m}$ particles at 17.12 V/cm, 450 mS/cm. Channel 2 is preferred at 17.12 V/cm. (c) Deflection of 10 $\mu\text{m}$ particles at 17.12 V/cm over a range of buffer conductivities. Channel 2 was preferred for all the buffer conductivities.....	188
7.8	(a) and (b) simulated particle trajectories for 3.18 $\mu\text{m}$ particles at 850 mS/cm medium conductivity and 6.85, 17.12 V/cm DC electric field strength conditions respectively, (c) and (d) simulated particle trajectories for 6.2 $\mu\text{m}$ particles at 600 mS/cm medium conductivity and 6.85, 17.12 V/cm DC electric field strength conditions respectively, (e) Channel particle fraction variability for 6.2 $\mu\text{m}$ particles at electric field conditions of 6.85 and 17.12 V/cm plotted as a function of medium conductivity, (f) and (g) simulated particle trajectories for 10 $\mu\text{m}$ particles at 850 mS/cm medium conductivity and 6.85, 17.12 V/cm DC electric field strength conditions respectively.....	190
7.9	(a) Channel particle fraction variability for 3.18 (green triangles), 6.2 (red squares) and 10 $\mu\text{m}$ (blue diamond) particles at electric field conditions of 17.12 V/cm plotted as a function of medium conductivity. (b), (c) and (d) simulated particle trajectories at 17.12 V/cm and 850 mS/cm for 3.18, 6.2 and 10 $\mu\text{m}$ particles. (e), (f) and (g) Simulated particle trajectories at 17.12 V/cm and 50 mS/cm for 3.18, 6.2 and 10 $\mu\text{m}$ particles.....	193

7.10	Deflection of 6.2 (blue triangles) and 10 $\mu\text{m}$ (orange squares) particles in a 2-channel system at different buffer conductivity values. Inset shows the 2-channel system where channel A is the sum of channels 1 and 2; channel B is the sum of channels 3 and 4. Positive particle fraction difference ' $\delta$ ' indicates particles are deflected into channel A and negative indicates deflection towards channel B. 6.2 $\mu\text{m}$ particles deflected towards channel B and 10 $\mu\text{m}$ particles deflected into channel A. Optimal buffer conductivity to achieve better separation is $\sim 600$ mS/cm.....	195
8.1	Representation of the microdevice developed in this research and the effect of DEP on the red blood cell at the insulating obstacle region. ....	208
8.2	Schematic representation of PDMS microdevice with patterned silicon (Si) wafer in the inset. ....	212
8.3	Detailed operation protocol of the planned red blood cell experiments, $t$ denotes time in minutes. ....	215
8.4	Experiment matrix to study all dependencies involving reproducibility, blood type, medium conductivity and DC Voltage.....	216
8.5	Schematic representation of interrogation windows (red boxes) drawn to obtain intensity profiles through custom-built software (Sandia National Laboratories). ....	218
8.6	Data analysis protocol using statistical functions available in excel library to calculate cell fraction in each channel outlets .....	221
8.7	Operating window for the red blood cell experiments at various DC electric field strength and range of medium conductivities. ....	223
8.8	Donor reproducibility studies for all the 8 blood types. Minimal variability between donors observed for all blood types. Each data point corresponds to 12 individual experiments at 68.5 V/cm and 100 mS/cm.....	224
8.9	Sorting of red blood cells into outlet channels 1, 2, 3 and 4 by its type at 100 mS/cm and 68.5 V/cm DC electric field. ....	226
8.10	Cells experiencing voltage and no voltage conditions to demonstrate dependency on electric field at 4X magnification (1.5 mm x 1.5 mm).....	228
8.11	Dependency on electric field for all the blood types. Channel fraction plotted at various DC electric fields. Dependency is negligible at different DC electric fields except for AB+. ....	229

8.12	Medium conductivity dependency on red blood cell sorting by its type at 34.25 V/cm. Blood type separations into different channels depends on medium conductivity conditions. Low medium conductivity optimal for better separation efficiency. ....	231
9.1	Experimental configuration showing the DC power supply applying a field across a microchannel and a 1 k $\Omega$ resistor. The DAQ measures voltage drop across the resistor. ....	239
9.2	(a) PDMS device with red dye and electrodes in the ports. (b) Microscope image, 4X magnified at the intersection highlighted in (a) showing red blood cells flowing from a loading port into the 200 $\mu$ m wide channel. The scale bar is 100 $\mu$ m wide.....	241
9.3	Experimental matrix to test different dependencies involved in resistance measurement for quantifying erythrocytes. ....	242
9.4	Average red blood cell counts for four dilutions were quantified from five independent sample preparations and five images of each suspension. ....	243
9.5	Representative measured voltage versus time for AB+ blood type suspended in 5% buffer medium (100 mS/cm) at 1:1000 dilutions and 100 V applied voltage. The step change in current corresponds to the replacement of buffer in the channel with the red blood cell suspension. ....	244
9.6	Calculated channel resistance for AB+ blood type suspended in 5% buffer medium (100 mS/cm) at 1:1000 dilution and 100 V applied voltage. 245	
9.7	Blood type dependency on resistance at 100 mS/cm and 100 V for 1:1000 concentrated erythrocyte sample. ....	247
9.8	Average change in resistance with standard deviations at different concentrations of erythrocytes. Resistance change can be accurately observed at high concentration of erythrocytes compared to lower concentrations.....	249
9.9	Representative image to show conductivity dependency on resistance measurement. O+ blood type at 1:1000 concentration and 100 V/cm DC electric field was employed at 3%, 4% and 5% D-glucose added buffers (100, 550, 700 mS/cm). ....	249



# CHAPTER I

## INTRODUCTION

### 1.1 Background

A lab-on-a-chip (LOC) device integrates all the necessary operations like sampling, mixing, reaction, analysis and detection on one chip. They are also commonly referred to in the literature as micro-Total Analytical Systems ( $\mu$ TAS), point of care devices (POC), microelectronicmechanical systems (MEMS), microdevices, etc. When these microdevices are catered towards medical diagnostics they are termed as biomedical microelectronicmechanical systems (BioMEMS). The phenomena investigated in this research involve controlled motion of particles and cells via electric fields (electrokinetics) and microfluidics. This technology blends science and engineering to quantify cell specific characteristics for the ultimate goal of furthering medical diagnostics. Here dielectrophoresis, a subset of electrokinetics has been used to sort human red blood cells by ABO type using an AC/DC electric field. From previous research by the group, sorting of red blood cells dielectrophoretically is influenced by ABO antigen expressions on the cell<sup>1</sup>. In the next sections, a more detailed discussion on current prevailing methods for cell diagnostics, microdevice technology, motivation and

objective of this study are presented. This chapter concludes with an outline of the remainder of chapters discussed in this dissertation.

### 1.1.1 Cellular Diagnostics

Identifying and visualizing a cell and its abnormalities is the key step in many diagnostic applications. Cells, discovered by Robert Hooke in 1665<sup>2</sup> are the basic building block of life. Cells constantly respond to the small changes in the living body. Supporting and retaining human cytoplasm, being a selective barrier, transportation, communication via receptors and recognition<sup>3</sup> are the major functions of the cells. Important information about identity, health and disease status are known from the cell and is key to many human and environment related problems<sup>4</sup>.

Understanding of biological processes greatly depends on analyzing single cell structures and behaviors. Very few conventional methods are used currently to analyze single cells: cytometry techniques and capillary electrophoresis<sup>5</sup>. Recently, due to developments in lab-on-a-chip technology, there are various techniques and improvements in the field of cellular diagnostics to analyze single cells. A number of researchers in the past have provided extensive reviews on the analysis of single cells, methodology, manipulation, separation of biological content from a single cell and detection<sup>6,7,8</sup>.

Cell manipulation is an important initial step in many biological processes to carry further experiments. Minimizing manipulation costs and finding a novel method to manipulate cells has been the focus recently by various researchers<sup>4</sup>. Cell manipulation could be distinguished based on the force used: magnetic, optical, mechanical and electrical manipulations. The most commonly used technique in LOC device is the

magnetic technique, where in magnetic particles are affixed to the cells selectively<sup>6</sup>. Optical manipulation has been a fast developing technique recently due to it being a contamination free and contactless technique; the most popular optical technique being the optical tweezers<sup>6</sup>. Optical tweezers offer high resolution but limited manipulation area for the cell. Another technological advancement in the field of optical manipulation is the “lab on microscope” which makes use of light intensity patterns<sup>6</sup> and optoelectronic tweezers developed by Wu *et al.* group<sup>9</sup>. Mechanical manipulation techniques are challenging due to the nature of complex properties in a biological cell. Some of the commonly used methods are microwells, microgripper, microfilters, modifying surface properties of microchannel, sandbag structure and dam structures<sup>6</sup>. Electric manipulation technique is the most widely used to manipulate cells, due to ease of structuring electric field in microdevices<sup>10</sup>. Electrophoresis, dielectrophoresis and optical traps are some of the electric manipulation methods used currently. Cell separation methods also fall under cell manipulation, which can be distinguished into immunological and non-immunological methods of separation<sup>4</sup>. Immunological techniques are conventional and commercialized techniques available currently such as magnetic-activated cell sorting (MACS), affinity based separation and fluorescence activated cell sorting (FACS). They are expensive, complicated and sometimes might damage the immunological content of the isolated cell but high selectivity and specificity are an added advantage. Non-immunological techniques are relatively cheap, fast and they explore the interactions of the cells with the medium. They can be separated by size, shape or other properties, but they lack specificity and sensitivity<sup>4</sup>. Some of the non-immunological methods of separating cells include dielectrophoresis, hydrodynamic separation, ultrasound separation and aqueous two-phase system separation. Cell treatment has to be integrated

in a microdevice to develop a lab on a chip device. Some of the treatment mechanisms include cell lysis- thermally, electrically, mechanically or chemically; culturing cells on plastic devices like PDMS; electroporation, electrofusion and optoporation<sup>6</sup>. A recent advancement in cell lysis technology is the use of handheld mechanical lysis chip with ultra-sharp nano blade arrays made of Si (110). This hand-held equipment doesn't need any external energy source for lysing and has been adopted for rapid protein analysis<sup>11</sup>. Electrofusion has not been explored very much, exceptions include Orwar *et al.*<sup>12</sup> and Takeuchi *et al.*<sup>13</sup>. Analysis of cells has been carried out by various methods due to recently developing lab on a chip technology<sup>6</sup>. Flow cytometers employing fluorescence, spectroscopy and light scattering have been the most common methods which are expensive and have the potential to be developed into a portable system to be integrated with microdevices. Small molecules, large proteins, DNA could be analyzed using these cytometers<sup>6</sup>. Another method of analyzing these cells is the biochemical sensing for metabolites in the cell. Due to the advancement in technology, whole cell assay has been made a possibility. By adapting this whole cell analysis, subpopulation of cells and cell-cell interactions could be further investigated. Figure 1.1 demonstrates all the steps involved in cellular diagnostics.

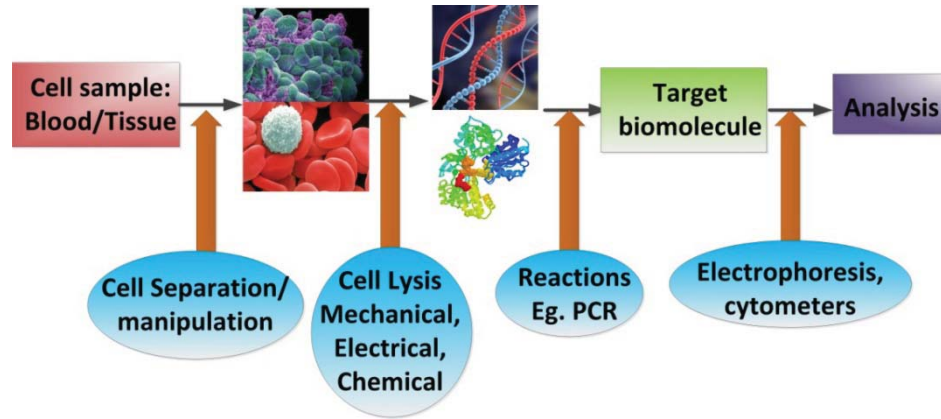


Figure 1.1 Steps involved in cellular diagnostics

To develop inexpensive, portable microdevices the physics beyond lab on a chip technology has to be known. The next two sections presents a detailed discussion of applications, methodology, functional units involved in developing a total analytical system and physics involved has been presented. By exploiting all these features, one can develop a highly specific and sensitive analytical system for medical diagnostic applications.

### 1.1.2 Lab-on-a-chip / Microdevices

Lab-on-a-chip devices or "micro Total Analytical Systems" ( $\mu$ TAS), the term coined by Manz *et al.* in 1990<sup>14</sup> when all sample preparation to answer are completed on one device, are microfluidics-based systems integrating several lab functions on one chip only a few centimeters in size having micron feature patterns and are capable of handling sub microliter sample volumes<sup>15</sup>. Manz *et al.* in his ground breaking work felt the need of such miniaturized system and introduced microchannels to increase separation efficiency in macro systems. In the early nineties, this technology was further successfully applied to separate fluorescent labeled amino acids and fluorescent dyes by capillary electrophoresis<sup>16</sup>. This innovative field motivated by the need to reduce operation costs,

analysis time and enhance automation combines physics, engineering, biology and chemistry to develop microdevices for a variety of applications ranging from DNA testing to medical diagnostic tools<sup>17</sup>. As cited by Whitesides *et al.*, microfluidic origins are related to molecular analysis, molecular biology, microelectronics and biodefense<sup>18</sup>. One can find such extensive capillary system in the human body where multiple reactions like gas exchange, metabolism, and functions in the kidney are performed in 5-10  $\mu\text{m}$  diameter capillaries and not in arteries or veins<sup>19</sup>. Figure 1.2 illustrates the relative scale range of creatures and different devices used in detection<sup>20</sup>.

To build a total micro analytical system, fundamental building units like sample injection/introduction or fluid transport, reactors/mixers, separation tools, and detection techniques have to be employed<sup>17</sup>.

A sample injector was first built by Harrison *et al.* on a single glass chip<sup>21</sup> and a lot of developments have happened since then. Some of the techniques used to inject sample are electrokinetic injection: pinched injection/gated injection<sup>22</sup>, hydrodynamic injection, piezo-injection technique, injection plugs, micro dialysis, electro-osmotic flow, pumping by pressure, centrifugal pumping<sup>22</sup>, thermally induced pumping, and micro pumps- with valves and valveless<sup>17</sup>. Recent advances include a powerless pumping method developed by Hosokawa *et al.* relied on gas permeability of PDMS, a micropump operated by its own generated power of production of oxygen by Choi *et al.*<sup>23</sup>, transport based on electrowetting, magnetohydrodynamic pumping<sup>22</sup>, volume change of bubbles, gravity induced convective flow<sup>24</sup>, microfabricated valves, and non-mechanical valves like plugs.

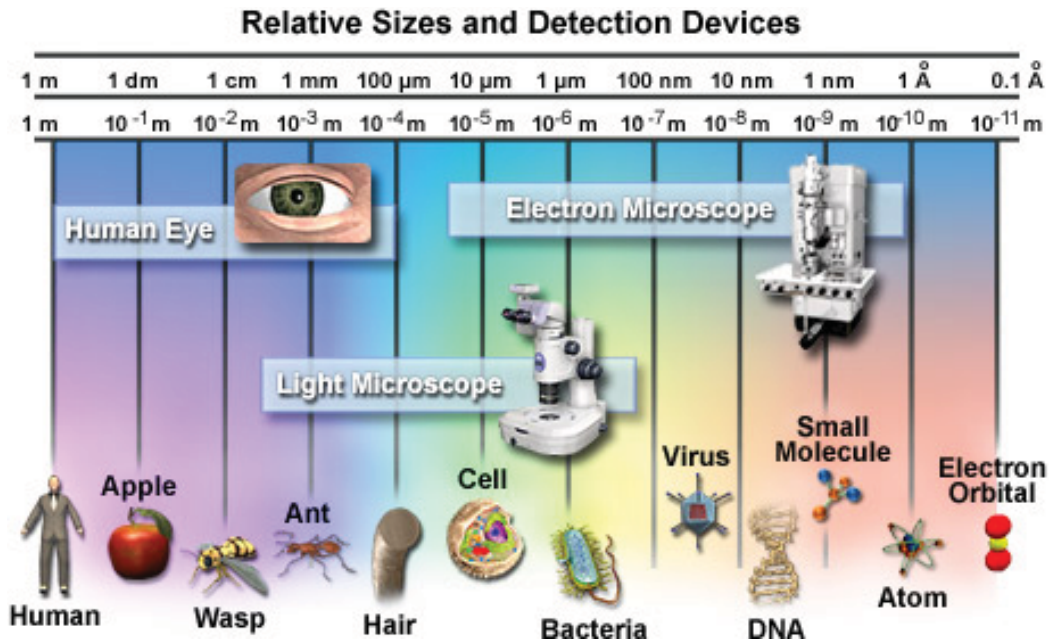


Figure 1.2 Dimensional comparison of scale range with most familiar objects<sup>20</sup> (Published with permission from Michael Davidson, Florida State University).

In microdevices, diffusion is the major process for mixing<sup>22</sup>, but this process is not quick and has prompted several researchers to build micro mixers. Some of the currently used techniques falls into two categories: active mixing and passive mixing<sup>25</sup>. Active mixers use external sources like chaotic mixing, acoustic mixing<sup>22</sup>, mixing by applying magnetic field, electro-osmotic mixing, and rapid switching of polarity<sup>23</sup>. Passive mixing techniques like fabricating channel geometries to introduce mixing<sup>26</sup>, distributive mixer, static mixer, vortex mixer, T-type mixer<sup>25</sup>, serpentine channel mixers have also been explored.

Separations in microdevices were conventionally achieved by chromatographic techniques, but currently electrophoretic techniques dominate. Efficiency, shorter analysis time and resolution power are the crucial factors considered in separations of analytes<sup>17</sup>. Pinched flow fractionation, insulating blocks in channel geometry, trapezoidal

electrode array, split-flow thin fractionation, free-flow magnetophoresis are some of the non-electrophoretic techniques explored in literature<sup>23</sup>. Some of the electrophoretic techniques by which separation can be achieved are capillary electrophoresis, capillary-gel electrophoresis, micellar electrokinetic capillary chromatography<sup>22</sup>, capillary electrochromatography<sup>22</sup>, synchronized cyclic capillary electrophoresis<sup>22</sup>, free flow electrophoresis, iso-electric focusing, dielectrophoresis, zone electrophoresis, and isotachophoresis<sup>23</sup>.

Detection of particles of interest is the last step in a  $\mu$ TAS system which is of prime importance. Various detection techniques are currently available and can be broadly classified into optical detection methods, electrochemical detection, mass spectrometry, thermal detection, acoustic wave detection, and nuclear magnetic resonance<sup>22</sup>. The most widely used detection technique for microdevice applications is the optical detection method: Single channel fluorescence detection, indirect fluorescent detection, multi-point fluorescent detection, absorbance detection, plasma emission detection, chemiluminescence detector, refractive index, thermal lens microscope, raman scattering, surface-plasmon resonance, infrared detection are the optical detection techniques currently explored<sup>22</sup>. Electrochemical detection involves measuring voltage, resistance or current in sample; amperometric detection, voltametric detection, potentiometric detection, conductivity detection are the commonly used detection methods.

Applications of micro-technology are in pharmaceutical industry, biomedical industry (drug design/delivery, detection and diagnostics), chemical, and environmental industries. Other applications are in transport of fluids in automotive and aerospace industries, printing, reaction engineering, and optical industries. Successful integrations



with mass spectroscopy, drug delivery systems, bioanalytical systems and single molecule analysis have been the latest innovations in microfluidics<sup>27</sup>. Novel electrical devices assembled by using microfluidics are an area of technological advancement. with an increasing impact on health, miniaturized devices are becoming very attractive for detecting diseases<sup>17</sup>. For clinical applications, bringing portability for point-of-care devices has the potential to reshape health care industry<sup>28</sup>. POC devices for use at home or in practitioner's offices will allow for infectious disease detection, cancers, and inherited diseases accurately and rapidly. Better administration of drugs thus reducing side effects and improving healing rate could be possible. Minute sample amounts, reproducibility and minimizing invasive ways of sample drawing from the body would be some of the advantages of using LOC devices. They are also cost effective and reduce sampling times and man power required<sup>17</sup>. Small sample volumes provide an added advantage of effective temperature control in the system and bulk use of dangerous and precious samples could be minimized, thus reducing operation costs, improving efficiency and increasing resolution, sensitivity<sup>19,27</sup>. Small sample volumes are also at a risk of clogging the microdevice and thus often requiring maintenance and calibration<sup>29</sup>. But despite these disadvantages, detecting or quantifying cells are much reproducible, accurate and highly sensitive in small sample volumes as the local concentration of cells of interest is high in small sample volumes<sup>30</sup>. Figure 2 demonstrates a lab-on-a-chip analysis, applications and its advantages<sup>31</sup>. Some of the most common LOC devices used in daily-life are the alcohol detecting breath analyzers, glucose monitors for the diabetics, and pregnancy test for hormone level detection<sup>17,30</sup>.

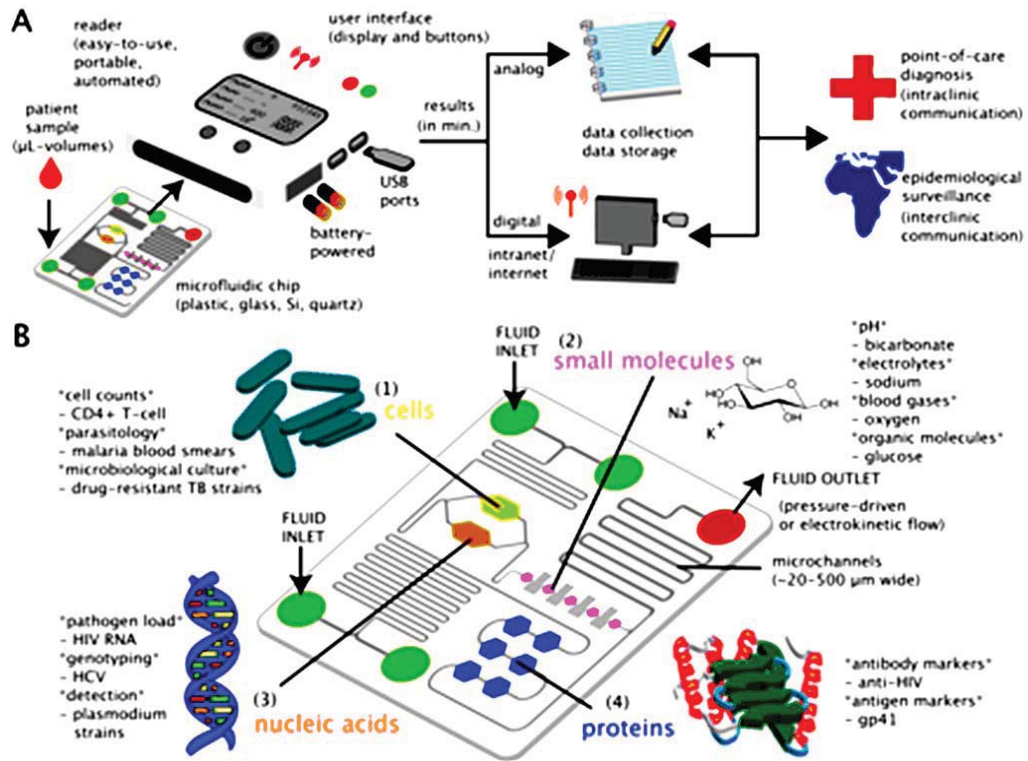


Figure 1.3 Lab-on-a-chip device, analysis and applications [Reproduced with permission]<sup>31</sup>.

Recent developments on lab-on-a-chip concept have extended to other different designs:

- Lab in a cell: This was developed for single cell analysis where micro and nano tools enabled precise control and manipulation of single cells<sup>10</sup>
- Lab on a foil: It has applications for nucleic acid analysis, home care testing, immunoassays, and cell-based assays. They use thin films (polymers, metals, paper) as their material for building these devices<sup>32</sup>.
- Lab on a tube (LOT): This is a disposable tube developed for point of care testing of multiple analytes. Sample collection and multi-sensing are performed in one step on the device. Currently the device quantifies glucose, oxygen and lactate in human serum samples. Samples could be

saliva, urine, water, tears, serum, and blood. They are cheap, user friendly, portable, and compact; high performance and high sensitivity could be achieved<sup>33</sup>.

Overall, detection and analysis of cells on one chip would have an impact for rapid manipulation of cells, thus more accurate and better quality information could be extracted. By using such miniaturized systems, single cell analysis could be performed at ease and they are more reliable and traceable compared to whole cell population results. Whole cell population results may generate more false positives and negatives and single cell analysis yield more information about the shape, abnormality, and rare cells thus enabling disease detection accurately<sup>34</sup>. Developments in nanotechnology is driving down the size of these devices much smaller to be able to administer drug locally or target tumor sites within the body, thus enabling high sensitivity and reproducibility in disease diagnostics<sup>30</sup>.

One very important factor other than geometry of the microdevice is choosing the substrate material. Silicon was commonly used for fabrication but recent advancements have propelled the use of polymer substrates, such as polyamide, polymethacrylate (PMMA), poly(dimethylsiloxane) (PDMS), polyethylene, or polycarbonate, offering different physical and chemical properties for the development of cheaper microdevices<sup>35</sup>. Plastics offer many advantages like cheap, fabrication ease, and rapid prototyping with different surface characteristics to be modified readily. Also, polymer manufacturing is a well known science and investigators can take advantage to create multifunctional, inexpensive, disposable LOC's.

In the next section a detail discussion on physics of fluids in microdevices is presented. Understanding the forces which cause fluid motion is important to be able to build a micro total analytical system.

### 1.1.3 Microfluidics

Microfluidics refers to the control of fluids enclosed in a small geometrical constrained structure. Commonly used fluids include whole blood, bacterial cell suspension, protein/antibody solution, saliva, breath and different buffers<sup>30</sup>. Microfluidic devices are used to obtain molecular diffusion coefficients, pH, chemical binding coefficients, fluid viscosity, and enzyme reaction kinetics<sup>27</sup>. Different forces dominate in microdevices compared to macro scale devices, and understanding of these forces would make new device design better suited for micro analysis. The important forces affecting these microdevices are diffusion, laminar flow, surface tension, fluid resistance and area to volume ratio<sup>25</sup>. Van der Waals forces, forces due to electric double layers (EDL) and surface tension when liquid/liquid interface exist are the dominant forces in small devices<sup>36</sup>. They have low Reynolds number due to the small geometry, thus making the flow laminar with no turbulence<sup>25</sup>. Transport of fluid in these devices are by<sup>36</sup>:

- Pressure driven flow- Also known as hydrodynamic flow, where the velocity distribution of the particle is parabolic in the channel because at the walls velocity is zero<sup>36,37</sup>.
- Electric fields- Here the flow of fluid could be electrophoretic (EP), dielectrophoretic (DEP) or electro-osmotic (EO). In EO flow regime, the fluid velocity profiles are uniform due to the forces exerted by the electrical double layer at the walls. In electrophoretic flow systems, the

velocity profile of particle of interest is linear. Dielectrophoretic motion caused by the electric dipole interaction renders the velocity response of the particle to be proportional to the square of electric field<sup>38</sup>.

- Capillary driven forces- due to surface wettability characteristic by the fluid<sup>36</sup>.
- Free-surface flows- gradients in the interfacial tension drive the fluid.

These can be caused by thermal or chemical gradients.

In this research study, sorting of particles and cells are investigated *via* dielectrophoresis (DEP) phenomena in the presence of AC/ DC fields. Dielectrophoretic motion is seen as a combination of electro-osmotic, electrophoretic and electrokinetic phenomena. In the next section, the fundamentals of electrophoretic motion will be discussed and a detailed discussion on dielectrophoresis and electro-osmosis will be dealt in Chapters 3 and 7.

#### 1.1.4 Electrokinetics

Electrokinetic phenomenon is a group of unique effects observed in liquids containing biomolecules or particles. They are caused by interfacial double layer of electric charges. Electric charge is a property of atoms and the particle interacting with the electric charge may be positive or negative. Two positively/negatively charged particles repel and a combination of positive/negative charged particles attracts each other. The interfacial electric double layer (EDL) consists of fluid layer containing stationary charges, charged surface and liquid layer of moving ions<sup>39</sup>. The net charge density is zero from the stationary ion layer to the bulk liquid phase. The boundary between the stationary liquid layer and the liquid layer of moving ions is the shear plane

and the potential in that region is the zeta potential<sup>38</sup>. The thickness of the liquid layer containing moving ions is termed as Debye length. Figure 1.3 demonstrates the electric double layer phenomena. When an electric field is applied, the excess counter-ions present in the bulk liquid phase, causes the fluid to move.

Electrokinetic forces have three components: electrophoresis, electro-osmosis and dielectrophoresis<sup>38</sup>. In electrokinetic flow mechanism, surface to volume ratio is high and heat dissipation is more efficient compared to macrodevices<sup>40</sup>.

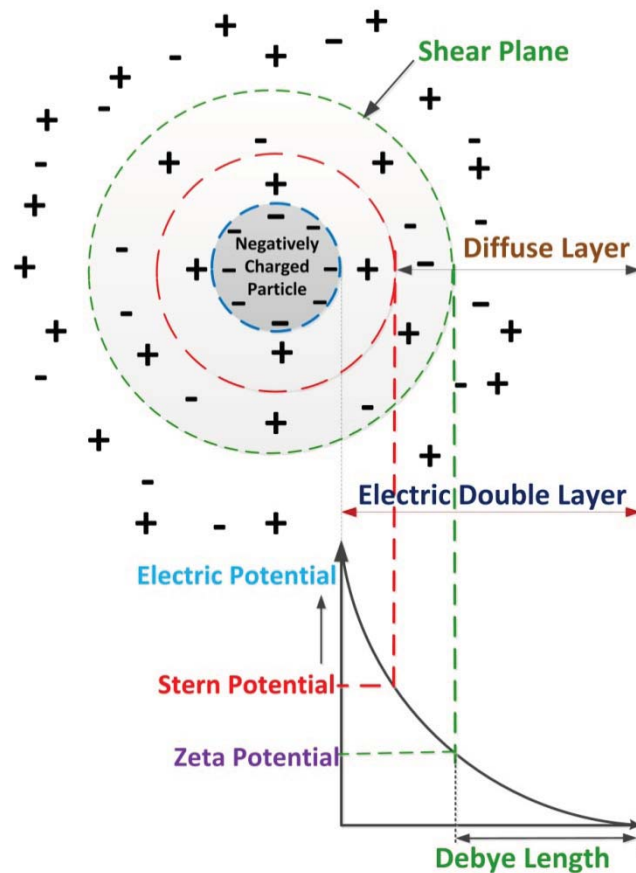


Figure 1.4 Electric double layer (EDL) representation of a negative charged particle experiencing electrokinetic phenomena.

#### 1.1.4.1 Electrophoresis

An electric field effect of electrokinetic phenomena is the electrophoresis for separating particles contained in liquid. Particles charged electrostatically in the bulk-liquid move comparative to the stationary or moving liquid when field is induced<sup>38</sup>. The charged particles continue to move until the frictional force equals to the electric force. Electrophoresis often compliments electro-osmosis due to the electric charge of the wall.

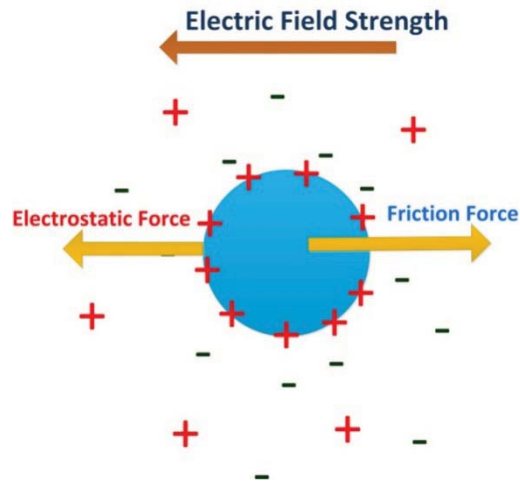


Figure 1.5 Charged particle demonstrating electrophoresis in a bulk-liquid phase under an applied electric field.

When a negative charged particle is under the influence of electric field, the electrophoretic motion causes it to move towards the positive electrode (anode). Electrophoresis is mostly used in separating biomolecules based on their charge to size ratio, as shown in equation 1 for spherical particles<sup>38</sup>.

$$\mu_{EP} = \frac{Q}{6\pi r\eta} \quad (1.1)$$

Here,  $\mu_{EP}$  is the electrophoretic mobility,  $Q$  charge on the particle,  $r$  radius of the particle and  $\eta$  viscosity of the fluid. In the next section, a brief introduction about electro-osmosis

and dielectrophoretic forces has been presented as they play a major role in sorting the blood cells in this research study.

#### **1.1.4.2 Electro-osmosis**

Electro-osmotic flow (EOF) is caused when the net charge in the Debye layer (EDL) causes the liquid to move on applying electric field. Generally, EOF is very high in small capillaries compared to large tubes. The bulk liquid phase moves relative to the stationary charged surface. Consider a negatively charged particle as shown in Figure 3, electrophoretically the particle moves towards anode, but electro-osmotically, the positive charges surrounding the particle will drive the particle towards negative electrode / cathode. In order for the particle to experience electrophoresis, it has to overcome electro-osmosis. Detailed discussion with the equations governing the flow will be discussed in Chapter 7.

#### **1.1.4.3 Dielectrophoresis**

Dielectrophoresis occurs when a dielectric particle subjected to electric field, experiences a net force directed towards field maxima or minima, depending on the medium properties and particle. For dielectrophoresis to occur the particles need not be charged and this can be observed for particle diameters in the range of 1-1000  $\mu\text{m}$ . For particle diameters less than 1  $\mu\text{m}$ , Brownian motion dominates dielectrophoresis and above 1000  $\mu\text{m}$  gravitational forces dominate<sup>41</sup>. Chapter 3 has been dedicated entirely to dielectrophoresis including a detailed discussion.

While these same charge / friction governing forces exist for all cellular electrokinetic applications, creative control of a) the applied electric field shape, type, and strength, b) electric field geometry, c) medium conditions, and cell properties, can



yield unique responses which are indicative of cell characteristics and can be used for cell diagnostic purposes. Next two sections present motivation and objectives in this research for building a point of care diagnostic device.

## 1.2 Motivation

There is an ever rising need in the area of medical diagnostics for early detection, high quality medical care and new technologies<sup>38,42</sup>. The driving force beyond this biomedical diagnostic application is the emphasis for accuracy, preventive care and least invasive procedures<sup>38</sup>. National institute of health and Bill and Melinda Gates foundation have prioritized to develop technology leading to identify disease conditions at point of care<sup>42</sup>. One such important diagnostic technique in urgent medical circumstances is blood typing. Knowledge of one's blood type is very important. Especially during urgent circumstances, vital judgments have to be taken rapidly for blood transfusion, so by knowing the blood type can save treasured minutes in the process following an accident. Blood type is decided by genetics widely, and is not modified through lifetime. Blood transfusions are life-saving in some circumstances, such as enormous loss of blood due to catastrophe, or to replace lost blood during a key surgery<sup>1</sup>. Blood transfusions are also used to treat some medical diseases like anemia. Frequent blood transfusions are required for people diagnosed with rare blood diseases like hemophilia or sickle-cell anemia.

The current technique for blood typing is by agglutination test in a practitioner's office, donation center, or a hospital by trained phlebotomists or medical lab technicians<sup>43</sup>. The test requires a medical environment, antibody tests for each blood type, and methodologies which are not transportable to the site of a catastrophe or calamity<sup>1</sup>. An agglutination test is carried out by handling blood with serum containing

antibodies. When different combining sites of one antibody react with antigen on two different red blood cells, cross linking of antibodies occur, thus causing agglutination<sup>44</sup>. Blood typing is often expensive (\$50 per test at Mississippi State University's Longest Student Health Center) and time consuming (~ 30 min at a major hospital trauma unit to ~ 1 day at Longest Student Health Center).

If a person does not obtain blood of similar type, serious risks are involved; severe transfusion reactions include agglutination of the blood inside the body or severe autoimmune responses, potentially resulting in death. Matching and verification is often required to avoid any error caused by the technician before blood is dispensed. Possible infections occur if blood transfusion is not dealt with utmost care. Current practices are time consuming and expensive in a catastrophe, so POC diagnostic tools would provide substantial improvements. Lab-on-a-chip diagnostic approaches aim to be accurate, less time consumption, easy operation, minute sample amount, reproducible and cheaper<sup>8</sup>. By adapting plastic devices, the operational costs could be minimal (~\$0.38) compared to the expensive quartz or silica devices<sup>42</sup>. Figure 1.6, illustrates the major differences between conventional lab tests and envisioned point of care LOC devices. Another advantage of LOC devices is that minimal power is required thus can be battery operated<sup>35</sup>. As the name suggests, POC can be run at home, office or any trauma locations without trained technicians and the results could be got in minutes compared to hours by the conventional testing methodology. This research investigates a novel method of using DEP as a tool for sorting blood types in the ABO blood type system.

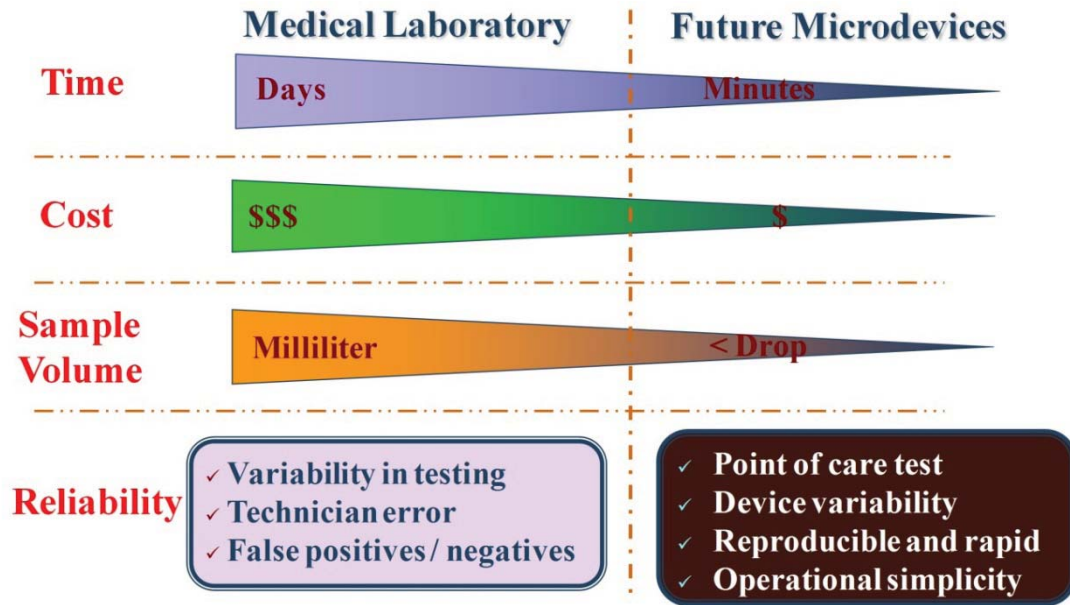


Figure 1.6 Comparison of medical laboratory and future lab-on-a-chip device for blood testing purpose.

By this technique, health care will be made affordable by the rural and lower group population in developing countries<sup>31</sup>. This micro-TAS or BioMEMS or lab-on-a-chip device technology has the potential to identify and prevent diseases, thus serving as an early diagnostic tool<sup>42</sup>.

### 1.3 Objective of the study

In this research study sorting a drop of blood by its ABO blood type using dielectrophoretic forces in a microdevice has been demonstrated. Determining the best possible electric field and other experimental parameters like conductivity of buffer and concentration of blood cells to achieve effective separation of blood cells by its type has been investigated.

From our group's previous work, dielectrophoretic behavior varies with blood type suggesting that dielectrophoretic fields polarize cells differently based on their antigen expression<sup>1</sup>. Prior to our group's publication in *Electrophoresis* in 2008,

dielectrophoretic blood responses were not blood types. Many previously reported methods involve altering the cells under non-physiological conditions<sup>6,11</sup>, but the research outlined in this dissertation involves a novel technique where the cells remain viable and the sorted red blood cells could be subsequently used for disease diagnostic purposes.

#### **1.4 Outline of Dissertation**

Chapter 2 reviews microdevices and fabrication techniques in detail including our preferred microfabrication technique of soft photolithography. This chapter also discusses different sealing methods and surface modification techniques to achieve desired electro-osmotic flow behaviors and better efficiency in separations of cells and particles.

Chapter 3 deals with traditional alternating current dielectrophoresis, theory, types and applications while Chapter 4 discusses the newer, novel field of direct current insulator dielectrophoresis (DC-iDEP), theory and applications. Important parameters governing separation of particles in DC-iDEP devices like electric field, pH and conductivity of the medium are presented.

Chapter 5 reviews about the human ABO blood system, Rh factor, other blood typing systems and specifically red blood cells / erythrocytes' shape, geometry and function in human body. Chapter 6 deals with blood typing using Alternating Current Dielectrophoresis (AC-DEP).

Chapter 7 presents particle separation using DC-iDEP while Chapter 8 discusses our progress on blood typing by DC-iDEP. Chapter 9 deals with a novel technique for quantification of red blood cells by resistance measurement. Chapter 10 concludes the dissertation and provides summary and conclusions about this research.

## CHAPTER II

### MICRODEVICE MICROFABRICATION

#### 2.1 Introduction

Microfabrication is a collection of engineering technologies for producing miniature structures at micron or submicron length scales involving film deposition, photolithography, etching, access-hole drilling, and bonding of microchip<sup>22</sup>. Semiconductor devices in integrated electrical circuit fabrication were the earliest microfabricated devices<sup>38,45</sup>. In this research polymers have been used to develop microdevices. To develop polymeric microdevices various methods are developed which include casting, laser ablation, injection molding, imprinting, and compression molding. The technique used in this research to manufacture polymeric device is soft photolithography via rapid prototyping involving a series of steps: designing the device in CAD (computer aided design) software; photoresist film deposition on substrate; replica molding; and bonding of microdevice<sup>38,46</sup>. In the next sections, a detailed discussion about different fabrication techniques has been presented.

#### 2.2 Fabrication techniques

Current fabrication techniques are categorized into hard and soft fabrication depending on the materials used in fabrication microfluidic devices<sup>38</sup>. There exist differences in the manufacturing process between these two techniques and each

technique has advantages / disadvantages. In the next section, discussions of these two techniques have been provided.

### **2.2.1 Hard fabrication**

Traditionally, microTAS platforms were made using hard inorganic materials as substrate, thus the name 'hard fabrication'<sup>38</sup>. Glass and silicon were the first inorganic material substrates used to build the  $\mu$ TAS platform<sup>47</sup>. Micromachining using film deposition, photolithography, etching, access-hole drilling, and bonding has been investigated on materials such as silicon, glass, and quartz<sup>45</sup>. Silicon substrates are rather expensive and they are not suitable for optical detection due to their opaque characteristic in the UV/visible region. Glass, on the other hand, is transparent and relatively cheap, but poses problems with etching due to scratch effects<sup>22</sup>. By pre-etching the glass surface with hydrogen fluoride (HF), scratch effects can be reduced. Micromachining quartz wafers are expensive and avoided by many researchers. Separating and sequencing DNA has been successful with glass microdevices but when manipulating proteins, they were adsorbed on the glass<sup>48</sup>. Overall, micromachining method of fabrication is expensive, labor intensive, requires special equipment, specialized skills and facilities. This method is more suitable for chemistry operations where high temperatures, strong solvents and chemically stable surfaces are required<sup>25</sup>.

### **2.2.2 Soft fabrication**

Soft fabrication techniques incorporate synthetic polymers, natural polymers like proteins and DNA, biological materials and self-assembled monolayers to create microstructures<sup>38</sup>. Bell labs in 1974 were the first to develop elastomeric micromolding, a type of synthetic polymer, by molding a soft material from a lithographic master. Soft

lithography involves stamping of patterned surface and fabricate microdevices by hot embossing or molding<sup>25</sup> (see Section 2.4). Soft fabrication may involve both hard and soft materials in fabrication processes, since soft fabrication technique can be a hybrid of silicon, glass and polymers. Soft fabrication materials have to meet a variety of constraints in order to make it a robust device. Some constraints are<sup>38</sup>:

- when fluorescence detection is incorporated in the device, the material should not absorb the detection frequency,
- no adverse effects should be detected between sample, solvents and the material,
- must be able to dissipate heat and hold up high temperatures, pressures and electric field, and
- channel walls fabricated by these materials might have to undergo surface modification.

Several advances have happened since the first elastomeric molding was developed. Whitesides *et al.* group<sup>46</sup> in 1998 transformed the way soft fabrication was employed to create microfluidic devices. In the next section, a more detailed discussion on the materials used in soft fabrication along with properties and advantages / disadvantages of using polymeric materials has been presented. In this research, rapid prototyping method, a soft photolithographic technique has been used to develop microdevices. A detailed discussion on the procedure involved is provided in Section 2.5.

### **2.3 Materials employed in soft fabrication**

Although fabrication using inorganic materials like silica, glass and quartz have been a success, but their cost, fragility, complex fabrication steps, and subsequently long

manufacturing times for concept design to completed device has limited their widespread use for lab-on-a-chip devices. As a substitute, synthetic polymeric materials are widely used in fabricating and offer many advantages<sup>38,47</sup>:

- light-weight, inexpensive, ease in fabrication
- biocompatible, fracture tolerant
- optical transparency for detection
- high aspect ratio of microstructures
- good thermal and electric properties
- able to modify surface and functionalize

Polymeric materials, in particular biomaterials can be classified depending on applications in medical diagnostics like *implantable* materials (having direct contact with the body), aiding in *transport* of biological samples and for *processing or analyzing* of biological samples. They can be divided into three classes depending on their glass transition temperature: thermosets, thermoplastic materials, and elastomers. Thermosets, rigid and heavily cross-linked which cure irreversibly and are malleable before curing, are used to develop devices using soft photolithography especially using the SU-8 technique. SU-8 is an epoxy photoresist and a very viscous polymer used in soft lithography process (more in Section 2.5.1). Thermoplastic materials such as poly(methyl methacrylate) (PMMA), polycarbonate, cyclo-olefin polymers, polyamide, polybutyleneterephthalate, polypropylene, polyethylene, polyoxymethylene, polysulfone, and polystyrene<sup>49</sup> are used in developing devices by hot embossing or injection molding, since they are linear or branched molecules and melt when heated. Elastomeric materials which are lightly cross-linked and can be reversibly stretched are most commonly used in rapid prototyping of microdevices due to cheap material cost and ease of handling. These materials swell



when organic solvents are brought in contact making it a limitation, but they are well adapted for cell-based systems<sup>50</sup>. Some disadvantages or problems using polymeric materials are<sup>22</sup>:

- Optical properties: UV transmittance is different for different polymeric materials. Autofluorescence emitted from the plastic materials and bonding substances might cause a problem depending on the method of detection used.
- Electrical properties: Low dielectric breakdown voltage is observed in many polymeric devices.
- Thermal properties: Low thermal conductivity compared to glass or silica. This might pose a problem with heat dissipation if a high electric field is applied to the system.
- Mechanical properties: Channels fabricated deep can collapse the device and also lateral collapse was observed when channels were not spaced at sufficient distance.
- Surface properties: Surface modification or functionalization needed to render channels hydrophobic or hydrophilic. But after rendering them hydrophilic or hydrophobic they need to be retained under certain solvents or gases to retain the properties.
- Solvent resistance properties: Some polymeric materials swell under organic solvents, some are not compatible with polar solvents and they have low adsorption of solvents.

In this research, poly(dimethylsiloxane) (PDMS), an elastomeric polymer, has been chosen as the polymeric material to fabricate the microdevice platform for sorting

erythrocytes by human ABO blood type and the next section deals with PDMS structure, properties and advantages / disadvantages.

### 2.3.1 Poly(dimethylsiloxane) (PDMS)

PDMS is a class of organosilicon compounds, commonly known as silicones, widely used in microdevice production. It is also referred to as silicone rubber and is liquid at room temperature but solidifies after mixing with a cross-linking agent (dimethyl, methylhydrogen siloxane). Some of the common applications of PDMS are in contact lens, shampoos, lubricating oils, heat resistant tiles, cosmetics, hair conditioners, and defoaming agents<sup>48</sup>. The chemical structure of PDMS as shown in Figure 2.1, has repeating units of  $-\text{OSi}(\text{CH}_3)_2-$  making it hydrophobic due to  $\text{CH}_3$  groups.

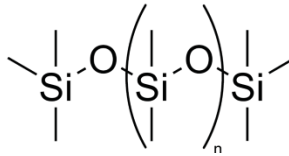


Figure 2.1 Chemical structure of poly(dimethylsiloxane) (PDMS).

Due to the hydrophobic nature of PDMS, wettability with solvents is an issue. In microchannels, this manifests as a propensity to trap air bubbles in channels when filling with fluid. However, PDMS elastomers offer these advantages<sup>48,51</sup>:

- controllable surface chemistry,
- fabrication of micron scale features with high accuracy by replica molding,
- transparency in UV/visible region allows for interfacing with various detection systems,
- low temperature curing and good thermal stability,

- non-toxic, so can be employed in biological systems and implantable devices are possible,
- reversible deformation, reversible and irreversible sealing on a wide variety of materials like glass and PDMS itself,
- elastomeric structure makes it easy to release off from the substrate / master with minimal damage depending on the shear rate,
- does not swell due to humidity,
- mechanically flexible and can be manipulated to the desired shape due to its homogenous structure,
- chemically stable due to low interfacial free energy; molecules patterned onto the surface do not adhere irreversibly,
- durable and the master pattern to create the PDMS mold can be used multiple times with minimal degradation.

PDMS also has few disadvantages when applied in soft lithography processes<sup>51</sup>:

- shrinks after curing and cured PDMS swells in presence of organic solvents,
- some limitation for multi-layer fabrication due to varying accuracy after fabrication,
- due to the softness of PDMS, aspect ratio is limited in microstructures.

Sagging is also seen in structures that are not mechanically well supported.

Despite all the disadvantages, PDMS is the most commonly researched elastomer for microfluidics in academic research labs because it is inexpensive, easy to fabricate, amenable to short concept design to finished device manufacture times, and suitable for biological samples<sup>27</sup>. Due to the different materials used in soft fabrication techniques

and to overcome some of the disadvantages of PDMS elastomer, a variety of methods have evolved to develop microdevices which are discussed in the next section.

## 2.4 Soft fabrication techniques

Soft lithography makes use of a group of processes: microcontact printing ( $\mu$ CP), microtransfer molding ( $\mu$ TM), molding in capillaries (MIMIC), replica molding, near-field phase shift lithography and decal-transfer microlithography (DTM)<sup>38</sup>. In the case of  $\mu$ CP, a patterned stamp is coated with an ink of alkanethiols and is brought in contact with the substrate. This method is used to transfer biologically active molecules and features of  $\sim 300$  nm have been achieved<sup>52</sup>. Microtransfer molding involves a patterned mold loaded with a precursor and then set on substrate to be patterned, which can generate small features up to 250 nm and also multilayer systems<sup>51,53</sup>. Another technology MIMIC can produce continuous channels and features of about 1  $\mu$ m. Here, the mold is first brought in contact with the substrate and by capillary action, the polymer precursor fills the channels where it is cured<sup>38,54</sup>. Recent advances in fabrication are the replica molding by Whitesides *et al.* group that allows making multiple copies from the master substrate without harming the original master. This technique can yield features up to 30 nm<sup>46</sup>. A number of such technologies like injection molding, microthermoforming, hot embossing, and casting where replication is optimal is discussed in a review article by Gartner *et al.*<sup>49</sup>. Hot embossing is one such technique which has advanced in the last decade. It involves transfer of a pattern micromachined into a plate onto a plastic sheet, more commonly polymethyl methacrylate (PMMA) by heat and pressure. They offer low cost devices, but expensive when the design has to be changed or if the micromachined, metal, silicon or glass wafer is broken due to high temperature and pressure<sup>25</sup>. Injection

molding is another method extensively used in fabricating microdevices. It involves feeding a melted polymer into an evacuated template cartridge to form a replica under high pressure. Once cooled, the replica is removed<sup>47</sup>. Injection molding is fast and less expensive compared to hot embossing, but cartridges must be made by thermoplastic polymers; there is a limited choice of materials and it has low resolution in producing small structures<sup>25</sup>.

Other recent advances in soft lithography include in situ construction, laser ablation, and SU-8 photolithography<sup>47</sup>. In situ construction of microdevices, also known as microfluidic tectonics uses liquid photopolymerizable materials, laminar flow and lithography to fabricate. It doesn't need any clean room facilities, fast, inexpensive, do not need expensive equipments and no bonding is required<sup>25</sup>. Also, complex microstructures and 3D devices could be fabricated in less time than even PDMS soft photolithography. UV radiation is used to polymerize the monomer and large variety of materials could be used to fabricate<sup>47</sup>. This technique is not widely used due to the fact that it cannot fabricate structures  $<100 \mu\text{m}$  because of the side reaction caused by UV-polymerization.

Another recent development in the field of fabrication is the microfluidic assembly blocks by Burns et al. group<sup>55</sup>. This technique involves fabricating basic building units by standard PDMS soft photolithography technique. The microfluidic building blocks like inlet/outlet, straight channel, T-channel, Y-channel, cross channel, chamber, connector, long channel, pneumatic valve, and zigzag channel are prefabricated and assembled later depending on the desired device and its application. The assembling doesn't require any cleanroom facilities and a non-expert user could easily assemble them by carefully

aligning the blocks<sup>55</sup>. This approach is good, if only a part of the device has to undergo surface modification. There is no limit on feature size and channel thickness.

FLASH, Fast Lithographic Activation of Sheets, was another recent discovery by Whitesides *et al.* group in lab on a chip technology. This method uses UV lamp source and hot plate (if unavailable, can use sunlight), producing hydrophilic structures ( $\mu$ PADS) as small as  $\sim 200 \mu\text{m}$ . This technology involves saturating paper with SU-8 photo resist; drying to remove the solvent used in photopolymerization of SU-8; covering one side with adhesive transparency and other side with black paper; printing the pattern using inkjet printing; exposing the patterned paper to UV light; removing the transparency film and black paper; baking the polymerized photoresist; and removing the unpolymerized resist<sup>56</sup>. Their applications lie in detecting and monitoring chronic diseases, agriculture, military applications, homeland security, and environmental monitoring.  $\mu$ PADS can be prepared in  $<30$  min, if FLASH is already made and the cost per device would average to 1-3 cents<sup>56</sup>.

A non-photolithographic technique of patterning structures in microdevice is the shrinky-dink microfluidics developed by Khine *et al.* group<sup>57</sup>. Shrinky-dinks are sheets of biaxially oriented polystyrene thermoplastics. Patterns developed by AutoCAD are printed onto shrink-sink sheets at 600dpi. Patterned sheets are placed in the oven for 3-5 min at  $163^{\circ}\text{C}$  to shrink the sheets. The shrunk sheets are then casted as a PDMS device. Once the device is cured, it is peeled and sealed onto glass slides. This technique yielded deep, rounded channels for mammalian cell assays<sup>57</sup>.

A plethora of modern technologies are available. However, soft lithography still uses a hard lithography technique to obtain the master (Si wafer) and once this is made available, the microdevices could be made with printing or replica molding. After hard

lithography is complete, there is no requirement for clean room facilities. Many fabrication facilities supported by National Nanotechnology Infrastructure Network (NNIN) offer services to create masters and can fabricate masters for satellite labs such as ours<sup>58</sup>. In the next section, a detailed discussion on the rapid prototyping soft lithography technique used in this research to build our microdevices is presented.

## **2.5 Fabrication of devices by rapid prototyping**

The rapid prototyping technique is one of the soft fabrication techniques pioneered by Whitesides *et al.* group in 1998 to fabricate microdevices in a cheaper and easier way<sup>46,48,59</sup>. By rapid prototyping, devices can be made in <24 h time period, cost is greatly reduced, and new configuration devices can be manufactured several times until the final design is obtained according to application<sup>59</sup>. This technique yields structures >20  $\mu\text{m}$  in size. A detailed protocol was recently published by Whitesides *et al.*<sup>58</sup> and Frienda *et al.*<sup>60</sup>. Figure 2.2 represents a detailed protocol of the rapid prototyping technology.

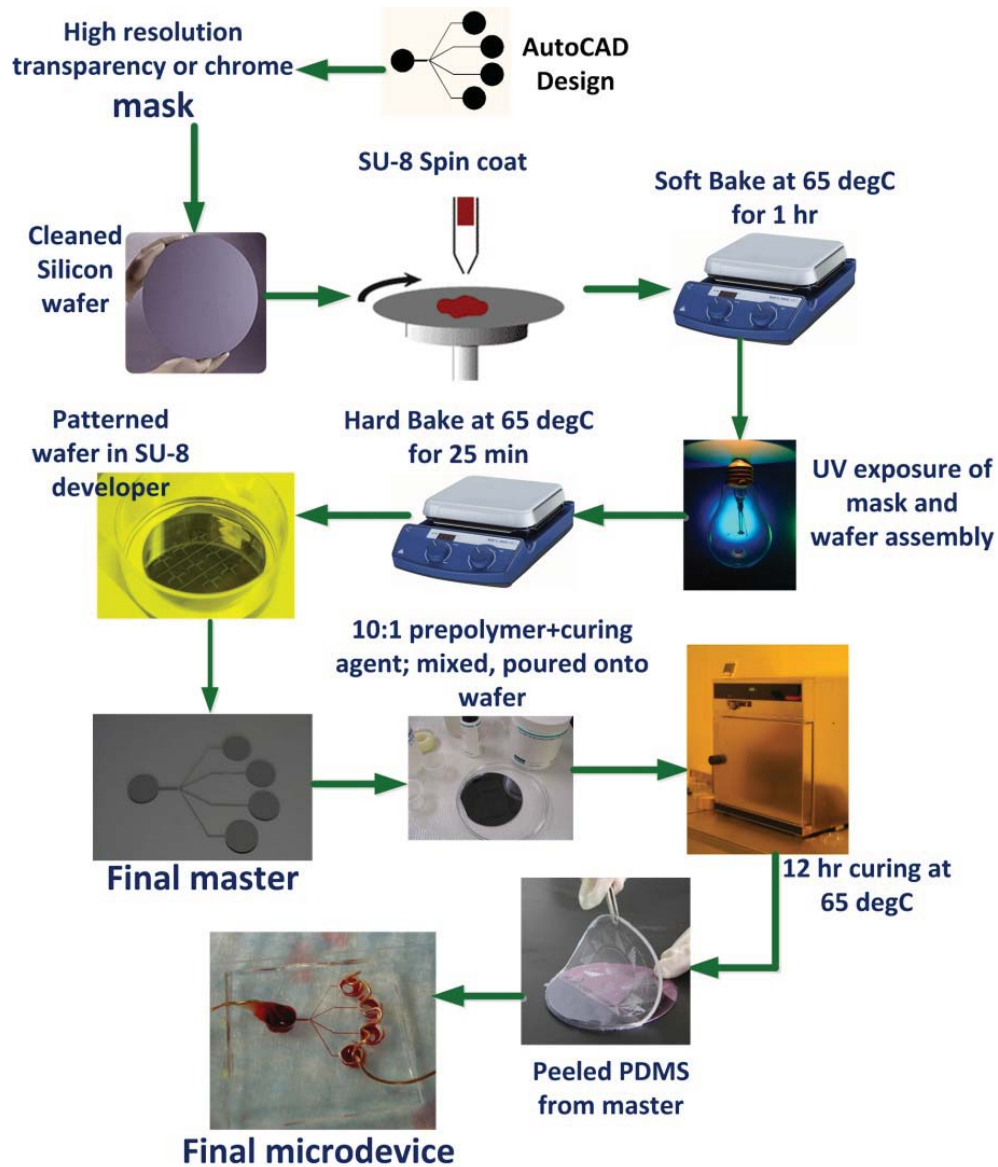


Figure 2.2 Detailed protocol of rapid prototyping technique for fabricating PDMS microdevice from silicon wafer master [some individual pictures adapted from Google images<sup>61</sup>].

### 2.5.1 Rapid prototyping

The first step in rapid prototyping involves designing the device in CAD (computer aided design) software and then printing a high resolution (32,000 dpi) transparency or a chrome mask with the pattern on it. Depending on the resolution needed for the mask, cost and time increases accordingly. Transparencies take less time



to be made and are less expensive compared to chrome masks. Once the mask is available, a master can be prepared from a silicon (Si) wafer on which a negative photoresist is spun.

Photoresist materials are light-sensitive viscous compounds used to pattern the design on the mask and most common being the SU-8<sup>62</sup>. SU-8 is an epoxy negative photoresist. It can be patterned with high aspect ratios (>20). SU-8 forms cross-linked structures when exposed to UV light at 365 nm. Once cured it is very hard to remove from a substrate, commonly used solvent is piranha (mixture of sulfuric acid and hydrogen peroxide). Different feature sizes could be obtained by using different SU-8 photoresist series e.g. SU-8 2000 series (1-200  $\mu\text{m}$  features can be developed). SU-8 2035 can develop features as small as 35  $\mu\text{m}$  (the last 2 digits of the series number signifies this).

Two different types of photoresists exist:

- Positive photoresist: Here, the portion exposed to light becomes soluble in the developer while the unexposed regions crosslink and harden. Thus, raised features exist where the UV light is blocked and an indented pattern is obtained. Smallest feature obtained by this is 0.5  $\mu\text{m}$ .
- Negative photoresist: Here the portion exposed to UV light cross-links and becomes insoluble in the developer. Thus raised patterns are obtained where UV light shines through the mask and a raised pattern is obtained. Negative photoresists are less expensive compared to positive photoresists and the smallest feature that could be obtained is about 2  $\mu\text{m}$ .

More information on these photoresists could be obtained from MicroChem<sup>®</sup>

([www.microchem.com](http://www.microchem.com)).

Usually the silicon wafer is cleaned with several solvents before spinning the SU-8 photoresist on it. These solvents are acetone, isopropyl alcohol (IPA), and ethanol; they clean and functionalize the surface to better bond the SU-8. After spinning the SU-8 photoresist, it is soft baked before exposing to UV light. The soft bake is at two different temperatures, 65 °C for 15 min and 95 °C for an hour on a hot plate. The time taken to completely bake the photoresist depends on the thickness of the deposited SU-8<sup>60</sup>. The times given here are for ~50 μm thick SU-8 layer. The mask is placed on the dried photoresist-coated master and then exposed to UV light (365 nm, 500 mJ/cm<sup>2</sup>) for 3-5 min depending on the depth of the photoresist. Exposure times also impact replication of the device features. Longer exposure times produce undesirable shadows around the microstructures due to a combination of reflection, refraction and Fresnel diffraction<sup>63</sup>. The shadow causes the channel walls to slope while vertical walls are most desired. The UV exposed master is now hard baked on a hot plate at 65 °C for 30 min or until firm to the touch (requiring some trial and error). At higher temperatures, the photoresist might develop some cracking or burn. Once the wafer containing the pattern is hard baked, the assembly is immersed in a developer solution for 15 min. This developer solution washes off the unexposed photoresist layer, thus leaving behind only the pattern. After removing from the developer, the wafer/master is washed with IPA and then finally with acetone. The master is dried at 65 °C for 15 min to obtain better stability of the pattern. The patterned master is now set for replica molding (casting PDMS) to obtain PDMS microdevices.

### 2.5.2 Replica molding

Replica molding involves developing the elastomer replica of the patterned design on the master by PDMS. Sometimes the master is silanized or sprayed with hexamethyldisilazane (HDMS) to prevent adhering of PDMS to the master. PDMS prepolymer base and curing agent (Sylgard Elastomer 184 Kit) from Dow Corning® in the ratio of 10:1 is used. The prepolymer base and curing agent is well mixed and degassed in a vacuum desiccator to remove air bubbles from the viscous PDMS elastomer mixture. Once degassed, this mixture is then poured onto the master containing the pattern. The assembly is cured at 65 °C for about 12 h; the cured device is peeled off and holes punched for inlet and outlet ports. The finished device is ready to be sealed.

In the next section different methods of sealing are presented with some surface modification techniques for rendering the PDMS channels hydrophilic.

### 2.5.3 Polymeric device sealing

Sealing is a method of fixing the three-sided PDMS channels to a surface to enclose the microchannels and features to contain fluid. The peeled device can be sealed onto glass or PDMS itself to form channels by different methods:

- Thermal bonding: In this technique, the polymer device and a base plate for forming the channels are clamped together and slowly heated to the glass transition temperature of the polymer. The temperature is lowered and the clamped assembly is released. This bond is sometimes weaker, but temperature and pressure can be optimized to achieve strong bonds<sup>64</sup>.
- Solvent bonding: Solvent bonding is relatively new technique, not explored by many researchers<sup>47,65</sup>. There are two methods available for solvent bonding, one is by spin coating solvent on the base plate and then

by applying pressure the patterned polymer is sealed to the base plate. Another method involves a sacrificial layer approach by melting wax. Patterned polymeric device is covered with PDMS to form an enclosed assembly which is heated above the melting point of the wax. Melted wax is filled into the channels. Assembly is cooled and the sacrificial layer is solidified. PDMS is removed from the patterned polymer device, and the sacrificial layer protects the channels. An organic solvent is poured on to the polymer surface, and base plate is compressed against the patterned substrate until solvent bonding is complete. The sacrificial layer can be removed by pipetting the melted wax by heating the bonded microdevice. Finally, hexane is used to dissolve any leftover sacrificial material in the channels<sup>47</sup>. The bonding appears to be stronger and less heat is required, but the channels may be modified or even obstructed due to the solvent.

- Adhesive bonding: Here a thin layer of adhesive glue having the same characteristic as the polymer substrate is painted on the casting<sup>66</sup>. Channels may be modified or obstructed with this approach as well.
- Resin-gas injection bonding: A new technology introduced in 2001 involves resin polymerization between two polymer substrates. Common resins used in this technology are hydroxyethylmethacrylate (HEMA), epoxy, and unsaturated polyesters<sup>47</sup>. An advantage of this method is channel modification can be performed while fabricating which saves time, but this might contaminate the channels.
- Chemical bonding: This is a type of permanent bonding technique. The bonding happens between the contact surfaces of the polymer-polymer or

polymer-glass devices. Due to varying chemical properties, different methods are available to seal the channels. The most common being the oxygen-plasma treatment<sup>59,67</sup>, described in the next section, which forms covalent bonds with the substrate and the base plate.

In this research, plasma-oxidation method was the optimal method used to functionalize the PDMS surface to chemically bond to glass and form the completed microdevices. But other methods like thermal bonding and solvent bonding were also explored and the results in terms of zeta potential and EOF mobility have been discussed in Chapter 7.

### 2.5.3.1 Surface modifications for PDMS

In this section, different surface modifications of the PDMS castings and channel walls are presented. The main topics are sealing PDMS to glass irreversibly by plasma oxidation and dynamically coating the PDMS channel to modify the surface charge temporarily. An in depth review article covering the entire scope of this topic has been published recently by Ho *et al.*<sup>68</sup>.

PDMS can be sealed reversibly by any of the methods described in Section 2.5.3. They form a weak contact by Van der Waal's forces. The easiest method is adhesive bonding by silicon tapes which allows for better flexibility of the device<sup>59</sup>.

Irreversible sealing of PDMS can be achieved by modifying the  $-O-Si-(CH_3)_2-$  groups aligned along the elastomer – air interface. They can be irreversibly bonded to a wide variety of materials like glass, PDMS, polystyrene, silicon, or polyethylene<sup>59</sup>. By exposing this to oxygen-plasma, covalent bonds of silanol polar groups are formed, destroying Si-CH<sub>3</sub> groups. When PDMS device is sealed to a glass plate, Si-O-Si bonds

are formed after losing H<sub>2</sub>O<sup>48</sup>. Attempting to separate the glass and PDMS device will result in structural breakage of the device, since a tight irreversible seal is formed. PDMS seals can withstand pressures between 30-50 psi, but this method doesn't work for polymers like PMMA, polyamide and polycarbonate<sup>48</sup>. Another method of irreversibly sealing two PDMS pieces is to add excess curing agent in one layer and excess monomer in the other. The two layers slowly react and bond together.

PDMS surfaces are generally hydrophobic and the channels have to be modified to render them hydrophilic<sup>69</sup>. Generally, surface modifications of PDMS are necessary to control the channel wall wettability, regulation of zeta potential and thus EOF, increase compatibility with biomolecules, and reduce unspecific adsorption. Some of the methods to modify PDMS surfaces are:

- Oxygen plasma treatment: The channels could be oxidized as specified above. Oxidizing of the channel walls has two advantages<sup>46</sup>: 1) hydrophilic<sup>70</sup> - easy to fill liquid into the channels and less bubble formation in the channels and 2) oxidized channels support electro-osmotic flow (EOF) towards negative electrode. Electro-osmotic flow is a mechanism that pumps the fluid through the channels so that both positively and negatively charged particles move towards the cathode (negatively charged electrode) on application of an electric field. To maintain the hydrophilic nature of oxidized channels, the device must be stored in water or any polar solvent<sup>59</sup>. If exposed to air, the oxidized channel wall reverts back to hydrophobic nature within 30 min of exposure<sup>48</sup>.

- **Dynamic coating:** This method is the simplest channel modification process. It involves mixing the coating with a specific buffer which is then flushed from the channel. The coating is adsorbed on the channel walls, thus modifying the channel properties temporarily. Most dynamic coatings are designed to reduce EOF<sup>71</sup> and prevent adsorption of biomolecules onto the channel walls<sup>72</sup>. The coatings are usually a type of surfactant, low molecular weight compound, charged compound or neutral polymer. Surfactants are commonly used due to the presence of both hydrophilic and hydrophobic groups such that adsorption to the wall occurs spontaneously through hydrophobic interactions. Commonly used surfactants are brij-35<sup>73</sup>, sodium dodecyl sulfate (SDS), tween-20<sup>74</sup>, triton X-100, n-dodecyl- $\alpha$ -D-maltoside, and didodecyldimethylammonium bromide<sup>47,64,75</sup>. Addition of SDS has been reported to increase EOF and thus improving separation efficiency of various biomolecules<sup>71</sup>. Another coating method is use of a neutral polymer like poly(ethylene glycol) (PEG), which helps in protein molecule desorption to the surface<sup>59</sup>. Other prepolymers used as dynamic coatings for manipulating EOF are polystyrene sulfonate, polybrene<sup>76</sup>, poly(vinylpyrrolidone) (PVP)<sup>77</sup>.
- **UV radiation:** This process requires a high energy source and it has shown to increase EOF<sup>78</sup>. Improved wettability and reduced adsorption was noticed. Here the PDMS device is treated in a UV cleaner for 15 min and the channel surface is modified permanently<sup>79</sup>.
- **Atom transfer radical polymerization:** This technique has been used for surface modification of PDMS and PMMA. This involves surface

activation of PDMS device by plasma-oxidation, initiator immobilization and grafting the chosen polymer to the surface<sup>47</sup>.

In this research study, plasma-oxidation was used as a method of surface modification, but UV-ozone and surfactants like tween-20 were used for comparing the EOF. The results on all of these modifications are discussed in detail in Chapter 7.

## 2.6 Summary

This chapter presents detailed overview of the various fabrication technologies, hard fabrication, and soft photolithography fabrication. A rapid prototyping method pioneered by Whitesides *et al.* group is discussed and adapted to develop microdevices for this research project. Different sealing methods and surface-modification techniques are presented and compared to our optimized sealing technique – plasma oxidation. Lastly, surface modification techniques to influence channel wall properties and thus electro-osmotic flow are discussed.

In the next chapter, a thorough review of electrokinetics with a particular focus on dielectrophoresis, theory, applications, and types is communicated.



## CHAPTER III

### DIELECTROPHORESIS

#### 3.1 Introduction

In the first and second chapters, a review of lab-on-a-chip (LOC) device, characteristic forces influence on small scale geometry, LOC applications, current cell diagnostics, soft fabrication techniques, materials used and a detailed discussion about rapid prototyping technology of microdevices has been presented. As discussed in Section 1.3, our research focuses on sorting red blood cells by dielectrophoretic phenomena depending on the antigen expression on these cells. In order to achieve this, an in-depth understanding of dielectrophoresis is required. In this chapter, a review of electric field gradient separation techniques especially dielectrophoresis, types and applications along with the types of bioparticles manipulated via dielectrophoresis in the literature is presented.

#### 3.2 Dielectrophoresis (DEP)

Dielectrophoresis (DEP), an electrokinetic effect, was discovered by Herbert A. Pohl in 1951 and later he coined the term in his book “*Dielectrophoresis the behavior of neutral matter in nonuniform electric fields*” in 1978<sup>41,80</sup>. This research dates back to the early 1960’s, but rapid advancement in this field started in the late 1980’s<sup>80</sup>. When a polarizable particle is subjected to non-uniform electric field, the force exerted on the

particle causes it to move towards high or low field density regions; this behavior is known as dielectrophoresis<sup>1,81</sup>. The motion of the particle is quantified by the polarity of charges and magnitude generated by the applied electric field and the phenomenon is often referred to as ‘classical DEP’<sup>82</sup>. Microelectrodes fabricated into nonlinear geometries are used to generate non-uniform electric field in these microdevices. Some of the characteristics of DEP force are<sup>41</sup>:

- observed only when non-uniform electric field is exerted on the particles because coulomb forces generated on both sides of the particle are different, thus facilitating motion of the particle towards regions of field maxima or minima. If a uniform field exists, the coulomb forces generated are equal but opposite in charge. This combined with the alternating orientation of the electric field makes the net force on the particle over time equal to zero<sup>82</sup>,
- both AC and DC electric fields can be applied to nonlinear field geometries and both will generate non-uniform coulombic forces across a particle thus yielding DEP behavior,
- when permittivity of the particle is more than the medium, particles move towards high field density regions; otherwise they move away from the high field maxima.

The DEP force exerted on a particle is dependent on 1) particle characteristics such as dielectric properties of that particle and particle size, 2) medium properties like pH and conductivity, and 3) applied electric field. In cases involving biological cells (bacteria, virus, mammalian cell), DEP is dependent on permittivity of the membrane and the pathological condition of cell in addition to the other dependencies stated above<sup>83</sup>.

DEP has been a commonly used technique for separation, trapping, and manipulation of cells, bacteria, DNA, virus, diseased cells, and inert microspheres<sup>84</sup>. Electrorotation, DEP migration, traveling wave dielectrophoresis (twDEP)<sup>38</sup>, dielectrophoretic field flow fractionation (DEP-FFF), DEP affinity or retention are some of the other phenomena developed after classical-dielectrophoresis for separation, trapping, isolation, and manipulation of select group of bioparticles<sup>85-86</sup>.

In electrorotation, four symmetric microelectrodes placed at  $90^{\circ}$  angles from each other are also subjected to AC electric fields that are  $90^{\circ}$  out of phase such that the signal maxima rotate around the four electrodes. The resulting torque induced on a single cell, causes rotation without direct contact<sup>87-89</sup>. This is quantified by measurement of rotation rates with respect to electric field frequency<sup>39,90</sup>. This technique was first introduced by Zimmerman *et al.* in 1982 and is more suitable for single cell manipulation compared to separation of groups of cells due to its confined, isolated geometry<sup>88,91-92</sup>. Traveling wave DEP involves multiple parallel electrodes where the electric signals are given in terms of four  $90^{\circ}$ -spaced phases to each consecutive electrode<sup>85,93</sup>. By this technique, high spatial separation of cells could be achieved and the cells are forced perpendicular to the electrode configuration<sup>39</sup>. It was first developed by Batchelder *et al.* at a low AC frequency; Fuhr *et al.* was the first to work on high frequency twDEP for manipulation of cellulose and pollen particles<sup>84,89</sup>. Traveling wave DEP can only be operated using AC fields as there is no phase change involved in DC voltages<sup>82</sup>. Dielectrophoretic field flow fractionation, another common technique used in separation, involves the passage of particles through a chamber wherein the dielectrophoretic force acts at right angles to the flow<sup>94</sup>. The particles move to different flow streamlines according to the DEP force they experience from the perpendicularly applied non-linear electric field and thus exit the

chamber at different times by a combination of dielectric, hydrodynamic, diffusion and other effects<sup>85,89</sup>. Dielectrophoretic field flow fractionation (DEP-FFF) is a phase gradient technique unlike dielectrophoresis which is a magnitude gradient technique.

Heterogeneous mixture of bacteria cells, cancer cells, latex beads have been separated by this technique<sup>84</sup>. Figure 3.1, provides a guide to the frequency ranges where DEP phenomena is applicable and this chart is applicable to separation methods where the medium conductivity is 50 mS/m<sup>95</sup>.

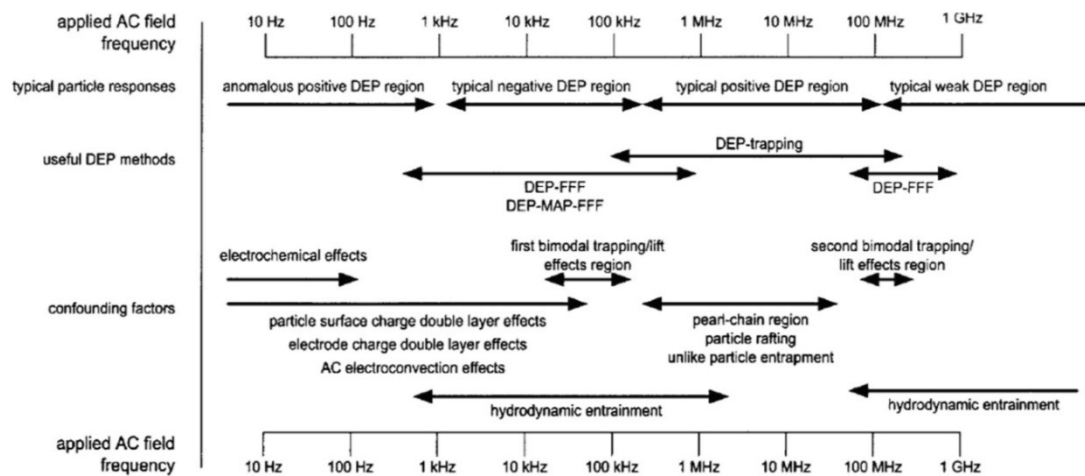


Figure 3.1 Chart showing the mammalian cell responses at frequency ranges applicable for dielectrophoresis<sup>95</sup> [Gascoyne, P. R. C.; Vykoukal, J., Particle separation by dielectrophoresis. Electrophoresis. 2002. 23. 1973-1983. Copyright Wiley-VCH Verlag GmbH & Co. KGaA. Reproduced with permission].

Dielectrophoresis is also an excellent focusing technique controlled by the electric field gradient. Other related gradient techniques developed in the last two decades are electric field gradient focusing (EFGF), dynamic field gradient focusing (DFGF), electrocapture (EG), temperature gradient focusing (TGF), and conductivity gradient focusing<sup>96-99</sup>. All these techniques are applicable to charged nano bioparticles separation like proteins and amino acids. EFGF or electromobility focusing is used to sort ions

based on electrophoretic mobility, first developed by Ivory *et al.*<sup>100</sup>. It is generally used in protein separations and is very different from the traditional isoelectric focusing (IEF) technique. Sorting in EFGF does not occur at the isoelectric point of protein and pH is constant throughout the chamber, unlike IEF<sup>100</sup>. Unlike traditional methods, a better efficiency in separation has not been achieved. EFGF has been operated using dialysis membrane, hollow fiber membrane and array of electrodes in combination with dialysis membrane outside the chamber. The electric field applied could be changed at will according to the shape desired and this gave rise to the development of dynamic field gradient focusing (DFGF), first reported by Ivory *et al.*<sup>100-101</sup>. This technique, would help in increasing the separation of charged particles especially proteins as electric field could be controlled. Another technique which makes use of temperature for separations is the temperature gradient focusing (TGF), a new technique developed recently by Ross *et al.*<sup>99</sup>. It depends on specific buffer which can cause temperature gradient; Joule heating was also considered to generate temperature gradient instead of an external source<sup>98</sup>.

These are specialized techniques for sorting nano bioparticles which are very complex and intricate like proteins and DNA<sup>98</sup>. They are applicable for separating highly charged species unlike erythrocytes which are slightly negatively charged. The techniques discussed above cannot be portable and requires time and money. By far, dielectrophoresis is the most commonly and widely used technique for focusing of micro bioparticles<sup>98</sup> like RBC, WBC, platelets, bacteria, yeast cells, and diseased cells<sup>102</sup>. An extensive review has been published by Hayes *et al.* group in 2009 discussing the different field gradient techniques available depending on the bioparticles of interest<sup>98</sup>.

In the next section, different electrode geometries and following that electric signal conditions for attaining dielectrophoresis will be discussed in brief.

### 3.2.1 Electrode geometry

Conventional electrodes were metal sheets, machined blocks, wires, rods or needles for generating non-uniformity in the electric field, but thanks to the advances in soft lithography techniques, microelectrode fabrication is possible and capable of creating precise electrode shapes and thus specific field gradients<sup>84</sup>. Adapting microelectrode has a number of advantages. One such advantage is the rise in DEP forces experienced by the particle. Dielectrophoretic force depends on gradient of the square of electric field ( $V^2m^{-3}$ ) and direct dimensional analysis demonstrates the substantial increase in force achieved with micron-sized electrodes. Another advantage is the use of low amplitude electric fields for manipulating cells if microelectrodes are used once again because a smaller voltage applied over a micron sized gap can achieve the same force as large voltages over large gaps. The miniaturization substantially reduces joule heating effects and electrode decay thus retaining viability of biosamples<sup>89</sup>. Some of the reported electrode geometries in the literature are trapezoidal electrode array<sup>103</sup>, interdigitated microelectrodes<sup>94,104</sup>, pyramidal arrangement<sup>105</sup>, checker board arrangement, polynomial geometry and multiphase electrodes<sup>106</sup>. An extensive review of the various electrode geometries has been recently published by Kalantar-Zadeh *et al.* group<sup>82</sup>.

### 3.2.2 Electrical signal considerations

The flow of charges in a complete circuit is called electric current. Conventionally, charges flow from positive to negative terminal. In an AC electric signal, the charges keep switching their polarity between + and - usually represented by a sine waveform. AC signal can also be triangular or square waves. The magnitude of the wave at its maximum peak is the amplitude of the signal, expressed in volts. Frequency is the number of complete cycles the wave goes through in a fixed time, usually seconds. It is

expressed in Hertz (Hz) and measured as cycles/sec. The distance travelled by a wave to complete one cycle is referred to as wavelength ( $\lambda$ ) i.e. distance between two troughs or crest in a sine wave. The opposition to the flow of AC signal is measured by impedance ( $Z$ ) which is phase dependent. In DC electric signal, the flow of charges is unidirectional, making it + or -. The flow of electrons is from negative to positive through a conducting media. It is frequency independent and the opposition to the flow of charge is referred as resistance ( $R$ ) measured in Ohm ( $\Omega$ ). Conductors are those that allow the electric charges to pass through them, whereas insulators do not allow charges to pass through them. Dielectrics are another class of materials, wherein the material behaves like an insulator and can be polarized by applying an electric signal, for e.g. a living cell. Dielectric particles depend on permittivity due to the frequency of the applied electric field.

The dependence of permittivity ( $\epsilon$ ) on frequency is termed as dielectric dispersion as described by Martinsen *et al.*<sup>107</sup> and Pethig *et al.*<sup>108</sup>. Permittivity decreases as frequency increases, and is usually very high at sub audio frequencies<sup>90,109</sup>. Since there is a time lapse between changes in electric field and polarization, permittivity is complicated and is a complex function of frequency<sup>108</sup>. These dispersions can be classified based on the magnitude of the frequency or by their physical nature<sup>90</sup>. Classification based on frequency gave rise to  $\alpha$  (low frequency),  $\beta$  (radio frequency) and  $\gamma$  (microwave frequency) dispersion ranges and  $\beta$  was further divided into  $\beta_1$  and  $\beta_2$  later<sup>90</sup>. Maxwell-Wagner and Debye dispersions were the two dispersion ranges according to the nature. Biological cells fall under Maxwell-Wagner or  $\beta$  dispersion range caused due to Maxwell-Wagner relaxation on cell membranes<sup>107,110</sup>. The Maxwell-Wagner effect is an interfacial relaxation process where the electric current must pass an interface between two different dielectrics<sup>107</sup>. Dielectric properties of cells at membrane

interface are dependent on physiological properties like morphology, size and conductivity and in the frequency range 5–200 kHz these dielectric properties are dominated by Maxwell-Wagner or  $\beta$  dispersion effects<sup>95</sup>. Since cells are morphologically distinct they have different dielectric phenotypes, which makes DEP an effective tool for cell manipulation<sup>95</sup>. This effect helps to detect polarization changes in red blood cells *via* dielectrophoresis<sup>110</sup>, thus sorting red blood cells by its type in this research study.

### 3.3 Types of dielectrophoresis

Dielectrophoretic phenomena have traditionally been associated with application of AC voltage and frequency in conjunction with spatially non-uniform electrode geometries to create novel electric field gradients in order to manipulate particles of interest<sup>111</sup>. However, in a new area of research, DC voltage can be applied to achieve dielectrophoretic separation, but the need to create a spatially non-uniform field is still evident. As discussed in Section 3.2, dielectrophoresis depends on a wide range of properties in both the medium and the particle. Due to differences in physical and chemical properties, one of two phenomenological DEP effects first explained by H.A. Pohl<sup>41</sup> are usually observed: positive DEP and negative DEP. These phenomena are discussed in the next two subsections in concert with a discussion on classical dielectrophoresis (AC-DEP) and the newly explored direct current dielectrophoresis (DC-DEP). In this research project, both AC and DC dielectrophoresis has been applied to achieve red blood cell sorting by human ABO blood type.

#### 3.3.1 Alternating Current Dielectrophoresis (AC-DEP)

This is the classical DEP technique employing AC voltages and frequency to manipulate particles of interest. Embedded microelectrodes positioned in a spatially non-



uniform manner are employed to achieve particle separation, trapping, and focusing by applying AC electric fields in the range from 1 kHz into the GHz range<sup>22</sup>. The use of high frequency (>100 kHz) AC field has some advantages: 1) no electrophoretic movement is observed due to the cell membrane being statically charged and 2) electrochemical reactions such as those producing gas (i.e. bubble generation) are reduced<sup>22</sup>. When a microparticle is suspended in a highly conductive medium, the particles experience less polarization compared to the medium. In such cases, the particles / cells exhibit negative dielectrophoresis (nDEP), wherein the particles move away from the high field density regions. In case of positive dielectrophoresis (pDEP), the particles are attracted towards the high field density regions by a translational force due to the polarizability of the particles being greater than that of the medium<sup>1,111</sup>. The transition between negative DEP and positive DEP as one moves up in AC frequency is known as the cross-over frequency. At this frequency the force experienced by the particle is zero<sup>84</sup>. Cross-over frequency is dependent on particle dielectric properties and medium properties. It is different for each particle or cell; this information can be used to optimize trapping or separation schemes. Some complex cells exhibit multiple cross-over frequencies. Most of biomolecules exhibit nDEP but mixed responses might also be possible due to the complex make up of their structure, composition and charge distribution<sup>102,112</sup>. Figure 3.2 cartoons nDEP and pDEP directional motion the particle experiences when subjected to a spatially differing AC electric field.

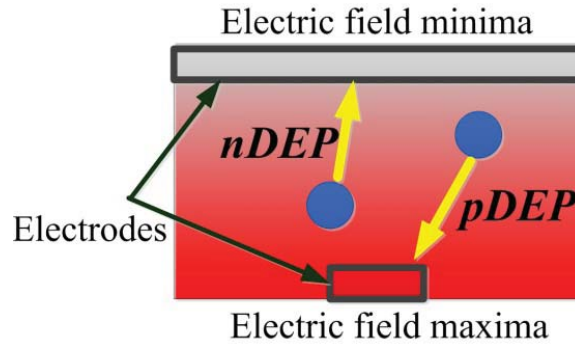


Figure 3.2 Demonstration of AC-DEP where dark red represents the region of high electric field density and grey represents regions of lower electric field density.

A detailed discussion on the theory and equations describing AC dielectrophoresis is in the Chapter 5.

### 3.3.2 Direct Current Dielectrophoresis (DC-DEP)

Direct current dielectrophoresis is a novel technique developed in the last decade. It employs insulating objects or hurdles fabricated by a variety of microfabrication methods within the channel to create spatial field non-uniformities<sup>81,113</sup>. It is also known as insulator based dielectrophoresis (iDEP) or electrodeless dielectrophoresis (eDEP) because electrodes are placed far outside the channel in inlet and outlet ports. The electrodes are immersed in the supporting media, but are not in direct contact with the particles being observed. This is a huge advantage over the traditional AC dielectrophoretic technique. In DC-iDEP, there is no frequency dependency involved so spatial electric field non-uniformities are solely responsible for the DEP forces experienced by the polarizable particles. The force exerted on the particle impels the particle to move away from the insulating obstacle region thus undergoing nDEP phenomena. In case of pDEP, the particles get trapped at sharp points or constrictions in the insulating region, which is the region of high field maxima in DC-iDEP devices<sup>114</sup>. A

particle in the insulating obstacle region experiences dielectrophoretic and electroosmotic forces; the relative magnitude of each determines whether the particle is trapped or flows through the constriction in a specific fluid flow streamline. The details about this will be provided in Chapter 6. Figure 3.3 demonstrates the phenomena of DC-iDEP where dark red represents the region of high electric field density and green represents regions of lower electric field density.

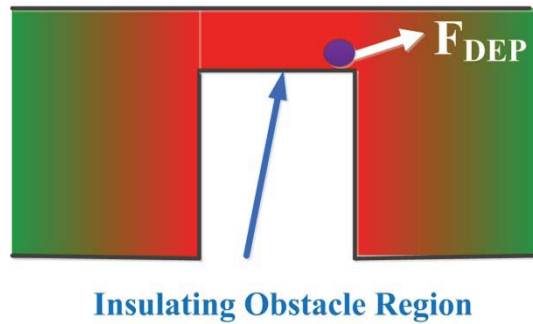


Figure 3.3 DC-iDEP phenomena on a particle at the insulating obstacle region in a microdevice.

Another manipulation technique which evolved from DC-iDEP is the use of both AC and DC fields in the insulating obstacle geometry to achieve trapping. By using both AC and DC signals, high voltage DC amplitudes could be reduced and replaced by low AC frequencies on the order of <100 kHz thus reducing the potential problem of Joule heating and sample degradation<sup>115</sup>.

Insulating obstacles of varying geometry are reported in the literature. Some of the common geometries are insulating posts<sup>113,116</sup>, rectangle<sup>81,117-118</sup>, spiral<sup>119</sup>, triangle<sup>118</sup>, oil droplet<sup>120</sup>, saw tooth channel<sup>121</sup>, and serpentine microchannel<sup>122-123</sup>. A variety of particles have been trapped and sorted with these geometries. Some of them are live vs. dead cells<sup>112</sup>, microbes in water<sup>124</sup>, yeast cells, bacteria<sup>125</sup>, protein<sup>126</sup>, DNA<sup>127</sup>, virus<sup>116</sup>,

and inert microspheres<sup>117,120</sup>. DC-iDEP techniques are advantageous compared to AC DEP separation which is discussed in Chapter 6. It is a very nascent technique and has the potential to improve the cell manipulation efficiency.

There is no complete picture available on the different DC-iDEP channel geometry, performance characterization of these devices and influence of particle, medium properties on DC-iDEP trapping or separation of bioparticles.

### **3.4 Manipulation of particles by dielectrophoresis**

Dielectrophoresis is a non-destructive and non-invasive technique that has the ability to manipulate very small bioparticles in the nano meter size like virus and DNA<sup>80</sup>. This field has seen considerable advancement from the 1960's and is now a popular and successful technique for manipulating and characterizing bioparticles. Electrophoresis and dielectrophoresis are the only two techniques which allow manipulation of nano meter sized particles as they are able to analyze dielectric properties in that range. In this section, a brief overview of the bioparticles manipulated by dielectrophoresis by researchers worldwide will be presented. Our research has focused on manipulating human red blood cells to carefully track the antigen expression dependencies via both AC and DC dielectrophoretic techniques.

- DNA: It is the hereditary or genetic material present in almost all organisms. This double helix structure is a natural polymer having long repeating units of nucleotides. Conventional methods for DNA separation involve filtering the sample like serum, extracting DNA from cell, centrifuging and finally adsorption. These techniques are not economical due to time, labor involved, special equipments, sample amounts and cost.

DEP and EP can increase the detection and separation efficiency. Another technique explored by researchers in the past is the capillary electrophoresis (CE). Since DNA is uniformly charged, it has a constant mass to charge ratio, which makes segments of different lengths easy to recognize because they have different mobilities. So using CE for concentration of DNA is not suitable as CE separates based on this charge to mass ratio. However, DEP can achieve concentration of similar DNA strands. Some of the research groups who have studied DNA separation and concentration by both AC-DEP and DC-iDEP techniques are Chou *et al.*<sup>128</sup>, Lapizco *et al.*<sup>127</sup>, Morgan *et al.*<sup>129</sup>, Washizu *et al.*<sup>130</sup>, and Parikesit *et al.*<sup>131</sup>.

- Proteins: Protein separation has been a challenge for many researchers in the past. Conventional methods for protein manipulation include 2D gel electrophoresis. Fewer researchers have explored manipulating proteins, but some groups explored DEP as a technique since it is non-destructive and does not denature proteins. Some of the researchers who have explored protein manipulation are Morgan *et al.* (manipulation of protein avidin by employing polynomial electrodes)<sup>80</sup>, Washizu *et al.* (manipulation of avidin, concanavalin, chymotrypsinogen and ribonucleaseA employing a set of corrugated electrodes and AC electric field; fractionating a mixture of DNA and protein by a combination of dielectrophoresis and field-flow)<sup>84,130</sup>, Lapizco *et al.* (manipulation of bovine serum albumin (BSA) using DC dielectrophoresis by employing insulating posts)<sup>126</sup> and Klenerman *et al.* (manipulation of yellow

fluorescent protein G and IgG)<sup>80,98</sup>. Other gradient techniques explored for manipulating proteins are EFGF, DFGF<sup>101</sup> and TGF (chiral separations of amino acids- aspartic acid, glutamic acid, glycine, alanine, serine, valine, and 2-aminoisobutyric acid)<sup>98-99</sup> as discussed in Section 3.2.

- Pathogens: Pathogens refer to virus, bacteria, and spores that are harmful to living organisms. Detecting them is important especially in areas involving environment and terrorism. Manipulating pathogens by dielectrophoresis has advanced in the past decade<sup>98</sup>. Dielectrophoresis has been used in viability studies<sup>112,132-133</sup>, detecting pathogens in environment<sup>124,134</sup>, separating pathogens from other particles<sup>113,118,135</sup>, and focusing of pathogens<sup>102,125</sup>. Research has been involved to understand dielectrophoresis on pathogens or single cell manipulation.
- Polymeric particles: Extensive research has been done in the area of inert particles as a method to explore dielectrophoretic phenomena<sup>81-82,104,115,117,123,135-139</sup>. Fluorescently tagged micro and nano particles, different size microspheres, and latex beads are used because they are cheap, readily available, predictable dielectrics with relatively inert chemical properties and uniform size / shape. Usually, when building a microfluidic system, researchers test the system first with polymeric particles, similar to the research presented in Chapter 7 of this dissertation which was a precursor to exploring DC-iDEP phenomena in blood typing.
- Mammalian cells: Dielectrophoretic approaches show strong potential in manipulating mammalian cells for medical diagnostic purposes. Separating diseased from healthy cells<sup>111,118,140-141</sup>, red blood cell from

plasma<sup>142</sup>, separating blood cells by (genotype) type<sup>1,88</sup>, cell viability studies, concentrating or trapping of cells, and size based sorting are studies already conducted<sup>81,140,143-146</sup>. Mammalian cells are complex in their composition and most of them experience nDEP over 1-100 kHz frequency range with crossover frequencies in the 100 kHz-100 MHz range<sup>147</sup>.

Dielectrophoretic techniques can also be applied in the manipulation of stem cells<sup>147</sup>. Stem cells are distinguished by their ability to selectively differentiate into specific cells needed by the body (immature cells). Hematopoietic stem cells are present in peripheral blood or bone marrow and no cell manipulation like antibody binding is required to sample them<sup>147</sup>. Pethig *et al.* group were the first to analyze manipulation of CD34+ cell subpopulation from bone marrow and peripheral blood stem cells using dielectrophoresis<sup>148</sup>. It is still an unexplored technique and has the potential to be applied to regenerative medicine<sup>147</sup>.

In order to manipulate cells by dielectrophoresis, knowing the cell's physiological characteristics including phenotype and genotype as well as the dielectric properties are important. The next section, briefly discusses the dielectric properties of the cell and what factors are most important when manipulating them.

### **3.4.1 Dielectric properties of cells**

Cells exhibit different dielectric properties based on the electric field they are exposed. Dielectric properties of the cell provide important information about structure, pathological status, metabolic mechanisms and functions due to dielectric properties dependence on frequency<sup>149-150</sup>. Membrane conductivity of a viable cell is about  $10^{-7}$  S/m

but the interior of the cell has very high conductivity ( $\sim 1 \text{ S/m}$ )<sup>15</sup>. A non-viable cell loses cytosol conductivity because ion pumps shut down and the membrane becomes permeable. Even small changes in membrane dielectric properties can be easily distinguished by applying DEP fields. The difference in dielectric properties of cells are due to various factors: membrane conductivity, morphology, cell size, internal cytosol conductivity, and charges on the cell wall<sup>89</sup>. Cells are frequently compared to an RC circuit (resistor-capacitor circuit) due to the membrane's insulative properties (resistance) and the cytosol's storage properties (capacitance)<sup>151</sup>. The cell membrane acts like a capacitor compared to a thin dielectric between two conductors (blood plasma and inside cell constituents)<sup>147</sup>. The membrane's ability to hold charges inside the cell like a capacitor is dependent on membrane composition, which dynamically responds when subjected to an electric field by selectively releasing charges and concentrating others at the membrane surface<sup>151</sup>. By exploiting this property, DEP can be used to separate different bioparticles like cells, virus, bacteria, yeast cells, human mammalian cells, cancerous cells, etc. since DEP depends on polarizability of the cell.

Dielectric properties of a cell could be quantified by a technique called dielectric spectroscopy (DS) developed seventy five years ago<sup>149,152</sup>. DS, a non-invasive technique, involves measurement of impedance by applying an AC signal<sup>153</sup>. DS can be applied to wide range of areas involving medicine, drug development, food production, polymers, and cryobiology<sup>149</sup>. It has been used to study plasma membrane properties of a living cell, protein activity, mammalian, and bacterial cells dielectric properties. This technique requires expensive and complex equipment due to the frequency ranges involved,  $10^{-5}$ - $10^{12}$  Hz, and many of the frequency ranges still remains unexplored due to the unavailability of ranges to work with. In the low frequency range, electrode polarization



occurs thus limiting the range of frequency available<sup>149</sup>. Low electrode polarization is the key to quantify the response of the cells, which can be achieved by suspending the cells in a low ionic strength buffer. Apart from all these challenges, recent advancement in the field of dielectric spectroscopy by developing new methods based on DS (time domain DS and broadband DS) has allowed to manipulate particles at macro, micro and meso levels<sup>149</sup>. To analyze the dielectric properties of cells in suspension, two mathematical models have been widely used, single shell and double shell models for spherical particles. The single shell model is based on a conducting sphere enclosed in a thin shell that is less conductive than the inner sphere. The double shell model is based on a smaller shell enclosing a sphere and enclosing both smaller shell and sphere is the bigger sphere. DS has also been applied to study dielectric properties of blood, especially erythrocytes. Erythrocytes are complex in shape and in order to apply the single shell model, they had to be made spherical by applying low osmotic pressure<sup>149-150,154</sup>. Apart from erythrocytes, yeast cells have also been studied by this single shell model<sup>155</sup>. Single cell analysis has also been accomplished using varied methods of dielectric spectroscopy like parallel plate capacitor (for larger particles  $>100 \mu\text{m}$ ), dielectrophoresis and electro-rotation ( $<10 \mu\text{m}$  particles)<sup>155</sup>.

In this research study dielectrophoretic technique to manipulate red blood cells by employing both AC and DC signals is explored.

### 3.5 Summary

Dielectrophoresis has great potential to be applied as a tool in the medical diagnostic field. Its ability to discriminate cell viability, isolate cells with minimum harm, detect morphology changes in the membrane of the cell, high separation efficiency of

specific type with no external treatment like fluorescent tagging, separate diseased from normal cells, and separate rare cancerous cell from a population of healthy cells has made it a promising tool to be applied to environmental, biological, biomedical and clinical applications.

In this chapter, a detailed review of dielectrophoresis is provided including its versatility by varying electrode geometry or varying electrical signal. Further, a literature survey of the particles manipulated by DEP was presented. The theory behind AC and DC dielectrophoresis was briefly discussed here, but will be dealt with in detail in Chapters 5 and 6. In this research, the dielectric properties of red blood cells including the physiological and chemical make-up, membrane properties, and antigen expressions are applied to sort red blood cells according to ABO types *via* both AC and DC dielectrophoresis.

## CHAPTER IV

### HUMAN BLOOD SYSTEM

#### 4.1 Introduction

Blood is an important and conveniently attained body fluid indicative of systemic health and body chemistry that is often used in medicine and research. This chapter presents some of the basic facts about blood, composition of blood and provides specific details about red blood cells in particular as these are the cells of prime interest in this research. There are also some challenges associated with sample preparation involving blood and this is discussed in brief. In this research, red blood cell responses are tracked based on their ABO blood type, so knowing about blood typing is of prime importance. A brief discussion about ABO blood types and other classification of blood types is also introduced here. In this chapter the terminology extensively used for red blood cells is RBC or erythrocytes and for white blood cells it is leukocytes or WBC.

#### 4.2 Blood

Blood, a specialized body fluid comprises about 8% of body weight and greater than five liters in an average human body has a plethora of information related to the functioning of the body; in other words, it is an indicator on the equilibrium of the entire body system<sup>7,156</sup>. Blood is viscous compared to water. It varies with the hematocrit value and generally the relative viscosity is 3-4 times that of water, but plasma's relative viscosity is about 1.8 times that of water. pH is between 7.35 and 7.45, and temperature of blood is slightly greater than that of the human body (100.4 °F). Blood alters its

function according to the body's needs by supplying immune cells in response to infection, tuning electrolyte composition in response to tissue equilibriums, increasing O<sub>2</sub> content as it passes through the lungs and flowing faster via heart pumping when the body is physically straining (exercise). Blood is referred to as "red gold" because it carries precious cells and proteins<sup>156</sup> and there exists no substitute for this unique fluid. Blood is essential in regulating body temperature and pH, coagulation and wound healing, and it also functions as a messenger between all of the body's systems (skeletal, nervous, chemical)<sup>7</sup>.

Some random facts about blood on the medical side is that blood is needed by someone every 2 s; blood transfusions are required by 4.5 million patients every year; and up to three lives can be saved by a single pint of blood<sup>157</sup>. Oxygen and nutrients are delivered by blood to the cells and waste products are collected from cells. The heart pumps the blood through two closed loops in humans, one to the lungs and the second which circulates through blood vessels to the tissues in the body. The concept of circulation was discovered by William Harvey in the 16<sup>th</sup> century<sup>7</sup>. Blood is a non-Newtonian fluid and thus it can flow effectively in tiny capillaries with less resistance.

Currently, analysis and sampling of blood are used to detect diseases and blood is extensively used for medical diagnostics. Due to the recent technological advancements, miniaturized device have shown great potential towards this application. In the following subsections, a brief overview on blood constituents and some challenges in blood sample preparation will be discussed.

#### 4.2.1 Composition of blood

The two main components of blood are the plasma and cells. Figure 4.1 represents the composition of whole blood in detail.

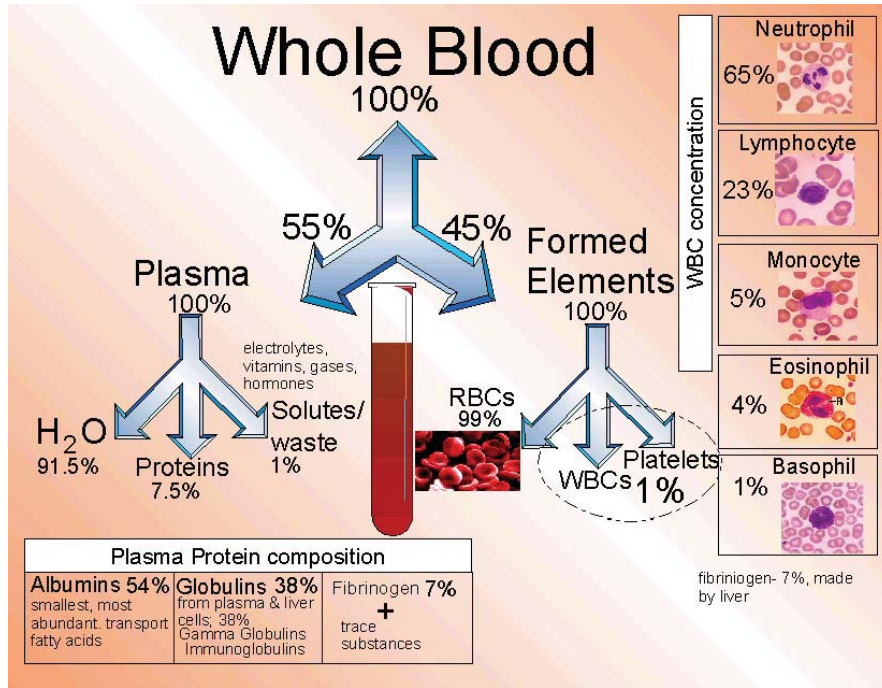


Figure 4.1 Composition of whole blood<sup>158</sup> [Reprinted with permission from Scott Potter]. [Copyright 2009].

Plasma accounts for 55% of blood and is pale yellow in color. It is mainly water but proteins, serum albumin, blood clotting factors, electrolytes and immunoglobulin are also present<sup>156</sup>. Frozen plasma has a life of about one year<sup>157</sup>. The cells comprise the remaining 45% of the blood and are generated from the bone marrow, primarily as immature stem cells; they mature into erythrocytes (red blood cells) which comprise 99%, of the total cell volume, leukocytes (white blood cells) and platelets account to a total of 1% in the 45% cell volume. The volume percentage of cells to plasma is known as the hematocrit and is tracked to determine all types of anemia. Figure 4.2 describes the process of hematopoiesis in which all three blood cells develop from stem cells.

## Immune cell development: Hematopoiesis

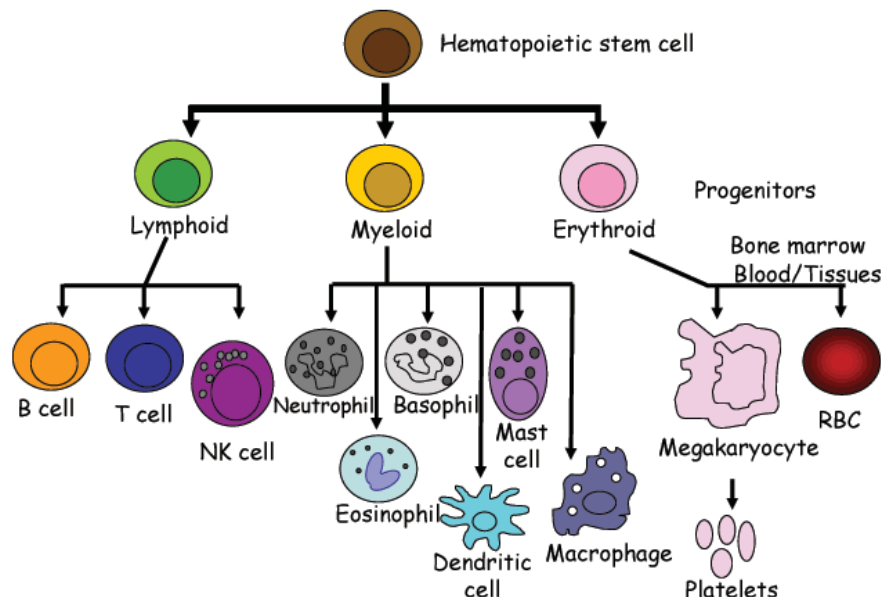


Figure 4.2 Process of the blood cell production in the body from immature stem cells in the bone marrow<sup>159</sup> [permission provided for educational purpose].

When whole blood is centrifuged or left to stand for several hours, it separates into three distinct layers: topmost layer being the straw colored fluid plasma (>50%), sandwiched layer represents the mixture of white blood cells and platelets (~1%) and the bottom most layer are the red blood cells (~45%). The measured packed cell volume of red blood cells (erythrocytes) is called hematocrit<sup>156</sup> and usually varies between 38% and 45% as suggested above. Anticoagulant, usually K<sub>2</sub>EDTA is added to the whole blood to prevent from coagulation.

Erythrocytes will be discussed in greater detail in Section 4.2.3. Leukocytes include all lymphoid and myeloid cell derivatives as shown in Figure 4.2 and are part of the immune system and between 4 and 11 thousand white blood cells per  $\mu\text{L}$  of whole blood are available in a healthy human body. They constitute approximately 1% of whole blood and are present in five diverse types: Neutrophil, Basophil, Eosinophil, lymphocytes and monocytes of varying diameter (10-15  $\mu\text{m}$ )<sup>7</sup>. The most common

lymphocytes are B and T cells. Monocytes become dendrite cells or macrophages. The most abundant of leukocytes are the neutrophils which kill the disease causing bacteria<sup>160</sup>. Eosinophils act on parasitic infections in the body and they are cytotoxic usually present in very low numbers. Basophils act when the body part has an infection by releasing mediators like histamine and serotonin<sup>160</sup>. Lifetimes of these cells in circulation vary between hours to years depending on the type of white blood cell. If WBC are present in low quantity, the person is at risk for more infections and diseases depending on the type of WBC low in number<sup>156</sup>. WBCs are either single round nucleus or multilobed nuclei. Platelets or thrombocytes are small irregularly shaped cell fragments of megakaryocytes cells in bone marrow and are about 2-3  $\mu\text{m}$  diameter with no nucleus. Platelets help in blood clotting at the site of an injury or in response to cancerous cells and can be stored for about five days for medical purposes. Excessive platelets cause thrombocythemia (blood clots) obstructing the flow of blood in capillaries and blood vessels, whereas low numbers cause excessive bleeding (thrombocytopenia)<sup>156</sup>. Figure 4.3 shows an SEM image of all the three cells in blood.

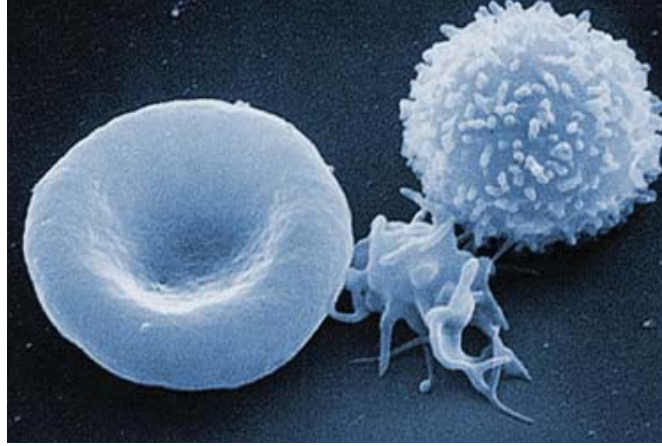


Figure 4.3 SEM image of all the three cells (RBC, WBC and platelets) in human blood [Reprinted from ABC Science, Australia]<sup>161</sup>[Permission provided for educational purposes].

To extract information from a complex and sophisticated system like blood is challenging. The information to be extracted remains cell specific and as a result, the cells must be separated from the rest of the unnecessary material available in the blood. In the next section, an overview of some challenges associate with sampling and analysis is presented.

#### 4.2.2 Erythrocytes

Erythrocytes or red blood cells are abundant in blood. They comprise about 45% of blood volume in a healthy adult. Higher or lower values of hematocrit can be causes for concern. The condition associated with lower hematocrit is known as anemia and in severe cases can lead to hemorrhages. In cases of excess hematocrit, the condition is called Polycythemia Vera where surplus amount of RBC's are produced in the bone marrow. This causes increased production of erythropoietin by the thus leading to pulmonary disorders like chronic obstructive pulmonary disease (COPD).

RBCs transport oxygen and nutrients to the tissues and organs in the body. RBC contains an important and vital protein called hemoglobin that contains a heme group



with four iron atoms which bind and transport oxygen. Hemoglobin imparts red color to the blood. Decrease in hemoglobin levels in blood causes anemia. RBCs do not contain a nucleus thus enabling the storage of hemoglobin as well as greater flexibility. It is biconcave in shape making it flexible enough to pass through small capillaries, especially in brain where the largest capillary is about 2  $\mu\text{m}$  in diameter. Erythrocytes range from 6 to 8  $\mu\text{m}$  in diameter and 2  $\mu\text{m}$  in width<sup>1</sup>. A single microliter of blood contains an average of 4 to 6 million cells. They are produced in the bone marrow by a process called erythropoiesis at a rate of 2 million/s. Their average maturation time is 7 days and life span in circulation is about 120 days<sup>1</sup>. The dead or old erythrocytes are removed by the spleen and liver with the help of specialized cells called macrophages<sup>156</sup>. Red blood cells have a net negative charge on their surface based on their linear electrophoretic behavior<sup>1</sup>. However, these surface charges deteriorate if the blood sample is stored for greater than six days; cell rigidity also decreases over this time-span<sup>1</sup>. In our research, blood is only tested within 24 h of donation to avoid these effects.

Many blood diseases developed due to imbalances in the red blood cell composition or structures. Some examples are: Anemia, hemolysis, polycythemia, and inherited and genetic diseases (sickle cell anemia, hereditary spherocytosis). Recently, scientists from a company (Advanced Cell Technology) in Worcester, MA reported a technique of growing red blood cells in the lab from embryonic stem cells. They claim that there will not be any shortage of blood cells in the future<sup>162</sup>.

The membrane of an erythrocyte is made up of proteins and lipids (cholesterol and phospholipids). Figure 4.4 shows images of the biconcave erythrocyte and the cell membrane.

Membrane proteins present in the red blood cell membrane are distinguished based on their functions: transport, cell adhesion, and structure maintenance. The proteins on the membrane are attached covalently to the lipids in the bilayer or the polypeptide chains pass through the lipid bilayer (transmembrane proteins)<sup>160</sup>. The proteins attached to the lipid bilayer are hydrophobic amino acids arranged in alpha helix pattern. The transmembrane protein projected out from the bilayer is hydrophilic amino acids, usually glycoproteins. Other proteins present on the membrane are loosely attached to the protruding transmembrane proteins are peripheral membrane proteins<sup>160</sup>. The maintenance of asymmetric phospholipids distribution in the membrane is very important for smooth functioning of the cell<sup>156</sup>. The cell membrane is also host to millions of antigens and many still remain unexplored. In the next section, a detail discussion of membrane antigens and how select ones determine blood type is explained.

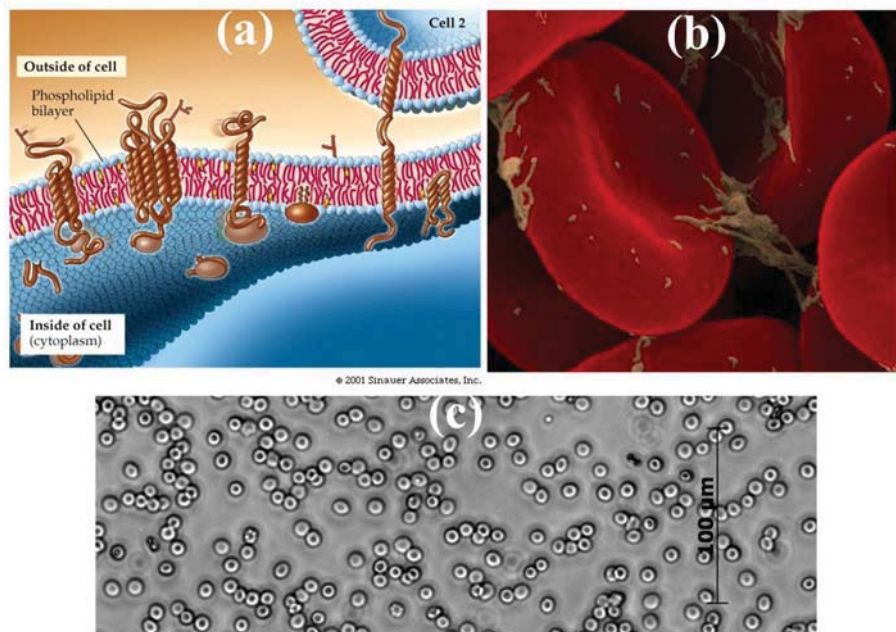


Figure 4.4 (a) Detailed view of a red blood cell membrane<sup>163</sup> [permission provided for educational purposes], (b) SEM close-up view of red blood cell, and (c) 16X microscope image of red blood cells.

### 4.2.3 Challenges in blood sample preparation

As discussed in Section 4.2.1, a plethora of information is hidden in blood.

Conventional technologies like flow cytometry are often used in macro scale diagnostics<sup>148</sup>. To extract information from the blood, a number of steps are involved<sup>7</sup>:

- identifying the pertinent target cells in the blood with the necessary information,
- separating the target cells from other irrelevant matter in the blood. This can be carried out by mechanical means (centrifugation separates based on density differences), molecular affinity schemes or by developing functional assays,
- after separation, detecting scientific and clinical information from the target cell is of utmost importance, and
- finally, only certain techniques are amenable to point of care diagnostics like dielectrophoresis or personalized drug treatments.

If white blood cells are the target of information, for each WBC there are more than 1000 RBC's. WBCs are also extremely diverse due to different types, extracting information from the required WBC and separating the target WBC at a high purity is very challenging. Some cells in the blood are very sensitive to handling (centrifugation) and this may modify the original composition of the cell thus affecting further analysis of identifying the target cells<sup>164</sup>.

Due to these challenges in blood cell analysis, a more gentle and precise control of manipulation / separation techniques is necessary. Microfluidics offers a great platform for handling individual cells of interest minimizing the risk of modifying the original composition of cells<sup>7</sup> by electrical, chemical, optical or mechanical techniques. One such

electrical technique that makes use of low amplitude electric fields is dielectrophoresis, which depends on polarizability of cells as discussed in Chapter 5. Mammalian cells readily polarize when electric field is applied without damaging the physiological composition of cells to a large extent<sup>7</sup>. Dielectrophoresis is established as a novel and gentle technique to control cells and extract information from them<sup>7</sup>. Dielectrophoresis has the ability to sort a single cell in a huge population of unwanted cells<sup>7</sup>. An excellent review article about the various techniques has been published by Toner *et al.* group<sup>7</sup>. In the research presented here, one such microfluidic platform is developed to manipulate red blood cells via applications of AC and DC electric field-based dielectrophoresis. In the next section, a more detailed discussion on erythrocytes, its properties and functions are presented.

### 4.3 Blood typing

Blood typing represents the classification of blood cells based on the antigens present or absent on and through the membrane of cell. Antigens are also referred to as cell markers which react to the immune system of the body. Antigens may be proteins, glycoproteins, carbohydrates, or glycolipids, all of which play a prime role in deciding blood type in humans. A blood group system is based on antigens inherited from an allele (one among a series of genetic locus)<sup>159</sup>. Blood type is inherited from both parents such that the mother and fetus may carry incompatible blood types. In such cases, the mother's body releases antibodies (IgG) that fight against the fetal RBC's and might cause hemolysis of fetus RBC's ranging from mild to severe<sup>159</sup>. Blood types do not change during a person's lifetime, but might change when the person experiences certain severe autoimmune disorders, infections or malignancies. Figure 4.5 shows wide range of

antigens either attached to the red blood cell membrane or traversing the membrane. The cell membrane contains three different proteins carrying antigens of specific blood groups: multi-pass proteins, single-pass proteins and glycosylphosphatidylinositol (GPI)-linked proteins<sup>156</sup>. The scope of this research study is limited to ABO and Rh system. Rh system carries transmembrane proteins in them and ABO antigens are carbohydrates attached to glycoproteins and thus on to lipid bilayer.

Currently there are thirty blood typing systems recognized by International Society of Blood Transfusion (ISBT)<sup>165</sup>. Among them the ABO blood typing system is the most common classification, and will be discussed in detail in the next section.

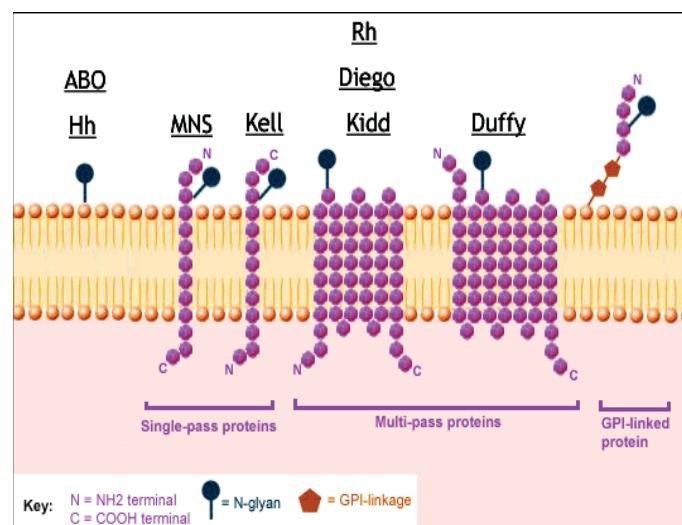


Figure 4.5 Schematic of red blood cell membrane with blood group antigens fixed on it<sup>156</sup> [permission provided for educational purposes].

#### 4.3.1 ABO blood typing system

The main two blood groups in the human body that are of prime importance in determining compatible blood transfusions are the ABO and Rh<sup>156</sup>. ABO blood typing system is one among 30 discovered by Karl Landsteiner in 1901 for which he was later

awarded the Nobel Prize in 1930<sup>1,166</sup>. ABO blood antigens also exist in apes including gorillas and chimpanzees. Two antigens (A and B) and two antibodies (anti-A and anti-B) are responsible for deciding the blood type. The presence or absence of an Rh antigen designate the + or – in the blood type. Rh antigens carry the transmembrane proteins<sup>156</sup>. A and B antigens are long chains of oligosaccharides attached to the membrane's lipid bilayer. O blood lacks both A and B antigens, but O blood cells still express the H-antigen backbone. All three antigens have H-glycoconjugate preceding them<sup>1</sup>. Figure 4.6 shows the structure of all the three antigens. All the three have the same backbone and they differ only in the last molecule of the chain.

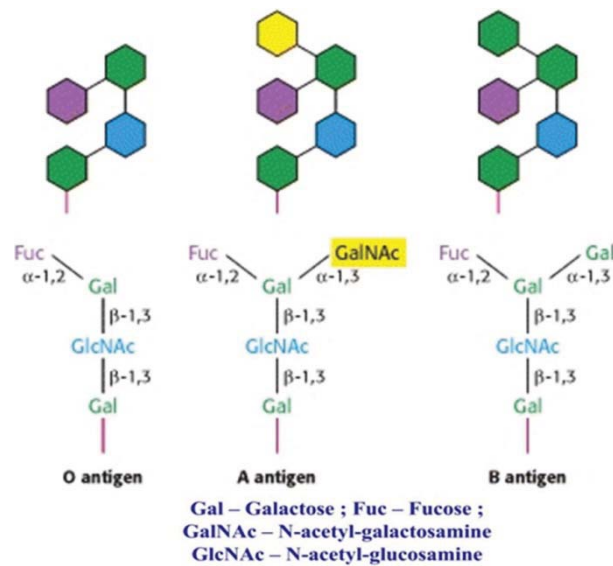


Figure 4.6 A, B and O antigen structure in the ABO blood typing system<sup>167</sup> [permission provided for educational purposes].

Antigens and antibodies are both integral to a blood type. Usually, a person must be exposed to an antigen in order to manufacture an antibody against it, but this is not the case with A and B antibodies which are genetically coded. For example, in type O blood, both A and B antigens are absent, but both A and B antibodies are present in the

surrounding plasma. In AB type blood, both antigens are present on the erythrocytes, whereas both antibodies are absent from the plasma. The implications of this on transfusions is that a type O person is a universal donor for all blood types, but can only accept other O blood, while type AB blood is a universal acceptor, but can only donate to another AB person. The absence of an antigen becomes a very important factor in blood transfusion to avoid agglutination of the blood transfused<sup>1</sup>. A type blood has B antibodies, and B type has A antibodies in the serum. If the transfusion is incompatible, the antibodies attack the antigen and blood coagulates. While this is matter of concern during blood transfusion, this attribute becomes useful when performing laboratory blood typing test. Figure 4.7 presents the combination of ABO blood types (A, B, AB and O) along with antigens and antibodies present in each blood type<sup>159</sup>.

**The ABO Blood System**








Blood Type (genotype)	Type A (AA, AO)	Type B (BB, BO)	Type AB (AB)	Type O (OO)
Red Blood Cell Surface Proteins (phenotype)	 A agglutinogens only	 B agglutinogens only	 A and B agglutinogens	 No agglutinogens
Plasma Antibodies (phenotype)	 b agglutinin only	 a agglutinin only	NONE No agglutinin	 a and b agglutinin

Figure 4.7 ABO blood typing system with antigens and antibodies representing A, B, AB and O groups<sup>159</sup> [permission provided for educational purposes].

For compatibility, it is important to consider the Rh factor antigen. Those people without the Rh factor antigen can develop anti-Rh antibodies after exposure to the Rh

antigen. Since it is nearly impossible for doctor's to know if exposure has occurred, they track Rh factor expression for transfusion compatibilities. There are 8 blood types in the ABO-Rh blood typing system: A+, B+, O+, AB+, A-, B-, O-, and AB-. As mentioned, type AB is the universal acceptor and Type O the universal donor. When Rh factor is considered, O- is the universal donor and AB+ is the universal acceptor. In this research study, all 8 red blood cell types are explored via dielectrophoresis as a function of antigen expression. Blood types vary according to population demographics worldwide. Some rare blood types are more prominent in certain races or nationalities. For example, in Korean population A and B are most prevalent with about 32% in each and about 10% are AB blood type with O representing the remaining population<sup>168</sup>. Comparing this with Native Americans, 16% of them are A, 4% are B, 79% are O and remaining population are type AB. The most commonly found blood type is O+ and rarest is AB- blood type. Figure 4.8 shows the distribution of all blood types in the ABO blood typing system in U.S.

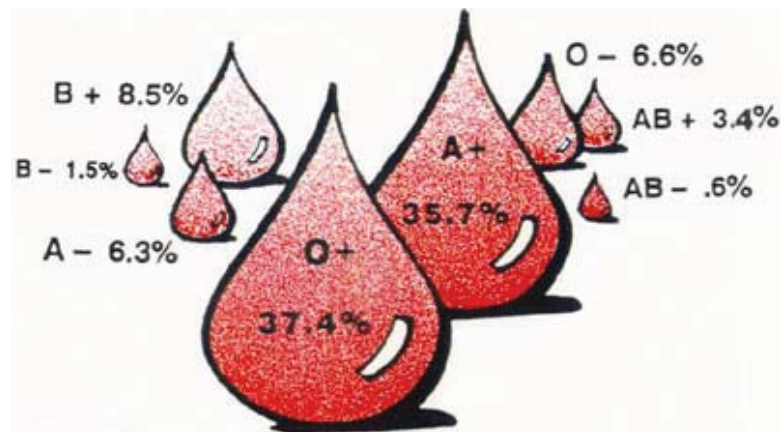


Figure 4.8 Blood type distribution in U.S. [Image adapted from Stanford Medical center]<sup>169</sup>.



Blood typing is accomplished most commonly using agglutination techniques. The premise of this is founded directly upon the antigen / antibody interactions. ABO blood typing tests are currently conducted in three steps<sup>43</sup>:

- i. Whole blood is suspended in two wells containing anti-A and anti-B antibodies. If coagulation occurs in any of the wells, then the blood reacted with one of the antibodies and it is type A or B. If it coagulates in both wells then it is type AB; if the blood doesn't coagulate in any, then it is type O,
- ii. second step is the back typing method where is serum of the unknown blood is used to suspend in the blood that is known to be type A or type B. If the blood agglutinates when type B cells are added, then the unknown sample is type A; otherwise vice versa. If blood cells agglutinate with both cells then it is type O, otherwise it is type AB. This determines the blood type accurately, and
- iii. third step involves suspending the unknown sample of blood in anti-Rh serum. If the blood agglutinates it is Rh positive, if not it is negative.

This method might take from 30 min to a day depending on the medical center. It involves a lab technician and has to be monitored carefully to avoid false designations. This involves money, time, labor and proper facilities where blood typing could be performed. The advances in the field of lab-on-a-chip technology have the potential to improve reliability, reduce time, and increase convenience with this point of care (POC) type technology. In this research, our aim is to study ABO blood cell types using dielectrophoresis in a lab-on-a-chip platform for medical diagnostic applications.

#### 4.3.2 Other blood typing systems

Apart from ABO and Rh blood typing systems, there are 28 other blood typing systems currently recognized by International Society of Blood Transfusion ([ISBT](#))<sup>165</sup>. Some of the common blood typing systems are: The P System, The Kell System, The MNSs System, The Duffy System, and The Fisher System. Table 4.1<sup>165</sup> shows the chart of all the blood typing system recognized by ISBT<sup>165</sup>.

Table 4.1 Thirty blood typing systems classified by ISBT<sup>165</sup>.

CONVENTIONAL NAME	ISBT SYMBOL	ANTIGENS
ABO	ABO	4
MNSs	MNS	37
P	PI	1
Rh	RH	47
Lutheran	LU	18
Kell	KEL	21
Lewis	LE	3
Duffy	FY	6
Kidd	JK	3
Diego	DI	2
Cartwright	YT	2
Xg	XG	1
Scianna	SC	3
Dombrock	DO	5
Colton	CO	3
Landsteiner-Wiener	LW	3
Chido/Rogers	CH/RG	9
Hh	H	1
Kx	XK	1
Gerbich	GE	7
Cromer	CROMER	10
Knops	KN	5
Indian	IN	2
Ok	OK	--
Raph	RAPH	--
JMH	JMH	--
Cost	COST	2
Ii	I	2
Er	ER	2
P, P1, LKE	GLOBO	3
Lewis-like: Le-c, Le-d	--	2
Wright	WR	2
Low Prevalence	--	36
High Prevalence	--	11

#### 4.4 Summary

In this chapter a detailed discussion about blood, the cells, fluid, and molecules that comprise it as well as its use as a diagnostic fluid was presented. This research is focused on studying red blood cells' responses in a dielectric field as a function of their ABO blood type classification. The antigens and antibodies characterizing this blood

typing system were covered in depth in this chapter. Due to the time, money, reliability, and convenience involved in traditional blood typing techniques, a microfluidic platform which is cost effective, less time consuming, rapid, and accurate point of care diagnostic tool to type blood cells based on their antigen expression has been presented.

In the next chapter, manipulation of red blood cells *via* dielectrophoresis under AC electric field thus sorting the positive blood types (A+, B+, AB+ and O+) has been explored.

## CHAPTER V

### DIELECTROPHORETIC CHARACTERIZATION OF ERYTHROCYTES: POSITIVE ABO BLOOD TYPES

#### 5.1 Introduction

This chapter has been reproduced in its entirety from the *Electrophoresis* publication, volume 29 that was published in 2008<sup>1</sup>. In this chapter, dielectrophoretic manipulation of erythrocytes/red blood cells is investigated as a tool to identify blood type for medical diagnostic applications. Positive blood types of the ABO typing system (A+, B+, AB+ and O+) were tested and cell responses quantified. The dielectrophoretic response of each blood type was observed in a platinum electrode microdevice; delivering a field of 0.025Vpp/mm at 1 MHz. Responses were recorded via video microscopy for 120 s and erythrocyte positions were tabulated at 20–30 s intervals. Both vertical and horizontal motions of erythrocytes were quantified via image object recognition, object tracking in MATLAB, binning into appropriate electric field contoured regions (wedges) and statistical analysis. Cells of O+ type showed relatively attenuated response to the dielectrophoretic field and were distinguished with greater than 95% confidence from all the other three blood types. AB+ cell responses differed from A+ and B+ blood types likely because AB+ erythrocytes express both the A and B glycoforms on their membrane. This research suggests that dielectrophoresis of untreated

erythrocytes beyond simple dilution depends on blood type and could be used in portable blood typing devices.

First a brief overview of some techniques used to manipulate of red blood cells have been discussed and more details could be found in Chapter 4. Theory of AC dielectrophoresis which uses embedded metal electrodes in the channel along with details about red blood cell properties has been presented. Section 5.4 deals with experimental part including material and methods, device fabrication, experimental conditions, image and data analysis. Results and discussion has been presented in Section 5.5 and the chapter wraps up with important take home conclusions derived from this research project.

## **5.2 Manipulation of red blood cells**

The rise of electrokinetics as a separation technique during the past decade has crafted new methods of analysis in medical applications. Dielectrophoresis (DEP), a subclass of electrokinetics, shows potential as a useful tool in developing inexpensive, easy-to-use medical microdevices capable of streamlining emergency medical diagnosis. Blood typing is a simple, yet life-essential diagnostic step preceding blood transfusion in major emergency medical situations. The antigens on the surface of donor blood must match the receiver's blood type or adverse immune responses can cause death in the recipient. The conventional serological methods for blood grouping used are the direct hemagglutination, antigen–antibody combined methods consisting of absorption, absorption elution, absorption inhibition and some other modified method along with histochemical methods<sup>170</sup>. Some methods available include using spectrophotometry to sort blood types, which utilizes antibody induced changes in the UV/visible spectra of

blood<sup>171</sup>. Advantages of using spectrophotometric method are: blood samples having abnormal spectra can be flagged and targeted for further analysis with no centrifugation required<sup>171</sup>. Magnetophoresis can also be a possibility for separating cells such as infected malarial from healthy erythrocytes. One of the advantages of using this technique is that it allows following mobility of hundreds of single cells in a relatively short period of time<sup>172</sup>. Portability of the power source and cell mobility can be less ideal than for a dielectrophoretic system. However, many blood typing technologies require time, a clinical environment, antibody assays for each blood type; such medical technological methodologies require skilled medical technicians and are not readily portable to emergency sites, which make the whole testing method more expensive and prone to false positives and negatives<sup>170-172</sup>. This research analyzes a novel technique of using DEP as a tool for distinguishing the positive blood types of the ABO system (A+, B+, AB+, O+). Dielectrophoretic characterizations in lab-on-a-chip devices are far more portable than current techniques. Microdevices have components on micrometer scales and are custom-made based on their specific application, ranging from microelectromechanical systems to DNA analysis and cellular testing<sup>173</sup>. The dielectrophoretic microdevice design used here was based on the prior microdevices fabricated for studying erythrocyte pearl chain formations with perpendicular platinum electrodes<sup>88</sup>. Several other designs have been studied for other applications including spiral arrangement of electrodes for cell separations<sup>140</sup>, interdigitated microarrays<sup>104</sup> and checkerboard arrangements of electrodes<sup>174</sup>. Analytical microdevices in various forms are being developed to make complicated multi-step biological analysis simpler<sup>175</sup>. Microdevices have the potential for sample analysis cost reduction and versatility in use<sup>176</sup>. Equipment used to perform medical tests, like a standard hematology panel of

hematocrits (erythrocytes, platelet and white blood cell counts), electrolyte balance, hemoglobin, etc., are expensive and range from \$55 to \$95<sup>177</sup>. Other tests like CD4, which test for HIV, rely on flow cytometers that can cost \$65000<sup>178</sup>. The fee for such blood tests outsourced to medical laboratories is about \$40 with medical costs rising annually<sup>178</sup>. In contrast, the cost of microdevices is minimal. As manufacturing of microdevices are scaled up, the price per device drops and is expected to cost less than \$3 each<sup>178</sup>. Once optimized, the reliability of data from microdevices is expected to exceed that of current medical laboratories. The use of the microdevices can be extended to diagnose chronic diseases like sickle cell anemia, which affects 1 in 500 African Americans (1 in 12 carry the sickle cell trait)<sup>179</sup>. Diagnosis of sickle cell anemia requires expensive medical kits ranging from \$69 to \$175 each along with the help of skilled medical technicians<sup>180</sup>. Medical microdevices have the potential to improve upon this by enabling point of care testing in less than 5 min, with only 1–3 drops of blood (~62  $\mu\text{L}$ ) while simultaneously eliminating human error. DEP is expected to play a major role in development of medical microdevices due to operational simplicity, lack of need for skilled medical technicians, small sample volumes and low voltage signals, all of which enable device portability.

### 5.3 Theory

DEP is a phenomenon, which results in movement of polarizable particles in non-uniform alternating current (AC) electric fields. The movement is due to a net force,  $\vec{F}_{DEP}$  resulting from transient polarization of particles<sup>41</sup> and the electric field<sup>181</sup>:

$$\vec{F}_{DEP} = 2\pi r^3 \varepsilon_m \alpha \nabla E^2 \quad (5.1)$$



The particle radius is ‘ $r$ ’, ‘ $\epsilon_m$ ’ is the medium permittivity, ‘ $\vec{E}$ ’ is the electric field strength, and ‘ $\alpha$ ’ is the real part of the Claussius-Mossotti factor, which is the effective polarizability of the particle relative to the suspending medium and is frequency dependent.

$$\alpha = \text{Re}[K(\omega)] \quad (5.2)$$

$$K(\omega) = \frac{\tilde{\epsilon}_p - \tilde{\epsilon}_m}{\tilde{\epsilon}_p + 2\tilde{\epsilon}_m} \quad (5.3)$$

$$\tilde{\epsilon} = \epsilon - \left( \frac{i\sigma}{\omega} \right) \quad (5.4)$$

where, ‘ $\tilde{\epsilon}$ ’ denotes complex permittivity and the subscript ‘ $p$ ’ refers to a lossless dielectric sphere particle suspended in a medium ‘ $m$ ’. The complex permittivity ‘ $\tilde{\epsilon}$ ’ is given by equation 5.4, which is a function of permittivity,  $\epsilon$ , medium electrical conductivity,  $\sigma$ , and the angular frequency,  $\omega$ <sup>41,181</sup>.

Equation 5.1 is a generalized equation for spherical, homogenous particles, but is only a precise relation of the dielectrophoretic force on erythrocytes because cells are non-homogenous complex biochemical entities with non-uniform distribution of insulating and conducting components. Analytical dielectric modeling has been done to interpret the movement of biological cells in electric fields using either sphere or ellipse as an approximation for their shapes, but remain approximations<sup>182</sup>. Further, it was shown that correct cell geometrical parameters are critical for understanding permittivity of cell suspensions<sup>183-185</sup>.

The transient polarization of particles results in their movement in the electric field that scales between two extremes depending on the exciting AC frequency. Herbert

Pohl, in his seminal text “*Dielectrophoresis: The behavior of neutral matter in nonuniform electric fields*” defined these two phenomenological extremes as positive dielectrophoresis and negative dielectrophoresis<sup>41</sup>. These two cases arise as a consequence of the polarizability of a uniform composition particle being greater or lesser than the polarizability of the medium in which it is suspended. If the real part of the effective polarizability,  $\text{Re}[\alpha]$  of the particle is greater than that of the medium, then the electric field lines pass through the particle causing a polarization which is slightly skewed due to the spatially varying electric field lines. A resultant force directs the particle to high field density regions and this observed movement is known as ‘positive dielectrophoresis’. If the effective polarizability,  $\text{Re}[\alpha]$  of the particle is less than that of the medium in which it is suspended, spatially non-uniform electric field lines divert around the outside of the particle causing ion depletion at the particle poles and subsequent polarization. The resulting force directs the particle to the low field density regions and this is termed ‘negative dielectrophoresis’<sup>41,186</sup>. This work examines these more complicated responses with a medically relevant system: erythrocytes expressing membrane antigens based on their blood type. These factors have been shown to influence the motion of the particles in a dielectrophoretic field.

Dielectrophoresis has been studied in detail by researchers over the past few years. In particular, the phenomenon was studied with regards to erythrocytes<sup>88</sup>; it was observed that A+ erythrocytes form pearl chains in a dielectrophoretic field. Dielectrophoresis is also studied to differentiate normal cells from leukemic cells<sup>186</sup>, metastatic breast cancer cells<sup>187</sup> and malarial cells<sup>188</sup>. Using a spiral electrode configuration, the dielectrophoretic movement of cells based on health was studied and malarial cells were separated from healthy cells<sup>140</sup>. Dielectrophoresis has also been used

to separate white blood cells from erythrocytes<sup>189</sup> and sample preparation for chip based hybridization assays in an integrated DNA or RNA system<sup>104</sup>. Furthermore, dielectrophoretic field flow fractionation was used to study differential analysis of human leukocytes<sup>144</sup>. However, systematic quantification as a function of blood type has not previously been performed.

### **5.3.1 Red blood cells (RBCs)/ erythrocytes**

Red blood cells or erythrocytes are the most abundant cells found in whole blood and, in a healthy adult male, 42 – 54% of the blood volume constitutes of erythrocytes. Erythrocytes are biconcave in shape to maximize surface area for gas (O<sub>2</sub> and CO<sub>2</sub>) transport across their membrane to the interior hemoglobin protein which transiently binds the gases. The diameter of a typical human erythrocyte disk is 6-8 μm, much larger than most other human cells. Their main function is to bind and carry oxygen from the lungs to the tissues in the body and remove CO<sub>2</sub> from the tissues for release in the lungs. The membrane of erythrocytes is composed mainly of proteins, lipids, and polysaccharides. Erythrocytes are manufactured in the red bone marrow of large bones, and lack a cell nucleus and have a life span of approximately 120 days in the human body<sup>190</sup>.

The antigens responsible for the A, B, and O blood types are one of many polysaccharides expressed on erythrocyte surfaces and are important for donor/recipient blood type compatibility<sup>190</sup>. The A and B antigen differ by the type of modification made to an acceptor glycoconjugate. The A antigen terminates in an α-1,3-linked N-acetylgalactosamine while B terminates in an α 1,3-linked terminal galactose<sup>191-193</sup>. O blood type cells have neither modification. According to the ABO blood typing system,

there are 4 base blood types, A, B, AB, and O. The presence or absence of a third antigen, termed the Rhesus (Rh) factor, determines the positive and negative blood types<sup>190</sup>. The blood type is assigned a '+' or a '-' sign based on Rh presence or absence respectively. Also, there are complimentary antibodies in the blood plasma (A and B antibodies) which are the recognition helpers of the immune system. The antibody A is present in B blood type plasma (both + and -) and antibody B is present in A blood type plasma (both + and -). O type plasma has both antibodies and AB has neither. Since antibodies are free in the surrounding blood plasma and not bound to the cell surface, they are assumed to not affect dielectrophoretic erythrocyte response.

Erythrocytes have a net negative charge based on their conventional linear electrophoretic behavior<sup>192</sup>. However, the surface charges of erythrocytes rapidly decrease if the blood is stored for more than 6 days. Cell rigidity also increases if stored for more than 6 days, which could be related to the surface charge phenomena<sup>192</sup>. Blood age as well as the storage container can also influence its properties. Hemolysis is less in cells stored in di-2-ethyl hexylphthalate (DEHP) plasticized bags than in butyryl-n-trihexylcitrate (BTHC) plasticized bags<sup>194</sup>.

In this study of work, qualitative and quantitative dielectrophoretic responses of erythrocytes based on positive blood types has been shown. Erythrocytes were subjected to dielectrophoretic fields of  $0.025 V_{pp}/\mu\text{m}$  at a frequency of 1 MHz<sup>88</sup> for 120 s and cell movements were observed using video microscopy. Quantification of cell movement with time included both the horizontal and vertical movement of red blood cells in a constant dielectrophoretic field. The results have shown dependency on the blood type for dielectrophoretic movement of red blood cells for positive blood types. Specific

trends for each blood type with time in both horizontal and vertical directions were tabulated.

#### **5.4 Materials and methods**

The parameters fixed in this research were frequency of the alternating current field and field strength. The parameters which changed were time in the electric field, and time of blood storage. From previous studies, the frequency was maintained at 1 MHz and the electric field strength was maintained at  $0.025 \text{ V}_{pp}/\mu\text{m}^{88}$ . Blood samples were analyzed in the dielectrophoretic field for 3 min on days 0 to 6 in storage. The important steps in the process were microdevice fabrication, experimentation (including microsample preparation), image analysis, quantification, and statistical correlation. Each of these steps is discussed in detail below.

##### **5.4.1 Microdevice fabrication**

The dielectrophoretic field was generated within a microdevice using  $100 \mu\text{m}$  platinum electrode wires positioned  $\sim 200 \mu\text{m}$  apart in a perpendicular configuration. This created a spatially non-uniform AC field. The microdevice was constructed by attaching a HybriWell chamber (HBW 75 and item # 10484908) to a glass microscopic slide thus creating a thin chamber (40 by 21 by 0.15 mm). Platinum wires for electrodes ( $100 \mu\text{m}$  OD, 99% pure, Goodfellow, PT005127/128) were placed perpendicular to each other (Figure 5.1) and the whole chamber was sealed by pressing the adhesive edges of the HybriWell chamber onto the microscopic slide. The microdevice then had two sample ports that enabled fluid to be introduced and removed. The outer ends of the electrodes were wrapped in conductive foil so that alligator clips from a 33250A Agilent Waveform

Generator could be attached. Programming of the generator resulted in a sinusoidal 1 MHz AC electric field in the chamber.

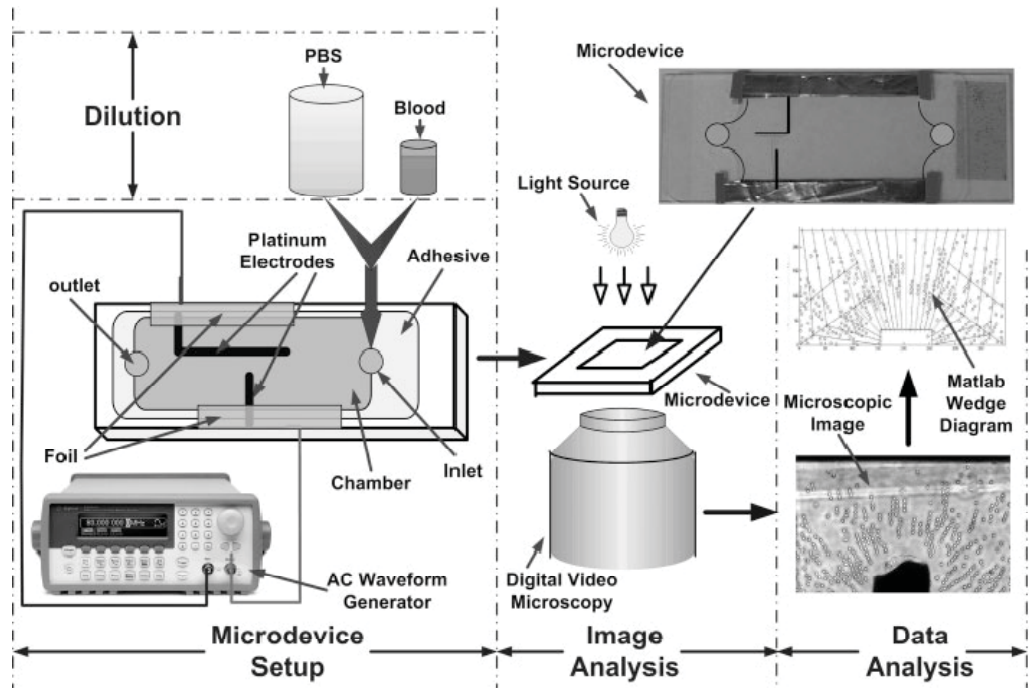


Figure 5.1 Experimental set-up illustrating the custom microdevice mounted on an inverted microscope. Microdevice electrodes are connected directly to an AC wave form generator. Sample inlet port is used to introduce dilute blood suspensions. Erythrocytes responses in the dielectrophoretic field are recorded digitally with a high resolution CCD camera and stored for subsequent image analysis.

#### 5.4.2 Microsample preparation

Whole blood was drawn from voluntary donors via venipuncture by a certified phlebotomist into Becton and Dickinson, 4 mL vacutainers. The donors were randomly selected, but varied in gender, age and ethnicity. The fresh human blood samples were stored in 1.8 mg  $K_2$  EDTA anticoagulant per mL of blood in a refrigerator at  $5^\circ C$ . Prior to conducting experiments, well-mixed whole blood was diluted (1:60) using Phosphate Buffer Saline (PBS; 0.14 M NaCl, 0.02498 M  $KH_2PO_4$ , 0.00907 M  $K_2HPO_4$ ). A 5000  $\mu L$

stock solution of blood suspension was prepared by mixing 4198  $\mu\text{L}$  of PBS solution and 82  $\mu\text{L}$  of whole blood. The solution was well mixed by gently swirling the mixing vial prior to sample loading into a clean microdevice. The day of the venipuncture was labeled as day 0 and subsequent days were 1, 2, 3, etc. For consistency, experiments were performed for 3 different days and two runs were conducted each day, resulting in 6 data sets for each condition set and were repeated for the same blood samples at the same conditions.

### 5.4.3 Experimentation

The microdevice was cleaned with e-pure water (Millipore Simplicity purification system, resistance: 18 Ohms), inspected under the microscope for any debris, and was rinsed five times with PBS. Diluted blood (about 15  $\mu\text{L}$ ) was micropipetted into the microdevice via sample ports labeled in Figure 5.1. The blood suspension was drawn across the HybriWell chamber using Kim Wipes which create a suction from the opposite sample port. This process was repeated five times to ensure that all PBS was displaced with a uniform spatial concentration of the blood suspension throughout the HybriWell chamber. The sample-filled microdevice was then positioned on the microscope stage and alligator clips were used to connect the foiled platinum electrodes to the waveform generator. A sinusoidal AC frequency of 1 MHz was maintained with electric field strength of  $0.025 V_{pp}/\mu\text{m}$ , which resulted from an applied voltage of  $5 V_{pp}$  over an electrode gap of 200  $\mu\text{m}$ . Since the distance between electrodes varied between 150  $\mu\text{m}$  and 200  $\mu\text{m}$ , the applied voltage was adjusted using the following relation to obtain a constant electric field:

$$E = \frac{V}{d} = 0.025 \frac{V_{pp}}{\mu\text{m}} \quad (5.5)$$

where 'V' is the voltage of the field in peak to peak volts and 'd' is the distance in microns between the electrodes.

The blood suspension in the microdevice was allowed to settle for 10 min while the microscope was focused and video capture settings adjusted. The output from the waveform generator was turned on and after 5 s the video microscopy recording was started. The movement of the erythrocytes was recorded via video microscopy at 10 s intervals for 4 min (Figure 5.2). These images were compiled and subsequently analyzed to quantify cell motion.

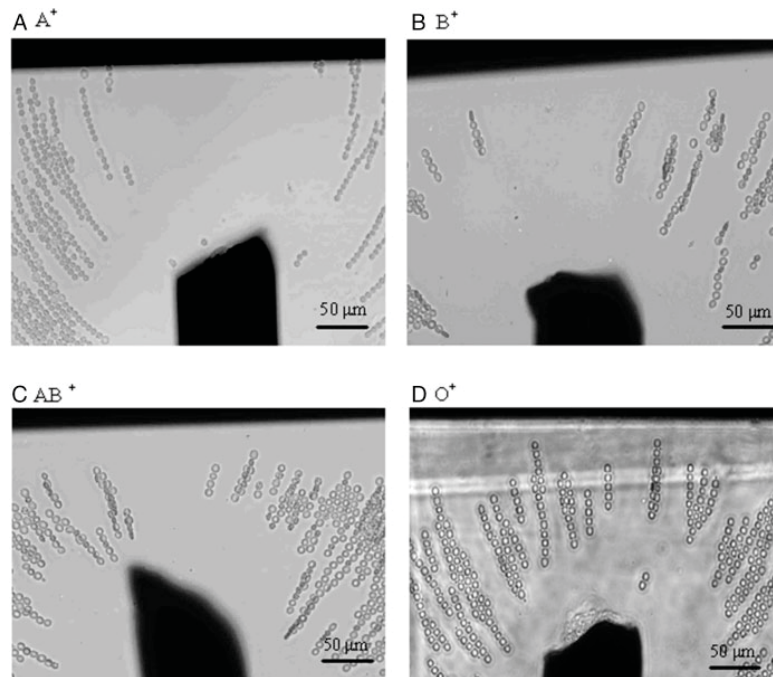


Figure 5.2 Untouched images of erythrocyte distributions in a dielectrophoretic field after 120 seconds of field application at 1 MHz for (a) A+ blood type, (b) B+ blood type, (c) AB+ blood type and (d) O+ blood type cells. The tip protruding into the bottom of the images is the electrode where field density is the highest and the horizontal dark region at the top of each image is the electrode where density is lowest. Red blood cells are aligned along field lines between the electrodes. The figure illustrates the difference in orientation of each of the positive ABO blood types studied after 120 seconds in a 1MHz, 0.025 Vpp/μm AC electric field.



As evident in the electrode profiles in the images in Figure 5.2, electrode shape and spacing differed slightly from microdevice to microdevice. Simulations of the electric field were performed in COMSOL Multiphysics<sup>195</sup> and are shown in Figure 5.3. Two cases are contrasted.

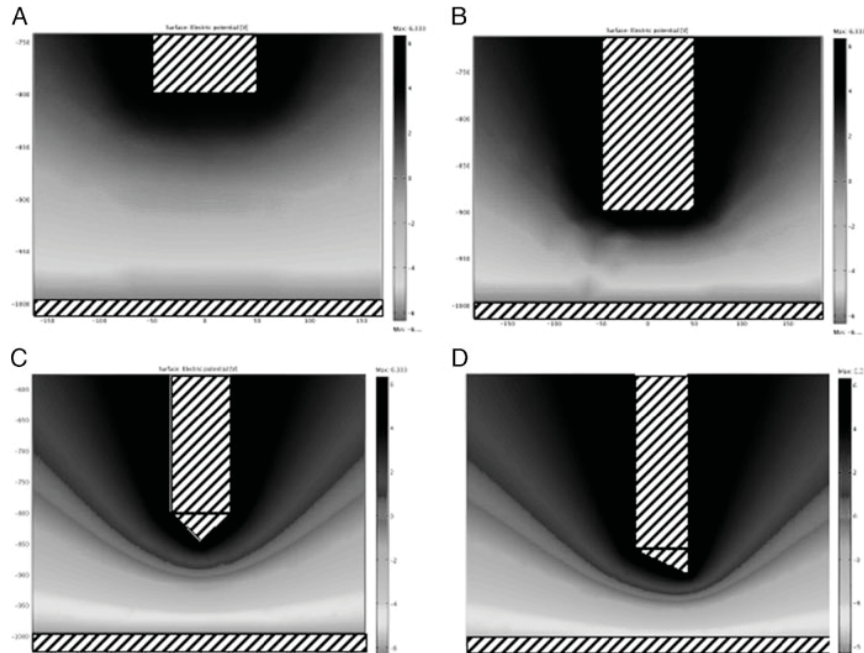


Figure 5.3 Simulations of the electric field in the microdevice were performed in COMSOL Multiphysics. The geometry of the electrode does not affect the separation of erythrocytes (compare Figs. A and B) whereas the distance between the high field density region and low field density region electrodes plays a vital role (compare Figs. C and D) in determining optimal separation of cells. Dark represents high field density regions while light represents low field density regions.

Comparison of Figure 5.3 a and b demonstrates the significant change in field gradient when the electrode spacing is changed from 200  $\mu\text{m}$  ( $E = 0.03 \text{ V}_{\text{pp}} / \mu\text{m}$ ) to 100  $\mu\text{m}$  ( $E = 0.06 \text{ V}_{\text{pp}} / \mu\text{m}$ ). Dark represents high field density region while light represents lowest field density region. A comparison of Figure 5.3 c and d illustrate that while symmetry of the field changes slightly with electrode shape, the gradient (the key

component in equation 1), is not significantly altered. It was concluded that electrode shape is a minor contributor to the field whereas the distance between the electrodes plays a major role in the dielectrophoretic response of erythrocytes. For this reason, considerable effort was dedicated to controlling the electrode spacing in the custom microdevices, but the wire available determined electrode shape.

All work was conducted in a certified Biosafety level II laboratory (BSL II) with Institutional Biosafety committee (IBC) and Institute Review Board (IRB) approval for human subjects.

#### **5.4.4 Image analysis**

The images were processed with image recognition software (Zeiss Axiovision 4.5) to get X/Y position, cell radius, cell area, bound width and bound height of the cells. Based on the difference in optical intensity of the cells and the image background, this edge recognition software selected cells or cell conglomerates. The software was then programmed to disregard objects that were not cells (either too big or too small). Manual selection of any missed cells occurred with a circle selection tool. For every selected object, the software recorded the following properties: X/Y position, radius, bound height and width in a spreadsheet. The cell count on each time-stamped image for every 10 s was also recorded. The images were analyzed for characteristic differences in their movement every 20 to 30 s up to 120 s into the experiment.

#### **5.4.5 Data analysis**

The X/Y data obtained was analyzed for variations with respect to blood type. The first analysis done was a sextant analysis where images were divided into six equal sextants using MATLAB. The sextants were created by dividing the image vertically into

two and then horizontally into three. Cell counts were analyzed in each region. However, the sextant approach proved not to be sensitive enough to quantify observed qualitative differences in motion; the regions were too large to show spatial differences in the dielectrophoretic movement of each blood type.

The next binning approach used was a Wedge Analysis where the image was divided into ~20 equally sized wedges in a manner such that they approximated electric field lines. In MATLAB, wedge lines from the high field density regions (bottom electrode) to the low field density regions (top electrode) were calculated from a geometry information file containing the dimensions of the high field density electrode, the distance between the electrodes, position of the low field density electrode and resolution of the image. Wedge size was determined by spacing the wedge lines 20  $\mu\text{m}$  apart at the low field density electrode (top region in Figure 5.4). Average movement of cells in the vertical and horizontal directions was tabulated for 0, 20, 30, 50, 60, 90 and 120 s for each sample. Data was compiled into a spreadsheet so that averages and standard errors were calculated over days 0, 3 and 5 for each blood sample. Data was further consolidated over independent blood samples for each type. This was done because cell properties do not change appreciably until after 6 days under the storage conditions at 5°C and 1.8 mg K<sub>2</sub> EDTA<sup>192</sup>. Lastly, a composite parameter which captured the distance that the cells moved in the electric field combined the vertical and horizontal positions via the distance formula.

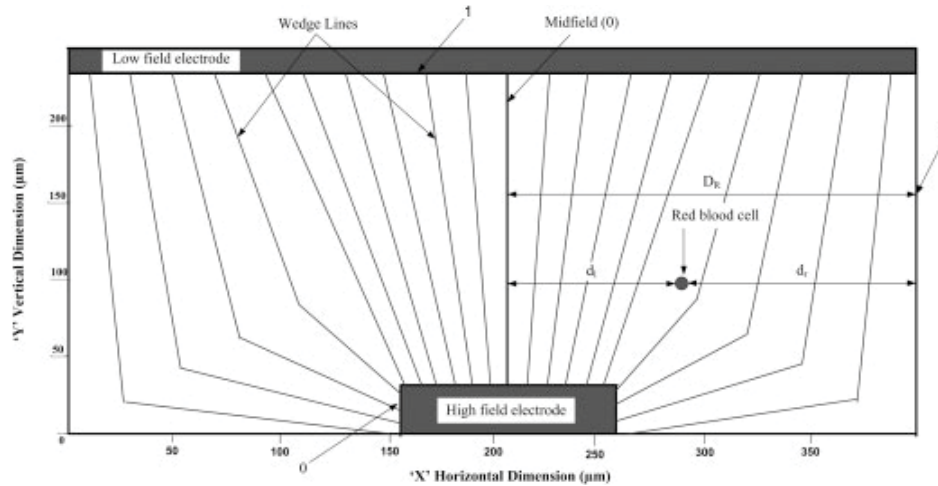


Figure 5.4 Wedge region construct for (X, Y) position tracking in MATLAB. The space between high field density and low field density electrode was broken into regions approximating the shape of the electric field. These wedge lines are calculated via an algorithm and cell movement is then tracked up or down each wedge region (vertical movement) as well as across wedge regions (horizontal movement).

The last approach taken, for assessing the significance of the vertical and horizontal movements of red blood cells was statistical analysis via SAS (Statistical Analysis Software version 9.1)<sup>196</sup>. Analysis of variance and least significance difference with multiple comparisons were performed on both vertical and horizontal movements' data. Analysis of variance was used to assess the primary effects (DAY, TIME, and BLOOD TYPE) and the interaction effects of DAY with TIME, DAY with BLOOD TYPE and TIME with BLOOD TYPE. However, it should be noted that in the current study, it is not possible to distinguish relative contributions of donor from device variabilities, so repetition dependence was not included in the statistical analysis. The model used for performing the analysis with interaction of the three variables is as follows:

$$Y = (\text{DAY TIME BLOOD TYPE}) (\text{DAY*TIME}) (\text{DAY*BLOOD TYPE}) (\text{TIME* BLOOD TYPE}) \quad (5.6)$$

Variance was analyzed separately for vertical and horizontal movements. DAY had three parameters 0, 2 and 5; BLOOD TYPE had four parameters A, B, AB and O; TIME had seven parameters 0, 20, 30, 50, 60, 90 and 120. Since the vertical movements of the cells up or down the wedges was tracked separate from the horizontal movement of the cells across wedge lines, the statistical analysis was also conducted on the vertical and horizontal parameters separately.

An analysis of variance and least significant difference was also conducted with multiple comparisons at 60 and 90 s for vertical and horizontal movements respectively, as these were the times where the best spatial separation of blood types were achieved. Hence the model in equation 5.6 was modified by neglecting the interaction effects as shown in equation 5.7.

$$Y = (\text{DAY TIME BLOOD TYPE}) \quad (5.7)$$

SAS output was utilized alongside movement data to ascertain whether blood types are distinguishable in a dielectrophoretic field. It aided in calculating the confidence level for distinguishing blood types for different movements depending on the DAY, TIME, and BLOOD TYPE.

## 5.5 Results and discussion

The quantitative and qualitative responses for all four blood types (A+, B+, AB+, and O+) in a  $0.025 \text{ V}_{pp}/\mu\text{m}$  electric field are presented in this work. The movements are discussed in the context of the traditional Clausius-Mossotti factor prediction of dielectrophoretic motion (Equation 5.4) and are found to not be entirely consistent. A set of images for all four positive blood types (A+, B+, AB+, and O+) were taken after 120 s of field application and the dielectrophoretic movement was found to be two-

dimensional. Figure 5.2 illustrates the difference in spatial distribution of each of the positive ABO blood types studied, at 120 s after the AC electric field (1 MHz, 0.025 Vpp/ $\mu\text{m}$ ) was applied. A+ had long chains of cells, which migrated away from the midfield region and were closer to the low field density electrode than the high field density electrode. B+ blood type cells demonstrated shorter chains with significant cell overlap and were positioned away from midfield, as well as the high field density and low field density electrode. AB+ erythrocytes had shorter chains that were agglomerated with some cell overlap. Significant repulsion from the high and low field density electrodes are observed with overall position much closer to the midfield than A+ and B+ blood types. O+ blood group cells had longer chains without overlap and conglomerations.

In order to quantify these different spatial distributions, the time sequence dielectrophoretic erythrocyte responses and mapping in MATLAB for O+ blood type is illustrated in Figure 5.5 for 5, 60, and 120 s respectively. Figures 5.5 (a), (c) and (e) show the time sequences of untouched images of dielectrophoretic responses.

As time progressed, prominent pearl chains and some conglomeration of cells were observed. The cells are closer to the central high field region at 5 s but moved away by 120 s. Similarly, cells at 5 s were closer to midfield where as at 120 s fewer erythrocytes were closer to the midfield region. Cell position tracking was achieved via image analysis object recognition that entailed recording X / Y coordinates of cell position and subsequently exported to MATLAB for binning analysis in wedges (Figures 5.4 and 5.5 (b), (d), (f)). Comparison between the untouched image and the X / Y position representation via MATLAB shows excellent agreement and reinforces that image analysis was reliable and robust. As demonstrated, a 1 MHz dielectrophoretic field

induced a fast response (less than 2 min) of the erythrocyte suspension. In order to quantify cell movements, three specific parameters were developed: cell counts by wedge region, vertical movement, and horizontal movement. These are discussed in detail in the following sections.

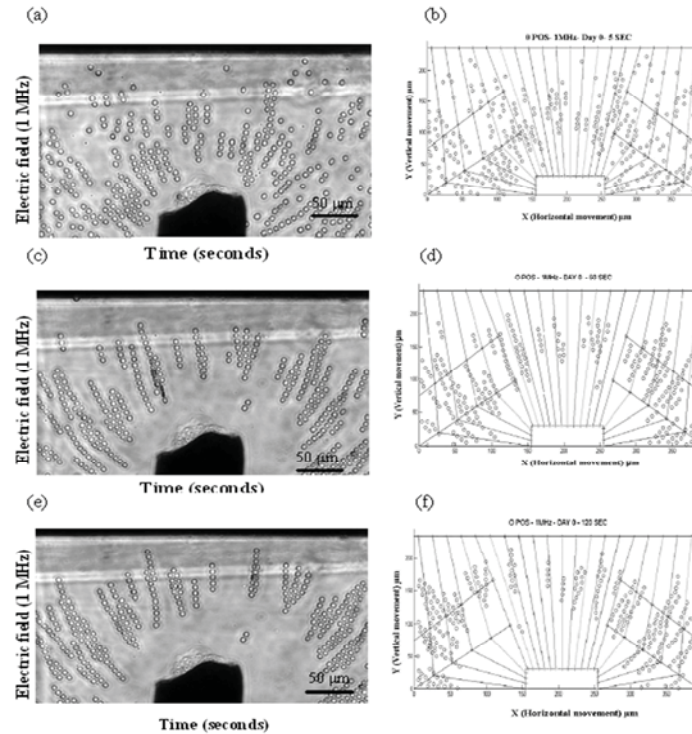


Figure 5.5 Comparison of the dielectrophoretic response of O+ blood type at times 5 (a, b), 60 (c, d), and 120 seconds (e, f) and their corresponding MATLAB representations (b, d, and f) within the wedge regions respectively. As demonstrated, the images and mapped (X, Y) cell position data from MATLAB are in good agreement.

### 5.5.1 Total cell counts by wedge region

MATLAB output for the dielectrophoretic response analysis for O+ after 120 s of field application corresponding to the MATLAB representation in Figure 5.5 (f) is shown in Figures 5.6 (a) and (b). Figure 5.6 (a) shows the horizontal spacing of total number of cells in each wedge region from L to R. Significant lateral movement of cells from

midfield is suggestive of negative dielectrophoresis. In Figure 5.6 (b) vertical distance along the wedges was scaled from 0 to 1 with 0 located near the high field density electrode and 1 near the low field density electrode.

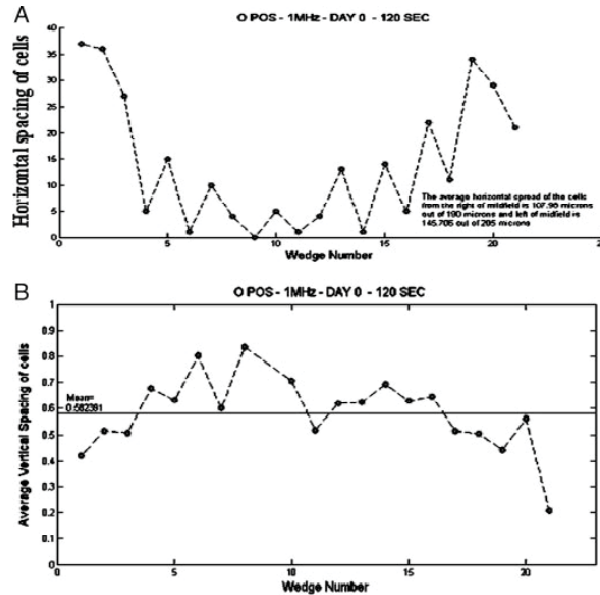


Figure 5.6 MATLAB output for the dielectrophoretic response analysis for O+ after 120 seconds of field application corresponding to the MATLAB representation in Figure 5.4 (f). Figure 5.5 (a) shows the horizontal spacing of total number of cells in each wedge region from L to R. Significant lateral movement of cells from midfield is suggestive of negative dielectrophoresis. In Figure 5.5 (b) vertical distance along the wedges was scaled from 0 to 1 with 0 located near the high field density electrode and 1 near the low field density electrode.

Total cell counts were tallied for all images analyzed (Days 0, 2, and 5 and on each of those days at 0, 20, 30, 50, 60, 90, and 120 s). The percentage of cells remaining in the image field of view was averaged over two independent blood samples and compiled for all four blood types in Table 5.1. As shown, there was a steady decline in the total number of cells in the image field of view as the experimental runs progressed.



This effect reduces the magnitude of the vertical and horizontal movement parameters as values computed at 90 and 120 s were based on fewer cells.

Table 5.1 Percentage of cells remaining in the image field of view for all four positive blood types. The percentage of cells remaining in the image field of view is compiled for all four positive blood types. There is a steady decline in the total number of cells in the field of view as the experimental run time progresses.

Blood Group Type	Total % of cells remaining from time 0 seconds						
	Time (seconds)						
	0	20	30	50	60	90	120
A+	100	93	90	86	80	73	68
B+	100	94	90	84	80	75	69
AB+	100	94	93	88	86	83	79
O+	100	93	92	87	90	90	89

### 5.5.2 Average vertical movement

Vertical movement captures movement of cells between the high and the low field density electrodes by tracking cell position in each wedge. It is determined by the cell's distance from the high field density electrode normalized by the total length of the wedge ( $l_j$ ). This results in a bounded number between 0 and 1: 0 would result when cells were clustered near the high field density region (positive dielectrophoresis) while 1 reflects cells aggregating at the low field density region (negative dielectrophoresis). Vertical movement,  $M_v$ , captures the movement of red blood cells up or down the wedges in the dielectrophoretic field. In equation form, it is given by

$$M_v = \frac{\sum_{i=1}^w \frac{\sum_{j=1}^n \frac{c_j}{l_j}}{n_i}}{W} \quad (5.8)$$

where ‘ $n_i$ ’ is the total number of cells in wedge ‘ $i$ ’, ‘ $c_j$ ’ is the distance along the wedge path from the cell to the high field density electrode for each cell for  $j=1$  to  $n$ , ‘ $l_j$ ’ is the total length of the wedge and ‘ $W$ ’ is the total number of wedges. An overall vertical position was obtained by averaging positions in all the wedges. This profile is depicted in Figure 5.4 where the average vertical position of the cells is shown as a function of the wedges from left to right. Wedge # 11 is the middle wedge and the symmetry in the X dimension can be observed (Figure 5.6 (b)). The information was further condensed by calculating a mean across all wedges to give the average vertical movement. This data was plotted as a function of experimentation time for all blood types and is depicted in Figure 5.7.

Points are shown for A+, B+, AB+, and O+ blood types and standard error is represented for each point. The standard error accounts for variability between the two independent blood samples as well as across experiment days 0, 2 and 5 since it is known that membrane fluidity of the erythrocytes does not change appreciably for the first six days of storage<sup>192</sup>. Standard errors were reasonable with values between 0.003 - 0.015 (0.6 – 3  $\mu\text{m}$ ) and were expected given that these were biological, micrometer scale experiments. In all cases, average cell position started near 0.5 (halfway between electrodes) corresponding to  $\sim 100 \mu\text{m}$  since a distance of 0.1 in wedge image represents erythrocyte movement of about 20  $\mu\text{m}$ . O+ continued to hover near 0.5 while all other blood types deviated towards the low field density electrode region. The best separation

achieved for all four blood types was at 60 s as shown in Figure 5.7. All the blood types converge back to a comparable average vertical position after 60 s due to the loss of cells from the field of view. Since these numbers are artificially skewed due to the data analysis tools, only 0 to 60 s are analyzed further (time frame where 80 % of cells exist in the field of view). The four blood types were fit to a linear trend; intercept and  $R^2$  values for each blood type are tabulated in Table 5.2 for experimental run time from 0 to 60 s.

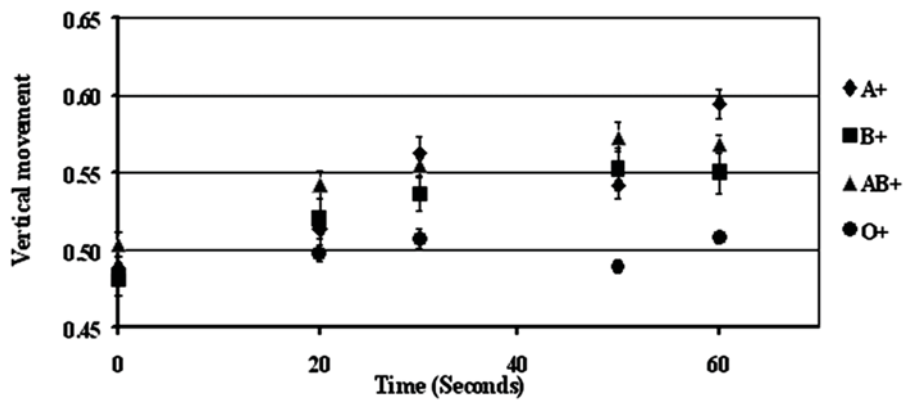


Figure 5.7 Vertical movement is calculated according to Equation 5.8 and is shown as a function of experimental run time up to 60 s. Points are shown for A+, B+, AB+, and O+ blood types and standard error is represented for each point. In all cases, average cell position starts near 0.5 (halfway between electrodes). O+ hovers near 0.5 while all other blood types deviate towards the low field density electrode. The best separation achieved for all the four blood types was around 60 s. All the blood types converge back after 60 s as shown in Table 5.1. Trend lines are not shown in the figure but are compiled in Table 5.2 for the experimental run time of 0-90 s.

Table 5.2 Linear trends of the vertical and horizontal movements for 4 positive blood types. The linear trends of the vertical and horizontal movements are shown for all the four positive blood types. The intercepts and slope are given along with the  $R^2$  value. These data are compiled for the experimental run time of 0-60 s for vertical movement and 0-90 s for horizontal movement as 60 and 90 s were the time where best spatial separation of all the four blood types were achieved for vertical and horizontal movements respectively.

Blood type	Slope		Intercept		$R^2$	
	Vertical	Horizontal	Vertical	Horizontal	Vertical	Horizontal
A+	0.0015	0.0012	0.49	0.54	0.78	0.91
B+	0.0011	0.0015	0.51	0.53	0.89	0.98
AB+	0.0012	0.0011	0.49	0.53	0.90	0.93
O+	0.0002	0.0008	0.49	0.53	0.28	0.95

Further, statistical analysis was performed as described in the data analysis section and three different tests were chosen: primary effects, interaction of primary effects and primary effects only at 60 s. First, the vertical means of primary effects, DAY, TIME, and BLOOD TYPE were compared. A goodness of fit test was performed on the model in equation 5.7, which yielded an observed significance level (p-value) of less than 0.0001. At this p-value, a conventional threshold significance level of 0.05 was chosen to study the variance. At this corresponding confidence level of 95%, it was concluded that all or at least one of the vertical movement means are different by Fisher's least significant difference method<sup>197</sup>. Least significant difference is the observed difference between any pair wise interaction effects sample means necessary to declare the corresponding population of interaction effect means different.

To know which means were different, interaction effects of (DAY \* TIME), (DAY \* BLOOD TYPE) and (TIME \* BLOOD TYPE) were compared, which is known as Multiple Comparisons carried out pair-wise<sup>197</sup>. Multiple comparisons of these interactions were performed using Fisher's method of least significant difference<sup>197</sup>. A

goodness of fit test<sup>197</sup> was performed on equation 5.7 which yielded a p-value of 0.001. At this p-value, a confidence level of 95% was chosen for this interaction analysis. Significant interaction of (DAY \* BLOOD TYPE) was observed, but there was no evidence to support interactions between (TIME \* BLOOD TYPE). Multiple comparison at an alpha of 0.05 suggested that O+ had a statistically significantly low mean vertical movement compared to the remaining blood types.

At this alpha value, there was no evidence to suggest that there was a difference between A+, B+, and AB+ blood types. In order to assess at which confidence level A+, B+, and AB+ could be discerned from each other, an iterative approach was taken. By successively decreasing the confidence level,  $\alpha$ , the confidence at which the blood types could be discerned was determined. It was found that AB+ is statistically different from B+ with a confidence of 85% and AB+ is statistically different from A+ with a confidence of 65%, which suggests that AB+ behaviors more closely mimic A+ vertical movement behavior. As shown in Table 5.3, it was only at a confidence level of 56% that all four blood types could be reproducibly distinguished.

Practical diagnostic devices may only consider a result at one point in time. Therefore least significant difference by multiple comparison of primary effect, BLOOD TYPE, was also studied by examining average vertical positions at 60 s, as this was the time where best separation of all the blood types was achieved (Figure 5.7). A goodness of fit test was again performed on equation 5.6 which yielded a p-value of 0.1172. Hence a confidence level of 85% was chosen for analysis. There was no influence of DAY on 60 s vertical movement data. At alpha of 0.15, multiple comparison on BLOOD TYPE showed O+ to be significantly different from A+ and AB+ but not from B+. There was no

evidence to suggest that A+, B+ and AB+ were significantly different from each other at an 85% confidence level.

Thus, the above quantitative results as well as qualitative observations suggests that vertical cell motion in a dielectrophoretic field is weakly dependent on BLOOD TYPE and that O+ dependencies are statistically significant with greater than 95% confidence, while other blood types are only significantly distinguishable at 56% confidence level.

Table 5.3 Least significant difference multiple comparison results for vertical movement. Least significant difference multiple comparison results for average vertical movement are shown. The confidence level at which the vertical movement parameter is able to distinguish blood type is tallied.

$\alpha$ Value	Confidence level	Significantly different blood types observed for Vertical movement
0.05	95%	O+ can be distinguished from A+, B+, AB+
0.15	85%	AB+ can be distinguished from B+
0.35	65%	AB+ can be distinguished from A+
<b>0.44</b>	<b>56%</b>	<b>All four blood types can be distinguished</b>

### 5.5.3 Mean fractional horizontal movement

The horizontal movement parameter captures the movement of erythrocytes away from the midfield towards the left or right edges of the image in the dielectrophoretic field (Figure 5.4). The distance from the electrode centerline (midfield) to the image edges on either side ( $D_L$  on the left side and  $D_R$  on the right side) was measured. The horizontal distance of the cells from midfield was calculated separately for the left hand side ( $d_L$ ) and the right hand side ( $d_R$ ) of the image (Figure 5.4). The total number of cells on either side of the centerline ( $N_L$  on the left side and  $N_R$  on the right side) were also calculated. Equation 5.9 shows how the position was normalized and averaged to give

horizontal movement; the resulting values were plotted for each blood type as a function of time in Figure 5.8.

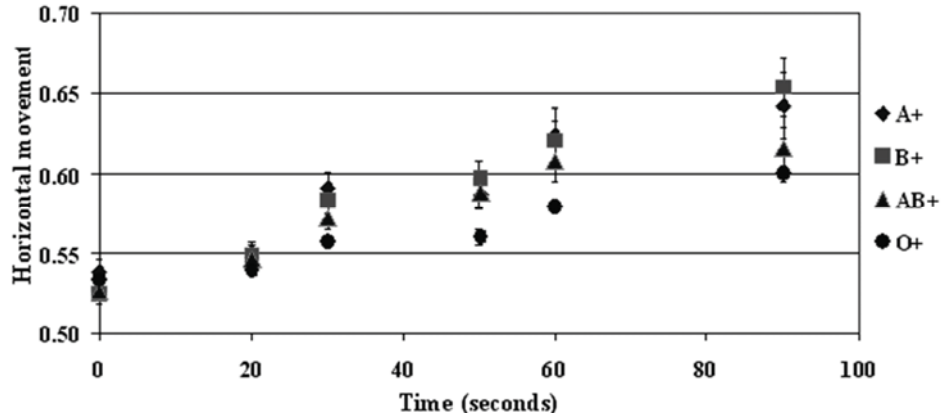


Figure 5.8 Movement in the horizontal dimension is calculated via equation 5.9. Data points for A+, B+, AB+, and O+ blood types are plotted and corresponding standard errors shown. For all four blood types, initial cell position is near 0.5, which is halfway between midfield and the far left or far right of the image. Movement with time is away from midfield in all cases. From the figure, the best separation was achieved at 90 s for all four blood types. All the blood types converge back after 90 s as shown in Table 5.1. Trend line data is again compiled in Table 5.2 for the experimental run time of 0-90 s.

Horizontal movement,  $M_H$ , aids in assessing the movement of the red blood cells either towards or away from the higher field gradient region (midfield) of the device. In equation form:

$$M_H = \frac{\sum_{i=1}^{N_L} d_L}{N_L \cdot D_L} + \frac{\sum_{i=1}^{N_R} d_R}{N_R \cdot D_R} \quad (5.9)$$

Data points for A+, B+, AB+, and O+ blood types are plotted with corresponding standard errors shown in Figure 5.8. Standard errors were reasonable with values between 0.0025 - 0.021 (0.5  $\mu\text{m}$  – 4.2  $\mu\text{m}$ ) and were expected given that these were biological, micrometer scale experiments. A distance of about 0.1 on the graph corresponded to ~20

$\mu\text{m}$  on the raw images from the device. For all four blood types, initial cell position was near 0.5 (100  $\mu\text{m}$ ), which represents the distance halfway between midfield and the far left or far right of the image (Figure 5.4). Movement with time was away from midfield, out of the image field of view for all four types. Type B+ cells horizontal movement was consistently greater than other blood types during the experiment from 20 to 120 s. In contrast, O+ cells demonstrated the smallest movement from midfield, which is consistent with qualitative observations (Figure 5.2). From Figure 5.8, the best horizontal spread achieved was at 90 s for all four blood types. As was observed with the vertical movement data, the loss of cells from the field of view artificially skewed the quantified position values, so only 0 to 90 s data were analyzed further. The four blood types converge back after 90 s and all blood types followed a linear trend; intercept and  $R^2$  values for each blood type are tabulated in Table 5.2 for experimental run time from 0 to 90 s.

Further, statistical analysis was performed as previously described. First the horizontal means of primary effects, DAY, TIME, and BLOOD TYPE were compared. A goodness of fit test was performed on the model in equation 4, which yielded an observed significance level (p-value) of less than 0.0001. As before, a threshold significance level of 0.05 was chosen to study the variance. At this 95% confidence level, it was concluded that all or at least one of the horizontal movement means were different by Fisher's least significant difference method<sup>197</sup>. To know which means were different on the primary effects, interaction effects of (DAY \* TIME), (DAY \* BLOOD TYPE) and (TIME \* BLOOD TYPE) were compared and significant interactions were observed for all the three interactions. By this method, DAY 0 was significantly different from 2 and 5. TIME periods 0, 90 and 120 were significantly different from the other periods. This



means that dielectrophoretic response is measurable at 0 and 90 s, and at 120 s, the total number of cells in the field of view are significantly impacting the profile of horizontal movement (see Table 5.1). The horizontal movement at other times of 20 and 60 s showed indistinguishable behaviors. It also showed that BLOOD TYPE O+ was significantly different from A+ and B+ but not from AB+ at a 95% confidence level. The confidence level,  $\alpha$ , was successively decreased until a level was reached where the blood types could be discerned. With 85% confidence, O+ could be discerned from AB+ by examining horizontal movement. At 75% confidence, AB+ could be distinguished from A+ and B+, but it was only with 8% confidence that all four positive blood types could be distinguished by examining horizontal movement alone. This data is show in Table 5.4.

Table 5.4 Least significant difference multiple comparison results for horizontal movement. Least significant difference multiple comparison results for horizontal movement is shown. The confidence level at which the horizontal movement parameter is able to distinguish blood type is tallied.

$\alpha$ Value	Confidence level	Significantly different blood types observed for Horizontal movement
0.05	95%	O+ can be distinguished from A+ and B+
0.15	85%	O+ can be distinguished from AB+
0.25	75%	AB+ can be distinguished from A+ and B+
<b>0.92</b>	<b>8%</b>	<b><i>All four blood types can be distinguished</i></b>

Again, to assess robustness if only one data point was used in a diagnostic device, the primary effect (BLOOD TYPE) was studied at 90 s, as this was the time where best spatial separation of all the blood types was achieved (Figure 5.8). A goodness of fit test<sup>197</sup> was performed on the model in equation 5.7, which yielded a p-value of 0.2718 so  $\alpha$  of 0.3 was chosen for further analysis. At this 70% confidence level, all blood types

were the same with the multiple comparison tests and there was no evidence to suggest that day or blood type were significantly influencing the horizontal movement values.

The statistical analysis conducted neglects the influence of the substantial number of cells that are lost from the analysis field of view. The impact of this is primarily on the horizontal movement because as the cells approach the edge of the field of view, their position drives the average up, but as they move out of the field of view, the average drops. This is likely the reason that blood type is discernable with horizontal movement at lower confidence levels than with the vertical movement tracking alone. Analyzing a large image space would likely help in addressing this issue. Thus, horizontal movement is not substantial enough to distinguish blood types, but tracking of vertical movement is far more reliable.

#### 5.5.4 Composite distance

The distance parameter captures the composite movement of erythrocytes in both the horizontal and vertical directions. This parameter is calculated using the distance formula with the vertical positions,  $M_V$ , and horizontal positions,  $M_H$ , always calculated as relative to the initial average position at time 0 as follows:

$$D_{xy} = \sqrt{(M_v^{time0} - M_v)^2 + (M_H^{time0} - M_H)^2} \quad (5.10)$$

This parameter allows to represent total movement in one number as a function of time. The resulting distances traveled are given in Figure 5.9 along with fitted trend lines.

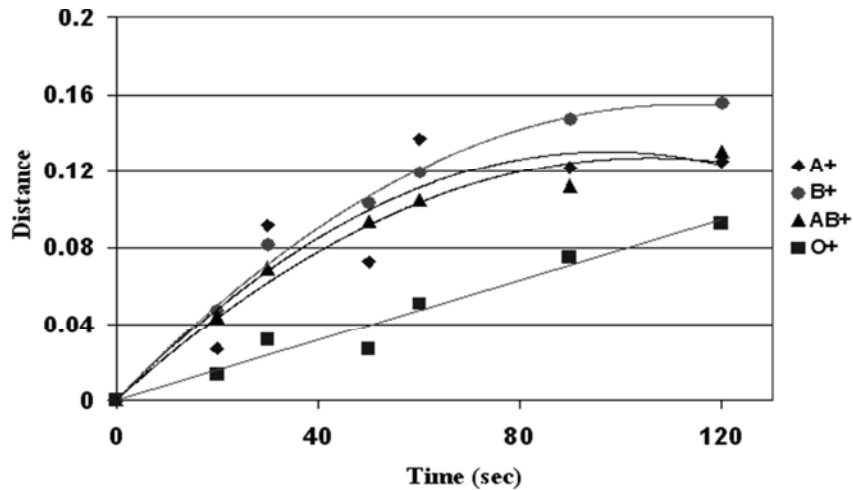


Figure 5.9 Composite distance combining horizontal and vertical movement figures via the distance formula in equation 5.10. Distance increases with time away from image center for A+, B+, AB+, and O+ blood types. From the figure, A+, B+, and AB+ movements cease to appreciably change after approximately 90 s due to the loss of cells from the analysis area as shown in Table 5.1.

Distance increases with time away from image center for all blood types. O+ cell distances followed a nice linear trend with an  $R^2$  of 0.96, while A+, B+, and AB+ cell types all required second order polynomial fits to attain acceptable  $R^2$  values. B+ and AB+ erythrocytes polynomial fits are 0.99 and 0.98, respectively. However, A+ blood type result varies and the fit is only good to an  $R^2$  value of 0.85. The need for a second order polynomial to estimate the trend of the data is necessary due to the loss of cells from the image field of view and thus the analysis area. From Figure 5.9, A+, B+, and AB+ erythrocyte movements cease to appreciably change after approximately 90 seconds due to the loss of cells from the analysis area as shown in Table 5.1. This causes a tapering off of the measured movement from the highest field density regions. This movement differs from that predicted by traditional dielectrophoretic theory (equations 5.1 and 5.2) suggesting that the polysaccharide antigens on the red blood surface impact the dielectrophoretic response. The single distance parameter demonstrates the same

movement patterns noted in the individual vertical and horizontal movement data and is a good tool for tracking blood cell motion in dielectrophoretic fields.

As demonstrated in Figure 5.2 and verified in analysis (Figures 5.7, 5.8, and 5.9), the dielectrophoretic responses of A+, B+ and AB+ blood types were similar to each other but differentiable from O+ blood type. The O+ blood type lacks both the antigens A and B and this may be the reason for the attenuated dielectrophoretic response to the applied field. The A and B antigen have a similar structure in terms of their modification of the H glycoconjugate<sup>192-193</sup>, N-acetyl-galactosamine and N-acetyl-glucosamine respectively. The horizontal and vertical movement tracking showed different trends in the dielectrophoretic movement of erythrocytes for A+, B+, AB+ and O+ blood types with time. Also, dielectrophoretic response of the O+ and AB+ blood types can be differentiated easily with greater than 95% confidence from vertical movement alone. This is of particular significance since O+ blood type, a universal donor (can be transfused to a person of any blood type) and AB+, a universal acceptor (can take any blood type via transfusion). Cells of O+ blood type were the least responsive to the dielectrophoretic field, while cells of the A+ blood type showed greatest response with time. This work, once improved upon, is significant for emergency blood transfusion applications and also in portable blood typing device for easy and rapid blood diagnostics.

## 5.6 Summary

Collectively dielectrophoretic movement of erythrocytes in the vertical and horizontal directions depends significantly on blood type. The dielectrophoretic movement of each positive blood type was seen to follow distinct trends with time. The

parameters, total cell count, vertical movement, horizontal movement, and distance were used to capture the total cells, and movements of the erythrocytes in each wedge in the dielectrophoretic field. From Table 5.1, for O+ blood type the total cells remaining in the field of view was about 90% without much change throughout the experimental run time, but drastic decreases in the total cells within the analysis window was observed for both A+ and B+ blood types. In case of AB+ blood type, the total cells remaining were in-between O+ and A+, B+ blood types. Vertical and horizontal movements indicated the best separation times to be 60 and 90 s respectively for all the blood types. The combined distance parameter illustrated this trend as was expected with the data following a linear trend away from dielectrophoretic field center before stabilizing off due to cell loss.

All parameters showed that O+ had an attenuated response compared to all other blood types. This was also verified from the statistical analysis on vertical and horizontal movements by Fisher's least significance difference method. At 95% confidence level, vertical movement showed O+ to be different from the other 3 types. O+ erythrocytes also showed relatively attenuated responses likely due to the absence of two antigens and this has large implications as type O blood is a universal donor. Also, A+ and B+ have very similar responses in the dielectrophoretic field with AB+ demonstrating similar spatial distributions. With both vertical and horizontal movement parameters and subsequently combined distance, AB+ demonstrated values between those shown by A+, B+ and O+. This is due to the fact that A+, B+ and AB+ all having antigens that are structurally similar<sup>191</sup> differing only by their side chains, on the polysaccharide backbone. AB+ responses differed from A+ and B+ likely because AB+ erythrocytes express both A and B glycoforms on their membrane. Wedge binning approach via MATLAB and

statistical analysis via SAS were able to capture the difference in the dielectrophoretic response of the RBC of different positive blood types.

The use of microdevices for blood typing can help increase the speed and efficiency of emergency medical diagnosis. Current blood typing technologies require time, a clinical environment, and antibody assays for each blood type; such medical technological methodologies require skilled medical technicians and are not readily portable to emergency sites which make the whole testing method more expensive and prone to false positives and negatives. Dielectrophoresis shows excellent potential for this purpose as it has many advantages over conventional blood typing techniques, spectroscopy and magnetophoresis. The capacity of dielectrophoresis as an analytical tool to differentiate positive blood types without any pretreatment or cell modification beyond simple dilution had been demonstrated. Four parameters were used to capture the differences in the dielectrophoretic movement of the erythrocytes based on their blood types: total cell count, vertical movement, horizontal movement, and combined distance. All parameters showed that O+ had an attenuated response compared to all other blood types. At 95% confidence level, vertical movement showed O+ to be different from the other 3 types with A+ and B+ having similar responses in the dielectrophoretic field with AB+ tracking close by. This work provides preliminary evidence that dielectrophoretic responses are influenced by the expression of polysaccharide molecules on the surface of cells, which has ramifications for future studies of the dielectrophoretic behavior of other biological cells. The current work is limited because it does not account for all the antigens on the blood cell surface, only ABO antigens. The results are accurate with acceptable standard errors, which is especially gratifying given that custom-made microdevices with electrode variability were utilized. Further work must be done to study

the dielectrophoretic response of negative blood types as well as field dependency and frequency dependency of the dielectrophoretic movement of all blood types. A pragmatic method for using this information for a commercial microdevice is also to be studied where analysis is performed using analytical equipment.

In the next chapter, a comprehensive review of the literature on DC dielectrophoresis has been provided. This project reveals that dielectrophoretic responses depend on antigen expression on the red blood cell membrane and this is treated as hypothesis to investigate red blood cell responses when DC electric field is applied.

CHAPTER VI  
DC INSULATOR-DIELECTROPHORETIC APPLICATIONS IN MICRODEVICE  
TECHNOLOGY: A REVIEW

### 6.1 Introduction

Dielectrophoresis is a non-invasive, non-destructive, inexpensive, and fast technique for manipulation of bioparticles. Recent advances in the field of dielectrophoresis (DEP) have resulted in new approaches for characterizing the behavior of particles and cells by using direct current (DC) electric fields. The spatial non-uniformities in the channel for observing separation or trapping is based on embedded insulating obstacle in the channel. This emerging field of dielectrophoresis is commonly termed DC insulator dielectrophoresis (DC-iDEP), insulator-based dielectrophoresis (iDEP) or electrodeless dielectrophoresis (eDEP). In many microdevices, this form of dielectrophoresis has advantages over traditional AC-DEP including single material microfabrication, remotely positioned electrodes, and reduced fouling of the test region. DC-iDEP applications have included disease detection, separation of cancerous cells from normal cells and separation of live from dead bacteria. However the need for a critical report to integrate these important research findings is necessary. The aim of this chapter is to provide an overview of the current state-of-art technology in the field of DC-iDEP for separation and trapping of inert particles and cells. In this article, review of concepts and theory leading to manipulation of particles via DC-iDEP, designs of insulating obstacle geometry and performance characterization of devices have been



discussed. The review compiles and compares the significant findings obtained by researchers in handling and manipulating particles.

## 6.2 Microfluidic platform

Microfabrication for the miniaturization of analytical laboratory procedures has relied heavily on the knowledge gained by the manufacture of integrated circuits by the electronics industry during the computer revolution<sup>198</sup>. Micro-total analytical systems ( $\mu$ TAS) have the capacity to perform diverse tasks ranging from DNA analysis to protein recognition and can also be catered to point-of-care medical diagnostic tools<sup>17</sup>, first coined by Manz *et al.*<sup>14</sup>. The first analytical laboratory miniaturization occurred at Stanford University in 1979 by Terry *et al.* group, where a gas chromatograph system was fabricated on a silicon chip<sup>198</sup>. Since this initial breakthrough, a plethora of micro-scale analytical devices have been developed with a variety of innovative technological strategies to achieve the  $\mu$ TAS dream. These devices are also termed lab-on-a-chip (LOC) devices and incorporate multiple laboratory functions on a single platform such that they can handle extremely small fluid volumes down to picoliters<sup>1,15,81,199</sup>. For robust operation and analysis, LOC's have to be designed as simple as possible to integrate different systems and perform separation, mixing and detection on a single chip<sup>19,30,34</sup>. Compared to traditional or macro-sized instruments, they provide better platform for handling bioparticles without the need of specialized instruments, environment and they perform better yielding higher efficiencies, reproducibility and affordability<sup>85</sup>.

Fluids are moved through channels and chambers on this chip via applied pressure differences, capillary driving forces owing to wetting of surfaces by fluids, and free-surface flows driven by gradients<sup>36,38-39</sup>. In addition to these forces, electrokinetics is

commonly utilized to move analytes because electric fields are versatile and can be precisely controlled for specific, quantifiable analyte responses. Furthermore, devices employing electric fields can eventually be simplified to only require a battery for power – a key characteristic for true portable diagnostic devices. Dielectrophoresis, the use of alternating current (AC) creates spatially non-uniform electric fields to polarize particles or cells is a key type of field to explore in analytical and diagnostic devices due to operational simplicity, lower voltage requirements, and small sample volumes - all of which enable device portability<sup>19</sup>. Separation and trapping can be achieved with a high degree of selectivity and sensitivity, which makes dielectrophoresis a powerful tool for diagnostic applications. An emerging new technology in the field of dielectrophoresis is DC dielectrophoresis, which employs insulative objects in the microchannel to create spatial non-uniformities in the electric field<sup>15,19</sup>. Remotely applied DC currents are utilized to create electric field around the insulating obstacles in the microchannel. DC dielectrophoresis differs from AC dielectrophoresis in that particle or cell polarization is accomplished only via spatial variations in the electric field and the alternating current (or frequency dependent) transient polarizations are not a factor in DC implementations of this technique.

Due to the relatively new nature of the field of DC-iDEP, a review of this field has not yet been conducted. The objective of this review is to depict the state-of-the-art technology on the use of DC insulator based dielectrophoretic devices (DC-iDEP) for the manipulation of inert and bioparticles. Here, an extensive review of the theory behind dielectrophoresis employing DC electric fields to create spatial non-uniformities in the channel, fabrication of insulator-based microdevices to accomplish DC insulator based dielectrophoresis has been provided. In order to fully explore this novel technique,

understanding the performance of such devices is important. Here some of the medium conditions suitable for performance of trapping or sorting particles via DC-iDEP employing glass and PDMS microdevices has been provided. A comprehensive review of different particles and biological cells manipulated leading to applications in analytical tests and medical diagnostics have been presented in the order of the size of the bioparticles. This article uses particle within the broad context that it can mean any geometry and composition of object including cells, inert particles and large biological molecules. This review provides a significant overview on DC-iDEP technology for researchers working or wishing to achieve sorting or trapping of particles.

### 6.3 Dielectrophoresis

The term ‘Dielectrophoresis’ was first coined by H.A. Pohl in his seminal text *“Dielectrophoresis the behavior of neutral matter in nonuniform electric fields”* 32 years ago<sup>41</sup>. Dielectrophoresis (or DEP) is a phenomenon observed when a force is exerted on a dielectric particle subjected to a non-uniform and traditionally AC field, albeit DC fields can achieve similar particle responses. Initially the term DEP referred to only translation effects of particles, but recently several other effects have been considered to broaden this area, some of them being travelling wave, quadrupole, and rotational effects. The DEP force experienced by a particle depends on the medium and particles' dielectric properties, shape and size, as well as on the frequency of the AC field<sup>83,88</sup>.

Dielectrophoretic force is given as a function of particle radius ( $r$ ), permittivity ( $\epsilon_m$ ), electric field ( $\vec{E}$ ) and the Clausius-Mossotti (CM) factor, ‘ $\alpha$ ’<sup>1</sup>:

$$\vec{F}_{DEP} = 2\pi r^3 \epsilon_m \alpha (\nabla E^2) \quad (6.1)$$

The spatial field gradients are captured within the  $\nabla \overline{E^2}$ , whereas the frequency dependence is captured within the Clausius-Mossotti factor. This CM factor is valid for a perfectly spherical particle and is a ratio of the effective permittivity's as follows:

$$\alpha = \frac{(\tilde{\epsilon}_p - \tilde{\epsilon}_m)}{(\tilde{\epsilon}_p + 2\tilde{\epsilon}_m)} \quad (6.2)$$

where,  $\tilde{\epsilon}_p$  is the permittivity of the particle and  $\tilde{\epsilon}_m$  the permittivity of the medium in which the particle is suspended. This CM factor guides polarization behaviors of the particles, which Pohl described as the two phenomena of dielectrophoresis, positive and negative dielectrophoresis<sup>41</sup>. Positive DEP occurs when the permittivity of the particle is greater than that of the medium resulting in positive values of CM factors and particle movement towards high field density regions (i.e. up the field gradient) and negative DEP occurs when permittivity of the particle is less than that of the medium, resulting in negative values of CM factors and particle movement towards low field density regions (i.e. down the field gradient)<sup>41,83</sup>. Conventional AC dielectrophoresis occurs by a) non-parallel metal electrodes in direct contact with the medium creating an electric field gradient directly controlled by an AC power supply or b) electrically free-floating metal electrodes in direct contact with the solution<sup>128</sup>. However, these embedded electrode systems face issues with Joule heating, electrode fouling<sup>200</sup>, fabrication complications due to metal micro fabrication in the micro chambers and electrochemical reactions on the electrode surface<sup>116</sup>. Another alternative to AC dielectrophoresis is insulator-based DC dielectrophoresis (DC-iDEP), which uses insulating obstacles, hurdles or protrusions in the channel to create spatial field non-uniformities.

In the next section, the novel technique of DC-iDEP is presented with equations describing the forces pertaining to DC-iDEP. A discussion on how the particles sort or trap with this technique using various insulating obstacle geometry is also described.

#### 6.4 DC dielectrophoresis: Theory

Direct Current insulator based dielectrophoresis (DC-iDEP) is a relatively new field developed in the past decade. Masuda *et al.*<sup>201</sup> was the first to develop this concept for a biological application involving cell fusion, which was later summarized by Lee *et al.* in 1994<sup>124,202</sup>. It utilizes the spatially nonuniform electric field component but not the frequency dependent component of dielectrophoresis, which has been shown to be adequate for manipulation of cells<sup>112</sup>. Spatial non-uniformities in the electric field are generated via insulating obstacles positioned in microdevice channels across which a remotely applied DC current is passed.

The advantages of using insulating obstacles include<sup>113,117,128</sup>:

- insulators are less prone to fouling than electrodes embedded in microdevices,
- no metal components are involved which reduces the complexity of fabrication of devices,
- ideal insulating obstacles are mechanically robust and chemically inert, and
- electrolysis gas evolution at the remotely located metal electrodes does not result in bubbles inside the microchannel.

Cummings and Singh were the first to observe two flow regimes in DC-iDEP systems<sup>113</sup>. This flow system resulted in the competition between electrokinetic flow

(electrophoresis and electro-osmosis combined) and dielectrophoresis. When DEP overcomes electrokinetic flow and dominates diffusion ‘Streaming DEP’ occurs, but when DEP forces dominate both diffusion and electrokinetic flow ‘Trapping DEP’ occurs. In streaming DEP, particles that are concentrated by electrokinetic forces flow in streams whereas in trapping DEP, the particles are immobilized onto edges of the insulating obstacle geometry and become more concentrated<sup>113</sup>. The streaming DEP can be thought of as the DC equivalent of negative DEP, while trapping DEP can be viewed as the DC equivalent of positive DEP. Such an analogy is based upon the direction that the DEP force acts on a particle as will be discussed below.

DC-iDEP is becoming increasingly utilized in LOC devices because the configuration is well suited for bulk manufacturing techniques like injection molding and precise particle manipulations are possible using even hybrid electric field condition<sup>203</sup>. For example, an insulator DEP device can be operated using simultaneous AC and DC fields, with the AC usually in the low frequency range. This will be discussed in more detail in the Section 6.6. First, let us review the theory behind purely DC field dielectrophoresis.

The non-uniform field force can be derived from the net dielectric force as shown:

$$F = (p \cdot \nabla) \vec{E} \quad (6.3)$$

where ‘ $p$ ’ is the dipole moment vector which is a function of particle’s effective polarizability, ‘ $\alpha$ ’, volume, ‘ $v$ ’, of the particle and the applied electric field, ‘ $\vec{E}$ ’ as shown:

$$p = \alpha v \vec{E} \quad (6.4)$$

The Clausius-Mossotti factor,  $\alpha$  estimates the effective polarizability term of the particle and is a ratio of complex permittivity’s  $\tilde{\epsilon}$  as given in equation 6.2 above.

$$\tilde{\varepsilon} = \varepsilon - i \frac{\sigma}{\omega} \quad (6.5)$$

where ‘ $\omega$ ’ represents frequency, ‘ $\varepsilon$ ’ the dielectric constant and ‘ $\sigma$ ’ the electrical conductivity of the medium.

Neglecting the frequency component for strict DC-iDEP, the dielectrophoretic force is estimated to be the residual of CM factor (equation 6.6) when the limit of the frequency approaches zero. This simplification is substituted into the dielectrophoretic field force equation yielding equation 6.7<sup>81,199</sup>.

$$\alpha = \frac{\sigma_p - \sigma_m}{\sigma_p + 2\sigma_m} \quad (6.6)$$

$$\vec{F}_{DEP} = \frac{1}{2} v \frac{\sigma_p - \sigma_m}{\sigma_p + 2\sigma_m} \nabla \vec{E}^2 = 2\pi \varepsilon_m d_p^3 \alpha \nabla \vec{E}^2 \quad (6.7)$$

where  $\sigma_p$  is the conductivity of the particle,  $\sigma_m$  the conductivity of the medium,  $v$  the volume of the particle,  $\varepsilon_m$  permittivity of the medium,  $d_p$  the diameter of the particle, and  $\nabla \vec{E}^2$  the magnitude of electric field applied.

From equation 6.6, if the conductivity of the particle is greater than the medium, the CM factor gives positive values and the dielectrophoretic force on the particle pushes the particle towards high field density regions thus trapping them i.e. the particle gets attracted towards insulating obstacle region whereas, if the conductivity of the particle is less than that of the medium, the particles are repelled from the high field density regions thus yielding in negative values of CM factor and movement of particles in the fluid streamlines i.e. particles are repelled from the insulating obstacle regions. The conductivity of the particle ( $\sigma_p$ ) is given as a function of surface conductivity and bulk conductivity<sup>204</sup>:

$$\sigma_p = \sigma_b + \frac{2K_s}{r} \quad (6.8)$$

where  $\sigma_b$ , the bulk conductivity,  $K_s$  is the surface conductance and ' $r$ ' the radius of the particle. In pure DC-iDEP technique, particle motion is governed by both electrokinetic and dielectrophoretic forces as:

$$\vec{j} \propto (\vec{u}_{EK} + \vec{u}_{DEP}) \quad (6.9)$$

where  $\vec{j}$  is the particle flux,  $\vec{u}_{EK}$  is the electrokinetic velocity and  $\vec{u}_{DEP}$  dielectrophoretic velocity. Electrokinetic velocity can be expressed as the sum of electro-osmotic and electrophoretic mobilities:

$$\vec{u}_{EK} = \mu_{EK} \vec{E} = (\mu_{EP} + \mu_{EO}) \vec{E} \quad (6.10)$$

where  $\mu_{EK}$  is the electrokinetic mobility,  $\mu_{EP}$  electrophoretic mobility,  $\mu_{EO}$  electro-osmotic mobility and  $\vec{E}$  applied electric field to create non-uniformities in the channel. Electrophoretic mobility could be neglected for large particles having lower surface charges<sup>204</sup>

$$\mu_{EK} \cong \mu_{EO} = \frac{\zeta \varepsilon_m}{\eta} \quad (6.11)$$

where  $\zeta$ ,  $\varepsilon_m$ ,  $\eta$  are zeta potential, permittivity of suspending medium and viscosity of suspending medium respectively.

A spatially dense non-uniform field ( $\vec{E}^2$ ) is created as the DC field lines diverge around the insulative obstacle. Due to the insulating obstacle, a high electric field density region is produced within narrow channel regions created by the obstacle. Fluid flow drives the particle through this narrow constriction, while the field gradient shape aids in particle motion. Since DC-iDEP forces push the particle towards or away from the high field density, the particle experiences an attractive or repulsive force as it flows around the corner of the obstacle, thus facilitating particle motion according to its polarizability.



Many geometrical configurations and operating conditions are possible as a result of DC dielectrophoresis.

In the next sub-section an overview of the insulating obstacle geometries explored by different research groups is provided. This is organized according to single obstacle, multiple obstacles and other geometries explored to achieve sorting or trapping of particles.

#### **6.4.1 Insulating obstacle geometry**

Researchers have created spatial non-uniformities using various insulating obstacle designs having single or multiple obstacles and in some cases modified channel geometry for achieving sorting or trapping of particles. Single obstacles embedded in the channel like an a rectangular obstacle<sup>81,114,117-118,137</sup>, a triangular hurdle<sup>118</sup>, a constriction in the depth of the channel rather than the width<sup>205</sup>, a single microchannel constriction<sup>115</sup> oil droplet<sup>120</sup>, and an oil menisci as field shaping barriers<sup>206</sup>; multiple obstacles like metallic trap<sup>128,207</sup>, insulating posts<sup>112-113,116,126-127,132,208-209</sup>, tetragon structures along the channel<sup>210-211</sup>, and multiple rectangular blocks<sup>212</sup>; and other geometries which modify the channels like non-converging saw tooth channels<sup>121</sup>, a set of aligned teeth<sup>102</sup>, saw tooth channel<sup>121</sup>, open top microstructures<sup>213-214</sup>, serpentine microchannels<sup>122-123</sup>, a series of iterative curves<sup>122</sup>, arrays of circular channels<sup>215</sup> and honey comb membrane design<sup>125</sup> are discussed below separately in different sections. Each obstacle shape yields differing spatial variations in the electric field. Devices were fabricated in quartz by standard lithography techniques and external gold electrodes were attached to a high voltage source.

### 6.4.1.1 Single obstacle geometry

In this, the channel contains one insulating obstacle for achieving manipulation of bioparticles. These may be made of different materials like PDMS, glass or oil. Rectangle and triangle obstacles fabricated using PDMS by soft lithography have been extensively applied to achieve sorting of particles and bioparticles by various groups<sup>114,117-118,137</sup>. An example showing how electric field lines diverge around an insulating rectangular obstacle is shown in Figure 6.1 reproduced from our research. The magnitude of the DEP force is proportional to the particle size as shown in equation 6.7. Larger particles tend to deflect away from the corner of the obstacle due to larger DEP forces experienced by particle<sup>118</sup> thus repelling away from the insulating obstacle region. The dark red region in Figure 6.1 represents high field intensity region and particles experience dielectrophoretic effect in that region which gets deflected into the channels depending on the polarizability of the particle. This is consistent with results observed in our group where smaller sized fluorescent polystyrene particles, 6.2  $\mu\text{m}$ , were deflected least from the insulating obstacle and larger sized particles 10  $\mu\text{m}$  were deflected most from the insulating obstacle geometry.

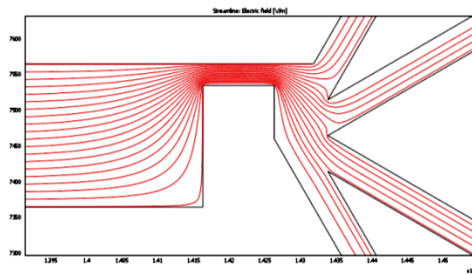


Figure 6.1 Electric field lines around the rectangular obstacle, darker regions represent high field density regions, as generated by COMSOL simulations.

Single curved constriction in the depth of the channel has been shown to control linear and nonlinear electrokinetic effects by employing both DC and AC fields<sup>205</sup>. Linear effects (electro-osmosis and electrophoresis) control the particle motion, whereas nonlinear effects (dielectrophoresis) are applied when the particle approaches the constriction. DEP is applied perpendicular to the channel constriction and the ratio between linear and non-linear decides whether the particle gets trapped or sorts. The authors sorted 2 and 3  $\mu\text{m}$  polystyrene particles by employing 3D shaped electric fields in a continuous throughput system<sup>205</sup>. Another group employed a microchannel constriction along the length of the channel<sup>115</sup> by employing both AC and DC fields to improve focusing efficiency of 5 and 10  $\mu\text{m}$  microparticles. Two electric field gradients are created in the channel due to the constriction and singularity around the corners. The electric field lines at these points are parallel and normal to the electric field applied respectively.

Another class of single insulating obstacles uses oil to create obstacles thus achieving spatial non-uniformities in electric field as shown in Figure 6.2. The greatest advantage of the oil droplet and oil menisci design is the controllable droplet size, providing a direct and dynamic control of the field gradient to achieve various separation configurations<sup>120,206</sup>. The gap width between the oil obstacle and the wall can be easily controlled and Li. D *et al.* group reported this gap width to be an important parameter to achieve good separation efficiency<sup>120</sup>.

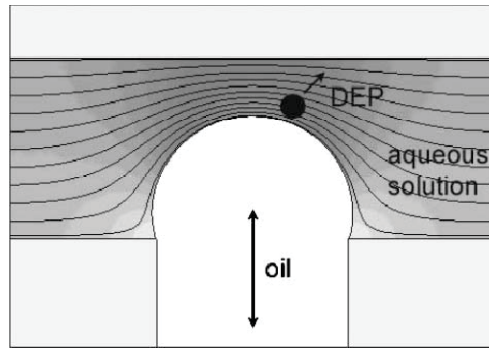


Figure 6.2 Electric field lines and contours of the field strength near the oil droplet. A particle in the high-field region is exposed to a negative DEP force. The darker region has stronger electrical field.<sup>120</sup> [Barbulovic-Nad I, Xuan X, Lee JSH, Li D (2006) Dc-dielectrophoretic separation of microparticles using an oil droplet obstacle. *Lab on a Chip* 6:274-279] – Reproduced by permission of The Royal Society of Chemistry.

Electric field gradient depends on this gap width and even if low voltages are applied, electric field gradient should be high enough to achieve separation of particles. This method can be applied for manipulation of biological particles that are sensitive to high voltages, which may avoid cell lyses and significant Joule heating of the medium<sup>120</sup>. But the only disadvantage of using low voltages is that the separation of cells becomes slow as the velocity of the particle decreases. For continuous separation of particles and to prevent trapping, electro-osmotic flow (EOF) of the medium is needed<sup>120</sup>; this can be controlled via judicious choice of wall materials or coatings. Higher DEP forces can be achieved by increasing the oil droplet size to increase the constriction in the channel thus compacting electric field lines to increase the field gradient as seen in equation 6.7. An oil menisci obstacle by Thwar *et al.* group succeeded in trapping particles by controlling the position and extent of the location of the oil menisci<sup>206</sup>. Oil filled syringes were used to create this hurdle. This allows for good trapping of conductive biomolecules like DNA, as the conductivity of these is much greater than the medium. The main

disadvantage is the absence of extensive reusability of the microchips due to fouling of channels by the use of oil.

#### 6.4.1.2 Multiple obstacle geometry

Chou *et al.* was the first to demonstrate DC-iDEP phenomena for sorting of single and double stranded DNA by employing dielectrophoretic traps in the channel<sup>128,207</sup>.

Figure 6.3, illustrates a schematic representation of a dielectrophoretic trap<sup>128</sup>. These DEP traps are insulating constrictions in the channel.

Another form of multiple insulating structures extensively used in DC-iDEP manipulation of particles is the array of insulating posts<sup>112-113,116,124,126-127,132,204,208-209,216-217</sup>. An array of insulating posts made of glass was utilized to create field non-uniformities in the channel. These insulating posts could be adjusted to achieve both streaming and trapping DEP as reported by Cummings and Singh. They could be made of any geometry diamond or circular. In the diamond shaped insulating posts, high electric field intensity regions occurred at the right and left vertices of the insulating post where as low field density regions were at the top and bottom of the insulating posts<sup>113</sup>. If the angle of the array of insulating posts is changed, the whole DEP behavior on the particle could be affected. In circular insulating posts, the region of high electric field density was between two insulating posts<sup>132</sup>.

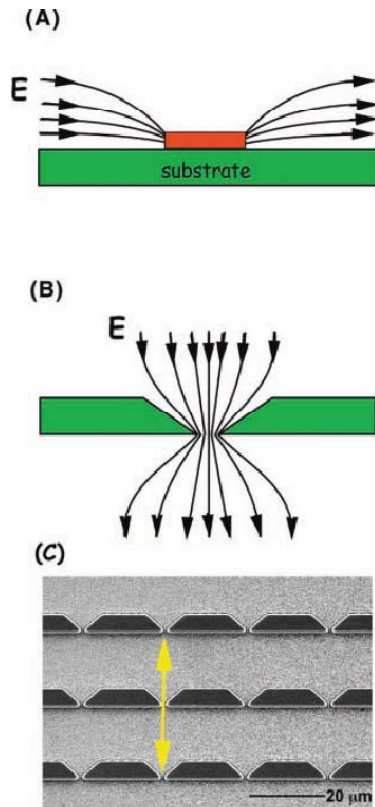


Figure 6.3 Schematic of a microfluidic DEP trap. (A) A metallic DEP trap made of micro fabricated wire(s) on a substrate. The wire(s) may be either free-floating or connected to a voltage source. (B) An electrodeless DEP trap made of dielectric constrictions. The solid lines are electric field lines  $\vec{E}$ . (C) A scanning electron micrograph of an electrodeless DEP device consisted of a constriction array etched in quartz. The constrictions are  $1 \mu\text{m}$  wide and  $1.25 \mu\text{m}$  deep. The whole chip measures  $1 \times 1 \text{ cm}$ . The double-headed arrows show the applied electric field direction  $z$ . [Reprinted from Biophysical Journal, 83, Chia-Fu Chou, Jonas O. Tegenfeldt, Olga Bakajin, Shirley S. Chan, Edward C. Cox, Nicholas Darnton, Thomas Duke, and Robert H. Austin, Electrodeless dielectrophoresis of single- and double-stranded DNA, 2170-2179, Copyright 2002 with permission from Elsevier]<sup>128</sup>.

Lapizco *et al.* group have simulated trapping zones in these insulating posts which could predict the location and magnitude at these trapping zones<sup>217</sup>. Sabounchi *et al.* group developed a novel technique by combining DC-iDEP and impedance measurement for trapping and analyzing bacteria employing DC and AC signals respectively<sup>209</sup>.

Conductless tetragon structures in the microchannels were applied to trap particles. Maximum electric field density region occurs at the corners of the tetragon structures. The spacing between the two tetragon structures could be adjusted to obtain maximum trapping efficiency<sup>211</sup>. Multiple rectangular insulating blocks were employed to concentrate and separate particles. Use of multiple blocks enhanced the dielectrophoretic effect on particles thus confining the particles in a small region for further analysis<sup>212</sup>.

#### 6.4.1.3 Channel variations

Apart from the insulating obstacles embedded in the microchannel, various channel geometry modifications exist to achieve trapping or sorting of particles as discussed in this section. Chen *et al.* explored non-converging saw tooth channel design for separation of small particles. Sharper corners of the teeth create a strong dielectrophoretic effect on the particles i.e. high electric field density region. Separation of these particles depends on electrophoretic and dielectrophoretic forces<sup>121</sup>. Blocking and trapping depends on particle properties and the channel geometry. If the channel geometry is fixed, the blocking depends only on the particle mobility ratio, the electric field and the spacing between the teeth. Selective blocking and trapping of particles can be achieved by varying the channel geometry<sup>121</sup>. Since, the same concept of non converging saw tooth channel design applies for saw tooth channel geometry and set of aligned teeth geometry, it is not explained in greater detail.

An open top microchannel design developed to trap cells could be used further for treatment of cells in a manner such as contact detection. Open-top microchannel adapted the same insulating obstacle geometry design as Chou *et al.*, DEP traps as shown in Figure 6.3. In this microsystem, loading of the sample into the device and cleaning after

analysis are much easier and faster compared to a closed channel design. Joule heating effects are lower due to dissipation of heat to the open air. This also offers no interference in fluorescence detection of the intensity of emitted light. Certain limitations arise in this design including sample evaporation<sup>213-214</sup> and convective currents. However, the open-channel concept was effective and constrictions in the channels created the necessary non-uniformity for trapping of human carcinoma (HeLa) cells. From the numerical results presented, the DEP force was still considered to be strong within 70  $\mu\text{m}$  of the constriction's height<sup>214</sup>.

In a serpentine channel design, the DEP force is stronger in the inner corners compared to outer corners<sup>123</sup> due to one left U-turn followed by right U-turn. Particles are uniformly distributed at the straight sections of the channel and become focused into streams along the channel centerline when exiting out of the serpentine channel. This behavior is consistent with streaming DEP indicative of nDEP where the dielectrophoretic force acts to push the particles down the electric field gradient while the particle simultaneously experiences larger translational forces due to EOF. The width of the focused stream is also dependent on the channel width and the length of serpentine section<sup>123</sup>. The same concept holds for iterative curve channel geometry and it is not explained in much detail here.

Another channel geometry explored is the circular channel design by Zhang *et al.* as shown in Figure 6.4<sup>215</sup>. The separation of particles depends on the particle's dielectric properties and they are driven through the channel by electro-osmosis<sup>215</sup>. The electric field gradient directs the particle to the center of the channel i.e. high field density region is observed towards the center of the channel. But due to nDEP, the particles move away from the center towards a different location depending on the dielectrophoretic effect on



them. Another novel design was presented by Cho *et al.* where microfabricated plastic membranes were used to concentrate bioparticles<sup>125</sup>. The membrane had honeycomb size pores that were positioned between two electrodes made of Indium tin oxide. High electric field density occurred at the corners of the pores and due to positive DEP effect the bioparticles were trapped. Trapping was achieved experimentally and COMSOL simulations resulted in characterizing regions in the membrane where highest trapping occurred.

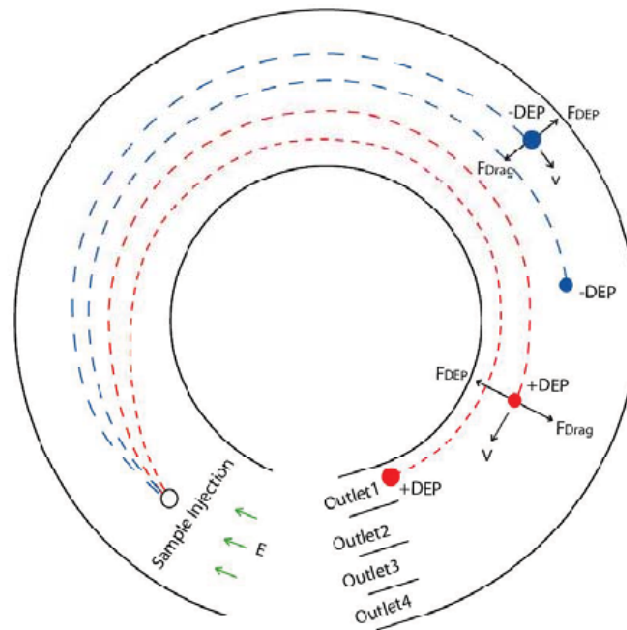


Figure 6.4 Schematic diagram of the dielectrophoretic separation in a circular microchannel. Reproduced with permission<sup>215</sup>.

#### 6.4.2 Comprehensive review of literature

In this review article, some of the above discussed insulating obstacle geometries have been compared as shown in Table 6.1. It provides a review of DC-iDEP research, including the media and particles used in those studies (potassium buffered saline solution and 10  $\mu\text{m}$  diameter polystyrene particles were considered for simulation study),

the obstacle geometries, and the applied electric fields. Estimates of the DEP force from COMSOL simulations and manual calculations, along with the COMSOL estimated relative DEP force with the orders of magnitude difference between the highest and lowest DEP force within the system are also listed. The latter value is a measure of how effective a given obstacle is increasing the DEP force. DEP force depends on size of the particle, electric potential applied and medium properties in which the particle is suspended. The geometry of the insulating obstacle is responsible for producing field non-uniformities thus affecting the gradient of electric field and impacting dielectrophoretic force experienced by the particle. Medium properties have a direct effect on CM factor as shown in equation 6.7 and this factor decides whether the particle will experience a negative DEP or positive DEP. Negative DEP causes streaming or sorting of particles into stream lines whereas positive DEP causes the particles to be trapped or attracted towards the insulating obstacle.

Table 6.1 Review of DC-iDEP research, including the media and particles used in those studies, insulating obstacle geometries, and applied electric fields. Estimates of the DEP force from COMSOL simulations and manual calculations, along with the COMSOL estimated relative DEP force, with the orders of magnitude difference between the highest and lowest DEP force within the system are also listed. The latter value is a measure of how effective a given obstacle is increasing the DEP force.

Reference	Device material properties	Coatings/sealing method	Particle of interest (Radius of particle) ( $\mu\text{m}$ )	Electric field	Insulating obstacle shape and geometry	Medium properties	Comments	Max. force (N)* (COMSOL)	Max. force (N)* (Manual calculation)	Difference in order of magnitude
<i>Chou CF et al.</i> <sup>128</sup>	Quartz	Oxygen plasma/POP-6 (polyacrylamide)	Single and double stranded DNA (0.001)	0-1 $\text{kV}_{pp}/\text{cm}$ , 200-1000 Hz	DEP trap: 1 $\mu\text{m}$ wide and 1.25 $\mu\text{m}$ deep	Tris borate EDTA, pH=8	Trapping and concentration via AC DEP	707 V/cm (RMS): $5.109 \times 10^{-11}$	707 V/cm (RMS): $1.39 \times 10^{-9}$	RMS: 11
								1 kV/cm (Max): $1.022 \times 10^{-8}$	1 kV/cm (Max): $2.78 \times 10^{-9}$	Max: 10
<i>Cummings and Singh</i> <sup>113</sup>	Glass	Thermal bonding	latex particles (0.1)	250-1000 V/cm	Diamond, square and circular posts: Distance between two posts is 63 $\mu\text{m}$	1 mM PBS, pH=7.7	Streaming and trapping DEP	Square: 1000 V/cm: $1.732 \times 10^{-10}$	Diamond: 1000 V/cm: $5.502 \times 10^{-10}$	Diamond: 3
								Circle: 1000 V/cm: $1.608 \times 10^{-11}$	Circle: $4.42 \times 10^{-9}$	Circle: 6
<i>Lapizco-Encinas BH et al.</i> <sup>116</sup>	Glass	NA	T4 virus (0.045)	400 V/cm	Array of microbumps	BU buffer	First article on trapping of virus	$2.480 \times 10^{10}$	$4.94 \times 10^{-9}$	8

Table 6.1 (Continued)

<i>Lapizco-Encinas BH et al.</i> <sup>112</sup>	Glass	Thermal bonding	<i>E. Coli</i> (0.25)	0-2000 V/cm	Square, triangle, circular insulating posts: 200 μm in diameter and 250 μm distance between two posts Circular insulating posts: 200 μm in diameter and 250 μm distance between two posts	DI water, 2.25 μS/mm	First separation and concentration of live/dead bacteria	2000 V/cm: 3.901x10 <sup>-10</sup>	2000 V/cm: 4.450x10 <sup>-11</sup>	6
<i>Lapizco-Encinas BH et al.</i> <sup>124</sup>	Glass	NA	<i>E. Coli</i> , <i>B. Subtilis</i> , Tobacco Mosaic Virus (0.009)	0-2000 V/cm	Circular insulating posts: 200 μm in diameter and 250 μm distance between two posts	DI water-NaOH-KCl, pH=7.5-8.0, 10-20 μS/cm		2000 V/cm: 2.560x10 <sup>-15</sup>	2000 V/cm: 4.450x10 <sup>-11</sup>	10 V: 2 2000 V: 3
<i>Barbulovic-Nad I et al.</i> <sup>120</sup>	PDMS	Plasma sealed	Fluorescent polystyrene particles (0.5; 2.85; 7.85)	80-240 V/cm	Oil droplet: Gap between oil droplet and channel wall is 46 μm	DI water	Separation of microparticles	240 V/cm: 6.260x10 <sup>-12</sup>	240 V/cm: 3.480x10 <sup>-12</sup>	7
<i>Kang KH et al.</i> <sup>117</sup>	PDMS (-80 mV)	-NA-	Carboxylate-modified polystyrene particles (2.85; 5.125; 7.85)	500-900 V/cm	Rectangular obstacle: 240x130 μm obstacle; 60 μm between wall and obstacle	1 mM sodium carbonate buffer	Separation of microparticles by size	360 V/cm: 9.743x10 <sup>-11</sup>	360 V/cm: 6.010x10 <sup>-12</sup>	4
<i>Zhang L. et al.</i> <sup>215</sup>		Simulation-based, discussion about particle trajectories	micro-particles (5 and 10)		Circular channel: 50 μm inner circle, 100 μm outer circle, 20 μm height		Separation of particles in a circular channel	6.006x10 <sup>-12</sup>	2.500x10 <sup>-16</sup>	3

Table 6.1 (Continued)

<i>Hawkins B.G. et al.</i> <sup>205</sup>	Zeonor 1020R	Hot pressing bonding	Microparticles (0.875; 1; 1.5)	DC biased AC field (25 or 50 V/cm; 1 kHz frequency)	Insulative constriction	-NA-	3D insulative technique first reported	10 μm -wide ridge: 50 V/cm: 1.195x10 <sup>-10</sup> 100 μm -wide ridge: 50 V/cm: 1.013x10 <sup>-10</sup>	10 μm -wide ridge: 50 V/cm: 6.95x10 <sup>-13</sup> 100 μm -wide ridge: 50 V/cm: 6.95x10 <sup>-14</sup>	<b>10 μm -wide ridge: 12</b> <b>100 μm -wide ridge: 8</b>
<i>Thwar et al.</i> <sup>206</sup>	PDMS	UV-Ozone	Fluorescent polystyrene microparticles  <i>Bacillus subtilis</i> , <i>E. coli</i> , and <i>Staphylococcus</i> (0.009)	DC voltage -500 and +500 V	Field shaping oil barriers	0.05 S/m	Simulation and experiments	6.080x10 <sup>-13</sup>	2.5x10 <sup>12</sup>	<b>6</b>
<i>Pysheer M. et al.</i> <sup>102</sup>	Glass and PDMS devices	Plasma sealed	<i>epidermidis</i> (0.009)	DC field 200 V/cm and 300 V/cm	Saw tooth: Varying tooth geometry. Max width is 500 μm	-NA-	Separation of complex biological particles	Height 150 μm, base 150 μm: 300 V/cm: 5.726x10 <sup>-12</sup> H 240, B 240: 300 V/cm: 1.600x10 <sup>-11</sup> H 100, B 200: 300 V/cm: 4.983x10 <sup>-12</sup> H 240, B 480: 300 V/cm: 1.410x10 <sup>-11</sup>	Height 150 μm: 300 V/cm: 7.150x10 <sup>-13</sup> H 240: 300 V/cm: 9.630x10 <sup>-13</sup> H 100, B 300 V/cm: 2.500x10 <sup>-12</sup>	<b>H150, B150: 3</b> <b>H240, B240: 3</b> <b>H100, B200: 2</b> <b>H240, B 480: 2</b>
<i>Zhang L. et al.</i> <sup>122</sup>	Silicon-SU8-Glass wafer assembly	Adhesive bonding	Carboxylate-modified FluoSpheres (1)	DC-biased AC field; DC 50-90 V/cm and 1 MHz	Iterative Curves: Inner radius is 100 μm and outer radius is 200 μm	-NA-	Separating submicron particles at low voltages	90 V/cm: 1.327x10 <sup>-13</sup>	90 V/cm: 2.250x10 <sup>-11</sup>	<b>8</b>

Table 6.1 (Continued)

<i>Sabounchi P. et al.</i> <sup>209</sup>	Zeonor 1060	Pressure and temperature bonding	<i>B. Subtilis</i> spores and carboxylate-modified microspheres (1.5, 1)	DC for concentrating and AC for flowing to impedance detection on port	Insulating posts	1-2 $\mu\text{S}/\text{cm}$	Coupling iDEP with impedance detection	$1.010 \times 10^{-10}$	$3.130 \times 10^{-11}$	6
<i>Sabounchi P. et al.</i> <sup>218</sup>	Zeonor 1060	-NA-	<i>E. coli</i> cells and <i>B. Subtilis</i> (1.5)	DC 500-1500 V/cm	Insulating posts	60-150 $\mu\text{S}/\text{cm}$	Experimental and numerical study of Joule heating effects in a polymeric iDEP device	1500 V/cm: $1.925 \times 10^{-15}$	1500 V/cm: $1.000 \times 10^{-10}$	2
<i>Ozuna - Chacon S. et al.</i> <sup>204</sup>	Glass	-NA-	Carboxylated polystyrene microspheres (0.5)	DC field: 200-800 V/cm	Cylindrical posts: 440 $\mu\text{m}$ diameter, 10 $\mu\text{m}$ height and 520 $\mu\text{m}$ center to center separation of posts	25-100 $\mu\text{S}/\text{cm}$	Higher fields, high conductivity and low pH-stronger negative DEP force for trapping	800 V/cm: $1.759 \times 10^{-10}$	800 V/cm: $2.230 \times 10^{-11}$	5
<i>Lapizco Encinas B.H. et al.</i> <sup>126</sup>	Glass	-NA-	Protein	DC field: 700-1600 V/cm	Cylindrical posts: 440 $\mu\text{m}$ diameter, 10 $\mu\text{m}$ height and 520 $\mu\text{m}$ center to center separation of posts	25-100 $\mu\text{S}/\text{cm}$	Trapping at low conductivity suspending medium conditions	1600 V/cm: $6.231 \times 10^{-10}$	1600 V/cm: $8.900 \times 10^{-11}$	5
<i>Kang Y. et al.</i> <sup>118</sup>	PDMS	-NA-	Fixed HIV infected WBC and live mammalian breast cancer cells (4-7; 10-30)	DC voltage 0-138 V/cm	Rectangular and triangular hurdle: 240x130 $\mu\text{m}$ obstacle; 60 $\mu\text{m}$ between wall and obstacle	NA	Separation by size	Rectangle: 138V/cm: $2.939 \times 10^{-12}$ Triangle: 138V/cm: $2.930 \times 10^{-12}$	138 V/cm: $8.830 \times 10^{-13}$	Rectangle: 10 Triangle: 2

Table 6.1 (Continued)

<i>Zhu J. et al.</i> <sup>123</sup>	PDMS (5.5 × 10 <sup>-8</sup> m <sup>2</sup> /Vs)	Plasma sealed	Polystyrene particles (2.5, 5)	DC 1000, 2000, 5000 V/cm	Serpentine channel: Serpentine: 200 μm height, 200 μm between two corners and 50 μm wide channels	160 μS/cm	DC-biased AC electric field in further experiments.	5000 V/cm: 1.725x10 <sup>-9</sup>	5000 V/cm: 1.390x10 <sup>-9</sup>	9
<i>Martinez-Lopez J.I. et al.</i> <sup>216</sup>	Glass (1.76-2.55 × 10 <sup>-8</sup> m <sup>2</sup> /Vs)	-NA-	Carboxylated polystyrene microspheres (0.5)	DC 800 V	Cylindrical posts	25, 50 and 100 μS/cm; 6-9 pH range	EOF increases by increasing pH or decreasing conductivity	1.030x10 <sup>-15</sup>	3.560x10 <sup>-11</sup>	2
<i>Zhu J. et al.</i> <sup>115</sup>	PDMS (6 × 10 <sup>-8</sup> m <sup>2</sup> /Vs)	Plasma sealed	Polystyrene particles (2.5, 5)	Pure DC 100 kV/m; DC-biased AC field 10 kV/m with 1 kHz frequency	Microchannel constriction: Constriction 56 μm height and 188 μm wide	160 μS/cm	Pure DC and DC-biased AC field compared	Pure DC: 2.580x10 <sup>-09</sup>	Pure DC: 4.970x10 <sup>-11</sup>	11
<i>Jen C.P. et al.</i> <sup>214</sup>	PDMS	Plasma sealed	Human carcinoma (HeLa) cells (5)	DC field 18 V/cm and frequency 10 Hz to 1 MHz	Open top microstructures: 500 μm wide between insulators and distance between Constrictions are 20 μm	1.76 mS/m	Cross over frequency between 3 and 4 kHz	1.765x10 <sup>-09</sup>	4.510x10 <sup>-12</sup>	5
<i>Gallo-Villanueva R. C. et al.</i> <sup>127</sup>	PDMS (2×10 <sup>-4</sup> cm <sup>2</sup> /Vs)	-NA-	Linear DNA particles (pET28b) (0.001)	DC field 500-2000 V/cm	Rectangular insulating post: 470 μm diameter and 510 μm center to center between posts	pH 10.8-11.15; 100-120 μS/cm	500-1500 V/cm cells immobilized, 2000 V/cm concentrated	2000 V/cm: 8.850x10 <sup>-11</sup>	2000 V/cm: 2.780x10 <sup>-10</sup>	4

Table 6.1 (Continued)

<i>Cho Y.K. et al.</i> <sup>125</sup>	Silicone	Plasma sealed	<i>E. coli</i> cells (1.5)	AC field (1280 V/cm and 300 kHz)	Honey-comb type pores made of SU-8 2100: Hexagonal pore; side length is 50 μm; distance between pores 112.6 μm	0.5 mS/m	Concentrating <i>E. coli</i> cells	4.05x10 <sup>-11</sup>	
<i>Chen D. et al.</i> <sup>138</sup>	PDMS	-NA-	Micro and nano particles (0.465)	DC 50-1000V (20-400 V/cm)	Insulating microstructures	1-10 mS/m	Microfluidic concentration application in concentrating target cells of interest Larger fields yield in trapping; different particle trajectory shifts	400 V/cm: 2.553x10 <sup>-9</sup>	20 V/cm: 9 400 V/cm: 10
<i>Ai Y. et al.</i> <sup>219</sup>		Numerical investigation using transient ALE finite element model	Microparticles	-NA-	Converging diverging microchannel			171.9 V/cm: 2.786x10 <sup>-15</sup>	2 2

To compare different insulating obstacle geometries reported in literature, the DEP force exerted on a 10 μm polystyrene particle was considered. The dielectrophoretic force was estimated using the COMSOL Multiphysics<sup>®</sup> 3.3 simulation software. The Conductive Media DC physics mode was used for the simulation. This physics mode is a time-independent model which can calculate electric field strength within a conductive medium, such as a microchannel filled with an aqueous solution. The governing equation for the system is,

$$\nabla d(\sigma \nabla V - J^e) = dQ_j \quad (6.12)$$

where  $\sigma$  is the electrical conductivity of the medium,  $V$  the electric potential and  $J^e$  is an externally generated current density.



A static mesh was used for the simulations. The material properties of the system were kept constant so that the differences in the estimated DEP forces would only be due to the different geometries and applied field strengths. A medium conductivity of 9 S/m (a typical value for potassium buffered saline solution) was used, and the CM factor was equal to -0.5 since the permittivity of polystyrene is very small compared to that of potassium buffered saline solution. The permittivity of the medium was  $7.08 \times 10^{-10}$  F/m. DEP force is maximum at the corners of the insulating obstacle and thus DEP force was estimated at this point. COMSOL automatically returns the value of the electric field strength in the direction of flow as a variable, and electric field gradient was calculated from this value and the width of the channel at the point where the DEP force was estimated using equation 6.7. The DEP force was estimated using equation 6.7 for spherical particle geometry.

$$\nabla |\vec{E}|^2 = \frac{|\vec{E}|^2}{w} \quad (6.13)$$

where  $\vec{E}$  is the electric field strength in the direction of the fluid flow calculated by COMSOL and  $w$  is the width of the channel or the distance between two obstacles at the point where the DEP force is estimated. For the values used in the simulation, the DEP force reduces to:

$$\vec{F}_{DEP} = 2.78 \cdot 10^{-15} \nabla |\vec{E}|^2 \quad (6.14)$$

In the cases of DC-biased AC-fields, only the DC component was taken into account. For cases of AC-iDEP, the DEP force was calculated both for the maximum field strength and the root mean square (RMS) field strength. In addition to the COMSOL simulations, the DEP forces in each system were also estimated by manual calculations,

which were also based on equations 6.6 and 6.7. Finally, the maximum and minimum DEP forces present in the system were compared to find out which geometries created a greater relative increase in the DEP force. The lowest DEP force present in the system is the “ambient” DEP force, which is the uniform value found away from the obstacles. Typically, the maximum DEP force was 3 to 10 orders of magnitude greater than the lowest value.

As the previous discussion demonstrates (also outlined in Table 6.1), a complete picture of insulator shape, insulator material, and voltage dependencies in channel geometries has not yet been attained. A number of models are notable such as rectangle, triangle, oil droplet, saw tooth, serpentine, circular, open-top microstructure and a model of four channel outlet with rectangular insulating obstacle geometry from our group but none give perfect agreement with experiments overall operating ranges.

Apart from DC-iDEP and traditional DEP technique, other techniques exist where in separation or trapping could be achieved as discussed in the next section. These alternative DEP techniques discussed in the next section vary from the DC-iDEP and AC-DEP in their electrode geometry to create non-uniformities. Not all dielectrophoretic systems use embedded metal electrodes or insulating obstacle geometries to manipulate particles; other different mechanisms exist and a brief overview has been presented in the next section. The objective here is to provide a review based on different electrode geometry available for dielectrophoresis and emphasizing particularly on insulating obstacle geometry.

### 6.4.3 Additional alternative dielectrophoretic schemes

Not all obstacles in a microchannel are created by insulating materials. Another approach is to use a floating electrode, where in long, coplanar uncoupled electrodes are used to generate DEP<sup>203,220-221</sup>. Figure 6.5 shows a comparison between classic DEP configurations and floating electrode DEP devices (feDEP) configuration devices. Only two electrodes are excited by a signal and the remaining electrodes are allowed to float as in Figure 6.5 (b).

These (feDEP) does not require an external signal source, making it easier to fabricate and miniaturize<sup>203</sup>. Some of the advantages seen in feDEP devices are: (i) decreased number of connections to the external signal source, (ii) reduced Joule heating, (iii) easier fabrication, (iv) ability to manipulate nanoparticles, and (v) reduced nanoparticle Brownian motions<sup>203,221</sup>. The DEP force experienced by the particle could be increased by choosing much smaller electrode features and reducing the gaps between them. However if electric potential applied is increased to create strong DEP effect, this may lead to Joule heating and sometimes hazardous for the bioparticles being manipulated<sup>203</sup>.

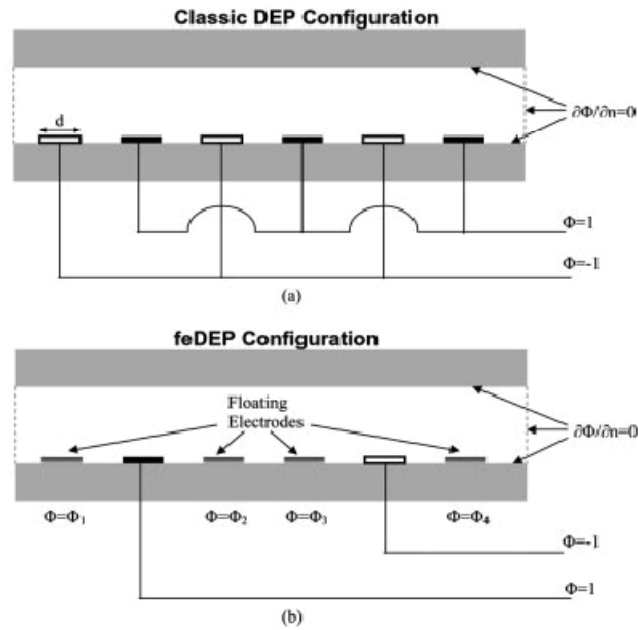


Figure 6.5 Models and boundary conditions used for the finite element calculations: (a) the classic DEP configuration and (b) the feDEP configuration<sup>203</sup> [Golan S, Elata D, Orenstein M, Dinnar U (2006) Floating electrode dielectrophoresis. *Electrophoresis* 27:4919-4926. Copyright Wiley-VCH Verlag GmbH & Co. KGaA. 2006 Reproduced with permission].

Another novel technique recently developed by Shafiee H. *et al.* is the contactless DEP (cDEP) technique, similar to DC-iDEP technique<sup>133,222</sup>. Here, the electrodes and the sample are not in contact and they are separated by thin insulating microbarriers. The absence of contact between the sample fluid and the electrodes prevents contamination, electrochemical effects, gas bubble generation, and Joule heating compared to the conventional dielectrophoresis. The electrodes are placed in a highly conductive medium isolated from the main channel by thin insulative barriers made of PDMS<sup>222</sup>. The main channel containing the sample has a funnel shaped design and thin insulating PDMS barriers are placed just at the intersection where the main channel tapers into small channel. Due to the geometry of the electrode channel, spatial non-uniformities are caused when a high frequency AC signal is applied. High electric field density regions at

the corners in the main channel is caused by the field non-uniformities in the side channel, thus exerting DEP effect on the particles to be focused and separated. According to the authors, this technique is robust, simple and inexpensive like DC-iDEP which can overcome some disadvantages of DC-iDEP devices. They have applicability in drug screening, disease detection and treatment and also in homeland security biomedical applications<sup>133</sup>.

All these insulating obstacle geometry needs to be fabricated to be integrated into the microfluidic platform. In the next section, a brief overview of the most often used fabrication technique in developing DC-iDEP devices has been presented. Detailed procedure is not discussed and has been provided elsewhere<sup>46</sup> (Chapter 2). Different sealing techniques and surface modifications are available to manipulate electrokinetic forces in the channel, which are also briefly included in the next section.

## 6.5 Fabrication of insulator-based microdevices

Different techniques have been employed by researchers to fabricate insulator-based microdevices<sup>49-50</sup>. Some common methods include soft lithography<sup>46,48,51</sup>, wet etching, injection molding<sup>223</sup> and hot embossing. The method of rapid prototyping developed by Whitesides *et al.* group has been extensively used for fabricating PDMS devices<sup>46,60</sup>. Not all polymers can be used to fabricate devices and the physical and chemical properties of these polymers need to be considered before they can be fabricated. To date many materials have been tried for fabricating these devices; Zeonor and PDMS<sup>224</sup> have been the most commonly used plastics<sup>225</sup>. Once the PDMS devices are developed, to form channels they can be sealed on to the same substrate as that of the microdevice or on glass. Different sealing methods exist like UV-ozone<sup>78-79</sup>, solvent

sealing<sup>65</sup>, temperature sealing<sup>66</sup>, pressure sealing and plasma-oxidation process<sup>46,67,70</sup>. In order to achieve dielectrophoretic trapping or separation of particles, it is important to consider surface characteristics of the channel to avoid particles being adsorbed onto the channel. Some of the surface modifications are the plasma-oxidation treatment, use of surfactants<sup>71-72,74</sup>, and dynamic coating of channels<sup>74,76,223,226</sup>.

The insulating obstacle geometry can have a substantial impact on the shape of the electric field and thus the electric field gradient each particle is exposed to as discussed above. But dielectrophoretic force is also dependent on the electric field applied to achieve separation. Electric field generated by the insulating obstacles are easily and more conveniently tunable to achieve particle trapping or separations. In the next section, the authors present a discussion where combined AC and DC fields can be used to achieve DC-iDEP trapping but with lesser magnitude of applied potential.

## **6.6 Electric field characteristics**

Traditionally DC insulator based dielectrophoresis employs DC electric fields to achieve particle manipulation like our own research work. The research carried in our lab employed very low DC electric field strength (17.12 V/cm) to achieve separation of fluorescent microparticles in rectangular insulating obstacle geometry microdevice, in which the inlet channel branches out into four outlet channels. Two DC electric fields (6.85 and 17.12 V/cm) were compared at different suspending medium conductivity conditions (50-850 mS/cm), higher electric fields yielded better separation of microparticles. Our approach is very novel since a very low electric field is used to achieve sorting into a four channel outlet system. Researchers have applied two channel systems in the past to achieve separation using DC-iDEP but our lab is the first to apply a

four channel system sorting of particles. High electric field gradient is caused by the insulating obstacle and this was achieved by manipulating the distance between the wall and the insulating obstacle geometry where the highest DEP effect on particles was exerted. Successful distinction of 6.2 and 10  $\mu\text{m}$  particles using a voltage of 25 V over a 1.46 cm long device has been achieved.

But recently, separations have been customized for certain systems by employing DC biased AC electric fields<sup>115,122,137,205</sup>. Independent control of linear and nonlinear electrokinetic effects can be achieved by employing a DC-offset, AC electric field. In this scenario, electric field magnitudes can be reduced and still achieve the same efficiency of separation<sup>122</sup>.

Hawkins *et al.* group aimed to overcome restrictions of traditional DC-iDEP by applying a DC offset to an AC electric field in addition to intelligently designing the insulating obstacle to activate nonlinear forces<sup>205</sup>. They explained the phenomena behind DC biased AC electric fields mathematically as,

$$\vec{E} = \vec{E}_{DC} + \vec{E}_{AC} = \vec{E}_{DC}(1 + \beta) \quad (6.15)$$

Where  $\vec{E}_{DC}$  is the DC field strength and  $\vec{E}_{AC}$  is the AC field strength; ' $\beta$ ' is the ratio of  $\vec{E}_{AC}$  to  $\vec{E}_{DC}$ .  $\beta=0$  it is the condition for a pure DC field. When ' $\beta$ ' is applicable, the dielectrophoretic force on a spherical particle from equation 6.7 would take the form:

$$\vec{F}_{DEP} = \frac{1}{2}(2\beta^2 + 1)v \frac{\sigma_p - \sigma_m}{\sigma_p + 2\sigma_m} \nabla \vec{E}^2 \quad (6.16)$$

The mean particle mobility is a sum of the mobilities due to dielectrophoresis (AC & DC field), electrophoresis (DC field) and electro-osmosis (DC field)<sup>205</sup>:

$$\vec{u} = \vec{u}_{DEP} + \vec{u}_{EP} + \vec{u}_{EO} \quad (6.17)$$

$$\vec{u} = \mu_{DEP} \nabla(\vec{E} \cdot \vec{E}) + (\mu_{EO} + \mu_{EP})\vec{E} \quad (6.18)$$

Equation 6.12 contains both linear and non-linear electric field terms. The first order dependence of electro-osmosis and electrophoresis are termed as ‘linear electro migratory effects’ and the second order dependence on dielectrophoresis is known as ‘non-linear electro migratory effects’<sup>205</sup>. Both these effects play an important role in separation when DC biased AC electric fields are applied. Further, by employing a DC-offset properly, pressure driven flow can be eliminated in the system.

If a very high DC voltage or a DC-biased AC field with a small DC component is applied, the dielectrophoretic motion reaches a threshold where it becomes dominant over the electrokinetic motion. As a consequence, fluorescent polystyrene beads were focused faster in serpentine microchannel geometry<sup>123</sup>. By simulations performed on serpentine channel geometry, the authors in<sup>122</sup> confirmed that 500 kV/m DC field is comparable to that at a 20 kV/m DC-biased AC field with the DC to AC field ratio ( $\beta$ ) being set to 0.04.

CM factor as shown in equation 6.6 depends on the medium the particle is suspended in along with the particle’s own physical properties. CM factor has a direct impact on dielectrophoretic effect on the particle as it decides the particle trapping or sorting. Some research groups have studied these medium properties and how it can be modified to maximize efficiency of manipulation of particles. In the next section these different characteristics like pH, conductivity of the medium, wall effects and Joule heating effects are presented.

## 6.7 Performance characterization

Performance measures are not uniformly studied with each custom DC-iDEP device. For example, systematic studies of the effects of pH, conductivity and electric field strength offer insight into insulator-based DEP device performance as is apparent in



equations 6.6 and 6.7 in Section 6.4. Suspending media parameters play an important role in separation and trapping of particles whenever electro-osmotic forces are significant in the microchannel<sup>204</sup>. Some research groups have attempted to study these effects on trapping of particles and cells which are discussed in detail below<sup>204-205,218,223</sup>, but universal correlations describing the effect of these factors in achieving separation of particles and cells in DC-iDEP devices has not been reported. The findings reported to date on medium pH, medium conductivity, device wall effects, and Joule heating effects have been compiled in this section.

### 6.7.1 Effect of medium pH

Lapizco-Encinas *et al.* explored the effects of medium pH on the dielectrophoretic effect. Glass microdevices with glass insulating posts were used to study the operating conditions on the DEP behavior of polystyrene particles. Conductivity, pH, and applied DC electric fields were varied in the ranges of 8-9, 25-100  $\mu\text{S}/\text{cm}$  and 200-850  $\text{V}/\text{cm}$  respectively. The researchers reported that by decreasing the pH of the medium, increased protonization of silanol groups on the glass surfaces were observed. Thus the overall negative charge on glass decreases due to protonization, which decreases the zeta potential and in turn decreases electro-osmotic mobility and velocity<sup>199,204</sup>. To suppress electro-osmotic flow (EOF), it was determined that a medium with a low pH should be used to decrease wall zeta potentials. As pH increases, a greater dielectrophoretic force is needed to overcome the strengthening EOF and still achieve trapping in such devices. To create higher DEP forces for particle trapping, higher electric fields are required<sup>204</sup>. Higher electric fields are not always compatible with biological samples and may want to be avoided. In another experiment conducted by the same group, optimal conditions for

concentrating 1  $\mu\text{m}$  polystyrene particles were studied and pH of the suspending medium were varied between 6-9<sup>216</sup>. Lower pH values, in this case 6 were found to be optimal condition for trapping due to lower electrokinetic flow at this pH.

### 6.7.2 Effect of medium conductivity

The effects of conductivity were also studied to determine impact on trapping<sup>204</sup>. Conductivity of the medium was varied between 25-100  $\mu\text{S}/\text{cm}$  and dielectrophoretic effect on 1  $\mu\text{m}$  polystyrene particles was studied. Increasing the medium conductivity increased the DEP force required for trapping in glass microdevices having cylindrical insulating posts geometry to create non-uniformities in the field<sup>204</sup>. This is also supported and explained by the Clausius-Mossotti factor (equation 6.6), which depends on the medium and particle conductivity. The greater the conductivity, the greater the CM factor which then increases the DEP force experienced by a particle. This is the only research publication which studied the effect of medium properties on glass devices for trapping 1  $\mu\text{m}$  polystyrene particles. As reported by this group a combination of low pH (6) and high conductivity (100  $\mu\text{S}/\text{cm}$ ) of the medium is optimal to achieve trapping of polystyrene particles in glass devices<sup>216</sup>. By safely controlling the suspending media properties, the energy supplied to the system can be minimized thus minimizing operation costs for DC-iDEP devices<sup>204</sup>. Insulator DEP is still a nascent technique. The findings by the Lapizco-Encinas *et al.* group could be further optimized to achieve higher degrees of particle separation by controlling the suspending medium properties. It should be noted that due to the complex nature of wall-fluid interactions, these findings are limited to glass microdevices and the field remains open to explore insulator / medium

interactions for plastic (PDMS, injection molded PMMA or PC, or cyclo-olefin) or quartz, ceramics, oil meniscus microdevices.

### 6.7.3 Wall effects

The electrophoretic motion of particles are affected by the presence of channel walls in three ways: (a) electro-osmotic flow due to the surface charges on the channel walls, (b) electric field around particles and cells are altered by these insulating channel walls, and (c) as the cells and particles move along or against the fluid, viscous retardation is enhanced by the presence of channel walls<sup>227</sup>. Wall effects were studied experimentally by Xuan *et al.* in 2006 on a converging-straight-diverging PDMS channel by using 10, 20 and 40  $\mu\text{m}$  diameter fluorescent microspheres. Estimated zeta potential of PDMS device was found to  $-82\pm 2$  mV at room temperature. Results show that larger particles are more viscously retarded compared to the smaller sized particles by the side walls of the channels<sup>227</sup>.

### 6.7.4 Joule heating effects

Joule heating effects were researched by Sabounchi *et al.* on glass and cyclo-olefin copolymer DC-iDEP devices with cylindrical insulating posts for creating non-uniformity in electric field<sup>218</sup>. They observed that Joule heating has a significant impact on the fluid and particle motion in DC-iDEP devices. Joule heating creates an asymmetric temperature distribution that disturbs the distribution of electric field lines and electrokinetic forces by producing complex 3D electric field<sup>218</sup>. Dielectrophoretic mobility and electric field change with conductivity and viscosity when an electric voltage is applied. Joule heating can be reduced by minimizing the current in the device either by reducing the applied field or reducing the medium conductivity. Electric field

required for achieving trapping or separation could be minimized by carefully adjusting the conductivity and pH of the medium. Experiments were conducted by Sabounchi *et al.* based on optical thermometry technique using fluorescence Rhodamine B dye to measure temperature sensitivity. At higher flow rates  $>40 \mu\text{L}/\text{min}$  (optimized by syringe pump), Joule heating was minimized. Another strategy to reduce Joule heating was to employ surfactants to influence wall zeta potential and thus reduce EOF and the electric field required to trap particles<sup>223</sup>. Davalos *et al.* demonstrated this technique by dynamically coating Pluronic F127 nonionic block copolymer surfactant on microchannels of Zeonor 1060R devices containing array of cylindrical insulating posts. The presence of these surfactants reacts with the hydrophobic surface of the polymer to render them hydrophilic by thus disrupting EOF by justifying the surface charge migration that occurs in an electro-osmotic flow condition. The phobicity is uniquely tailorable by utilizing one of the various surface modifications for microdevices<sup>71,75,228</sup>, which suppress or enhance EOF. These surface modifications have been explored with capillary microdevices, but to the authors knowledge this is first group to have reported dynamic coating surface modification in DC-iDEP devices.

By controlling medium and wall characteristics as well as tuning the applied electric field, diverse particle manipulations are possible as is discussed in the next section.

## **6.8 Separation and trapping of biomolecules, bacteria, microparticles, and cells**

A variety of particles and cells have been manipulated using DC-iDEP technology. It is non-invasive and non destructive especially for living cells. Electric field gradient could be controlled according to the particle to be manipulated by adjusting the

insulating obstacle geometry. In this section, separation and trapping of particles using DC-iDEP technique from smallest to largest size have been discussed i.e. biomolecules like DNA and proteins, bacteria, microparticles of different sizes and mammalian cells.

### 6.8.1 DNA and proteins

Initial work for trapping single and double stranded DNA with DC-iDEP was conducted by Chou *et al.* in 2002<sup>128</sup>. DNA trapping was demonstrated using insulating constrictions at far lower frequencies (See Figure 6.3). In conventional AC-DEP, metallic electrodes embedded in the channels fabricated by thin-film deposition decay the field gradient and thus reduce trapping efficiency. When the electric field is too high, complex electrochemical reactions occur at the microelectrodes changing local medium ion compositions and degrading the electrodes<sup>128,200</sup>. Chou *et al.* also showed that for a given trapping voltage, the DEP force increased with the increase in length of DNA molecule. Chou *et al.* in 2003 published an article about constructing dielectrophoretic traps using dielectric constrictions for a sample-to-answer, lab-on-a-chip chemical analysis system<sup>207</sup>. In this article, the differences between electrodeless trapping employing insulating constrictions in the channel and conventional trapping employing metal electrodes embedded in the channel along with principles behind electrodeless dielectrophoresis have been discussed. They showed several examples where DC-iDEP can be applied including DNA trapping, cell lysing and cell sorting<sup>207</sup>. Protein purification and recovery has been a very challenging task for pharmaceutical industries. Not much has been reported on manipulating protein in DC-iDEP devices. Traditional methods of purification are expensive and cheaper alternatives are being explored. One such method is the use of DC-iDEP for manipulation of Bovine Serum Albumin (BSA)

proteins, first explored by Lapizco-Encinas *et al.* in 2008 on a glass microdevice containing an array of insulating posts<sup>126</sup>. Motion of protein particles were affected by the dielectrophoretic force, electro-osmotic flow and electrophoretic flow. Effects of electric field on the dielectrophoretic response of protein and effect of suspending medium properties on trapping of BSA particles were studied. Strong negative dielectrophoretic trapping occurs at high electric field strengths; by increasing medium conductivity and lowering medium pH, dielectrophoretic trapping can be achieved at lower electric field strengths. Trapping of protein particles occurred between 700-1600 V/cm electric field strength ranges depending on the suspending medium properties<sup>126</sup>.

### **6.8.2 Bacteria and virus**

As discussed in the theory section, Cummings and Singh studied DC-iDEP in 2003 containing an array of diamond insulating posts where streaming and trapping DEP operating regimes were observed<sup>113</sup>. Simulations based on fluid velocity and electric field was also developed to predict particle transport around the insulating posts. Typically, Poisson and Navier-Stokes equations for direct numerical simulation of electrokinetic flow have to be solved, but they simplified by taking advantage of the fact that fluid velocity is proportional to the electric field, and hence, both the electric potential and fluid flow can be computed by solving only the Laplace equation for electric potential<sup>113</sup>. Subsequently, Lapizco-Encinas *et al.* used cylindrical insulating posts to concentrate and sort live and dead *E.coli* where live cells exhibited trapping DEP and dead cells exhibited streaming DEP<sup>112</sup>. In these cases, cell size was constant while cell chemical properties varied suggesting cell composition is sufficient to impact cell polarizability and thus susceptibility to DEP forces. In the device, narrow regions between the insulating posts

generated the highest electric field. Negative DEP into low field gradient regions was observed with live *E.coli* whereas dead cells experienced less negative DEP and were carried by flow streamlines through the array. This was the first report of separating live and dead bacteria in a DC-iDEP device.

In 2003, Lapizco-Encinas *et al.* also demonstrated trapping and concentration of viruses. They performed experiment on a glass chip but their ultimate goal was to create a high throughput polymeric device<sup>124</sup>. For this they created an array of circular microbumps (100 μm in diameter and 40 μm in height) as insulating posts to create locally concentrated electric fields. They tested several polymeric substrates for this purpose and observed polyethylene and Zeonor had excellent fabrication characteristics and yielded streaming and trapping of two forms of T4 viruses at 400 V/cm with the insulating DEP. In 2004 they also worked on concentration of live-bacteria in water by DC-iDEP<sup>132</sup>. Here four types of bacteria were studied, all of which exhibited negative dielectrophoresis. Among them *E. coli* was gram-negative and the other three, *Bacillus subtilis*, *B. cereus*, and *B. megaterium* were gram-positive species. In this study, a relation for dielectrophoretic trapping was established as shown in equation 6.18.

$$\frac{\mu_{DEP} \nabla(\vec{E} \cdot \vec{E}) \cdot \nabla \vec{E}}{\mu_{EK}(\vec{E} \cdot \vec{E})} > 1 \quad (6.18)$$

It was demonstrated that membrane conductivity did not account for change in DEP behavior of cells. Single bacteria and mixed-species experiments were performed on glass devices having circular insulating posts of 150 μm diameter at electric fields ranging between 250-900 V/cm. DEP trapping was achieved with lower electric fields in this range for *E. coli* species compared with other gram-positive species. A trend was established based on size of the bacteria and the cell properties: *E. coli* < *B. megaterium*

<*B. subtilis* <*B. cereus*. Selective trapping experiments were conducted between two different types of bacteria to concentrate one species at high electric field and selectively elute a species by incrementally lowering the DC voltage. Trapping of *E. Coli* bacteria grown in brain-heart infusion broth at 37 °C was achieved in a membrane type DC-iDEP device<sup>125</sup>. The side length of the hexagonal pore was 50 mm and the thickness of the wall between pores was 112.6 mm. The diameter of the membrane area was 5 mm and 517 pores were located with a honeycomb pattern. The void fraction in the membrane was 18.7%. Trapping efficiency varied between 61-73% for a dilute bacteria solution flowing at a rate of 100 µL/min under 1280 V/cm electric field strength and 300 kHz frequency. The trapped bacteria were released with an efficiency varying between 86-100% when AC field was turned off. Viable bacteria were quantified using the standard colony forming units (CFUs) counting method. The capture efficiency of the bacteria was >80% at flow velocities lower than 10 mm/s, but increase in the flow velocity (>50 mm/s) of the bacteria suspension decreased the capture efficiencies by 30%<sup>125</sup>.

Sabounchi *et al.* demonstrated a novel platform for concentrating *Bacillus Subtilis* spores by combining iDEP, pressure driven flow and impedance measurement for further analysis of the concentrated sample<sup>209</sup>. This was the first report published where a detection system was built on the same platform used for manipulation of particles. The electrodes used for the impedance measurement were coplanar and rectangular; passivated with SiO<sub>2</sub> to maintain stability of the system for longer time periods. Sample concentration involved applying DC electric fields of 500 V/cm on insulating post geometry whereas impedance measurement involved AC signal at 100 mV amplitude and 100 Hz sine wave frequency. The lower detection limit established was injecting sample at 40 µL/min containing 10 spores/mL<sup>209</sup>. Once the spores are trapped at 500 V/cm, the



DC voltage was lowered for the spores to enter the side channel for impedance measurements. This platform is foreseen to act as a decision-making component to determine if downstream identification assays are required<sup>209</sup>.

### 6.8.3 Polystyrene particles

Many researchers have worked on separation and trapping of polystyrene particles of varying size ranges (1-15  $\mu\text{m}$ ) on varying insulating geometry and field strengths (DC and DC biased AC fields). Mela *et al.* demonstrated trapping of polystyrene particles in injection-molded hot-embossed cyclo-olefin DC-iDEP device. Trapping of carboxylated microspheres was observed at 340 V/cm in serpentine microchannels of 32 cm long, 160  $\mu\text{m}$  wide and 70  $\mu\text{m}$  deep<sup>123</sup>. Barbulovic-Nad *et al.* (2006) used an oil droplet as an insulating obstacle to separate 1, 5.7, and 15.7  $\mu\text{m}$  fluorescent carboxylated-modified microspheres under electric field ranging between 80-240 V/cm<sup>120</sup>. The particles were exposed to a negative DEP force. Since that force is linearly dependent on their volume, particle separation was achieved by size. The greatest advantage of this oil droplet obstacle was dynamic droplet size control, which is adaptable to separation requirements of various particles<sup>120</sup>. PDMS microdevices on a glass substrate were fabricated by standard photolithography technique containing four 40  $\mu\text{m}$  deep microchannels<sup>120</sup>. Effects based on droplet size, particle size and electric field were explored in this study. They were able to demonstrate that separation was effective at very low field strength for particles as small as 1 and 5.7  $\mu\text{m}$ . Employing low voltages for separation makes the separation efficiency and velocity of the particle slower, which was the main drawback<sup>120</sup>. Zhang *et al.* simulated and modeled separation of positive and negative DEP particles of 5 and 10  $\mu\text{m}$  radiuses in a circular channel driven by electro-osmotic

flow<sup>215</sup>. The particles with different dielectric properties move towards different locations across the channel. The circular channel was enclosed with an inner circle of 50  $\mu\text{m}$ , an outer circle of 100  $\mu\text{m}$  and height of 20  $\mu\text{m}$ . The principle behind this concept is shown in Figure 6.5. For small particles, the DEP force is balanced by the fluid drag force thus slowing the particle motion in the channel. But for larger particles, due to higher mobility they travel faster towards the inner or outer circle depending on positive or negative DEP effect experienced by the particle. In this system, the dielectrophoretic mobility of a particle moving in an electric field gradient is dependent on the surface area of the particle. The direction of movement of particle depends on the sign of the CM factor ( $\alpha$ ) as discussed in equation 6.7. The particles following the inner path of the circular channel move faster compared to the outer path particles. When the electric field was reduced, the particles move slower due to the slower electro-osmotic flow. Under higher electric field conditions, the particles move with the greater electro-osmotic flow, so the particles to arrive at the end of the channel quicker<sup>122</sup>. Separation efficiency of particles was improved by employing higher electric field strengths as electro-osmotic force is increased at higher DC field strength. So the particles travel faster to reach the end of channel, but the particles tend to be over separated due to large DEP effect on them. In a serpentine channel system, Zhu *et al.* studied the focusing of 5 and 10  $\mu\text{m}$  polystyrene particles using pure DC fields and DC biased AC fields<sup>123</sup>. The ratio ' $\beta$ ' from equation 6.7 was varied and the total magnitude of DC and AC fields was maintained at 100 V/cm. With increase in ' $\beta$ ' values, or increasing AC with respect to DC amplitudes, the width of focusing stream was narrowed thus achieving higher degree of focusing in the channel. Zhu *et al.* group also achieved continuous separation of mixture of 5/10  $\mu\text{m}$  particles and 3/5  $\mu\text{m}$  particles in an asymmetric double-spiral microchannel by applying DC

voltage<sup>119,139</sup>. 100% separation was achieved with 5/10  $\mu\text{m}$  particles at 600 V DC ( $\sim 265$  V/cm at the high electric field density region), whereas for 3/5  $\mu\text{m}$  particles 100% separation could not be achieved even with an applied voltage of 1500 V DC ( $\sim 465$  V/cm at high electric field density region)<sup>119</sup>. Another study by the same group involved particle focusing by adopting a microchannel constriction and DC-biased AC electric fields<sup>115</sup>. The microchannel constriction was 56  $\mu\text{m}$  high and 188  $\mu\text{m}$  long placed in the middle of a 2 cm long, 310  $\mu\text{m}$  wide channel. Pure DC voltage experiments involved electric field strength of 100 V/cm whereas in DC-biased AC case, the total electric field strength was 100  $V_{pp}$ /cm with 1 kHz frequency. Separation efficiency was the same in both cases with an added advantage of using lesser voltage in case of DC-biased AC experiments<sup>115</sup>.

A recent development in DC-iDEP was a nanoparticle concentrator developed by Chen *et al.*<sup>138</sup>. The concentrator was composed of a series of microchannels constructed with PDMS as shown in Figure 6.6. The regions shown in Figure 6.6 were designed such that field increases gradually from region 4 up to region 1. The device performance was evaluated using 930 nm green fluorescent polystyrene microspheres at field ranges between 20-400 V/cm. Both streaming and trapping DEP occur in the Chen *et al.* device depending on the electric field applied. Streaming aids in the transport of the trapped nanoparticles and trapping DEP aids in concentrating and filtering of the particles. In this concentrator, the structure of the channel is designed to highly focus and thus amplify the electric field. At 200 V/cm, complete trapping of particles occurred in the device. For collecting the trapped particles, the electric field was turned off and a pressure source was applied at the inlet with a syringe. The concentration of 930 nm polystyrene particles was rapid and efficient at this stage. Further experiments were also conducted for 500 nm

nanoparticles, which required higher electric field to completely trap all nanoparticles. One notable aspect of this implementation of DC-iDEP is that it has achieved manipulation of smaller particles than other studies. This technique could be implemented to concentrate biomarkers for disease diagnostic applications and also for sample preparations and concentrations for biological assays. The design could be further improved by changing the trapping regions based on the applications<sup>138</sup>.

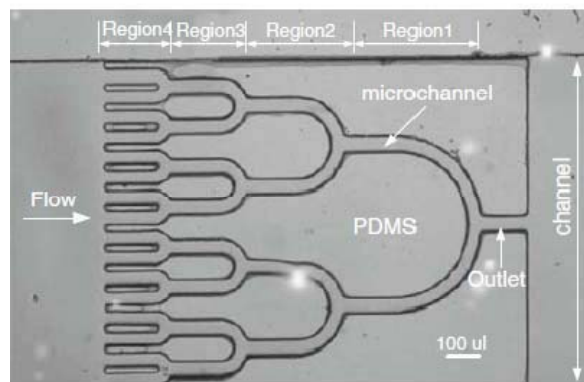


Figure 6.6 Photograph of the PDMS-insulating microstructure for concentrating of particles. Electric field strength increases gradually from regions 4-1. DEP trapping begins at region 2. “With kind permission from Springer Science + Business Media: Chen D, Du H, Tay CY (2010) Rapid concentration of nanoparticles with dc dielectrophoresis in focused electric fields. *Nanoscale Research Letters* 5:55-60, copyright 2009”<sup>138</sup>.

To improve DEP focusing of small particles, the number of constrictions or insulating obstacles in the channel can be increased. This is apparent when compared against just one constriction<sup>115</sup>. Particle focusing is more effective when the particle size is comparable with the constriction width or the applied field is sufficiently high. If the width of the constriction is reduced, the chances of particle clogging and chip fouling increases. This is usually countered with higher electric fields. This choking phenomena was recently modeled by Ai *et al.* using a finite element model in a converging-diverging

microchannel<sup>219,229</sup>. Choking phenomena was observed when the DEP force increased with electric field at a much faster rate than electro-osmosis and electrophoresis, thus preventing the particle from moving into the converging channel. A high non-uniformity in the electric field, a high particle size ratio and high zeta potential ratio are predicted to be the main causes of this choking phenomenon in DC-iDEP converging-diverging channel geometries. The results presented in this study are not applicable to nanoparticles due to the assumption made by the authors that particle size is much larger than the electric double layer (EDL) present between the charged wall and the particle<sup>229</sup>.

#### **6.8.4 Yeast cells and mammalian cells**

Kang *et al.* reported a technique combining AC and DC dielectrophoresis for a continuous separation of a mixture of 5 and 10  $\mu\text{m}$  microparticles and yeast cells achieved by employing a PDMS obstacle and a pair of embedded electrodes to generate localized AC electric fields<sup>137</sup>. Embedded electrodes were viewed as advantageous in this system because low voltages were applied; it avoided electrokinetic flow and yielded a confined area for manipulation of particles. It was found that pressure driven flow adopted in the rectangular hurdle microchannel for separation was advantageous as it minimized Joule heating effects. However, the particle streamlines were close to each other which affected the separation efficiency. The crossover frequency was estimated to be 200 kHz; above this crossover frequency the efficiency of separation decreased and below AC amplitudes of 7 V, no separation occurred. The authors concluded that optimum flow rates for the highest throughput have yet to be determined to improve this technique of separation<sup>137</sup>. However, cell viability decreased as the electric field increased due to Joule heating<sup>115,230-231</sup>. Previous researchers have reported that the high

electric field strength could cause increase in temperature at the constrictions due to Joule heating and thus damage cells or disturbances to particle motions<sup>218</sup>.

DEP is an excellent technique for manipulating mammalian cells and many researchers have accomplished cell manipulation and single cell analysis by fine tuning electric field gradient via traditional AC dielectrophoresis to achieve sorting, focusing, concentrating or trapping in microdevices<sup>1,10,29,34,89,111,135,147-148,232-235</sup>. But not many researchers have investigated DC-iDEP behavior on mammalian cells, except our group<sup>81</sup>, Kang *et al.* group<sup>118</sup> and Jen *et al.* group<sup>213-214</sup>. Our group investigated separating red blood cells via DC-iDEP technique using a rectangular insulating geometry<sup>81</sup>. The red blood cells (RBC) are separated according to its human ABO type into one of the four channels depending on the RBCs polarization capacity. Our previous work involved using AC-DEP for sorting RBCs based on blood type by using an AC electric signal. Here O+ is distinguished from all the other blood types with >95% confidence<sup>1</sup>. From previous research, dielectrophoresis depend on antigen expression on the RBC membrane which helped in sorting of the RBCs by its type<sup>1,81</sup>. Kang *et al.* studied the separation of human white blood cells and breast cancer cell groups (MCF7) individually were studied in a rectangular and triangle insulating obstacle geometries by applying DC electric field<sup>118</sup>. White blood cell solution was composed of monocytes, granulocytes, lymphocytes along with other components in blood (red blood cells, platelets, and other debris). Breast cancer cell lines had varying sized cells in the range of 20-60  $\mu\text{m}$ . White blood cells were separated in the rectangle design and triangular obstacle was used for manipulating live cells. They claim that since the rectangular obstacle is so long, the cells may die (due to extra stress on the membrane and strong electric field in the insulating obstacle region) in between and triangular obstacle geometry would be better for

handling live cells<sup>118</sup>. The applied voltage in the rectangular geometry was 345 V (138 V/cm), whereas in triangular geometry lower voltages of about 180 V (72 V/cm) were applied to achieve separation. Jen *et al.* group studied trapping of human carcinoma cells (HeLa) by employing open top microstructures containing DEP insulating traps similar to Chou *et al.* group<sup>128,207</sup>. HeLa cells displayed both positive and negative DEP under frequencies >100 kHz and <1 kHz respectively at an applied electric field of 60 V<sub>pp</sub>/cm. Cross-over frequency where the shift occurs from negative to positive DEP was estimated to be ~3.5 kHz. HeLa cells were trapped completely at 180 V<sub>pp</sub>/cm and 1 MHz frequency<sup>214</sup>.

As discussed in the above section, many investigators have researched separation or trapping of different types of cells and microparticles by employing low and high DC, DC-biased AC fields. DC-iDEP is a very novel technique and can be used for manipulation of any type of particles by maintaining viability of bioparticles. There might be Joule heating experienced in some device geometry and careful selection of electric field ranges and surface modification techniques would help to overcome this problem.

## 6.9 Summary and conclusions

In this review article, an extensive review of the major contributions observed in insulator based dielectrophoresis has been provided. It is a nascent field which has yielded >40 publications in the last decade. The publications for this review paper have been searched through Google Scholar and Web of Science data base by applying several individual and combination of key-words like “insulator + dielectrophoresis”; “electrodeless + dielectrophoresis”; and “DC current + dielectrophoresis”. DC-iDEP

devices have various advantages compared to the traditional AC dielectrophoretic devices wherein metal electrodes are embedded inside the fluid channels. Insulator based dielectrophoretic devices are less prone to fouling, gas generation and are easier to fabricate because the metal electrodes are remotely positioned in sample wells. DC-iDEP devices can also be operated as continuous flow devices or even employ both DC and AC electric fields for optimal particle manipulations. Insulating obstacles in the channel fabricated create electric field non-uniformities that yield DEP forces on polarizable particles and can be harnessed to achieve separation or trapping of such particles of interest. This review has outlined the standard and novel insulating obstacles explored thus far. Most obstacles are robust, inert and can be fabricated by soft lithography in diverse geometries including single obstacle (rectangular obstacle, a triangular hurdle, a constriction in the depth of the channel rather than the width, a single microchannel constriction, oil droplet, and an oil menisci as field shaping barriers) embedded in the channel; multiple obstacles (metallic trap, insulating posts, tetragon structures along the channel, and multiple rectangular blocks) and other channel geometries modifications (non-converging saw tooth channels, a set of aligned teeth, saw tooth channel, open top microstructures, serpentine microchannels, a series of iterative curves, arrays of circular channels and honey comb membrane design). The most extensively used channel geometries are the insulating posts (be cylindrical or diamond shaped) made of glass and single rectangular obstacle geometry made of PDMS.

Trapping or separation of particles is dependent on various factors. These factors have been discussed in this article at various stages and a great potential exists for future improvement of this technique. Efficiency of trapping, focusing, separation or concentrating of particles can be improved by carefully selecting the suspending medium



properties and electric field strengths suitable for the particle of interest. Specific dependencies with medium pH, medium conductivity and judicious selection of electric fields are areas that need further exploration in DC-iDEP devices.

Traditional DC-iDEP devices have yielded separation and trapping of DNA, viruses, bacteria, isolation of live and dead cells, protein manipulation and fluorescent polystyrene microparticles by employing suitable DC fields and various insulating obstacle geometries like rectangle, triangle, oil droplet, array of insulating posts, multiple rectangular block, serpentine channels, series of iterative curves and circular channels. To achieve separation, high voltages are often necessary which is not conducive for cell viability. Further, large electric fields promote Joule heating with slower particle velocities and fluid flow. To overcome these difficulties, a hybrid approach of simultaneously applying a low DC field with an AC frequency can frequently achieve more efficient separation and trapping of particles. Some examples discussed include a nanoparticle concentrator<sup>138</sup>, bacteria concentrator<sup>125,209</sup>, open top microstructure for human carcinoma cell trapping<sup>214</sup>, and micro particle focuser with lower power utilization and greater efficiencies than traditional DEP approaches<sup>102,115,122,137,205</sup>. Mammalian cells have not been explored much by investigators in literature exceptions include two groups<sup>118,214</sup>; Kang *et al.* studied the separation of breast cancer cell lines (MCF7) and white blood cells individually by employing DC electric fields<sup>118</sup> and Jen *et al.* studied the trapping of human carcinoma cells (HeLa) by employing DC-biased AC fields<sup>214</sup>.

In summary, DC-iDEP remains an underexplored yet powerful particle manipulation technique and much work is needed to fully recognize its potential. The plethora of applications that have utilized traditional dielectrophoresis are likely adaptable to this more user-friendly platform enabling mobile lab on a chip diagnostic

applications. Some such prospective applications include manipulation of bioparticles, bioseparations and purifications in the pharmaceutical industry, concentration of biomarkers from body fluids for disease detection, environmental purification or remote monitoring systems by concentrating and quantifying bacteria, viruses, or hazardous waste, drug delivery, biodefense, food applications and other diverse applications in medicine and biology.

In the next chapter, sorting of polystyrene particles based on size is presented. A study of three dependencies: size, electric field and medium conductivity on particle sorting is investigated.

CHAPTER VII  
DC-INSULATOR DIELECTROPHORETIC SEPARATION OF FLUORESCENT  
POLYSTYRENE PARTICLES

### 7.1 Introduction

Lab-on-a-chip device for sorting of fluorescent polystyrene microparticles employing direct current insulating dielectrophoresis (DC-iDEP) is described in this chapter. Particles were sorted by combining electrokinetics and dielectrophoresis in a 250  $\mu\text{m}$  wide microchannel containing a rectangular insulating obstacle and four outlet channels. Microdevice fabricated from PDMS by soft-photolithography process was sealed by plasma-oxidation. The DC-iDEP particle flow behaviors were investigated with 3.18, 6.2 and 10  $\mu\text{m}$  fluorescent polystyrene particles which experience negative DEP force depending on particle size, DC electric field magnitude and medium conductivity. Due to negative DEP, particles are repelled away from the high electric field density region (around the obstacle) and larger DEP forces create larger deflection or repulsion on the particles. Particles suspended in dextrose and phosphate buffer saline (PBS) at conductivities ranging from 50-850 mS/cm at pH 7.0 were compared at 6.85 and 17.12 V/cm. Simulations for the same conditions as experiments were conducted with *COMSOL Multiphysics*<sup>®</sup> modeling software. Results from both simulations and experiments suggest that DEP force depends on medium conductivity, particle size and applied DC potential. Overall results from both simulations and experiments prove that smaller particles prefer channels 3 and 4, whereas the larger particles prefer channels 1

and 2. Deflection of 10 and 6.2, 3.18  $\mu\text{m}$  particles can be independently directed into one of four channels by tuning the voltage or the medium conductivity. This is accomplished at lower DC potential than other researchers. This work is an essential first step in employing DC-iDEP for multiparticle sorting in a continuous flow lab-on-a-chip device.

In the next sections, a brief over-view of DC-iDEP in literature is presented followed by theory and modeling of the experiments. Section 7.4 deals with experimental methods and image analysis followed by results and discussion section. Electro-osmotic mobility and base-line conditions for the experiments have been discussed along with the results for the dependencies affecting particle separation in our 4-channel system. The chapter concludes with a comparison of 2-channel system investigated by past researchers and how novel is our system from them has been derived.

## 7.2 DC-iDEP in literature

Lab-on-a-chip systems have the capacity to perform a variety of tasks ranging from DNA analysis to protein recognition and could be catered to point-of-care medical diagnostic tools. Lab-on-a-chip (LOC) devices integrate multiple laboratory functions on a few centimeter(s) sized chip and are capable of handling extremely small fluid volumes down to picoliters<sup>1,15,81,199</sup>. They commonly utilize electrokinetics to move analytes since electric fields are versatile and can be precisely controlled for specific, quantifiable analyte responses. Furthermore, devices employing electric fields can eventually be simplified to only require a battery for power – a key characteristic for true portable diagnostic devices. One type of electrokinetic phenomenon, dielectrophoresis (DEP), has traditionally employed alternating current (AC) electric fields to create spatial non-uniformities in a channel, which controls particles or cells through transient polarizations.

Dielectrophoresis could also be achieved using direct current (DC) electric fields and this paper focuses on using DC electric fields to achieve sorting of fluorescent polystyrene particles (DC-iDEP). Dielectrophoresis is a key type of field to explore in medical diagnostic devices due to operational simplicity, requirement of lower voltages, and small sample volumes, all of which enable device portability<sup>81</sup>.

Direct current insulating dielectrophoresis (DC-iDEP) is a relatively new field that has yielded ~40 journal publications since the last decade. It utilizes a spatially non-uniform electric field component but not the frequency dependent component of AC-dielectrophoresis, which has been shown to be adequate for manipulation of cells<sup>112</sup>.

Spatial non-uniformities in the electric field are generated via insulating obstacles embedded within the microdevice channels, while remotely positioned electrodes at the ends of the channels deliver direct current or DC with low frequency AC current. The advantages of using such insulating obstacles to create non-uniformities in the channel include<sup>117</sup>: (a) insulators in microdevices are less prone to fouling than embedded electrodes and they retain functionality despite of fouling (b) fabrication is simple, since there is no metal components involved (c) insulating obstacles are mechanically robust and chemically inert (d) electrolysis gas evolution at the remotely located metal electrodes causes minimal or no bubbles inside the channel, and (e) can be operated by both AC and DC fields with continuous flow system.

Initial work on DC-iDEP was conducted by Cummings and Singh in 2003<sup>113</sup>. Their configuration contained an array of insulating posts where two operating regimes were observed, namely streaming and trapping DEP<sup>113</sup>. In streaming DEP, particles of interest concentrate at electric field maxima but travel through the device in flowing streamlines; and in trapping DEP the forces reversibly immobilize the particles of interest

on the insulating posts. Subsequently, Lapizco-Encinas *et al.* used insulating posts to concentrate and sort live and dead *E. coli*<sup>112</sup> where live cells exhibited trapping DEP and dead cells exhibited streaming DEP in fields of 160 V/cm. They also demonstrated that dead cells exhibited less negative DEP compared to live cells. In these cases, cell size was maintained constant while cell dielectric properties varied. There were many efforts to explore other insulating materials for iDEP including oil droplet obstacle<sup>120</sup> and pairs of insulating oil menisci to shape the DC electric field<sup>206</sup>. Lapizco-Encinas *et al.* (2008) studied the performance characterization of DC-iDEP microdevice as a function of suspending medium properties by using insulating posts with polystyrene micro particles of 1  $\mu\text{m}$  diameter<sup>204</sup>.

Fabrication of these microdevices have been achieved utilizing silica or glass, thermal plastics such as polymethylmethacrylate (PMMA), polyolefins, polyethylene terephthalate, and polycarbonate or elastomers such as poly(dimethylsiloxane) (PDMS)<sup>48</sup>. The differing materials influence wall surface charge and thus electro-osmotic velocities, but all achieve field non-uniformities governed by obstacle geometry. Other researchers have explored a number of insulating obstacles comprising of different shapes like rectangle<sup>118</sup>, triangle<sup>118</sup>, circular<sup>215</sup> and saw-tooth<sup>102,121</sup>, serpentine channels<sup>122-123</sup>, and open top microstructures<sup>213-214</sup>. Another recent development was by a group of researchers who developed a technique to concentrate nanoparticles<sup>138</sup>. The concentrator was composed of a series of PDMS microchannels wherein both streaming and trapping of particles occurred. At higher voltages of 200 V/cm, trapping of particles occurred whereas at lower voltages streaming or flow of particles was observed.

Many researchers have explored using DC biased AC fields for achieving greater separation of particles and cells<sup>115,122,125,205,212</sup>. A complete picture of particle shape,

insulating obstacle geometry and voltage dependencies direct current insulator-based dielectrophoresis (DC-iDEP) has not yet been attained.

In this research, only direct current (DC) electric fields are applied to sort microparticles in a channel with multiple outlets. Streaming DEP is desired to sort particles based on size and it was achieved by the presence of an insulating obstacle embedded in the microchannel. PDMS insulating obstacles of rectangular geometrical configurations were utilized to create a spatially non-uniform electric field to sort particles of three different sizes (3.18  $\mu\text{m}$ , 6.2  $\mu\text{m}$  and 10  $\mu\text{m}$ ) into four channel outlets.

Baseline electro-osmotic flow (EOF) determinations were performed in order to tune simulation results and to determine how long a single particle experiences the DEP force as it passes the obstacle in the channel. The faster the EOF, the less time the particle resides in the obstacle region potentially reducing the deflection effect into specific outlet streams. Negligible DEP force yields particle trajectories driven by EOF and hydrodynamic effects and no channel preference will be observable at lower electric fields. All particles experience the same EOF, but the magnitude of the DEP force will repel the particles away from the obstacle into certain streamlines that are then bifurcated into the four outlet channels. Results reported are primarily based on three dependency studies including a) polystyrene particle size, b) electric field strength, and c) suspending media conductivity. The device design is novel to the best of authors' knowledge as it relies on DC voltage and insulating obstacle to create field non-uniformities thus bifurcation into four channels to quantify deflection around the rectangular insulating obstacle.

This developed technique can be further applied for use in portable diagnostic devices for easy, accurate and rapid analysis. Dielectrophoretic characterizations in

continuous flow lab-on-a-chip devices relying on a DC power source would be far more portable and better to be adapted to diagnostic applications requiring larger cell event numbers. DC-iDEP technique is the viable option for disposable, inexpensive DEP devices because insulating-based-devices can be made from inexpensive substrates and are much simpler and more economical than electrode-based-devices. Also employing DC voltages allows using EOF to pump liquid, thus eliminating micro-pumps and increasing portability.

### 7.3 Theoretical background

In this section, a detailed discussion of particle motion and modeling for experiments conducted are discussed.

#### 7.3.1 Particle motion

Particle transport along the microchannel is assumed to depend on electrokinetic (EK) and dielectrophoretic (DEP) mechanisms only. The particle flux  $\vec{j}$  can be expressed in terms of an electrokinetic velocity  $\vec{u}_{EK}$  and dielectrophoretic  $\vec{u}_{DEP}$  velocities as:

$$\vec{j} \propto (\vec{u}_{EK} + \vec{u}_{DEP}) \quad (7.1)$$

The electrokinetic velocity,  $\vec{u}_{EK}$  takes into account the electrophoretic and electro-osmotic contributions to the particle transport. The apparent velocity is taken to be proportional to the applied electric field  $\vec{E}$ , as:

$$\vec{u}_{EK} = \mu_{EK} \vec{E} = (\mu_{EP} + \mu_{EO}) \vec{E} \quad (7.2)$$

where  $\mu_{EK}$ ,  $\mu_{EP}$ ,  $\mu_{EO}$  are the electrokinetic, electrophoretic, and electro-osmotic mobilities, respectively. For relatively large particle size with low surface charge it is possible to neglect the electrophoretic mobility<sup>204</sup>, thus:



$$\mu_{EK} \approx \mu_{EO} \quad (7.3)$$

$$\mu_{EO} = \frac{\zeta \varepsilon_m}{\eta} \quad (7.4)$$

where  $\zeta$ ,  $\varepsilon_m$ ,  $\eta$  are zeta potential, permittivity of suspending medium and viscosity of suspending medium respectively.

The dielectrophoretic velocity  $\vec{u}_{DEP}$  is related to the applied electric field as:

$$\vec{u}_{DEP} = -\mu_{DEP} \nabla \vec{E}^2 \quad (7.5)$$

where  $\mu_{DEP}$  is the dielectrophoretic mobility. For a spherical particle of diameter  $d_p$ , the dielectrophoretic mobility  $\mu_{DEP}$  can be expressed as<sup>199</sup>:

$$\mu_{DEP} = \frac{\pi d_p^2 f_{CM} \varepsilon_m}{12\eta} \quad (7.6)$$

where  $\varepsilon_m$  is the permittivity of the suspending medium,  $\eta$  is the viscosity of the suspending medium and  $f_{CM}$  is the Clausius-Mossotti factor, which accounts for the particle polarizability. Under a DC electric field, for a spherical particle with a conductivity  $\sigma_p$  suspended in a medium with conductivity  $\sigma_m$  the  $f_{CM}$  is given by<sup>89</sup>:

$$f_{CM} = \frac{\sigma_p - \sigma_m}{\sigma_p + 2\sigma_m} \quad (7.7)$$

As it can be observed from equation 7.7,  $f_{CM}$ , DEP can be positive or negative, depending on the relative conductivities of the particle and suspending medium. It has been shown that for a DC electric field polystyrene particles<sup>204,236</sup> and bacterial cells<sup>102,112</sup> exhibit negative dielectrophoresis: *i.e.*, they are less polarizable than the suspending medium and are repelled from the regions of higher field density. In this research, the

microdevice developed hopes to exploit these characteristics in order to sort the particles into four outlet channels *via* unique device design. In this study, conductivity of polystyrene particle was considered negligible ( $\sigma_p = 0$  mS/cm)<sup>236</sup> compared to that of the suspending medium. This assumption was supported by calculations of  $f_{CM}$  employing  $\sigma_p$  values reported in the literature<sup>236</sup> where all values for  $f_{CM}$  were very close to -0.5.

A spatially dense non-uniform field is created around the obstacle as the DC field lines diverge around the insulating obstacle. Due to the presence of the insulating obstacle, a high electric field density region is produced between the obstacle and the channel wall, which imparts a DEP force on particles flowing down the channel, thus, altering their trajectory into one of the four outlet channels. These negative DC-iDEP forces push the particles away from high field density regions resulting in a repulsive force exerted on the particle as it flows around the corner of the obstacle, thus facilitating particle motion. From equation 7.7, since  $\epsilon_p < \epsilon_m$  the particles experience repulsive forces or streaming or negative DEP trapping. Here, streaming DEP is desired given by the condition in terms of electric field,  $\mu_{EK}$ ,  $\vec{E}$  and  $\mu_{DEP}$ <sup>237</sup>:

$$\frac{\mu_{DEP} \nabla(\vec{E} \cdot \vec{E}) \cdot \nabla \vec{E}}{\mu_{EK} (\vec{E} \cdot \nabla \vec{E})} \leq 1 \quad (7.8)$$

This condition was monitored in the following study *via* our unique device design employing rectangular insulating obstacle and DC electric field.

### 7.3.2 Particle pathlines

In this study, since all the polystyrene particles had very similar dielectric properties, the effect of nDEP on a particle pathline is assumed to depend only on particle diameter. From simulation work, it can be observed that this effect becomes important to

determine which one of the four outlet channel the particle will take. The magnitude of nDEP force depends on the gradient of  $\vec{E}^2$ , which reaches its maximum over the region where the insulating obstacle is located. Particles coming out of the region of the constriction will be deflected due to nDEP to different channel outlet, depending on their diameter.

### 7.3.3 Mathematical model

The performance of the microdevice was studied employing a mathematical model built with *COMSOL Multiphysics*<sup>®</sup> and implementing Finite Element Analysis (FEA). The geometry of the microdevice utilized was carefully mapped out with COMSOL. By solving the Laplace equation, it was possible to predict the distribution of electric potential across the microdevice, and the magnitude of the electrokinetic forces involved as well as particle trajectories.

For the mathematical model, the applied DC electric potential was assumed to remain constant along the microchannel depth; it has been demonstrated that the electric field does not decay in a significant manner along the depth<sup>25</sup>. Therefore, the simulation was treated as a 2-dimensional electrostatics problem.

A triangular mesh was built in order to solve the Laplace equation using the *Lagrange element* implemented in the software. FEA was applied in a triangular mesh consisting of 1200 elements and 2800 nodal points. The electric potential  $\phi$  was approximated by a polynomial of low order at each mesh point. From the obtained numerical solution it is possible to obtain values for the parameters describing the electrokinetic and dielectrophoretic behavior of the particles, such as the electrical field  $\vec{E}$ , gradient of  $\vec{E}^2$ , and particle pathlines.

Values for the electrokinetic mobility were obtained from reported experimental results (shown in Table 7.1) as a function of suspending medium conductivity; this is described in the Experimental methods section under sample preparation.

The microchannel contains one rectangular insulating obstacle and four different outlet channels (Figure 7.1). When applying a DC electric potential, the presence of the insulating obstacle creates a region of non-uniform electric field that affects particle pathlines by means of negative dielectrophoretic effects. Further information regarding microchannel geometry is included in Section 7.4.1. The model solves the electrical potential inside the microchannel as described by the Laplace equation:

$$\nabla^2 \phi = 0 \quad (7.9)$$

with boundary conditions:

$$\vec{n} \cdot \vec{J} = 0 \text{ at the boundaries} \quad (7.10)$$

$$\phi = \phi_{in} \text{ at the inlet of the microchannel} \quad (7.11)$$

$$\phi = 0 \text{ at the outlet of the microchannel} \quad (7.12)$$

From the numerical solution obtained, it is possible to predict the motion of the spherical particles along the microchannel<sup>217</sup>.

#### 7.4 Experimental methods

From equations 7.6 and 7.7, dielectrophoretic force on the particle depends on magnitude of the applied DC electric field, medium conductivity, and size of fluorescent polystyrene particles. All these dependencies are explored here. For electro-osmotic mobility determination in PDMS channels, current monitoring method was used<sup>238</sup>. In this section device design and microdevice fabrication by soft lithography,

experimentation (including microsample preparation) for electro-osmotic flow and fluorescent polystyrene particle experiments, image analysis and quantification are discussed in detail.

#### **7.4.1 Device design and fabrication**

AutoCAD 2008 software (Autodesk, Inc) was used to design the microdevice mask, which was printed on high resolution transparencies of 32,512 dpi (Fine-Line Imaging, Inc.). The microdevice developed consists of one inlet (250  $\mu\text{m}$  wide) and four outlet channels of 90  $\mu\text{m}$  in width. The distance between the inlet and outlet ports was 1.46 cm with 3 mm diameter ports. An insulating obstacle of rectangular geometry was positioned in the inlet channel at a distance of 150  $\mu\text{m}$  upstream from the bifurcation to the four outlet channels. The width of the rectangular obstacle was 330  $\mu\text{m}$  and the height was 190  $\mu\text{m}$  as shown in Figure 7.1.

Standard techniques of soft lithography were used to pattern the microdevice and microchannels<sup>46</sup> that were cast into poly(dimethylsiloxane) (PDMS) device and sealed onto a glass slide. Some modifications in the process included employing increasing exposure times with the masked UV light and soft / hard bake temperatures and baking times. The device was fabricated with a sample injection port and four outlet ports. Biopsy punches were used to create inlet and outlet ports of 3 mm in diameters. Pt electrodes were weaved through the outlet ports followed by cleaning of the PDMS mold with scotch tape to remove any dust particles before plasma oxidation treatment<sup>67,70</sup> (Harrick Plasma, Inc) using room air and temperature for 1 min; this ensured an irreversible seal between the PDMS mold and a cleaned glass slide. Glass slides were cleaned with e-pure water and dried in a clean air stream before sealing the microdevice.

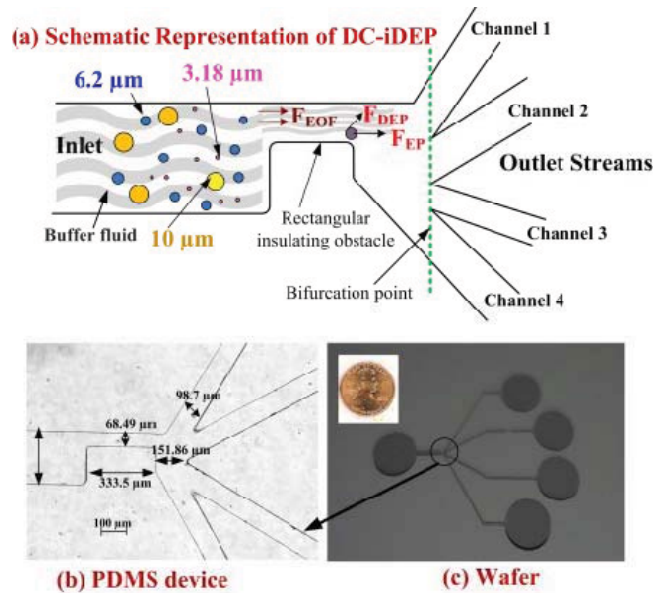


Figure 7.1 (a) A particle at the insulating obstacle due to electric field  $\vec{E}$ , experiences electrophoretic force ' $F_{EP}$ ' (negligible in this research due to particle size), electro-osmotic force ' $F_{EO}$ ' from the fluid, and the dielectrophoretic force ' $F_{DEP}$ ' (b) Rectangular obstacle geometry enlarged from (c) at the point highlighted bifurcating into four channels (c) Master on Silicon wafer showing device design of 1.46 cm in length compared to the size of a penny.

#### 7.4.2 Sample preparation

Dextrose was used to augment phosphate buffer saline (PBS) in order to manipulate medium conductivity. D-Glucose (dextrose) (Fisher Scientific, >99% pure, anhydrous) was added to PBS at concentrations ranging from 1-5 wt%. pH was adjusted to 7.0 for all the buffers using HCl and NaOH (Fisher Scientific, HPLC grade) as necessary and final conductivities were recorded for each buffer. Table 7.1 indicates the average conductivity values with standard deviations obtained for all the dextrose-added buffers over a range of solutions prepared ( $n$ ). The conductivities varied between 20-850  $\text{mS}\cdot\text{cm}^{-1}$ . Here 0% buffer refers to 0.14 M PBS at pH 7.0.

Particle movement depends on dielectrophoretic and electrokinetic mobility as shown in equation 7.1. To calculate dielectrophoretic mobility, electrokinetic mobility

needs to be known. Electrokinetic mobility refers to EOF in this research, and EOF causes particle movement towards the outlet direction whereas DEP deflects the particles into different channels. For the electro-osmotic flow determination experiments freshly prepared 0.14 M and 0.56 M PBS was used along with dextrose-diluted buffers. The electrokinetic mobility of buffers shown in Table 7.1 was calculated by the current monitoring technique<sup>238</sup>.

Table 7.1 Average conductivities of various dextrose added buffers with standard deviations and electrokinetic mobility with standard deviations for each buffer at 10.27 V/cm. The number *n* represents the number of solutions averaged for calculating buffer conductivities. The values ranged between 20-850 mS/cm and do not show a mobility dependence on buffer conductivity.

% Dextrose added buffers	Average conductivity (mS/cm)	Electrokinetic Mobility ( $\times 10^{-4}$ cm <sup>2</sup> /Vs)
5%	23.8 $\pm$ 9.3 ( <i>n</i> =5)	41.9 $\pm$ 2.4
4%	508 $\pm$ 28.1 ( <i>n</i> =4)	36.9 $\pm$ 0.96
3%	616.2 $\pm$ 41.9 ( <i>n</i> =5)	41.0 $\pm$ 1.53
2%	732.7 $\pm$ 35.5 ( <i>n</i> =4)	53.5 $\pm$ 5.05
1%	823 $\pm$ 31.8 ( <i>n</i> =4)	54.2 $\pm$ 1.92
0% (PBS)	847.4 $\pm$ 23.7 ( <i>n</i> =2)	32.9 $\pm$ 1.07

In this, the higher concentration buffer (0.56M) replaced the lower concentration buffers (50-850 mS/cm dextrose buffers). The time required to reach a voltage plateau when the buffers are replaced are noted and thus the electrokinetic mobilities for various buffers are calculated by:

$$\mu_{EK} = \frac{L}{tE} \quad (7.13)$$

where  $L$ ,  $t$ , and  $\vec{E}$ , are the length of microdevice, time taken to reach the voltage plateau when one buffer replaces the other in the microchannel and applied DC electric field, respectively. It is important to note that in this system the EK mobilities do not vary greatly and do not demonstrate a dependence on the conductivity of the buffer as shown in Table 7.1.

### 7.4.3 Operation

As demonstrated in equation (7.6), the dielectrophoretic force that a particle experiences is proportional to its volume (and subsequently its size) as well as the conductivity difference ( $f_{CM}$ ) from the surrounding medium<sup>112</sup>. Therefore, dependencies on fluorescent polystyrene particles of three sizes were studied here as well as on six different conductive buffers. The details of electro-osmotic mobility measurement experiments and polystyrene particle experiments are presented in the next two sections.

#### 7.4.3.1 Electro-osmotic flow measurement

Electro-osmotic flow rate experiments within the main channel into the four outlet channels were conducted by current monitoring methods<sup>238</sup>. The set-up consists of 1 k $\Omega$ -1/2 kW resistor, multimeter (0-500V) (Radioshack, Inc), and a DC power supply (Hewlett Packard 6030A, 0-200V, 17A). Electrical connections with PDMS microdevice were made by using copper electrodes. The experiment was conducted at 10.27 V/cm for plasma-sealed devices using 0.56 M PBS buffer and dextrose added buffers of varying conductivity ranges (50-850 mS/cm) as shown in Table 7.1. The impact on EOF from alternative sealing mechanisms were also explored including common methods like UV-Ozone sealed<sup>79</sup> solvent method using IPA<sup>65</sup>, thermal treatment<sup>64</sup> and no treatment for PDMS and glass slide-sealed by pressure application.



The EOF current monitoring configuration involves a 1 k $\Omega$  (1/2 kW) resistor connected in series to the microdevice. A multimeter was connected across the resistor for constant monitoring of voltage. The microchannels were pre-conditioned by rinsing with e-pure water at least five times, and then filled with lower conductivity buffer (50-850 mS/cm) individually for each experimental set. DC power supply was turned on and initial voltage on multimeter was recorded when low conductivity buffer was present in the microdevice. To minimize pressure driven flow, 30  $\mu$ L of buffer was added to each inlet and outlet ports. The high conductivity buffer (0.56 M PBS) replaced lower conductivity buffer (50-850 mS/cm dextrose added buffers) and the time required to reach a new constant voltage plateau across the resistor was measured. The experiment was repeated at least five times (standard deviation values in Table 7.1) at each DC electric field strength and statistical analysis performed on the measured times to replace the fluidic path with high conductivity buffer.

#### 7.4.3.2 Polystyrene particle experiments

Fluorescent polystyrene particles (Spherotech Inc.) of three different diameters 3.18  $\mu$ m (fluorescent pink, 580 nm emission), 6.2  $\mu$ m (fluorescent ocean blue, 700 nm emission) and 10  $\mu$ m (fluorescent yellow, 480 nm emission) were selected. Fluorescent polystyrene particles were diluted at 1:100 for 3.18  $\mu$ m particles, 1:200 for 6.2  $\mu$ m particles and 1:50 for 10  $\mu$ m particles with all six buffers shown in Table 7.1. The dielectrophoretic mobilities,  $\mu_{DEP}$  for the different sized particles were calculated from equation (7.6): 3.18  $\mu$ m particles:  $2.98 \times 10^{-11}$  cm<sup>4</sup>/Vs; 6.2  $\mu$ m particles:  $1.13 \times 10^{-10}$  cm<sup>4</sup>/Vs and 10  $\mu$ m particles:  $2.95 \times 10^{-10}$  cm<sup>4</sup>/Vs.

A DC power supply was used to deliver 10 or 25 V for separation of the particles over a distance of 1.46 cm between the inlet and outlet ports (corresponding to fields of 6.85 and 17.12 V/cm). The channels were filled with buffer initially and then 30  $\mu$ L of buffer was replaced with sample in the inlet port (similar approach as described in the electro-osmotic flow experiments) after the DC power supply was turned on. Experiments were repeated at least three times and statistical analysis performed on the results.

Raw images of different sized fluorescent particles were taken with a CCD camera (Carl Zeiss, AxioCam MRm, 14 fps) attached to a pseudo-confocal microscope for 5 min at 0.25 s interval for each of the buffer conditions (50-850 mS/cm) and at DC field strengths of 6.85 and 17.12 V/cm. Quantification of particles in each channel was accomplished by using Maximum Intensity Projection (MIP) program in Zeiss AxioVision software (Version 4.6.3) by combining all raw images taken at every 0.25 s for 5 min. For 6.2  $\mu$ m and 10  $\mu$ m particles, analysis was also verified by optically counting the particles in each channel for every 0.25 s un-altered video frames. Detailed image analysis process is explained in the next section.

#### **7.4.4 Image analysis**

Two different analysis techniques were employed as a method of verifying the results obtained: 1) Indirect quantification by intensity profile analysis (all three sizes of particles) 2) Direct quantification by optical counting of particles in each channel (6.2  $\mu$ m and 10  $\mu$ m particles). Indirect quantification involved combining all raw images using MIP program in Zeiss AxioVision software. An example of the composite image is shown in Figure 7.2.

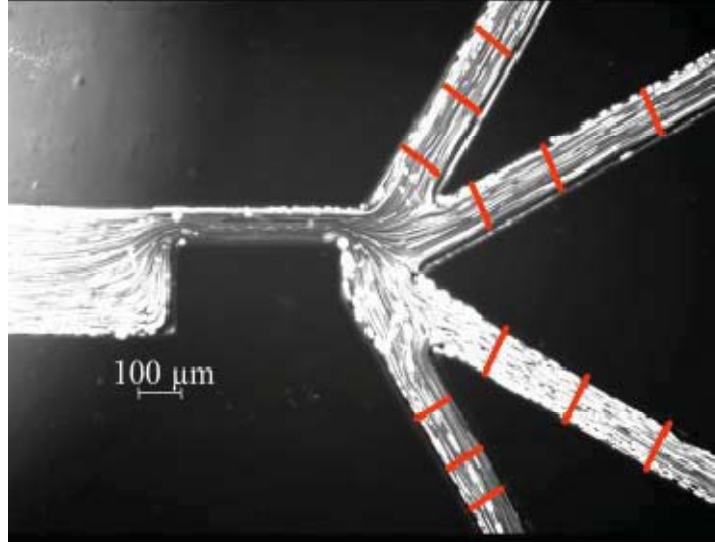


Figure 7.2 Raw images from 3.18  $\mu\text{m}$  particle experiments added by Maximum Intensity Projection (MIP) in AxioVision 4.6.3 software. Intensity profiles (shown in red lines) are drawn across each outlet channel at three different positions. Particles quantified by comparing relative profile intensity across each channel.

An intensity profile was drawn across each channel at three different positions. Care was taken to draw profile excluding a) walls of the channel b) particles trapped at any points of field singularity and c) particles settled in the channel. The particles were quantified by using equation (7.14), where  $N_{Avg}^{Ch}$  is the number of particles present in each channel (Ch) averaged over three different positions ( $X = 1, 2, 3$ );  $I_{Total}^{Ch}$  is the total intensity of all the particles in a channel at one position X;  $I_{p,avg}$  is the average intensity of one particle. Total particle fraction in each channel was calculated by eqn. (15), where  $F^{Ch}$  denotes the fraction of particles present in one outlet channel ( $Ch = 1 \dots 4$ ). Thus particle fractions for all the three sizes of particles at different buffer conditions were calculated by indirect quantification *via* the relative intensity profile method.

$$N_{Avg}^{Ch} = \frac{Avg \left[ \sum_{X=1}^3 I_{Total}^{Ch} \right]}{I_{p,avg}} \quad (7.14)$$

$$F^{Ch} = \frac{N_{Avg}^{Ch}}{\sum_{Ch=1}^4 N_{Avg}^{Ch}} \quad (7.15)$$

$$F^{Ch} = \frac{P_T^{Ch}}{\sum_{Ch=1}^4 P_T^{Ch}} \quad (7.16)$$

In the direct quantification approach to image analysis, particles in each channel were optically counted and fractions were calculated by using equation (7.16), where  $F^{Ch}$  denotes the fraction of particles present in one outlet channel ( $Ch = 1 \dots 4$ ). This method of quantification was only used for large sized particle (6.2 and 10  $\mu\text{m}$ ), as individual particles were optically more distinguishable than 3.18  $\mu\text{m}$  particles.

## 7.5 Results and discussion

### 7.5.1 Electro-osmotic flow measurement and baseline study

Particle motion depends on electro-osmotic and dielectrophoretic mobilities. In order to calculate DEP mobility, electro-osmotic flow measurements have to be achieved. Electro-osmotic mobility was calculated using equation (7.13) for the four sealing methods at 6.85 and 10.3 V/cm electric field strengths. The average electro-osmotic (EO) mobility for plasma-sealed devices across different conductivities at 10.3 V/cm was found to be  $(40 \pm 2.3) \times 10^{-4} \text{ cm}^2/\text{Vs}$ . Comparisons were made between literature reported values and experimental values determined in this work with the four sealing methods. Literature values were compared for native PDMS channels and PDMS channels sealed by plasma treatment<sup>73,239-242</sup> for PBS buffer at  $\sim 850 \text{ mS/cm}$ . Figure 7.3 compiles and compare these literature values to the experimental values obtained in this research.

In native PDMS channels, EO mobility was highest at 10.3 V/cm and 830 mS/cm buffer conductivity. It was ~10 times greater than literature reported values from Ross D. *et al.* group<sup>242</sup>. From Figure 7.3, UV-ozone sealing treatment of PDMS device increased the EO mobility and in this research, a decrease in EO mobility was desired. To reduce electro-osmotic mobility in PDMS channels, two surface modification treatments were explored. Microdevice channels were coated with Tween-20<sup>74</sup> (99.9 %, Fisher Scientific) diluted to 1 % with 0.14 M PBS for 30 minutes before rinsing with the buffer for running experiment; this yielded a 161 % increase in EOF and clustering of particles. A 5 % 8000 MW polyvinyl propylene (PVP) coating was also conducted, following the same procedure<sup>77</sup>. This coating reduced EO mobility by 10 % but plasma-oxidation sealing surpassed this significantly to a final mobility of  $(40 \pm 2.3) \times 10^{-4} \text{ cm}^2/\text{Vs}$ . Therefore, surface modification using plasma-oxidation treatment was adopted for all subsequent experiments to reduce EO mobility in channels. EO mobilities in plasma sealed devices showed small dependencies on buffer conductivities. This change in electro-osmotic mobility influences the length of time a particle flowing through the system experiences a DEP force as it passes by the insulating obstacle. This is explored in greater detail in the polystyrene particle experiments section.

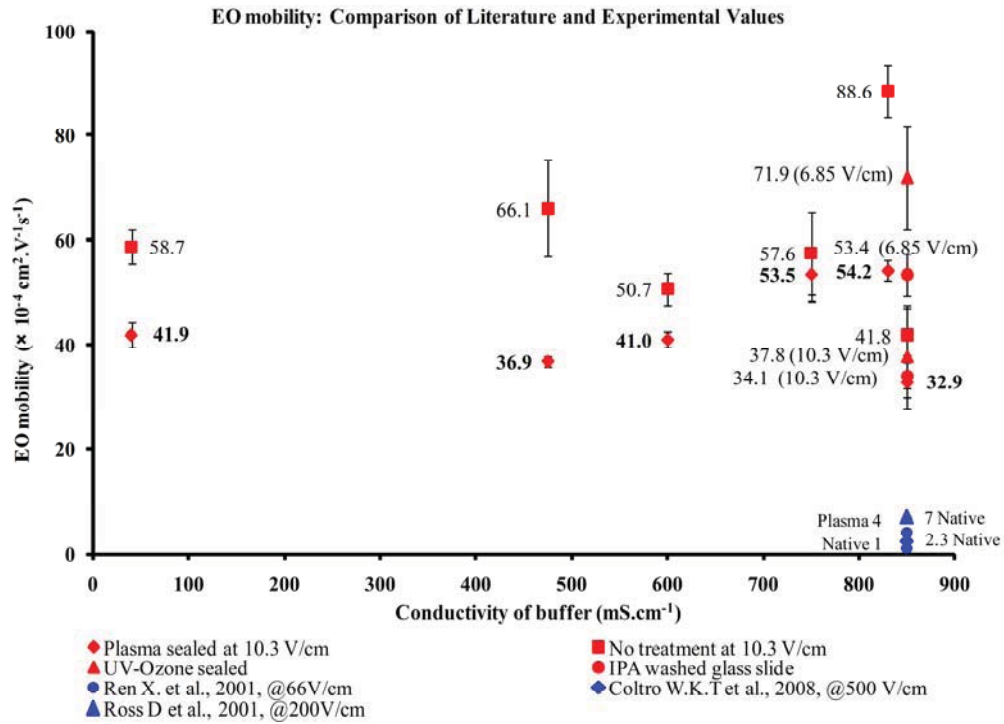


Figure 7.3 Electro-osmotic mobility of plasma-oxidation (in bold numbers), UV-Ozone, IPA washed glass slide and no treatment (native PDMS channels) sealing methods. Comparison of literature reported values from Ren X<sup>239</sup>, Ross D.<sup>242</sup> and Coltro W.K.T.<sup>241</sup> groups are included for plasma sealed and native PDMS channels for PBS buffer. Our EOF results are much greater in magnitude at lower applied fields and the average EOF value for plasma sealed device was  $(40 \pm 2.3) \times 10^{-4} \text{ cm}^2/\text{Vs}$  at 10.3 V/cm.

Before testing the size dependency, baseline was established to fix the best operating parameters like DC voltage and medium conductivity. This is shown in Figure 7.4, where two different behavior regions were observed for the six different buffers in electric fields from 6.85 to 136 V/cm. At lower conductivities (50 mS/cm) there was no noticeable electrolysis observed until 200 V over the 1.46 cm device, but at higher conductivities (475-850 mS/cm) the maximum voltage to operate without any detectable electrolysis was sequentially reduced. 1 % dextrose buffer (830 mS/cm) had severe electrolysis at the inlet ports, which increased the precipitant formation in the inlet thus blocking the inlet channel. The blue diamonds in Figure 7.4 indicate the safe operating

regions for all the experiments at different conductivities and electric fields; red circles identify adverse operating conditions due to electrolysis and precipitant formation at electrodes, thus blocking the microchannels.

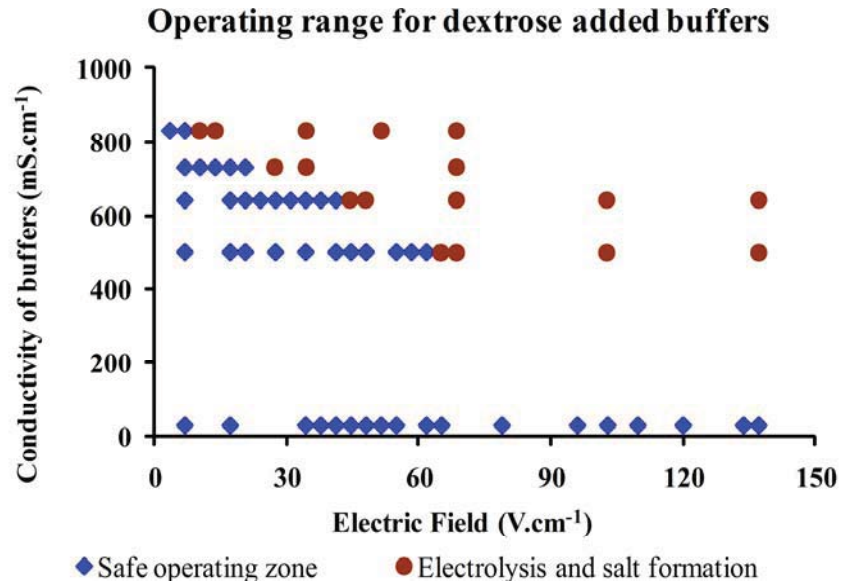


Figure 7.4 Operating window for size dependency experiments at different buffer conductivity (50-850 mS/cm) and electric field strength (6.85-136 V/cm). Blue area is the safe operating zone for experiments, whereas in the red area heavy salt precipitation occurred at the inlet thus blocking the channels.

## 7.5.2 Polystyrene particle experiments

Here, three different dependencies were explored: size, magnitude of the DC electric field and medium conductivity.

### 7.5.2.1 Size dependency

Fluorescent polystyrene particles of three different sizes were chosen for experiments. These experiments were conducted in order to observe the deflection pattern near the insulating obstacle region based on size in the multi-channel outlet design. As discussed earlier, particles experience nDEP and the magnitude of deflection depends on

dielectrophoretic force experiences by these particles. The force experienced is again dependent on the particle polarizability and size of the particle.

#### 7.5.2.1.1 3.18 $\mu\text{m}$ particles

Samples were prepared with different buffer conductivities as described in sample preparation section. Due to the smaller particle size and their high velocity in the DC-iDEP channel system, 3.18  $\mu\text{m}$  particle flow events were quantified in each of the four channels with MIP as described under Image analysis section. Intensity as a function of the position was generated for each image in the time sequence. As a result, one can observe intensity spikes for each particle flowing event. At different conductivities, the particle concentration varied in each channel as shown in figure 7.5 (g). From Figure 7.5 (g), channel 3 had the highest particle fraction at 50, 475 and 600 mS/cm (low conductivity). Quantified and observed results at 50, 475 and 600 mS/cm conductivities (Figures 7.5 (a), (c), (e) and (g)) shows that channel 3 is slightly preferred compared to other channels.

A set of simulations were carried out to predict the electrokinetic trajectories of these particles (3.18  $\mu\text{m}$  diameter) at 50, 475 and 600 mS/cm by applying DC voltage of 25 V ( $E= 17.12$  V/cm). These specific conductivities were chosen depending on the experimental results observed in Figures 7.5 (a), (c), (e) and (g). Each line in Figures 7.5 (b), (d) and (f) are equivalent to the path of a single particle. By comparing these results with the experimental results, some agreement was established, indicating slightly preferred channel to be 3.



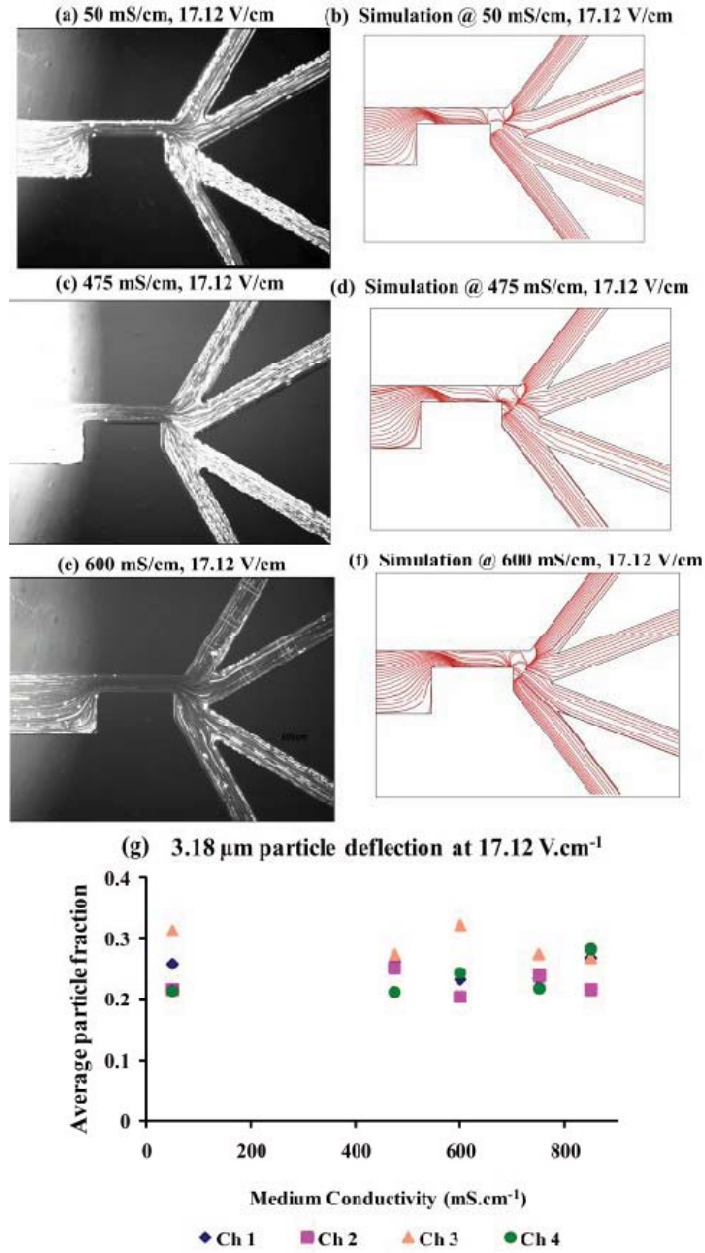


Figure 7.5 (a) Raw images of 3.18  $\mu\text{m}$  particle trajectories combined by MIP program at 50, 450 and 600  $\text{mS}/\text{cm}$  and 17.12  $\text{V}/\text{cm}$ . (b) Particle trajectories obtained for 3.18  $\mu\text{m}$  particles at 17.12  $\text{V}/\text{cm}$ , 50, 450 and 600  $\text{mS}/\text{cm}$ . Channels 3 and 4 are preferred at 17.12  $\text{V}/\text{cm}$ . (c) Deflection of 3.18  $\mu\text{m}$  particles at 17.12  $\text{V}/\text{cm}$  over a range of buffer conductivities. Channel 3 was the slightly preferred channel for all the buffer conductivities.

#### 7.5.2.1.2 6.2 $\mu\text{m}$ particles

The flow patterns of 6.2  $\mu\text{m}$  particles were also quantified using the raw image by MIP. This resulted in composite images showing particle streaks down the length of outlet channels (Figure 7.6 (a)). Experiments were run at 17.12 V/cm and five different buffer conductivities. Using equations (7.14) and (7.15), the total number of particles, and fractions for each channel and for each electric field condition were obtained. Experimental results suggested that the channel preference for 6.2  $\mu\text{m}$  particles was channel 4 for low buffer conductivities as shown in Figure 7.6 (c). To verify the results obtained by intensity profile analysis, direct quantification method using equation (7.16) was also conducted. The particle fractions obtained by this method were in close agreement with the indirect quantification method. Simulations were conducted to predict the electrokinetic trajectories of the 6.2  $\mu\text{m}$  particles employing 600 mS/cm buffer conductivity and 17.12 V/cm to verify the experimental observations. Figure 7.6 (b) shows the electrokinetic particle trajectories predicted. 6.2  $\mu\text{m}$  particles seem to prefer channel 4, which is in agreement with the experimental results.

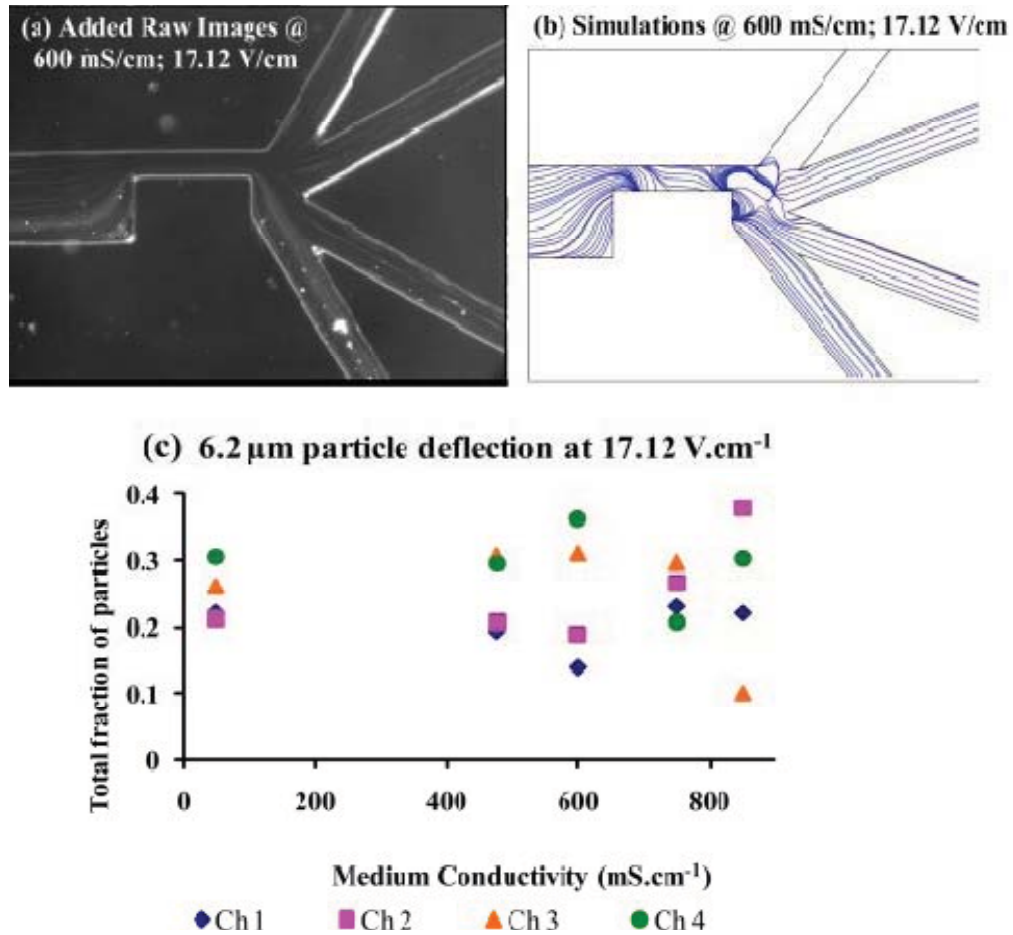


Figure 7.6 (a) Raw images of 6.2 μm particle trajectories combined by MIP program at 600 mS/cm and 17.12 V/cm. (b) Particle trajectories obtained for 6.2 μm particles at 17.12 V/cm and 600 mS/cm. Channel 4 is preferred at 17.12 V/cm and lower conductivities. (c) Deflection of 3.18 μm particles at 17.12 V/cm over a range of buffer conductivities. Channel 4 was preferred for all the buffer conductivities.

### 7.5.2.1.3 10 μm particles

Raw images from the microscope were quantified by obtaining a composite image from MIP as shown in figure 7.7 (a) for 450 mS/cm, 17.12 V/cm conditions. The particle events in each channel were compiled in Figure 7.7 (c); channels 1 and 2 each captured a third or greater of the total particles at 17.12 V/cm.

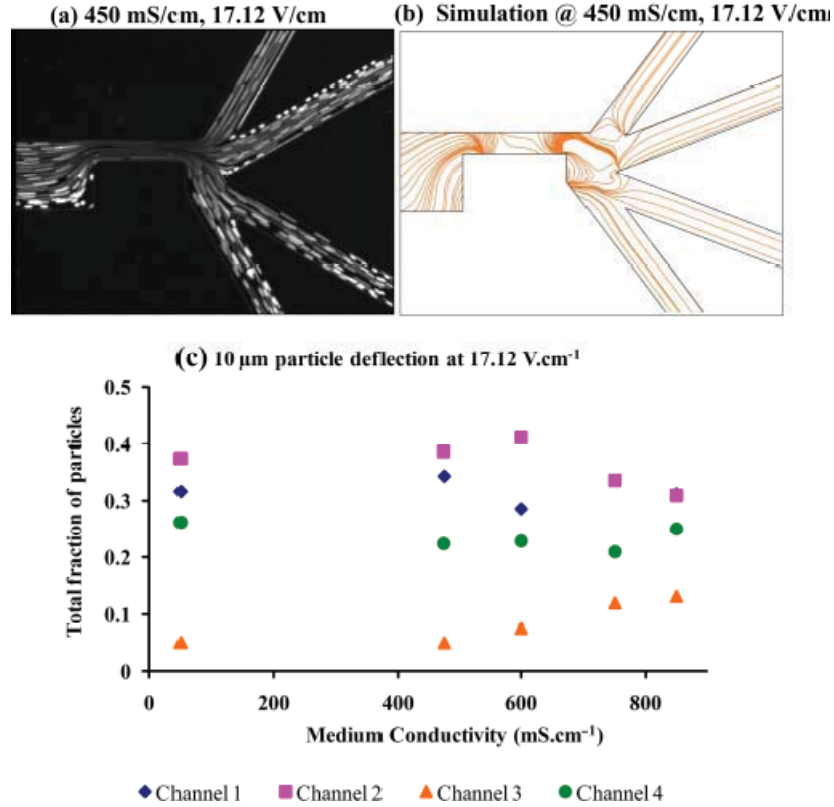


Figure 7.7 (a) Raw images of 10 μm particle trajectories combined by MIP program at 450 mS/cm, 17.12 V/cm. (b) Simulated particle trajectories obtained for 10 μm particles at 17.12 V/cm, 450 mS/cm. Channel 2 is preferred at 17.12 V/cm. (c) Deflection of 10 μm particles at 17.12 V/cm over a range of buffer conductivities. Channel 2 was preferred for all the buffer conductivities.

To verify the experimental results obtained by intensity profile analysis, direct quantification method was also conducted using equation 7.16. The particle fractions obtained by this method were in close agreement with the indirect quantification method. A set of simulations to predict the trajectories for the 10 μm particles was conducted at all five medium conductivities. In Figure 7.7 (b) particle trajectories at 450 mS/cm, 17.12 V/cm are shown which indicates that 10 μm particles preferred channel 2.

From size dependency studies, it is possible to observe that 3.18 μm particles deflection showed a slight preference toward channel 3, 6.2 μm particles experienced the

least dielectrophoretic effect and were deflected from the insulating obstacle into channel 4 and 10  $\mu\text{m}$  particles experienced the greatest DEP force effect and were repelled from insulating obstacle into channel 2. From equation 7.6, dielectrophoretic force is proportional to the square of the diameter of particle i.e. dielectrophoretic effect is high for larger particles compared to smaller particles. In this research, this phenomenon was demonstrated, showing that there is size dependency and thus they are deflected into different channels.

#### **7.5.2.2 Electric field dependency**

Dielectrophoretic force on the particle is proportional to the square of the gradient of electric field strength from equation 7.6. This effect will cause the particle deflection to be altered. To verify the same phenomena in this study, electric field dependency studies were conducted. Comparison experiments for 3.18 and 10  $\mu\text{m}$  particles at different electric field strengths were not conducted. The results obtained for 6.2  $\mu\text{m}$  particles were treated as a standard for estimating better separation conditions at different electric fields (6.85 and 17.12 V/cm); 17.12 V/cm field yielded higher separation efficiency compared to 6.85 V/cm.

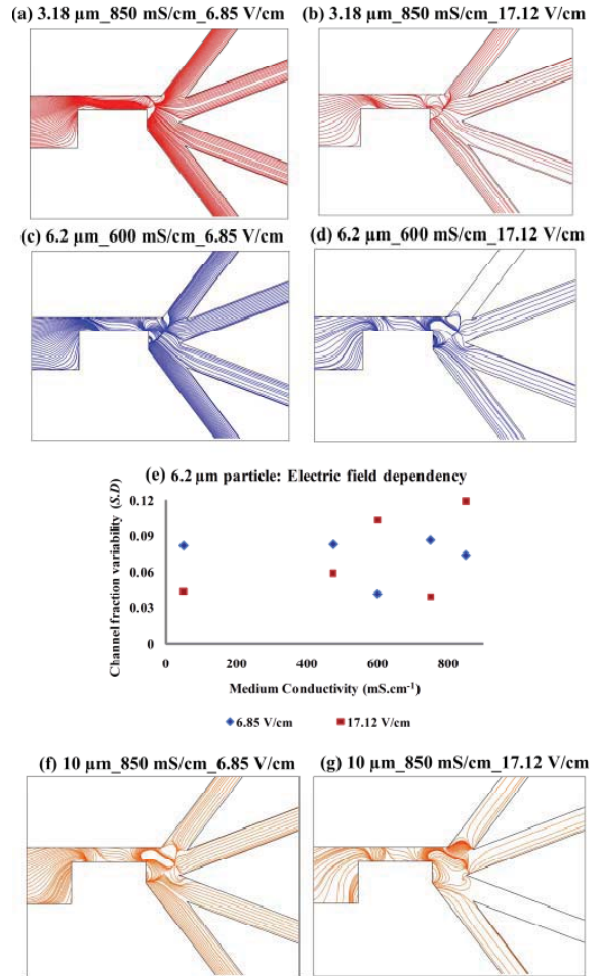


Figure 7.8 (a) and (b) simulated particle trajectories for 3.18  $\mu\text{m}$  particles at 850 mS/cm medium conductivity and 6.85, 17.12 V/cm DC electric field strength conditions respectively, (c) and (d) simulated particle trajectories for 6.2  $\mu\text{m}$  particles at 600 mS/cm medium conductivity and 6.85, 17.12 V/cm DC electric field strength conditions respectively, (e) Channel particle fraction variability for 6.2  $\mu\text{m}$  particles at electric field conditions of 6.85 and 17.12 V/cm plotted as a function of medium conductivity, (f) and (g) simulated particle trajectories for 10  $\mu\text{m}$  particles at 850 mS/cm medium conductivity and 6.85, 17.12 V/cm DC electric field strength conditions respectively.

From simulations comparing Figure 7.8 (a) and (b) at 850 mS/cm buffer condition, there is no significant effect on particle trajectories at lower field but by increasing the magnitude of the DC field to 17.12 V/cm, a change in the particle

trajectories is noticeable. For 6.2  $\mu\text{m}$  particles, experiments were conducted at 6.85 V/cm and 17.12 V/cm DC field strengths to compare the variability of particle fractions in different channels. This variability was quantified by taking standard deviation (*S.D.*) of particle fractions  $F^{Ch}$  for all the four outlet channels. *S.D.* was calculated by equation (7.17) and plotted as shown in Figure 7.8 (e).

$$S.D. = \sqrt{\frac{1}{4} \sum_{Ch=1}^4 (F^{Ch} - F_{avg})^2} \quad (7.17)$$

where  $F_{avg}$  is the average of the particle fractions in all four channels. *S.D.* is used to compare particle flow at two voltage conditions. Higher values of *S.D.* indicate better channel separation.

From Figure 7.8 (e), better separations were achieved at 17.12 V/cm (red squares) with some dependency on buffer conditions compared to 6.85 V/cm (blue diamond). From simulations, comparing Figures 7.8 (c) and (d) for 6.85 and 17.12 V/cm at 600 mS/cm, 17.12 V/cm has better separation compared to 6.85 V/cm *i.e.* in the 17.12 V/cm case, channel 1 is not available and channels 2 and 3 are the least preferred, thus yielding better separation at higher electric field strength.

For 10  $\mu\text{m}$  particles simulations were compared (Figures 7.8 (f) and (g)) at 850 mS/cm buffer condition, there was no significant effect on particle trajectories at lower field strength (6.85 V/cm) but by increasing the DC electric field to 17.12 V/cm, there were no particle trajectories in channel 3.

Dependency on field strength exists and separations could be best achieved by manipulating the electric field. In this research, 17.12 V/cm DC field strength provides high sorting efficiency compared to 6.85 V/cm. From equation 7.6 dielectrophoretic

mobility is proportional to the square of the gradient of electric field strength (DC applied potential). An increase in electric field strength increases the dielectrophoretic force experienced by the particle and is attributed to DEP trapping behaviors. These trends are consistent with experimental results observed as well as simulations (see Figures 7.5, 7.6 and 7.7).

### 7.5.2.3 Medium conductivity dependency

From equations 7.6 and 7.7, dielectrophoretic force depends on medium conductivity properties. Here, comparison were made to study conductivity dependency by considering total particle fractions for all three particle sizes at 17.12 V/cm. Channel fraction variability was calculated by standard deviation (*S.D.*) using equation 7.17. Larger values of *S.D.* indicate better separation.

From Figure 7.9 (a), greater variability (*S.D.*) values were found at 600 mS/cm, which indicates optimal buffer conditions to maximize DEP force in the device and thus more pronounced separations into channels. In general, 10  $\mu\text{m}$  particles have better separation efficiency based on large variability (*S.D.*) values.

From simulations results, negative DEP effect becomes more important at high buffer conductivity (850 mS/cm) as can be seen by comparing Figure 7.9 (b), (c) and (d) at 17.12 V/cm. It can be seen that pathlines located at the downstream corner of the obstacle exhibit greater deflection with increasing particle size. Also DEP effect increases substantially with small variations of particle size (variations in diameter from 3-4  $\mu\text{m}$ ). At lower buffer conductivities (50 mS/cm), Figures 7.9 (e), (f) and (g) at 17.12 V/cm are considered.



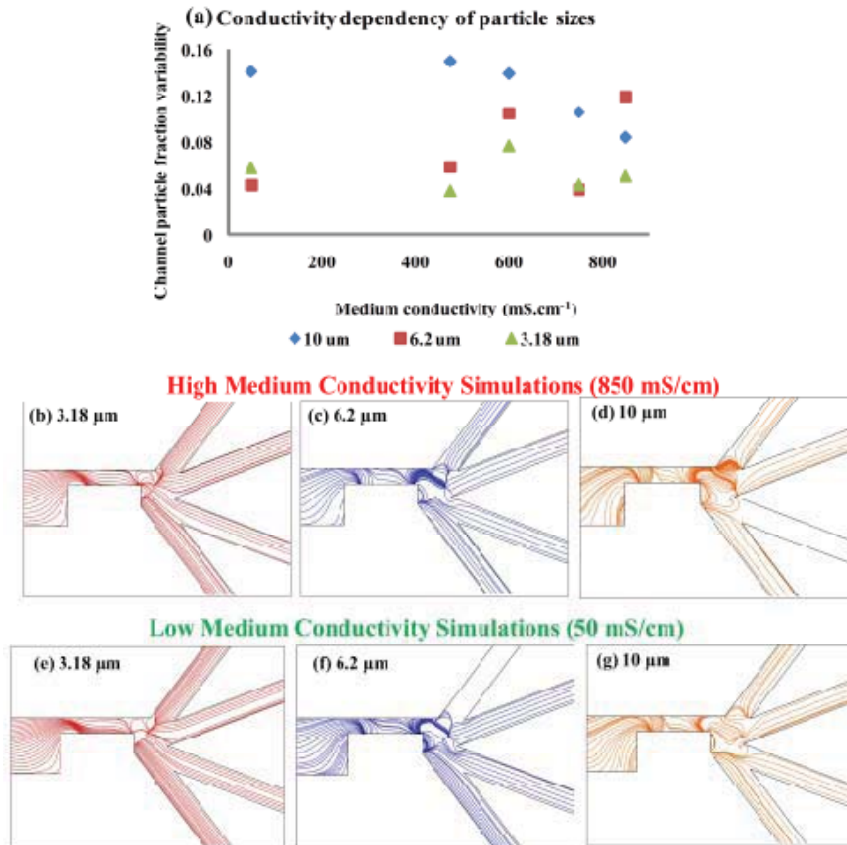


Figure 7.9 (a) Channel particle fraction variability for 3.18 (green triangles), 6.2 (red squares) and 10  $\mu\text{m}$  (blue diamond) particles at electric field conditions of 17.12 V/cm plotted as a function of medium conductivity. (b), (c) and (d) simulated particle trajectories at 17.12 V/cm and 850 mS/cm for 3.18, 6.2 and 10  $\mu\text{m}$  particles. (e), (f) and (g) Simulated particle trajectories at 17.12 V/cm and 50 mS/cm for 3.18, 6.2 and 10  $\mu\text{m}$  particles.

The two cases presented in here (low and high medium conductivity conditions at 17.12 V/cm), show that there is a channel that is not available depending on the size of the particle. Results from experiments and simulations, shows that medium conductivity also influences separation and sorting of particle along with other parameters like size and electric field. Also from experiments, the optimal buffer condition for spatial sorting into channels of these three different particles was 600 mS/cm.

### 7.5.3 2-channel system

In a 4-channel system, 6.2  $\mu\text{m}$  particles experiences least dielectrophoretic effect and were deflected by the rectangular obstacle into channel 4, whereas 10  $\mu\text{m}$  particles were deflected into channel 2 thus experiencing strong DEP effect. The 3.18  $\mu\text{m}$  particles at most buffer conductivities slightly preferred channel 3. These experimental results are in agreement with simulations results obtained in this research study and by other groups that have achieved continuous separation of particles into two channels in a rectangular obstacle. Here, only 6.2  $\mu\text{m}$  and 10  $\mu\text{m}$  particles are considered for proving the two-channel system in line with other groups of researchers<sup>117</sup>. The conditions and design adopted in this research is different from the past researchers<sup>117</sup> because they adopt: (1) 2-channel system, (2) inlet position different, (3) DC potential applied at all 4 ports (2 inlet and 2 outlet ports), and (4) DC electric field applied is  $\sim 10$ -15 times greater than the applied electric field in this research project. By reducing our 4-channel system into a two-channel system *i.e.* by combining channels 1 and 2 labeled as channel (A) and channels 3 and 4 labeled as channel (B) in Figure 7.10 (inset), reproduces the same result. Figure 7.10 shows a two-channel system with the deflection of 6.2  $\mu\text{m}$  and 10  $\mu\text{m}$  particles at different buffer conditions. First, the particle fractions were converted into 2-channel system by adding particle fractions of individual channels by,

$$F_A^c = F_1^c + F_2^c \quad (7.18)$$

$$F_B^c = F_3^c + F_4^c \quad (7.19)$$

Particle fraction difference  $\delta$  between channel A and B is,

$$\delta = F_A^c - F_B^c \quad (7.20)$$

If the difference  $\delta$  in channel (A) and (B) is positive, then particles prefer channel (A); but if the difference is negative, particles prefer channel (B). The deflection pattern for 6.2  $\mu\text{m}$  particles indicated towards channel (B), but for 10  $\mu\text{m}$  particles they were repelled from insulating obstacle region towards channel (A). This supports prior experimental observations that smaller particles experience lesser nDEP effect compared to larger particles whose trajectories are dominated by electrophoretic and electro-osmotic flow forces with a greater DEP force from the obstacle.

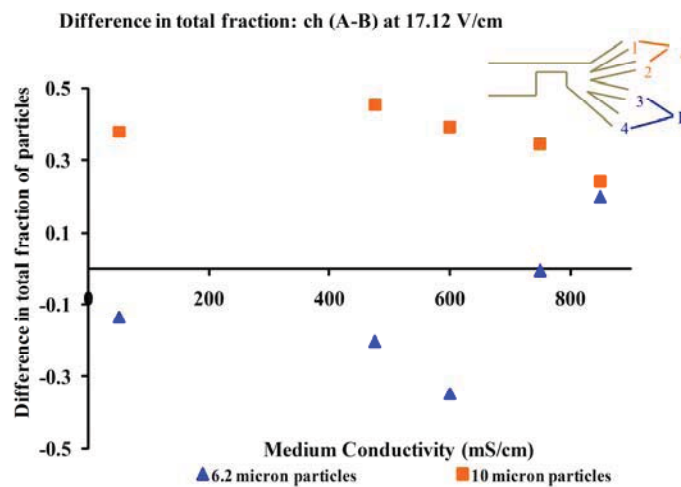


Figure 7.10 Deflection of 6.2 (blue triangles) and 10  $\mu\text{m}$  (orange squares) particles in a 2-channel system at different buffer conductivity values. Inset shows the 2-channel system where channel A is the sum of channels 1 and 2; channel B is the sum of channels 3 and 4. Positive particle fraction difference ' $\delta$ ' indicates particles are deflected into channel A and negative indicates deflection towards channel B. 6.2  $\mu\text{m}$  particles deflected towards channel B and 10  $\mu\text{m}$  particles deflected into channel A. Optimal buffer conductivity to achieve better separation is  $\sim 600$  mS/cm.

Further examination of the dependence on medium conductivity shows greater average deflection of 6.2  $\mu\text{m}$  particles with decreasing conductivities due to lesser DEP force experienced by the particles. The 10  $\mu\text{m}$  particles experience greater negative DEP

force at the obstacle, thus displaying a more pronounced separation into A (Channels 1 and 2) with decreasing conductivity. The optimal buffer conductivity for separations appears to be  $\sim 600$  mS/cm.

## 7.6 Conclusions

Direct current insulator-based dielectrophoresis (DC-iDEP) is a relatively new technique that emerged within the last decade. It has a great potential for technological applications in medicine, biology and industry yielding in point of care devices.

In this research, fluorescent polystyrene microparticles motion was studied in a PDMS microchannel with a rectangular insulating obstacle and four outlet channels by applying only DC electric fields at various buffer conductivities. The impact of the field non-uniformities in the channel was studied by examining particle trajectories into the four outlet channels. Particle deflection in DC-iDEP depends on two forces: negative dielectrophoresis and electro-osmosis. To quantify electro-osmotic mobility baseline experiments were performed at different buffer conditions and different sealing mechanisms. Electro-osmotic mobility did not vary considerably with different buffer conductivities and for a plasma-sealed device the mobility was  $(40 \pm 2.3) \times 10^{-4}$  cm<sup>2</sup>/Vs at 10.3 V/cm.

Three dependencies were studied: size dependency, DC electric field dependency, and medium conductivity dependency. Simulations were carried out to support the experimental work using *COMSOL Multiphysics*<sup>®</sup> software. From size dependency experiments and simulation results at 17.12 V/cm, 3.18  $\mu$ m particles slightly preferred channel 3, 6.2  $\mu$ m particles experienced a weaker DEP force at the rectangular insulating obstacle, thus pushing particles into channel 4, while 10  $\mu$ m particles experienced

strongest negative DEP force repelling the particles into channels 1 and 2. Two different electric field strengths (6.85 and 17.12 V/cm) were compared to study field dependency on separation of 6.2  $\mu\text{m}$  particles; experimental and simulation results suggested that 17.12 V/cm yielded a better spatial separation efficiencies compared to 6.85 V/cm. Medium conductivity was also a dependent factor for particle separations and simulations and experimental work suggested 600 mS/cm as the optimal buffer condition for separation. The 4-channel system with an insulating obstacle geometry explored in this research was reduced into a two channel system (channel A and channel B). The results obtained were similar to the past research on polystyrene particles by different research groups in a 2-channel system. But the novelty of the research here is due to: (1) multiple outlets sorting, (2) low DC electric field applied to achieve sorting and this minimizes Joule heating effects, (3) due to low DC voltages, portability of these devices could be easily achieved, (4) fine tuning of DC electric field and medium conductivity; particles could be guided into different channels because separation of particles depend on DC electric field and medium conductivity from Figures 7.8 and 7.9, and (5) at low medium conductivity, separation of the particles better; thus avoiding electrolysis and electrode fouling<sup>200</sup>.

The study presented here could be applied to multiparticle sorting and separation, *e.g.* bioparticles of interest as the DC field applied is not high enough to damage bioparticles. The properties of the medium (conductivity and pH) and electric field applied could be further controlled in order to achieve higher separation efficiency. Electro-osmotic mobility could be manipulated by employing different surface-modification techniques.

The results presented here illustrate the great potential of DC-iDEP to be employed for rapid and effective sorting of bioparticles, with potential applications in clinical analysis and medical diagnostics. Future work is envisioned to develop DC-iDEP as a powerful and robust method for the continuous separation of a wide array of bioparticles, from bacterial to red blood and mammalian cells.

In the next chapter, the same microfluidic platform developed here will be utilized to sort red blood cells based on DC insulator dielectrophoretic phenomena based on human ABO blood typing system.

CHAPTER VIII  
INSULATOR BASED DC DIELECTROPHORETIC BLOOD TYPING: HUMAN ABO  
SYSTEM

### 8.1 Introduction

In this chapter, a microfluidic platform is developed for quantifying the dependence of erythrocyte responses by ABO blood type via direct current insulator dielectrophoresis (DC-iDEP) phenomenon. The DC-iDEP device utilized a 400  $\mu\text{m}$  wide rectangular insulating obstacle embedded in a 1.46 cm long, 200  $\mu\text{m}$  wide channel to create spatial non-uniformities in field density. Immediately past the insulating obstacle the main channel bifurcates into four outlet channels each 50  $\mu\text{m}$  wide. The goal of this configuration is to spatially sort into the channels based on individual erythrocyte deflection from the insulating obstacle by DC-iDEP forces. The PDMS device and insulating obstacle were fabricated using the rapid prototyping soft-photolithography process developed by Whitesides *et al.* group<sup>46</sup>. The PDMS device was sealed to a glass slide by plasma oxidation and ports drilled with a biopsy punch. The DC-iDEP red blood cell flow behaviors were investigated with all 8 blood types (A+, A-, B+, B-, AB+, AB-, O+, and O-) in the human ABO blood typing system. Red blood cells were isolated from plasma and suspended at a concentration of 1:750. Different conductivity buffers ranging from 100 to 900 mS/cm and electric fields from 17.12 to 68.5 V/cm were applied to investigate separation dependencies. An SVM microscope from LabSmith<sup>®</sup> was used to capture video at 30 fps for 5 min. The data analysis was conducted with custom-built

software from Sandia National Laboratories that utilizes image intensity profiles at locations prior to the obstacle and in all four outlet channels. The resulting intensity profiles identify particle flow events in the channel at each position as a function of time. Erythrocyte concentration factors were estimated from the total intensities exhibited by a composite sum of cells in the 5 min experimental run. It is hypothesized that antigens expressed on the RBC membrane will impact the resulting DC-iDEP force the cell experiences thus causing deflection of the cell type predominantly into a single channel. By tracking concentrations in each channel, our goal is to correlate dominant channel with blood type.

This lab-on-a-chip technology application could be applied to emergency situations, natural calamities, accidents, etc. for blood typing in an accurate, portable, and minimal error free way.

This chapter is organized into a discussion of electrokinetic cell manipulation techniques especially DC-iDEP, the theory behind the DC-iDEP technique as pertinent to red blood cells membrane properties, followed by experimental materials and methods, results, and finally conclusions from this study. The results and discussion section presents donor reproducibility studies, sorting of RBCs by blood type, effect of conductivity of the medium and effect of electric field. The chapter concludes with summary and application of this explored novel technique to sort red blood cells by ABO types.

## **8.2 Manipulation of bioparticles by DC-iDEP**

Dielectrophoresis is a non-invasive and non destructive technique popularly used for manipulating bioparticles like mammalian cells, bacteria, virus, yeast cells, cancerous



cells, and other<sup>85,89,105,146-147,187,207,230</sup>. A bioparticles' dielectrophoretic behavior can be explored by employing both DC and AC signals to generate non-uniform electric fields<sup>80</sup>. Traditionally, dielectrophoresis utilizes embedded metal electrodes in the channel in concert with AC electrical signals to create non-uniformities in the electric field<sup>1,41,243</sup>. In a distinctly different approach, direct current insulator based dielectrophoresis (DC-iDEP) phenomena utilizes an embedded insulating obstacle of varying geometry in the channel to create spatial non-uniformities in the applied electric field<sup>81,113,128</sup>.

Direct current insulator based dielectrophoresis is a novel technique first explored by Masuda *et al.* group for cell fusion studies<sup>201</sup>. Its exponential growth over the last decade has expanded to the point where this is now a viable technology for medical diagnostic applications involving point of care devices that is portable and can be applied in emergency situations or for early disease diagnostic purposes. DC-iDEP is a better technology for portable medical diagnostics than AC dielectrophoresis as summarized in the following Table 8.1:

Table 8.1 Difference between AC and DC dielectrophoretic system

<b>AC-DEP</b>	<b>DC-DEP</b>
Operated by AC field	Operational by both AC and DC fields
Electrodes response create field non-uniformity	Insulator obstacle creates field non-uniformity
Electrodes inside channel	Electrodes in inlet and outlet ports
Fabrication difficult- metal components in channel	Fabrication easier- Insulators from soft lithography
Batch process	Continuous process

To avoid these problems in cell manipulation due to embedded electrodes, insulating based dielectrophoresis was developed. This technique was further explored by Chou *et al.* by employing insulating constriction in the channel for manipulating DNA<sup>128</sup> and then by Cummings and Singh employing insulating posts made of glass<sup>113</sup>. Two flow regimes were explored by Cummings and Singh called ‘streaming DEP’ and ‘trapping DEP’<sup>113</sup>. Cells are focused by the electrical field then flow in streamlines during streaming DEP, but cells get immobilized at the electrode surface during trapping DEP. Traditional DC-iDEP devices have yielded separation and trapping of DNA<sup>128</sup>, viruses<sup>116</sup>, bacteria<sup>125</sup>, isolation of live and dead cells<sup>112</sup>, and protein manipulation<sup>126</sup> by employing suitable DC fields and various insulating obstacle geometries. There are not many researchers who have investigated DC-iDEP behavior on mammalian cells, Kang *et al.* group<sup>118</sup> and Jen *et al.* group<sup>213-214</sup>. But with this technique researchers could achieve separation of yeast cells by its phenotype using pressure driven flow in a rectangular insulating obstacle geometry via low frequency AC-iDEP technique<sup>137</sup>. This technique is discriminating enough to detect yeast phenotype when the genotype is identical, so based on this hypothesis DC-iDEP will be able to discern antigen expression on RBC surfaces. This is further supported by AC-DEP results (Chapter 5) which yielded sorting of red blood cells by its type at  $0.025 V_{pp}/\mu m$  and 1 MHz frequency<sup>1</sup>. O+ could be distinguished from all the other positive blood types with >95% confidence<sup>1</sup>. Studies on performance of microdevice based on medium properties and prediction of trapping zones in DC-iDEP devices were also reported by Lapizco *et al.* group<sup>204,217</sup>.

Blood typing is an essential step in blood transfusions, which frequently occur under time-sensitive conditions due to trauma. The human ABO blood type system was discovered by Karl Landsteiner and is one of 30 blood typing systems recognized by the

International Society of Blood Transfusion (ISBT)<sup>1,165</sup>. The Rhesus factor (Rh) is also one among the 30 blood typing systems. The ABO blood typing system involves antigens A and B that share a common polysaccharide backbone but terminate differently. The A antigen terminates in an  $\alpha$  1,3-linked N-acetylgalactosamine while B terminates in an  $\alpha$  1,3-linked galactose<sup>166</sup>. Human blood types are classified based on (1) membrane surface antigens that span the entire membrane and (2) blood plasma antibodies thus yielding 8 blood types: A+, B+, AB+, O+, A-, B-, AB- and O-<sup>166</sup>. Type A blood cells express antigen A on their membrane surface, type B blood cells express antigen B, type AB blood cells have both A and B antigens while type O blood has only the non-functional antigen backbone. In the blood plasma, antibodies against other antigens exist; e.g. A+ blood has anti-B antibodies in the plasma. Currently, the accurate typing of blood is time, money and labor intensive and is performed by agglutination methods. This involves an assay where the unknown blood sample is treated with antibodies A and B thus yielding the blood type in three steps<sup>43</sup>. This method takes a lab technician approximately 30 min, but medical laboratory proximity and overhead may increase this wait beyond a day. Advances in lab-on-a-chip technology have the potential to reduce these concerns while simultaneously providing the convenience of completing the blood classification at the patient's bedside. This kind of point of care (POC) technology is the focus of our research to rapidly sort blood cells using low voltage DC fields in a lab-on-a-chip platform.

Traditional red blood cell manipulations were accomplished by flow cytometry and spectrophotometric techniques<sup>1</sup>. Due to the advancement in microfluidics for lab-on-a-chip platforms, many other mechanical, electrical, and chemical methods evolved. One such electrical technique is dielectrophoresis, which is gentle on cells and allows for high

degrees of sensitivity when positioning target cells for identification. Recently, our group investigated red blood cell responses using AC dielectrophoresis and observed a dependence on blood type<sup>1</sup>. O+ could be distinguished from all other positive blood types with greater than 95 % confidence at 1 MHz frequency and 0.025 V<sub>pp</sub>/μm AC electric field. Only two other articles have investigated the antigen responses of O<sup>141</sup> and A<sup>88</sup> blood groups. All of these investigations utilized embedded metallic electrodes which may pose harm to the sample due to the use of high electric field to accomplish focusing, trapping, separation or manipulation. AC DEP is predominantly a microbatch setup so cell behaviors are composite for a finite number of cells. Further, portability of final LOC devices is a concern; batteries and electronics to produce alternating current electrical signals are less portable than for direct current signals. This is the premise for our DC-iDEP investigations of ABO blood types.

The only publications in the literature on DC-iDEP and human cells or blood are manipulation of human cancerous cell lines (HeLa) and separation of human white blood cells from breast cancer cell groups<sup>118</sup>. The application of DC-iDEP for manipulating red blood cells remains unexplored and according to the authors' knowledge, this is the first study where dependencies related to erythrocyte responses in DC-iDEP have been studied. This investigation builds off our prior findings that AC DEP cell polarizations differ due to the difference in red blood cell antigen structures. The implications of this are that the cell polarizations yield motion along an electric field gradient based on ABO blood types such that blood type can be ascertained in less than 5 min. The current work improves upon this by continuously sorting human ABO blood types depending on the red blood cell surface antigens *via* DC-iDEP electric fields in a novel microfluidic platform with an embedded rectangular insulating obstacle in the inlet channel and four

outlet channels. This research study has been split into four sections dealing with donor reproducibility studies, blood type sorting into the four channel geometry, dependence on DC electric field strength, and dependence on medium conductivity.

The next section discusses the forces governing DC insulator based dielectrophoresis and some of the important properties of erythrocytes.

### 8.3 Theory

Dielectrophoresis is the motion of polarized dielectric particles when subjected to non-uniform AC or DC electric fields<sup>1,41</sup>. In AC DEP, non-uniformity is caused by spatial orientation of the electrodes as well as the sigmoidal electrical signal. However, in DC-iDEP, field non-uniformity is only spatial in nature and is created with insulating structures embedded in the microchannel. As a result, the observed DC-iDEP polarized particle motion depends on two forces: electrokinetic and dielectrophoretic as shown in equation 8.1.

$$\vec{j} \propto \vec{u}_{EK} + \vec{u}_{DEP} \quad (8.1)$$

where  $\vec{j}$  is the particle flux. Electrokinetic mobility  $\vec{u}_{EK}$  is expressed as the sum of electrophoretic and electro-osmotic forces.

For large diameter particles like red blood cell, electrophoretic mobility can be neglected because of the substantial drag on the particle<sup>204</sup>. The particle motion now depends only on electro-osmotic flow induced by the charged channel walls and dielectrophoretic mobility created by the spatial non-uniformities in the electric field.

For a spherical particle, dielectrophoretic mobility is dependent on the diameter of the particle, conducting medium properties and the particle polarizability captured by the Clausius-Mossotti factor as shown in equation 8.2.

$$\mu_{DEP} = \frac{\pi d_p^2 \epsilon_m f_{CM}}{12\eta} \quad (8.2)$$

Where  $\mu_{DEP}$  is the dielectrophoretic mobility of the particle,  $d_p$  particle diameter,  $\epsilon_m$  permittivity of the medium,  $f_{CM}$  Clausius-Mossotti factor and  $\eta$  viscosity of the medium. In AC DEP, the Clausius-Mossotti factor depends on the permittivity of medium and particle which both contain real and imaginary terms due to the AC frequency.

$$\alpha = \frac{(\tilde{\epsilon}_p - \tilde{\epsilon}_m)}{(\tilde{\epsilon}_p + 2\tilde{\epsilon}_m)} \quad (8.3)$$

where,  $\tilde{\epsilon}_p$  is the permittivity of the particle and  $\tilde{\epsilon}_m$  the permittivity of the medium in which the particle is suspended. But in the DC-iDEP limit, the imaginary term reduces to zero due to no frequency contribution.  $f_{CM}$  in DC-iDEP is expressed as a function of the conductivity of particle and medium as in equation 8.4.

$$f_{CM} = \frac{\sigma_p - \sigma_m}{\sigma_p + 2\sigma_m} \quad (8.4)$$

$\sigma_p$  refers to conductivity of red blood cell and  $\sigma_m$  refers to conductivity of the medium.

From  $f_{CM}$  induced dipole moment of the particle could be positive or negative and is reflected in the direction of the resulting DEP force on the particle as shown in equation 8.4<sup>15,88</sup>.

The dielectrophoretic velocity  $\vec{u}_{DEP}$  related to the applied electric field is given as:

$$\vec{u}_{DEP} = -\mu_{DEP} \nabla E^2 \quad (8.5)$$

When cells are attract towards the insulating obstacle (toward higher electric field density), the phenomena experienced is positive DEP (pDEP) i.e. when polarizability of

cell is greater than that of medium. When cells are repelled from the insulating obstacle region (down the electric field gradient), this leads to the cells focusing into flow streamlines, at it is said that cells experience negative DEP (nDEP)<sup>199</sup>. Previously, in the literature it has been shown that live cells under DC electric fields experience nDEP thus moving away from the insulating obstacle region<sup>102,204</sup>.

Due to the insulating obstacle geometry, a spatially dense non-uniform electric field is created around the obstacle region as the DC electric field lines diverge around this insulative zone. The resulting electric field gradient is maximum at the outside corners of the obstacle and much greater between the obstacle and the channel wall. It is in this region, that the cells experience the greatest DEP force, while in other regions of the channel, EOF forces dominate. As shown in equation 8.1, both forces contribute to cell motion. DC-iDEP forces will push the cells away from the high field density zones such that they experience nDEP due to repulsive forces as it flows around the corner of the obstacle. The strength of this DEP force will depend on the red blood cells ABO antigen polarizability, thus facilitating particle motion into specific flow streamlines which will proceed to one of the four channels. In order to achieve flow of cells or streaming DEP effect as reported by Cummings and Singh<sup>113</sup>, “the dielectrophoretic mobility should be less than or equal to electrokinetic mobility” as shown in equation 8.6. In this research, electrokinetic mobility is only comprised of electro-osmotic mobility as discussed above<sup>237</sup>.

$$\mu_{DEP} \nabla(\vec{E} \cdot \vec{E}) \cdot \nabla \vec{E} \leq \mu_{EO} (\vec{E} \cdot \nabla \vec{E}) \quad (8.6)$$

The cell motion is also aided by electro-osmotic forces. If electro-osmotic flow dominates over dielectrophoretic forces, then the cells move slowly into channel 4. As

dielectrophoresis increasingly dominates electro-osmosis flow, the red blood cells deflect from channel 3 up to channel 1. This phenomenon is cartooned in Figure 8.1.

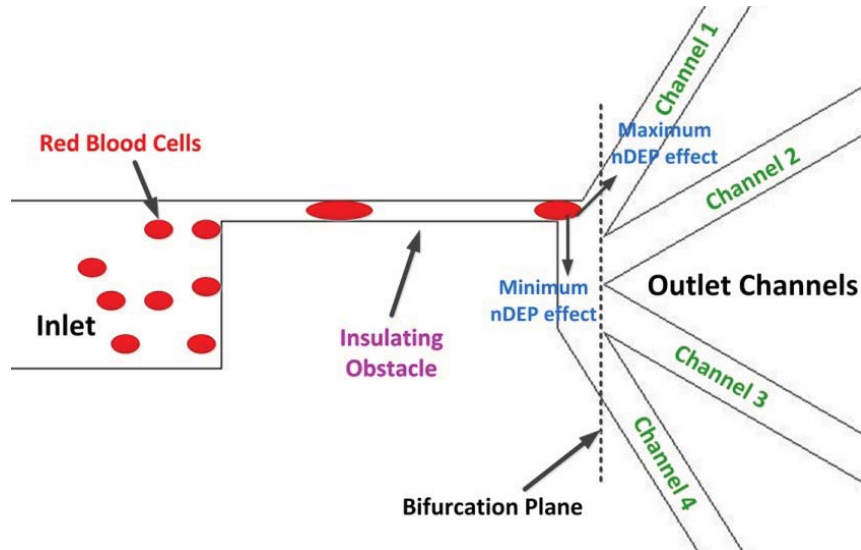


Figure 8.1 Representation of the microdevice developed in this research and the effect of DEP on the red blood cell at the insulating obstacle region.

### 8.3.1 Red blood cells / erythrocytes

Blood is an important diagnostic fluid containing a plethora of information about genetics and pathological state of a human being. It is made up of 54% of plasma and 45% of cells: RBC (erythrocytes), WBC (leukocytes) and platelets. In this work, only erythrocytes are retained for testing in the microdevice and will be briefly discussed here. Detailed explanation of blood, its composition and properties have been discussed in Chapter 3. Erythrocytes are 6-8  $\mu\text{m}$  in diameter, biconcave shaped, lacks nucleus and carries hemoglobin inside. The biconcave shape helps to maximize surface area for gas ( $\text{O}_2$  and  $\text{CO}_2$ ) transport across their membrane<sup>1</sup>. RBCs are responsive to the slightest changes in solvent conditions, pH and temperature. They have a net negative charge based on their conventional linear electrophoretic behavior with their outer membrane



being non-conductive ( $\sigma \leq 1 \mu\text{S/m}$ ) and the interior being conductive ( $\sigma = 0.53$  to  $0.31 \text{ S/m}$ )<sup>15</sup>.

## **8.4 Materials and methods**

Experimentation involved specific device design and fabrication by standard soft photolithography techniques. Sample preparation involving blood is often challenging due to various leukocytes and platelets present in blood. Section 8.4.1.2 provides the details of sample preparation along with protocol for running experiments in our 1.46 cm long microdevice. Human diversity influences antigen expression of erythrocytes so the following variations were considered: donor reproducibility, blood type dependency, electric field and medium conductivity dependencies. Meticulous experiments to cover all these dependencies were planned and details are discussed in Section 8.4.1.3. This section concludes with video analysis obtained from the SVM LabSmith<sup>®</sup> microscope and data analysis using statistical functions available in Microsoft Excel's library.

This research protocol was approved by the Institutional Review Board (IRB) for the protection of human subjects and Institutional Biosafety Committee (IBC) at Mississippi State University. All experiments were performed in a certified Biosafety Level II laboratory.

### **8.4.1 Experimentation**

This section, covers the details of the experiment including device design by poly(dimethylsiloxane) (PDMS), sealing the PDMS device to form microchannels, blood sample preparation to target erythrocytes and the experimental matrix to study dependencies influencing red blood cell behaviors.

#### 8.4.1.1 Device design and fabrication

AutoCAD design software (Autodesk, Inc) was used to design the microdevice mask, which was etched in chrome on 5” soda lime glass (Bandwidth Foundry International Pty Ltd., Australia). The actual PDMS microdevice consists of one inlet (200  $\mu\text{m}$  wide), an insulated obstacle, and bifurcation into four outlet channels (50  $\mu\text{m}$  wide). The distance between the inlet and outlet ports was 1.46 cm. An insulating obstacle, 400  $\mu\text{m}$  across with a rectangular geometry was positioned in the inlet channel at a distance of 100  $\mu\text{m}$  upstream from the bifurcation to the four outlet channels. The distance between the wall and the obstacle in the PDMS device was 30  $\mu\text{m}$ .

The microdevice was fabricated by the rapid photolithography technique developed by Whitesides *et al.* group<sup>46</sup>. The procedure was modified according to the desired channel depth and wall thickness needed. Silicon wafer substrates were used to create a master from soda lime chrome mask by using cleanroom facilities at Michigan Technological University. The steps involved in creating Si masters were:

- Spinning negative photoresist SU-8 2025 from MicroChem® onto wafer by:
  - ✓ Ramping spin coater to 800 rpm at the rate of 100 rpm/s and holding for remainder of 10 s
  - ✓ Ramping spin coater from 800 rpm to 1750 rpm at the rate of 300 rpm/s and holding for remainder of 30 s
- Pre-bake wafer on hot plate to allow drying of the spun photoresist in two steps:
  - ✓ Step 1: 65°C for 5 min
  - ✓ Step 2: 95°C for 10 min

- UV Exposure to pattern Si wafer from the soda lime mask
- Position the mask onto EVG mask aligner and then place Si wafer to be patterned on substrate holder of EVG mask aligner
- Expose for  $200 \text{ mJ/cm}^2$ : when power reading is  $\sim 20 \text{ mW/cm}^2$  which translates to an exposure time of 10 s
- Post-bake Si wafer to fix the pattern (photoresist polymerizes in the UV exposed areas) in two steps:
  - ✓ Step 1:  $65^\circ\text{C}$  for 2 minutes
  - ✓ Step 2:  $95^\circ\text{C}$  for 6 minutes
- Develop the pattern by placing the Si wafer in SU-8 developer for 10 min. Occasional agitation was used to move excess photoresist away from wafer.
- Rinse with isopropyl alcohol (IPA) to wash off the unpolymerized photoresist
- Dry the patterned Si wafer under Nitrogen stream.
- Final pattern on Si wafer master is the device pattern having raised walls yielding thickness of  $\sim 73 \mu\text{m}$  as measured with a Veeco Dektak Stylus profilometer.

To create PDMS device from the patterned Si wafer master, a 10:1 PDMS prepolymer base and curing agent from Dow Corning<sup>®</sup> were mixed thoroughly and degassed in vacuum desiccator to remove bubbles. The Si master was placed on aluminum foil and degassed PDMS mixture was poured over it. The whole assembly was left in the oven for about 12 h at  $65^\circ\text{C}$  to set the polymer. The cured PDMS device was

gently peeled from the Si master to avoid damage. Inlet and outlet ports were drilled with 3 mm biopsy punches.

To form channels in the PDMS microdevice, the peeled PDMS device was sealed onto a cleaned glass slide by plasma-oxidation treatment (Harrick Plasma<sup>®</sup>) using air at room temperature for 1 min. This yielded hydrophilic channels and irreversibly sealed the PDMS casting to the glass slide. To retain hydrophilicity for longer periods, the channels of the completed PDMS device were kept in constant contact with e-pure water. Platinum electrodes in the inlet and outlet ports were soldered in place to make electrical connections. A schematic representation of the patterned wafer and PDMS microdevice is shown in Figure 8.2. The PDMS microdevice can be compared to the size of a penny having a length of 1.46 cm.

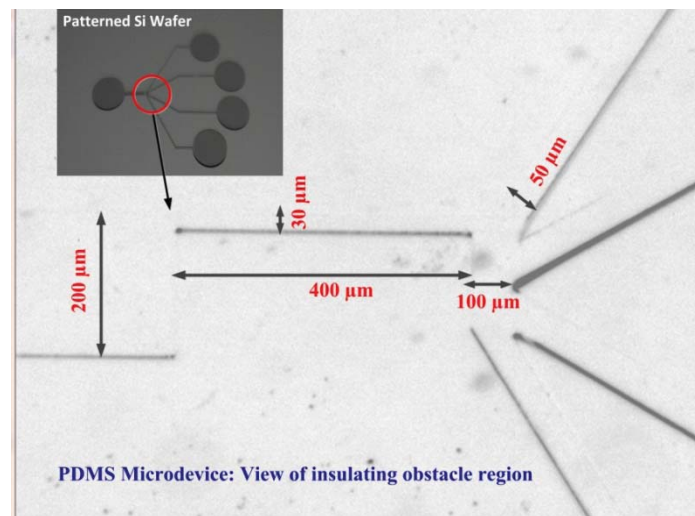


Figure 8.2 Schematic representation of PDMS microdevice with patterned silicon (Si) wafer in the inset.

#### 8.4.1.2 Sample preparation

Blood samples from volunteers with verified blood type were drawn by trained phlebotomists at the Longest Student Health Center in Mississippi State University.

Volunteers were recruited without regard to age, race, ethnicity or gender and donor confidentiality was strictly maintained. Fresh whole blood samples were stored in 4 ml vacutainers suspended in K<sub>2</sub> EDTA anticoagulant. The samples were allowed to settle by gravity. Red blood cells settle at the bottom due to their density with plasma forming a layer above the cells. Separated red blood cell samples were then diluted with isotonic buffer comprised of glucose and phosphate buffer saline (PBS) salts.

Erythrocyte responses in the DC electric field were studied as a function of conductivity. D-Glucose can maintain isotonicity with the erythrocyte interior without contributing to ionic conductivity and was therefore used to supplement PBS<sup>154</sup>. Red blood cells osmolarity value varies between 280-310 mOsm/L and 5% glucose solution is considered isotonic<sup>244</sup>. Glucose concentrations were varied between 5-1% and the corresponding amount of NaCl and potassium phosphate salts were calculated for buffer preparation. Red blood cells are stable at pHs of 7.0. Buffers at all glucose concentrations were adjusted to 7.0 and the corresponding conductivity shift was noted. The buffers were made fresh for each blood type experiment. The average conductivity with standard error and pH values obtained for 'n' samples are shown in Table 8.2. The conductivity of the buffer medium varied between 100 and 900 mS/cm for corresponding glucose concentrations of 5 to 1%.

The red blood cells were suspended in these different buffers and examined to verify that the cells maintain their original shape and composition. Repeated experiments were conducted before concluding the buffers maintained the isotonicity and osmolarity of the blood sample. Since buffers can be hypotonic or hypertonic and cause the red blood cells to swell or shrink due to the osmotic pressure, the above effort was designed

to ensure the DEP responses observed in our microdevice were free of osmotic pressure effects.

Table 8.2 Average conductivity and pH values for the buffers prepared by adding D-Glucose

<b>% Glucose added buffers</b>	<b>Average Conductivity (mS/cm)</b>	<b>Average pH</b>
<b>5</b>	95.21 ± 2.47 (n=20)	6.95 ± 0.017
<b>4</b>	579.3 ± 0.95 (n=6)	6.97 ± 0.005
<b>3</b>	693.7 ± 0.35 (n=6)	7.08 ± 0.013
<b>2</b>	711.6 ± 0.37 (n=6)	7.17 ± 0.017
<b>1</b>	917.2 ± 0.16 (n=6)	7.01 ± 0.047

#### 8.4.1.3 Operation protocol and experiment matrix

Separated red blood cell samples were suspended in appropriate buffer (5%-1% glucose added) depending on the experimental matrix in 1:750 dilutions. On average, there are about 5 million RBCs in 1  $\mu$ L of whole blood sample. Approximately 7000 RBCs are present in 1  $\mu$ L of 1:750 diluted samples of RBCs. The microdevice was loaded with 30  $\mu$ L buffer after rinsing at least 5 times. DC voltage was provided through LabSmith<sup>®</sup> high voltage supply (HVS448; 0-3000V) connected through Pt electrodes. The microdevice assembly with electrodes connected to the high voltage supply was mounted on the LabSmith<sup>®</sup> SVM340 microscope stage. Video recording and the DC power supply were started and the buffer in the inlet well was replaced with 30  $\mu$ L of diluted red blood sample. A continuous video at 30 fps was captured for ~5 min by the high sensitivity video camera in the SVM microscope. The 4X magnification in the SVM340 has a 0.1 numerical aperture and provides a 1.5  $\times$  1.5 mm field of view. This field of view covered a part of the inlet channel, the entire obstacle region and of the

entrances to the four diverging outlet channels. Bright field illumination was used to run the experiments without fluorescence. Each experiment was repeated at least two times to maximize reproducibility and accuracy in experiments. A detailed protocol is provided in Figure 8.3 where sample preparation, sample injection, experimentation and analysis are highlighted with the approximate starting time  $t$  in minutes of each step.

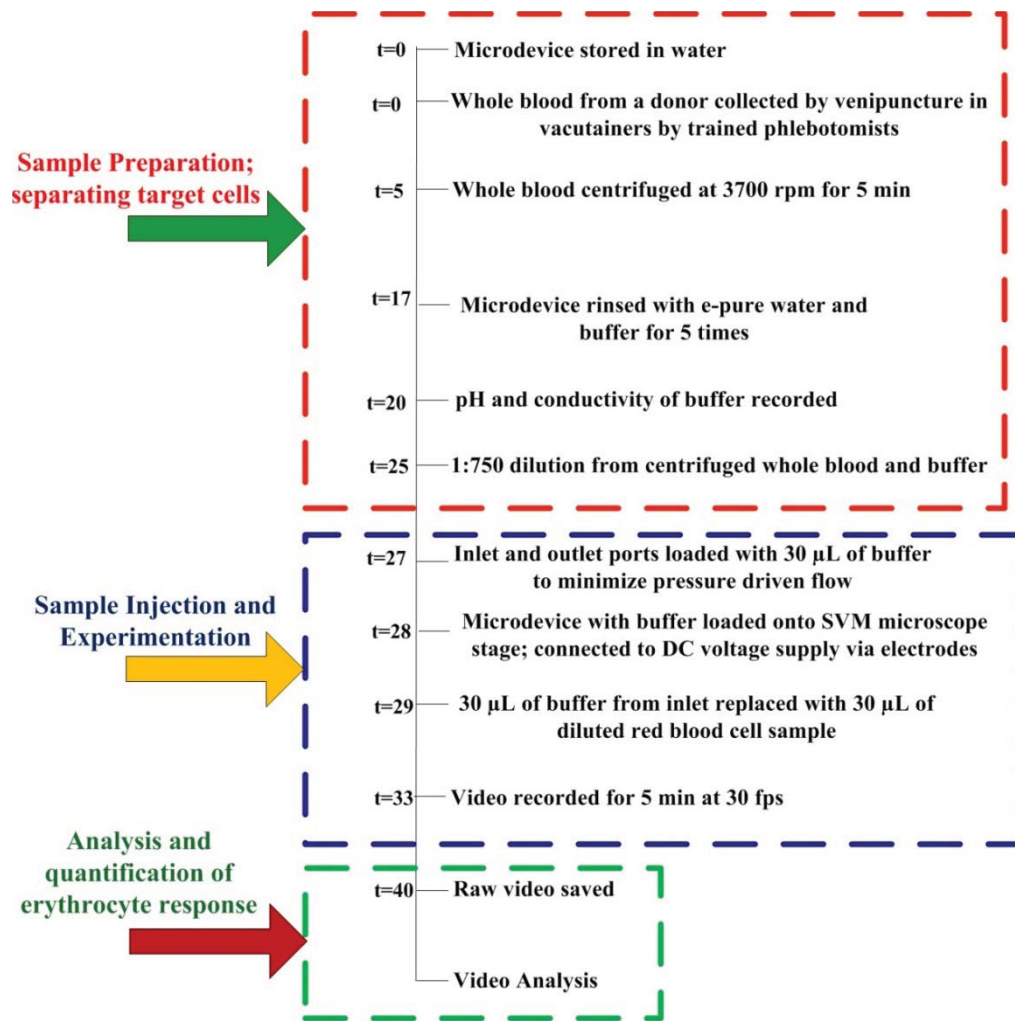


Figure 8.3 Detailed operation protocol of the planned red blood cell experiments,  $t$  denotes time in minutes.

The aforementioned experimental matrix consisted of three unique donors for each blood type, repetition of one donor for each blood type, voltage dependency experiments, and conductivity dependency experiments as shown in Figure 8.4.

blood type	Days							
	1		2		3		4	
	Donor	Voltage (V)	Donor	Voltage (V)	Donor	Voltage (V)	Donor	Voltage (V)
	<b>D</b>	<b>50, 100</b>	<b>D</b>	<b>100</b>	<b>D</b>	<b>100</b>	<b>D</b>	<b>10, 25, 50, 75, 100</b>
<b>O+</b>	5% to 1% @ 50 V D1a 5% @ 100V		Reps=3 D2 5% @ 100V		Reps=3 D3 5% @ 100V		5% @ 10,25,50,75,100 D1b	
<b>O-</b>	5% to 1% @ 50 V D1a 5% @ 100V		Reps=3 D2 5% @ 100V		Reps=3 D3 5% @ 100V		5% @ 10,25,50,75,100 D1b	
<b>B+</b>	5% to 1% @ 50 V D1a 5% @ 100V		Reps=3 D2 5% @ 100V		Reps=3 D3 5% @ 100V		5% @ 10,25,50,75,100 D1b	
<b>A+</b>	5% to 1% @ 50 V D1a 5% @ 100V		Reps=3 D2 5% @ 100V		Reps=3 D3 5% @ 100V		5% @ 10,25,50,75,100 D1b	
<b>AB+</b>	5% to 1% @ 50 V D1a 5% @ 100V		Reps=3 D2 5% @ 100V		Reps=3 D3 5% @ 100V		5% @ 10,25,50,75,100 D1b	
<b>A-</b>	5% to 1% @ 50 V D1a 5% @ 100V		Reps=3 D2 5% @ 100V		Reps=3 D3 5% @ 100V		5% @ 10,25,50,75,100 D1b	
<b>AB-</b>	5% to 1% @ 50 V D1a 5% @ 100V		Reps=3 D2 5% @ 100V		Reps=3 D3 5% @ 100V		5% @ 10,25,50,75,100 D1b	
<b>B-</b>	5% to 1% @ 50 V D1a 5% @ 100V		Reps=3 D2 5% @ 100V		Reps=3 D3 5% @ 100V		5% @ 10,25,50,75,100 D1b	

Figure 8.4 Experiment matrix to study all dependencies involving reproducibility, blood type, medium conductivity and DC Voltage.

It is known that red blood cell's molecular characteristics differ by genotype (different donors) as well as in response to environment, so the dependencies considered in this study were:



- i. Donor reproducibility: Reproducibility is a very important parameter in any microfluidic platform especially for medical diagnostic purposes. Three different donors (D1, D2 and D3) were selected for this purpose and among them one of the donors was repeated on a different day to study variability inside a donor (D1a and D1b).
- ii. Blood type dependency: Red blood cells have ABO antigens on the surface and Rh factor antigens through the membrane. The number of ABO antigens as well as antigens from the other 29 blood typing systems likely varies with each donor and are uncontrolled for in this study. ABO antigens impact cell polarizability thus yielding different responses to the applied electric field. All 8 ABO-Rh blood types were considered. Sorting into the four outlet channels was monitored and quantified.
- iii. Electric field dependency: Dielectrophoretic force is proportional to the square of the electric field gradient. Four different DC voltages, 25 V, 50 V, 75 V and 100 V corresponding to 17.12 V/cm, 34.25 V/cm, 51.37 V/cm and 68.5 V/cm were considered for the experiments to study voltage dependency. These four voltages were considered based on the baseline study responses as discussed in Section 8.5.1.
- iv. Medium conductivity dependency: Erythrocyte's DC-iDEP responses depend on the conductivity of the medium as indicated in equation (8.4) according to the Clausius-Mossotti factor. Depending on the conductivity properties of medium and cell, cells can experience streaming or trapping DEP. To study these dependencies, different D-glucose conductivity buffers were prepared as indicated in Section 8.4.1.2. Five different

conductivity buffers ranging from 100-900 mS/cm were considered at 50 V on donor D1a.

#### 8.4.2 Video analysis

Uncompressed video from the microscope were saved in .avi format. Custom built software from Sandia National Laboratories (VideoProc 1.1) was used to analyze these raw videos from the experimental run of 5 min at 30 fps. Five interrogation windows were drawn just prior to the obstacle and in each of the four outlet channels as shown in Figure 8.5.

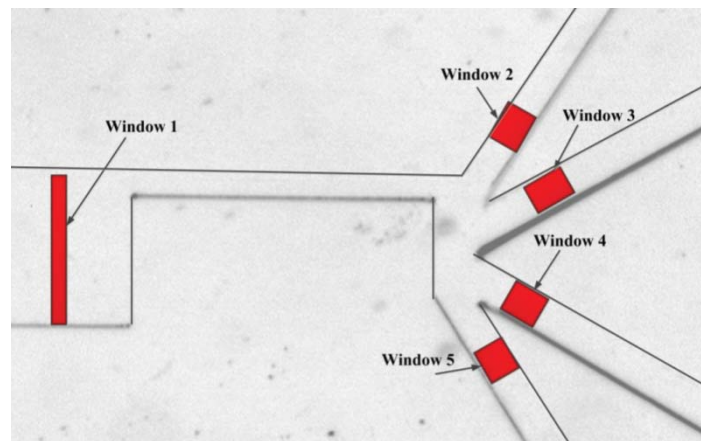


Figure 8.5 Schematic representation of interrogation windows (red boxes) drawn to obtain intensity profiles through custom-built software (Sandia National Laboratories).

The videos were processed and intensities from the five windows as a function of time were produced. When drawing the interrogation windows the following steps were adopted:

- interrogation windows were drawn based on the order of the results desired. The windows were drawn first prior to the obstacle region and then in outlet channels.

- care was taken to not draw windows on stationary or trapped cells in the window
- care was taken not to touch the walls when drawing the windows
- approximately equal area windows were drawn in each channel

The intensity values provided as a function of time along with the area of each window was entered into excel to analyze the data statistically and calculate fraction of cells in each outlet channel as discussed in the next section.

### 8.4.3 Data analysis

The intensity values from the experiment in each channel were further analyzed by using statistical functions present in Microsoft Excel's library. The first and foremost step was to subtract background intensity values from the intensity values obtained with the cells present in the channel. Background intensity value were calculated when no cells were present in the interrogation window. However, since the microscope relied on ambient light for illumination, the background value was sometimes less than or greater than the intensity values with particles. Intensity values ranged between 0 (black) and 255 (white). The subtracted intensity values (both positive and negative) were plotted against time to visualize the distribution of data. Periodically, sharp peaks were detected in the graph and were attributed to:

- diluted red blood cell sample might contain other cells like WBC and platelets,
- dust accumulation on the microdevice,
- discrepancies due to room light usage for experiments, and

- discrepancies due to small movements on the microscope stage, since the device assembly is not in a secured position on the microscope stage.

The sharp peaks are false positives and false negatives in the intensity values. Before calculating the cell fraction in each channel, removal of these unnecessary peaks was essential. For that, statistical outliers were detected and removed from the data set.

Outliers are those data that are abnormally placed from other values in a random sample of population<sup>197</sup>. These outliers could be detected by examining the plotted data via a normal scattered Excel plot or a box plot. Here, a scattered plot was used to identify outliers. For this, the lower quartile range (25<sup>th</sup> percentile) and upper quartile range (75<sup>th</sup> percentile) were calculated by,

$$Q1 = (N + 1) \times 0.25 \quad (8.6)$$

$$Q2 = (N + 1) \times 0.75 \quad (8.7)$$

where Q1 is the lower quartile range, Q2 upper quartile range and N is the population size (number of time frames in an experimental run). Interquartile range IQ also known as fourth spread is calculated as the difference between upper and lower quartile ranges. There were two types of outliers, mild and extreme<sup>197</sup>. Here, mild outliers were detected by equations 8.8 and 8.9:

$$Upper\ OB = Q2 + 1.5 \times IQ \quad (8.8)$$

$$Lower\ OB = Q1 - 1.5 \times IQ \quad (8.9)$$

Extreme outliers are also detected in the same way but they are based on 3 times IQ instead of 1.5 times IQ as in mild outliers. Once the outliers were taken off from the sample set, total intensity of all the cells in each channel was calculated over the entire frame of experiment. For accuracy, the total intensity of cells in each channel was divided

by the area of the respective interrogation window. Fraction of the cells in each channel is given by,

$$F_{Ch} = \frac{I_{Total}^{Ch}}{\sum_{Ch=1}^4 I_{Total}^{Ch}} \quad (8.10)$$

where  $F_{Ch}$  is the fraction of cells in a particular channel,  $I_{Total}^{Ch}$  is the total intensity of one channel. A detailed analysis protocol employing the above equations and using statistical functions available in the Excel library is provided in Figure 8.6.

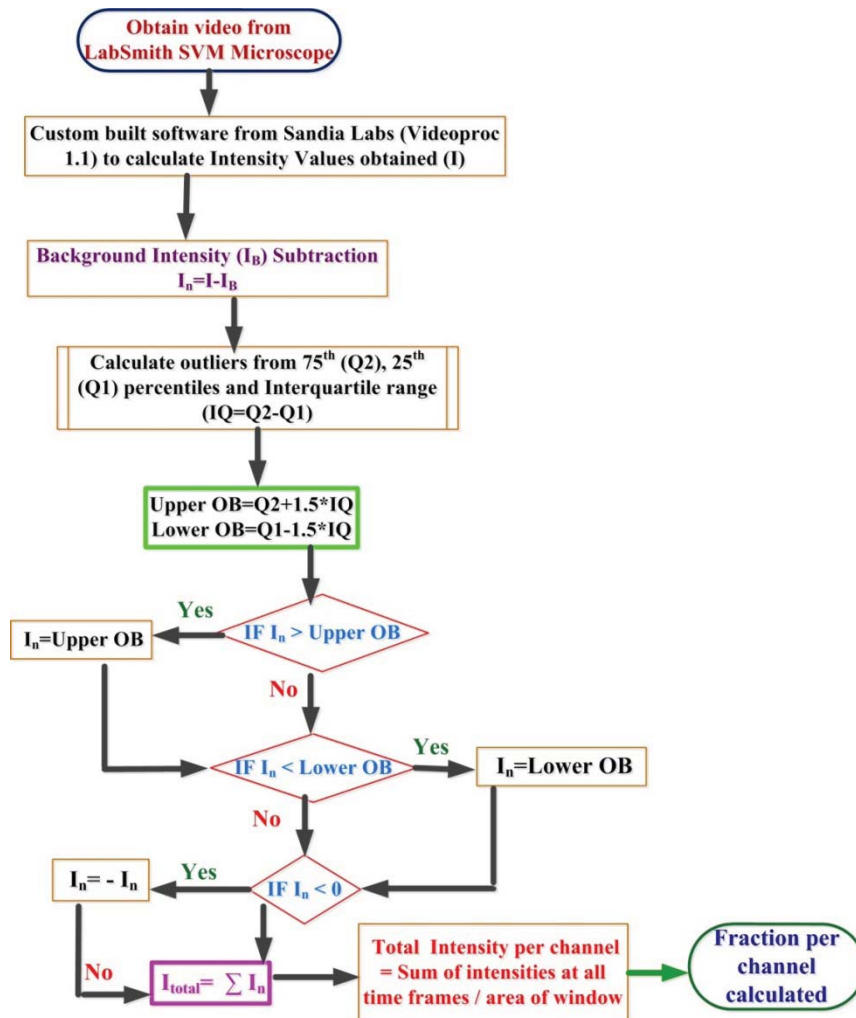


Figure 8.6 Data analysis protocol using statistical functions available in excel library to calculate cell fraction in each channel outlets

## 8.5 Results and discussion

This section deals with the results of the experiments conducted to observe red blood cell responses by ABO blood type via DC-iDEP. Various dependencies were studied and each of them is discussed in detail.

### 8.5.1 Baseline study

A baseline study was conducted to determine the voltage and buffer stable operating ranges that minimized harm to the red blood cell sample, maintain buffer integrity, and avoid electrolysis reactions at the electrode surface. High voltages are known to lyse cells and promote electrolysis at electrode surfaces. By establishing a suitable operating window, lysing the red blood cells is avoided. Also in this research, streaming or flowing DEP is desired, but based on the electric field applied, trapping might also be achieved. This baseline established an operating electric field range where streaming was observed and thus avoided trapping of red blood cells. The baseline study was conducted by running the diluted red blood cells in the channel for  $> 5$  min and observing their behavior at different electric field strengths. Figure 8.7 demonstrates the operating window for our experiments. As shown in the Figure 8.7, two different zones exist: one where no trapping or clustering of cells was seen (blue dots) and the red dots represent flow reversal and clustering of cells. Flow reversal may happen due to buffer interactions with charges present on the wall. This could be temporarily treated by flushing the channels with e-pure water at least five times, thus changing the charge distribution back to the native PDMS channel walls. The final operating window for our experiments was limited to less than 100 V corresponding to 68.5 V/cm for most experiments. Conductivity dependency studies were conducted at 50 V corresponding to

34.25 V/cm due to the high conductivity, high field null operating conditions demonstrated in Figure 8.7.

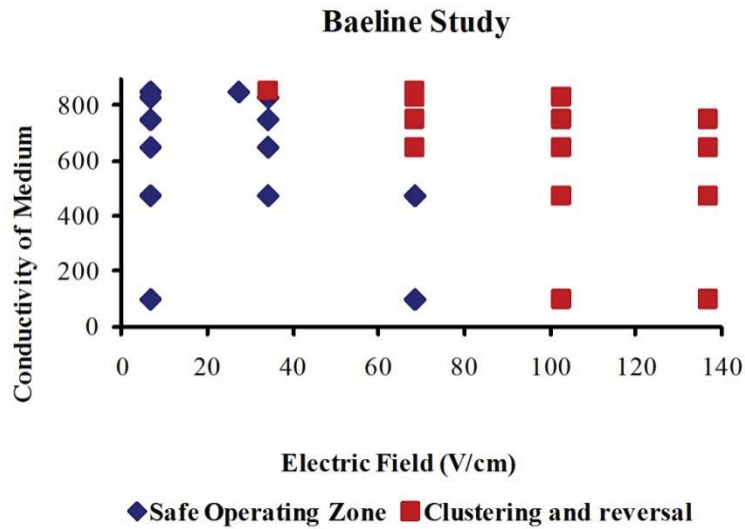


Figure 8.7 Operating window for the red blood cell experiments at various DC electric field strength and range of medium conductivities.

### 8.5.2 Reproducibility Studies

Donor reproducibility studies were conducted by recruiting three donors for each blood type as shown in the experimental matrix in Figure 8.4. Total particle fractions were calculated for each donor and plotted against the outlet channels 1, 2, 3 and 4 as seen in Figure 8.8. As shown in Figure 8.8, all 8 ABO blood types were considered in this study and experiments were performed in a 100 mS/cm conductivity buffer with an applied DC electric field of 68.5 V/cm. The channel fractions were plotted against different outlet channels 1, 2, 3 and 4.

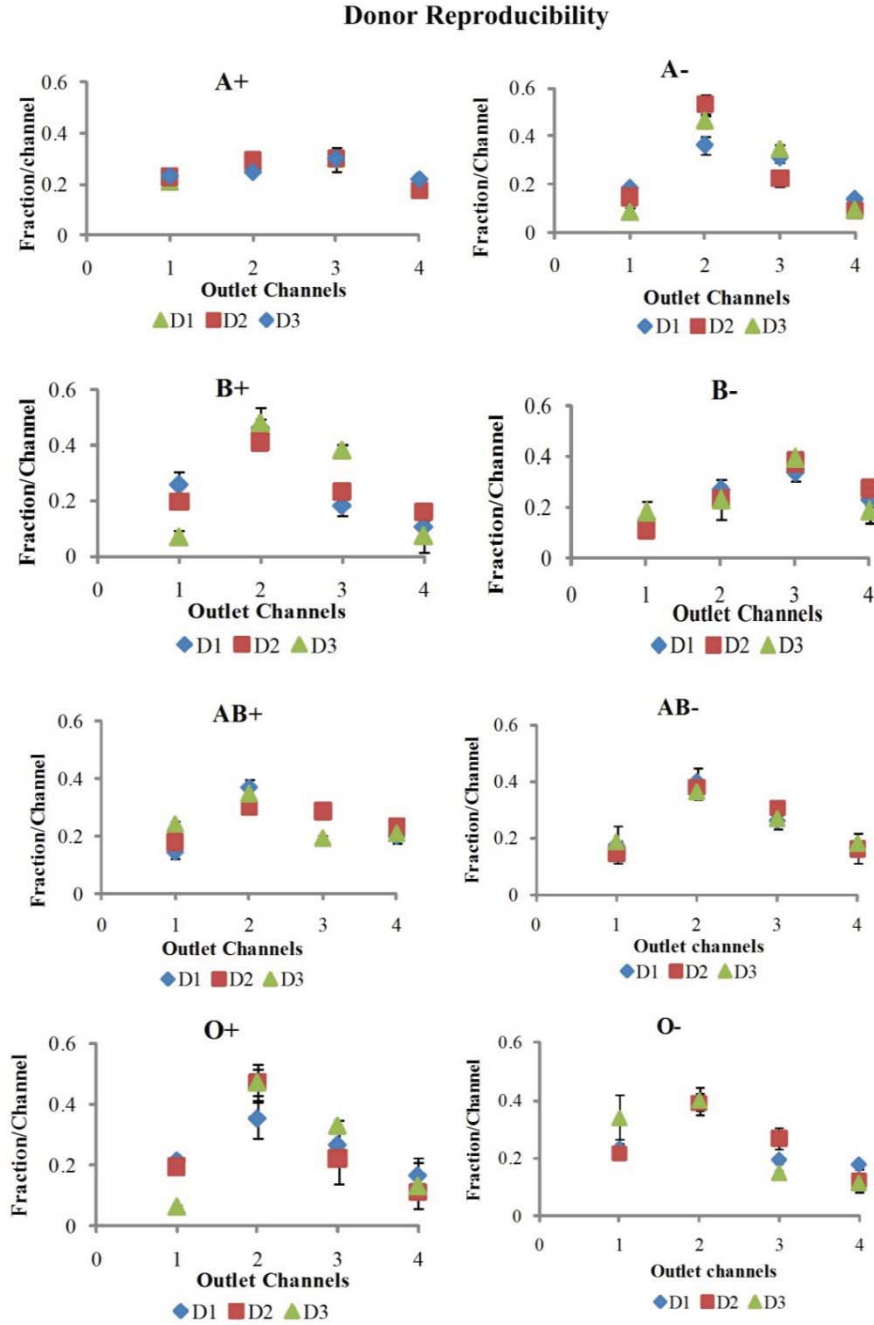


Figure 8.8 Donor reproducibility studies for all the 8 blood types. Minimal variability between donors observed for all blood types. Each data point corresponds to 12 individual experiments at 68.5 V/cm and 100 mS/cm.

The error bars for most of the blood types in most of the outlet channels overlap showing that reproducibility of data exists. Minimal differences are observed in the



channel fractions for different donors D1, D2 and D3. Each of the donor experiments was repeated at least twice to reduce standard error between donors.

From the above graph (Figure 8.8) it is shown that slight variability exists between donors, but donors of the same ABO blood type exhibit comparable responses suggesting they have very similar physiological composition of red blood cells. This counters the concern one encounters when using samples from a population whose genotypes / phenotypes are not fully screened. In this study, only the expression of ABO antigens was controlled, but did not collect data on the antigen expression of any of the other 29 blood typing systems nor was any data collected on patient immunological history (i.e. antibody expressions), nor blood disorders. The fact that multiple donors of the same blood type exhibit similar responses (and differences between blood types are observed as is discussed in Section 8.5.3) supports our hypothesis that DC-iDEP polarizability is influenced by the expression of ABO-Rh antigens, but not appreciably influenced by other factors. Donor variability was therefore neglected for further dependencies and all same blood type donors were averaged together for a composite response.

### **8.5.3 Blood type dependency**

Dependency studies on blood types involved experiments at 100 V DC corresponding to 68.5 V/cm fields on all blood types at 100 mS/cm buffer conductivity. These conditions were selected based on the baseline study discussed in Section 8.5.1 where maximum operable conditions were found. There were three donors involved for each blood type and for each donor experimental runs were repeated at least three times. As seen in the donor reproducibility studies discussed in Section 8.5.2, different donors

have comparable responses and therefore all donors of a single blood type were averaged together for the blood type dependency analysis. A graph of cell fractions in each channel is plotted against blood type to study the blood type sorting into channels as shown in Figure 8.9. The error bars indicate the standard error for all donors in the same blood type. This standard error is calculated from an experimental run number greater than 12 (3 repeats, 3 unique donors, 1 donor repeat).

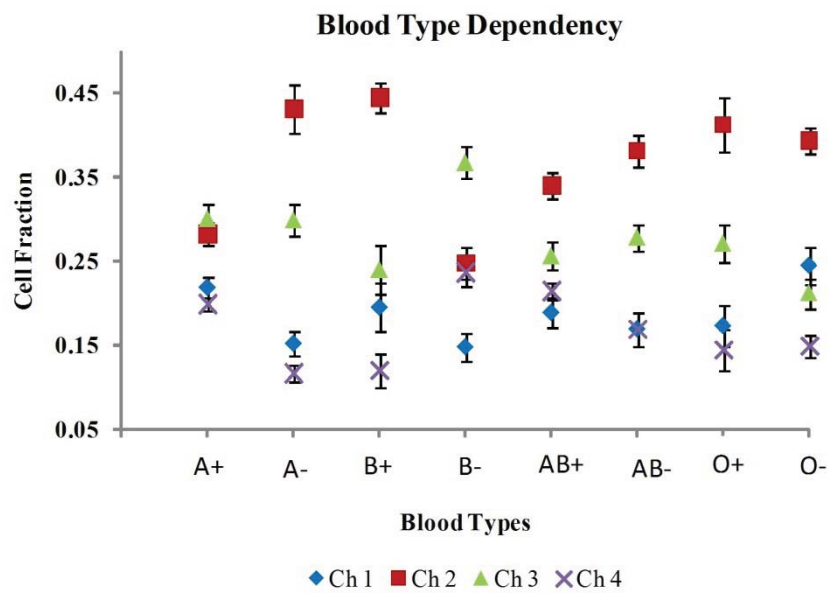


Figure 8.9 Sorting of red blood cells into outlet channels 1, 2, 3 and 4 by its type at 100 mS/cm and 68.5 V/cm DC electric field.

As shown from the Figure 8.9, different blood types show different distributions of blood cell flow into the four channels. Thirty microliters of diluted red blood sample were loaded onto the device, which correspond to about 210,000 red blood cells in the inlet. Overall trends in the data show that channels 1 and 4 were the least preferred for all blood types and channels 2 and 3 were most preferred. However, the relative distribution into these channels changed with blood type. Based on simple preference for one

channel, A- and B+ both show ~45% of their cells are directed into channel 2, but the error bars overlap with O+, which overlaps with O- and AB-, etc. A simple fraction into channels will not be able to discern blood type at an appreciable confidence level.

However, relative channel concentrations are more informative. For example, AB+ can be discerned from all other blood types easily because the ratio of Ch3:Ch4 is 1.2 (lowest ratio), while all other blood types have ratios that vary from 1.42 to 2.56. For A, B, AB and O blood, the presence of the Rh factor can be discerned with high confidence by examining the Ch3:Ch4 ratio as seen in Table 8.3. All blood types are distinguishable from each other as standard deviations between them are <5 % (< 0.05 channel fraction difference).

Table 8.3 Ratios of the fraction of blood cells in channel 3 to the fraction of blood cells flowing into channel 4. All 8 blood types are distinguishable from each other.

Blood type	Ratio: Ch3/Ch4	Distinguishable?
<b>A+</b>	<b>1.51</b>	<b>YES</b>
<b>A-</b>	<b>2.56</b>	
<b>B+</b>	<b>2.00</b>	<b>YES</b>
<b>B-</b>	<b>1.56</b>	
<b>AB+</b>	<b>1.20</b>	<b>YES</b>
<b>AB-</b>	<b>1.65</b>	
<b>O+</b>	<b>1.89</b>	<b>YES</b>
<b>O-</b>	<b>1.42</b>	

Sorting depends on many factors and the most important being the polarizability of the cell. Antigens present on the red blood cell membrane polarize differently and there is a dependency seen for various blood types. To conclude, blood type depends on antigen expression present on red blood cell membrane.

#### 8.5.4 Electric field dependency

To study the dependence on the applied electric field, four different DC voltages were chosen: 25, 50, 75 and 100 V corresponding to fields of 17.12, 34.25, 51.37 and 68.5 V/cm at 100 mS/cm buffer conditions. This is an important factor to study because the dielectrophoretic force depends on square of the gradient of electric field as shown in equation 8.5. Figure 8.10, shows the electric field effect on red blood cells near insulating obstacle region.

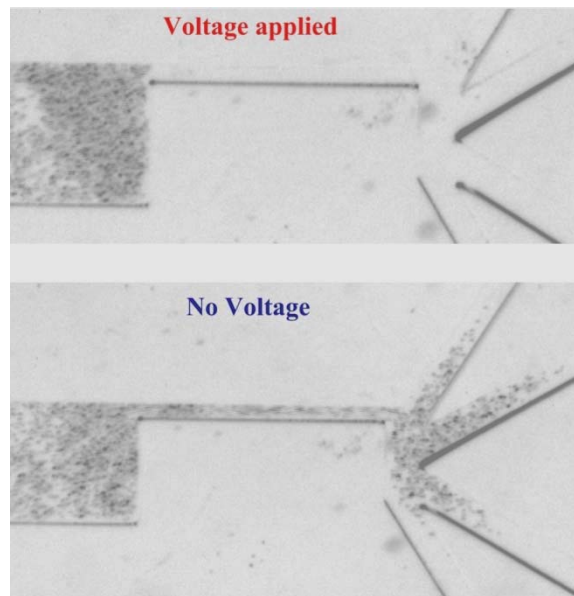


Figure 8.10 Cells experiencing voltage and no voltage conditions to demonstrate dependency on electric field at 4X magnification (1.5 mm x 1.5 mm).

High resistance is offered near the insulating obstacle region when 68.5 V /cm DC electric field is applied; as the field is withdrawn, cells flow into the four outlet channels as seen from the snapshot image. As the voltage is adjusted down to achieve streaming DC-iDEP, cells flow through the insulating obstacle region and into the four outlet channels.

For the electric field dependency study, videos from the experiments were analyzed in the same manner and cell fractions were calculated for each outlet channel. All 8 blood types were considered and a graph of cell fraction in each channel vs. electric field applied for each blood type was plotted as shown in Figure 8.11.

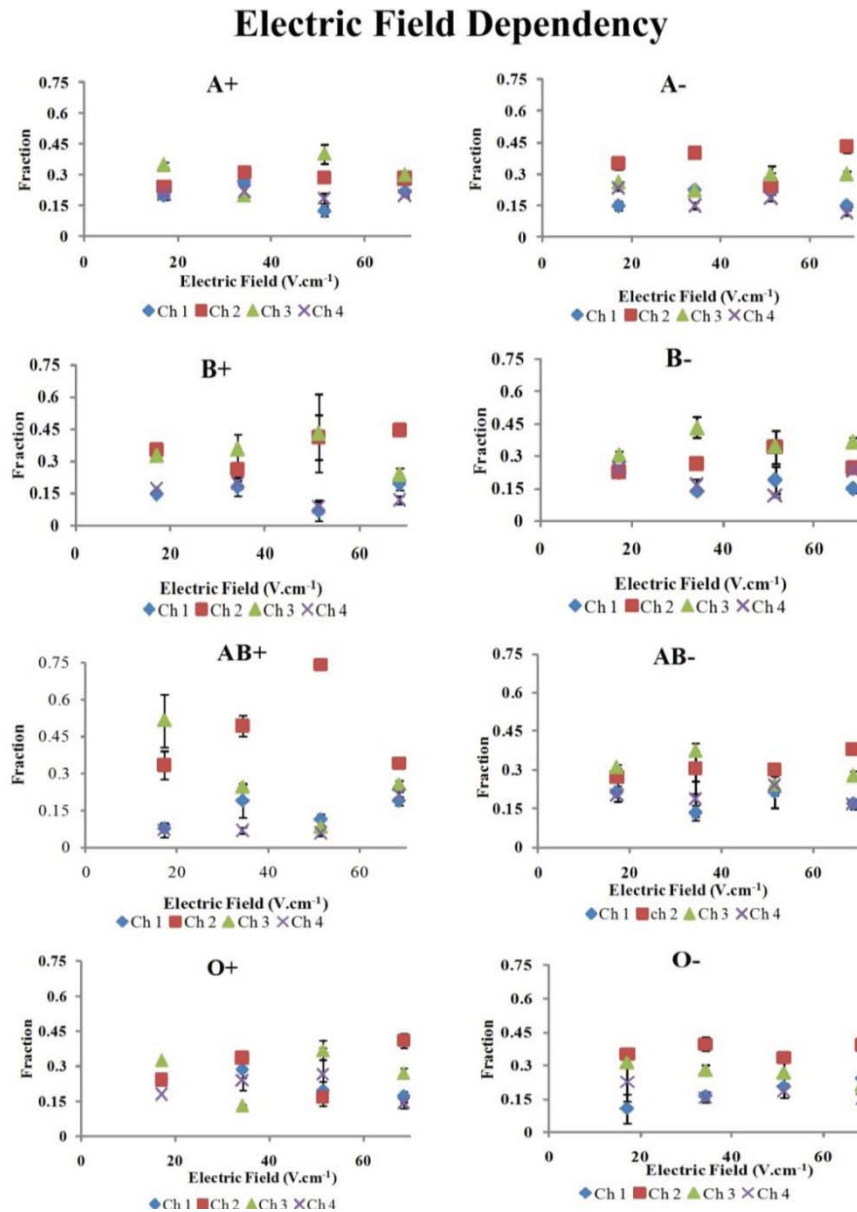


Figure 8.11 Dependency on electric field for all the blood types. Channel fraction plotted at various DC electric fields. Dependency is negligible at different DC electric fields except for AB+.

The values at 68.5 V/cm in each plot are the same as those shown in the blood type dependency Figure 8.9. By close examination of Figure 8.11, there is not much dependency seen on separation of blood types in each channel at different electric fields. Electric field dependency could be neglected and thus the DC voltage required for dielectrophoretic separation could be further reduced from 100 V.

Error bars are greater for 25, 50 and 75 V DC (17.12, 34.25, and 51.37 V/cm respectively) runs, because as shown in the experimental matrix in Figure 8.4, the voltage dependency runs were completed for donor D1a so  $n=3$  in contrast to  $n=12$  for the 100 V DC (68.5 V/cm) case. A range of electric fields applicable for sorting red blood cells is 34.25 - 68.5 V/cm, but since blood types do not show preference to a voltage, it is concluded that electric fields less than 68.5 V/cm are sufficient for any subsequent experiments.

#### **8.5.5 Conductivity dependency**

Various D-glucose added buffers at varying conductivities and pH 7.0 were considered for conductivity dependence studies. The conductivities of the five buffers ranged between 100-900 mS/cm. All the experiments for exploring this dependency were conducted at 50 V (34.25 V/cm) due to uninterrupted flow of cells at all buffer conditions established from the baseline study discussed in Section 8.5.1 and Figure 8.7. The dielectrophoretic force experienced by a cell depends on medium conductivity in the manner described by the Clausius-Mossotti factor in equation 8.4. All experiments were repeated at least three times and cell fractions calculated for each outlet channel in the same manner as described in Section 8.4.3. Figure 8.12 shows graphs for all 8 blood types where cell fraction in each channel is plotted against medium conductivity values.

## Medium Conductivity Dependency

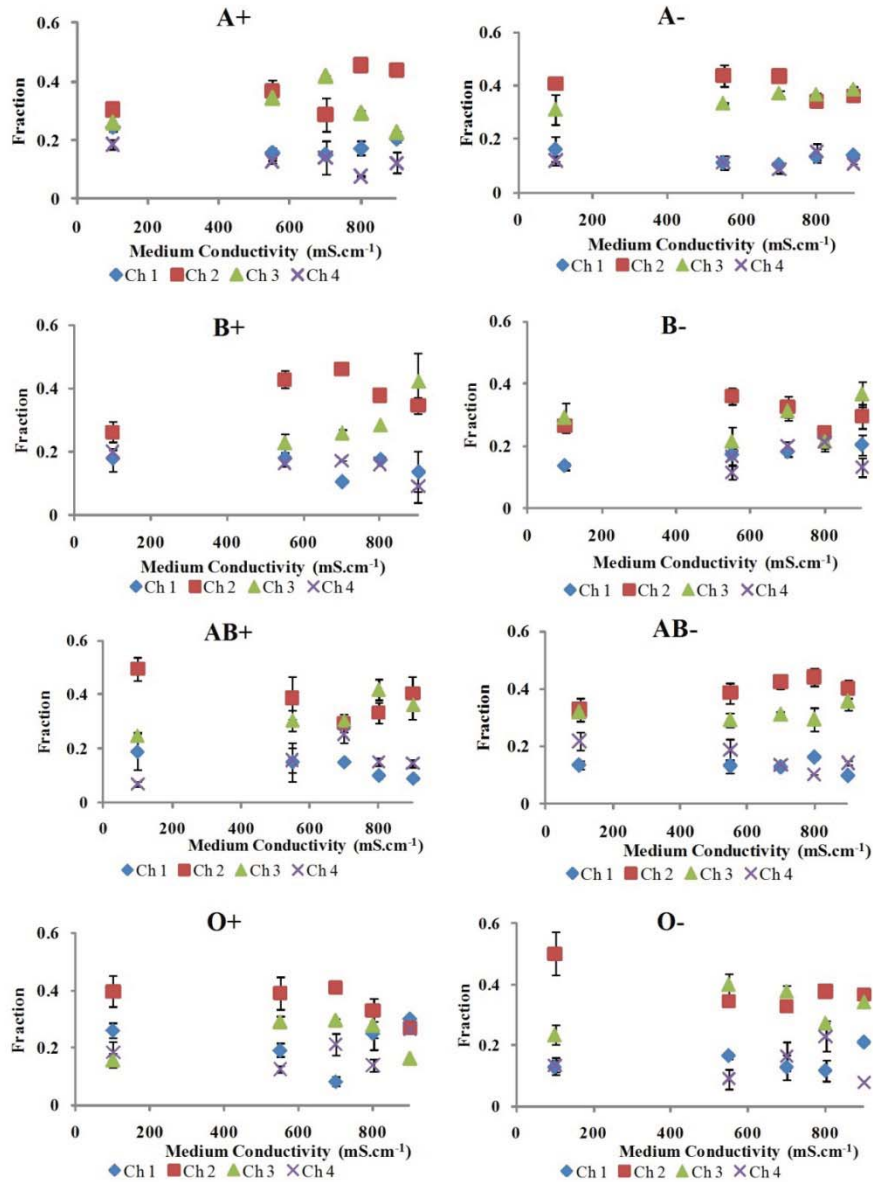


Figure 8.12 Medium conductivity dependency on red blood cell sorting by its type at 34.25 V/cm. Blood type separations into different channels depends on medium conductivity conditions. Low medium conductivity optimal for better separation efficiency.

Figure 8.12 illustrates that blood type separation varies with the medium conductivity. Low conductivity buffers were preferred over high conductivity buffers in most of the blood types.

Overall these dependencies suggest that red blood cell sorting by its blood type depend on the antigens expressed on the red blood cell which influences the polarizability of the red blood cells. This polarizability influences the dielectrophoretic force experienced by the cells and thus cells experience deflection around the insulating obstacle channel yielding separations into different channels.

## 8.6 Conclusions

Insulator-based DC dielectrophoresis is a novel technique experiencing exponential growth in exploration and applications over the last decade. This technique has great potential in portable lab on a chip devices and their use for disease diagnostics applications. In this chapter, a novel technique for sorting red blood cells based on human ABO typing by DC-iDEP is presented. A PDMS polymeric device by standard soft photolithography technique was developed and tested under a wide range of voltage and conductivity conditions. Fresh blood samples from 24 volunteer donors were used for experiments. A LabSmith SVM microscope and a high resolution CCD camera at 30 fps captured continuous video of the experiments which were analyzed to quantify blood cell dielectrophoretic deflection from an insulating obstacle into four outlet channels.

DC electric fields applied across the device cause the cells within the inlet channel to experience dielectrophoretic forces at the insulating obstacle region thus yielding separation into four different channel outlets. The separation is based on polarizability of the red blood cell which in turn depends on the antigen expressed on



(ABO) and in (Rh) the red blood cell membrane. Different dependencies were studied to determine their affect on this separation: blood type, electric field and medium conductivity.

Donor reproducibility and variability studies were also conducted which indicated no variability between donors of the same blood type. Blood type dependencies indicated that most of the blood types preferred channel 2, some preferred 3 and some preferred both 2 and 3. However, the ratio of channel preferences was more informative in distinguishing the blood types from each other. Different channel fractions and channel preference ratios suggest that the dielectrophoretic force that a cell experiences is dependent on erythrocyte antigen expression as all other variables were controlled. Antigen expression on the membrane cannot be controlled and thus the dielectrophoretic behavior is attributed to antigens on the membrane. All blood types could be distinguishable from each other by examining different combination of channel ratios and standard deviations between the channel fractions were within 5% range. Electric field dependency studies indicated much less variation and consistent optimal separations were achieved at all electric fields considered in this study. Medium conductivity was varied along with blood type and while differences by blood type were observed, there was no simple trend established. Some blood types had higher separation efficiency at lower conductivity but some behaved more ideally at higher conductivity. Lower conductivity of the medium was optimal to achieve higher separation of red blood cells.

Overall, in this research study, a demonstration of a novel technique for manipulation of red blood cells in a microfluidic platform by DC insulator-based dielectrophoresis has been presented. The results show promise for a continuous flow style device to determine blood type for an unknown blood sample. This is the first

reported technique using DC insulator dielectrophoresis to manipulate red blood cells based on blood type using a multi-channel microdevice for sorting. A complete picture of electric field and medium conductivity dependence for manipulating red blood cells has been presented.

CHAPTER IX  
QUANTIFYING ERYTHROCYTES BY SOLUTION RESISTANCE  
MEASUREMENT

**9.1 Introduction**

In many cell diagnostic lab-on-a-chip technologies, it is necessary to control or monitor cell counts per volume closely. The purpose of this research project is to relate DC solution resistance to the concentration of erythrocytes within microchannels. This will serve as a microfluidic means to determine hematocrit in blood samples. A microdevice with a single, straight channel 200  $\mu\text{m}$  in width, 1 cm long and 50  $\mu\text{m}$  in depth was fabricated with soft lithography and cast into a PDMS device by soft photolithography technique. D-glucose added buffers were used to maintain isotonicity for the cells with varying solution conductivity, DC voltages were applied via remotely-positioned platinum electrodes, and voltage change was measured across a resistor using a LabVIEW DAQ. This method has the potential to be used for dynamically monitoring cells concentration at multiple outlet ports simultaneously with minimal analysis.

In this chapter, a brief overview of some of the quantification methods used to quantify bioparticles has been presented. Three dependencies were studied and the results are discussed. The chapter concludes with some of the important conclusions based on the dependencies explored.

## 9.2 Quantification techniques in literature

Lab-on-a-chip (LOC) technology is the use of small-scale manipulations and reactions on chip-like devices for processes such as biomolecular separations and analysis<sup>17</sup>. Researchers have used many methods to quantify cells and particles in the nano-volumes contained in microchannels and micro-chambers. Examples include optical means such as laser path detection in flow cytometry, fluorescent tagging with relative intensity analysis, impedance detection, manually counting via micro-Coulter counters<sup>245</sup> and software-based image analysis such as Image J distributed by the National Institute of Health (NIH). These approaches either require sophisticated and expensive laboratory equipment, large sample concentration or they are laborious and time consuming<sup>245</sup>. To quantify cells, an efficient and sensitive non-optical approach is scarce in the literature<sup>246</sup>. Some of the bioparticles quantified in literature utilizing non-optical technique include bacteria<sup>247</sup> and human spermatozoa cells<sup>245</sup>. The non-optical technique utilized for quantifying was by impedance detection by building a complex electric circuit and applying sigmoidal AC electric signal.

An integral aspect of desirable lab-on-a-chip devices is the ability to detect and adjust concentration of analytes in different locations within the device to maintain quality control or combine more than one laboratory process on a single chip. Further, a prominent goal in LOC devices is to develop the ability to dynamically control cell concentrations for subsequent diagnostic applications<sup>1</sup>. Currently for blood-based devices, the primary methods for quantifying red blood cells flowing in microchannels are optical tools that monitor image intensity changes. PIV (Particle Imaging Velocimetry) is an example of this approach<sup>246,248</sup>; it utilizes a pulsing laser in concert with image capture to back out particle velocities via algorithm analysis of the images. If

the sample is stationary, still frame images can be counted using object recognition algorithms such as those employed in Image J or MATLAB- Image processing software or our lab's Zeiss AxioVision software. However, both PIV and still frame analysis approaches require substantial computing power, which is not conducive to transforming the LOC device to be small and portable.

Because many lab-on-a-chip systems use constant DC electrical signals for electrophoretic separations, concurrent relative electrical resistivities of fluid and analytes in the system can potentially be monitored to determine the concentrations of those analytes without altering normal device operations. The electrical resistance of an object is a measure of its opposition to the passage of a steady electric current. An object of uniform cross-section will have a resistance proportional to its length and inversely proportional to its cross-sectional area, and proportional to the resistivity of the material. A DC current was chosen so the simplified model will only involve resistance rather than impedance. Impedance involves resistance and reactance in AC circuits. Electrical impedance extends the concept of resistance to AC circuits, describing not only the relative amplitudes of the voltage and current, but also the relative phases in the imaginary term of the number. A DC system only yields real values and is much more straightforward to interpret. This method is widely applicable and has the potential to monitor the concentration of analyte in a simple, inexpensive, and dynamic manner.

The research study outlined herein explores monitoring solution resistance to dynamically and unobtrusively measure erythrocyte concentrations in buffer dilutions. The RBC count (hematocrit) in a healthy human being typically varies between four to six million cells per microliter of blood<sup>156</sup>. In the ABO-Rh system, red blood cells can be characterized by two antigens, A and B, with the Rh factor either present (positive) or

absent (negative). The combination of these three antigens makes eight different blood types: A+, B+, AB+, O+, A-, B-, AB-, and O-. Prior results from our group have suggested that each blood type has unique electrical characteristics<sup>1,15,88</sup>. This dependence is tested alongside red blood cell concentrations in different buffer conductivity solutions.

### **9.3 Theory involved in resistance measurement**

In this research DC voltages are applied to measure the resistance offered by the flow of red blood cells in a straight 200  $\mu\text{m}$  wide, 50  $\mu\text{m}$  deep microchannel. A simple circuit is designed by using a resistor in series with the microdevice. The aim is to correlate changes in the resistivity to relative concentrations of red blood cells in the microchannel of the microdevice. A single microchannel with one inlet and one outlet port is considered here for this proof-of-concept investigation. The amount of current flowing in the microchannel for an applied DC voltage is very small, generally in the mA range. Due to this small current, a very high resistance exists in the microchannel for the electrons to flow. The resistor placed in series with the microchannel is 1  $\text{k}\Omega$ , which yields a substantial change in the voltage drop across the resistor when red blood cells flow through the microchannel. The system configuration involving the source / microchannel / resistor circuit is shown in Figure 9.1.

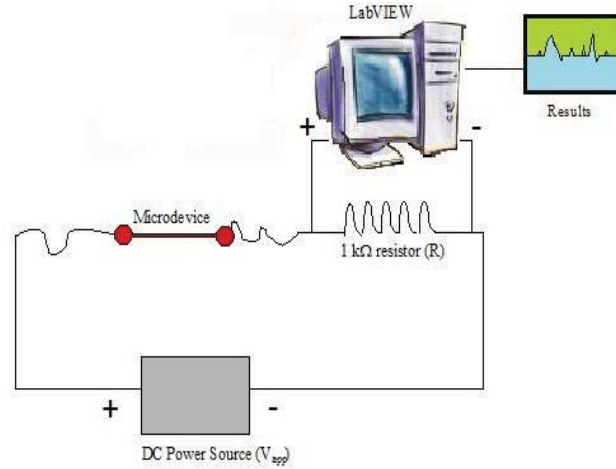


Figure 9.1 Experimental configuration showing the DC power supply applying a field across a microchannel and a 1 kΩ resistor. The DAQ measures voltage drop across the resistor.

The voltage applied by a DC power supply is  $V_{app}$ . ' $R_{ch}$ ' is the resistance across the microdevice, and ' $V_m$ ' is the voltage measured by the LabVIEW system across the 1 kΩ resistor  $R$ . The measured current,  $I_m$ , and channel resistance,  $R_{ch}$ , are calculated by equations 9.1 and 9.2, respectively. Since the resistance depends on the ions in the solution, channel resistance is expected to change as the solution conductivity changes with the presence of erythrocytes.

$$I_m = \frac{V_m}{R} \quad (9.1)$$

$$R_{Ch} = \frac{V_{app}}{I_m} - R \quad (9.2)$$

#### 9.4 Materials and methods

In this section, details about the device design, fabrication and red blood sample preparation has been discussed. Experimental matrix was developed to test all the dependencies and procedure for the experimental run has been presented. This section

concludes with a discussion on the data analysis to calculate resistance from the LabView raw data.

#### **9.4.1 Experimentation**

This section is split into device fabrication, red blood sample preparation and discussion of experimental matrix and operation.

##### **9.4.1.1 Device design and fabrication**

Microfabrication was completed through the process of soft lithography and the master wafer cast with PDMS polymer according to the procedure outlined in Chapter 8 Section 8.4.1.1. The design utilized in this study was a 1cm long, 200  $\mu\text{m}$  wide, and 50  $\mu\text{m}$  deep straight channel with a consistent cross section to simplify calculations as shown in Figure 9.2. PDMS device was sealed onto a glass slide by plasma-oxidation process utilizing air and room temperature for 1 min. Biopsy punches was utilized to drill ports in the sealed PDMS device. Copper (Cu) electrodes were placed in the inlet and outlet ports; soldered to make electric connections as shown in Figure 9.2.



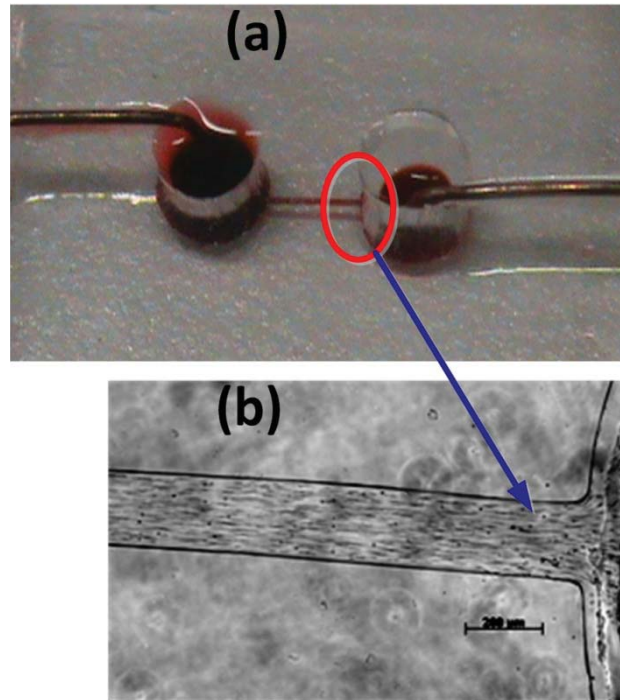


Figure 9.2 (a) PDMS device with red dye and electrodes in the ports. (b) Microscope image, 4X magnified at the intersection highlighted in (a) showing red blood cells flowing from a loading port into the 200  $\mu\text{m}$  wide channel. The scale bar is 100  $\mu\text{m}$  wide.

#### 9.4.1.2 Sample preparation

Blood samples were obtained from volunteer donors in accordance with the procedure outlined in Chapter 8 Section 8.4.1.2. Experiments were completed according to the schedule laid out in Figure 9.3. Fresh blood samples were obtained from volunteers and drawn via trained phlebotomists into 4 ml vacutainers containing  $\text{K}_2\text{EDTA}$  anticoagulant. Blood samples were centrifuged to separate red blood cells from other components of bloods, plasma and white blood cells.

Blood Type	Days					
	1		2		3	
	Donor	Voltage	Donor	Voltage	Donor	Voltage
	D	100	D	100	D	100
O+	D1 Reps = 2 3%, 4%, 5% @ 100V		D2 Reps = 2 5% 1-600, 1-800 1-1000, 1-2000		D1 Reps = 2 5% 1-600, 1-800 1-1000, 1-2000	
AB-	D3 Reps = 2 3%, 4%, 5% @ 100V		D4 Reps = 2 5% 1-600, 1-800 1-1000, 1-2000		D3 Reps = 2 5% 1-600, 1-800 1-1000, 1-2000	
B+	D5 Reps = 2 3%, 4%, 5% @ 100V		D6 Reps = 2 5% 1-600, 1-800 1-1000, 1-2000		D5 Reps = 2 5% 1-600, 1-800 1-1000, 1-2000	
A+	D7 Reps = 2 3%, 4%, 5% @ 100V		D8 Reps = 2 5% 1-600, 1-800 1-1000, 1-2000		D7 Reps = 2 5% 1-600, 1-800 1-1000, 1-2000	
AB+	D9 Reps = 2 3%, 4%, 5% @ 100V		D10 Reps = 2 5% 1-600, 1-800 1-1000, 1-2000		D9 Reps = 2 5% 1-600, 1-800 1-1000, 1-2000	
A-	D11 Reps = 2 3%, 4%, 5% @ 100V		D12 Reps = 2 5% 1-600, 1-800 1-1000, 1-2000		D11 Reps = 2 5% 1-600, 1-800 1-1000, 1-2000	
O-	D13 Reps = 2 3%, 4%, 5% @ 100V		D14 Reps = 2 5% 1-600, 1-800 1-1000, 1-2000		D13 Reps = 2 5% 1-600, 1-800 1-1000, 1-2000	
B-	D15 Reps = 2 3%, 4%, 5% @ 100V		D16 Reps = 2 5% 1-600, 1-800 1-1000, 1-2000		D15 Reps = 2 5% 1-600, 1-800 1-1000, 1-2000	

Figure 9.3 Experimental matrix to test different dependencies involved in resistance measurement for quantifying erythrocytes.

The red blood cells were extracted and then suspended in appropriate amounts of Phosphate Buffer Saline (NaCl,  $\text{KH}_2\text{PO}_4$ ,  $\text{K}_2\text{HPO}_4$ , double distilled  $\text{H}_2\text{O}$ ) (PBS) at constant pH 7.0 with D-glucose. 5% D-Glucose is isotonic for the red blood cells, i.e. there is no osmotic pressure experienced by the cells at this concentration. Different amounts of D-Glucose ranging from 5-1% were added to maintain isotonicity and

proportional amounts of PBS salts were added to change conductivity of the buffer medium according to the data shown in Table 8.2 of Chapter 8.

In order to ensure consistent final cell concentrations of cells, dilutions of blood were prepared from 10  $\mu\text{L}$  of centrifuged erythrocytes and the appropriate amount of buffer to attain the different concentrations shown in Figure 9.4. This data was obtained optically using manual counting. The dilutions were repeated five times and the standard deviations were within 5% of each other. The dilutions were performed for all 5 conductivity buffer mediums in order to examine the practical isotonicity of the D-glucose added buffers and ascertain any physical effects on the morphology of the erythrocytes. All D-glucose buffers were deemed acceptable.

Dilution of Blood	Avg # RB Cs/ $\mu\text{L}$
1-600	8333
1-800	6250
1-1000	5000
1-2000	2500

Figure 9.4 Average red blood cell counts for four dilutions were quantified from five independent sample preparations and five images of each suspension.

#### 9.4.1.3 Operation

The device was prefilled with the same D-glucose buffer solution as the red blood cell / buffer suspension that was going to be tested. Once full, the microdevice electrodes were attached to the power supply and circuit as shown in Figure 9.1. A voltage was applied across the circuit by a HVS448 high voltage sequencer and a LabView program written for the Keithley 6512 voltmeter which was turned on to record the voltage every second for 600 s. Once the voltage for the D-glucose PBS buffer solution in the device leveled out, 30  $\mu\text{L}$  was removed from the inlet well and instantly replaced by the

applicable erythrocyte suspension. Immediately, 30  $\mu\text{L}$  of the D-glucose PBS buffer solution was removed from the outlet well to force pressure-driven flow of the erythrocyte dilution through the device due to the hydrostatic pressure differences across the channel. The flow was visually monitored with a LabSmith SVM340 microscope while the LabView program simultaneously recorded the voltage for 600 s and automatically saved the data into an Excel file. The voltage was turned off, the device channel was washed with double distilled water and then with D-glucose added buffer solution and refilled for another run. An example resistance versus time profile is shown in Figure 9.5; the initial resistance when the microchannel was full of D-glucose PBS buffer is noted as well as the point where the inlet well was replaced with the erythrocyte suspension and pressure driven flow induced.

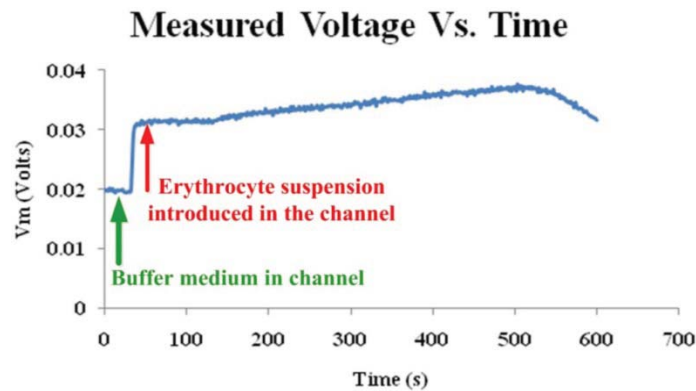


Figure 9.5 Representative measured voltage versus time for AB+ blood type suspended in 5% buffer medium (100 mS/cm) at 1:1000 dilutions and 100 V applied voltage. The step change in current corresponds to the replacement of buffer in the channel with the red blood cell suspension.

#### 9.4.2 Data analysis

The Excel file produced by LabView included data for voltage,  $V_m$  with respect to time in seconds. From each voltage in time, current was calculated using equation 9.1.

Resistance was then calculated using current and voltage for each point as shown in equation 9.2. The voltage versus time was plotted for the full 600 s (Figure 9.5) and using that, the resistance versus time was graphed for the interval that included the introduction of the erythrocytes (Figure 9.6).

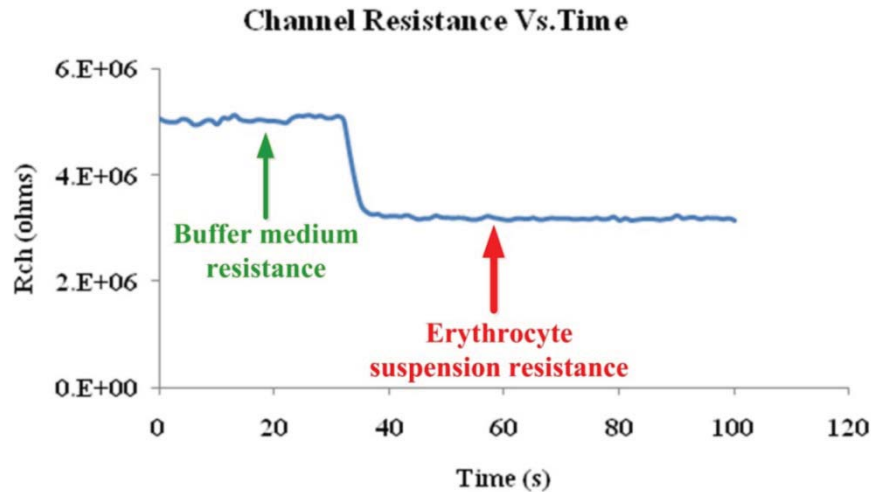


Figure 9.6 Calculated channel resistance for AB+ blood type suspended in 5% buffer medium (100 mS/cm) at 1:1000 dilution and 100 V applied voltage.

The average resistance over the device before introduction of erythrocytes recorded, ranged between 8 k $\Omega$  and 1 M $\Omega$  for medium conductivities between 700 and 100 mS/cm (5-3% D-glucose added buffers), respectively. The average resistance over the device immediately after the addition of the erythrocyte dilution was also recorded for different buffer conductivities (700-100 mS/cm) and the values remained in the M $\Omega$  range, but depended on the blood type and medium conductivity. The difference in resistances was calculated as well as the percent change with respect to the resistance before red blood cell suspensions were introduced into the channel.

Three dependencies were tested: (1) blood type dependency (2) concentration dependency and (3) medium conductivity dependency. Blood type dependency

experiments were reported for 100 V/cm and 100 mS/cm buffer conductivities at a 1:1000 suspension of red blood cells to buffer. Concentration dependency experiments utilized dilutions of 1:600, 1:800, 1:1000, and 1:2000. Conductivity dependency experiments included 3%, 4%, and 5% D-glucose solutions at 100 V/cm DC electric field as higher conductivity buffers could not be operated at high voltages due to noticeable salt formation at the ports entering into channels thus blocking the channel. The purpose of this was to test the effects of the dilution and medium conductivity on the changes in resistance.

## **9.5 Results and discussion**

In this section, the three types of dependency results have been discussed. All the 8 blood types of the human ABO-Rh blood typing system were utilized.

### **9.5.1 Blood type dependency**

The initial values for resistance varied slightly for each run due to conductivity variations between buffer preparations. The absolute changes in resistance as well as the percent change, which was defined as the change in resistance over initial resistance, were used to show relative differences. The more positive the % change in resistance, the larger the increase in absolute resistance was when the erythrocytes were introduced. Negative % change in resistance meant that the resistance decreased when erythrocytes were introduced; greater negative % changes corresponded to lower the final resistances compared to the initial value. The percent change in resistance was consistently more negative for the blood types devoid of the Rh factor, and B and AB blood types had the most negative % change. Blood type A was the only positive % change.

Erythrocytes from most blood types were more conductive than the 5% glucose solution they were suspended in (100 mS/cm). B- was the most conductive blood type, followed by AB-. A+ and A- were the least conductive blood types. A definite difference in the conductivities of the blood types and their effects on resistance in the microdevice channel are seen in Table 9.1 and Figure 9.7.

Table 9.1 Average values for initial and final resistances, change in resistance, and % change for each blood type in 1-1000 dilution in 5% D-glucose solutions (100 mS/cm).

Blood Type	Initial Resistance (M $\Omega$ )	Final Resistance (M $\Omega$ )	Change in Resistance (k $\Omega$ )	% Change
A+	0.13	0.14	4.23	3.22
A-	0.35	0.35	3.37	1.56
B+	0.78	0.75	-37.2	-4.74
B-	4.3	3.07	-1215	-28.39
AB+	2.4	1.8	-567.2	-13.06
AB-	0.36	0.3	-61.04	-16.915
O+	3.25	3.04	-214.5	-6.58
O-	3.3	2.88	-415	-9.51

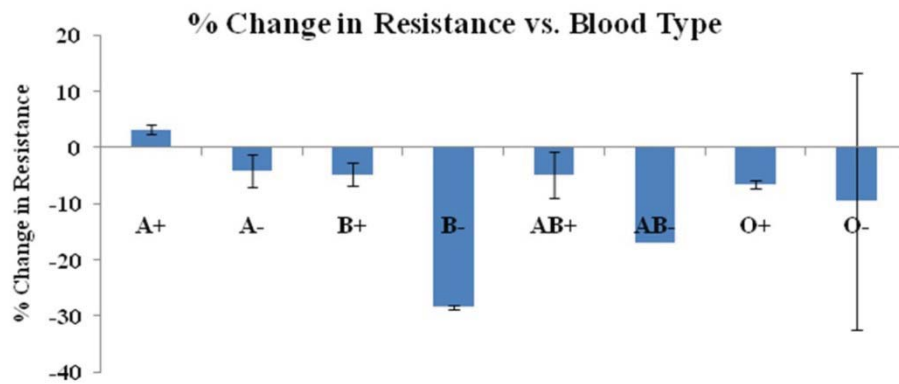


Figure 9.7 Blood type dependency on resistance at 100 mS/cm and 100 V for 1:1000 concentrated erythrocyte sample.

The error bars shown were calculated as the standard deviation of the experiments performed. The number of successful runs varied by blood type so sample numbers varied from n=1 (AB-) to n=22 (A-). O- has an extremely large error bar because only two runs were completed which were in stark disagreement with each other.

### 9.5.2 Concentration dependency

For each blood type, the change in resistance became steadily smaller as suspension became more dilute. The percent change in resistance decreased to near zero for the 1-2000 dilutions. In conclusion, the dilution of erythrocytes directly affects the percent change in resistance as shown in Table 9.2 and Figure 9.8.

If the blood type of a sample used in a microchannel and the resistance to electrical flow in the device for each run is known or fixed, the relative dilution can be determined by the drop in voltage across the microchannel.

Table 9.2 Average values for initial and final resistances, change in resistance, and percent change for each concentration of A- blood type in 5% D-glucose solution.

Dilutions	Initial Resistance	Final Resistance	Change in Resistance	% Change
1-600	855297	915197	59900	5.71
1-800	352979	365526	12546	3.55
1-1000	344978	348349	3371	1.56
1-2000	371744	368001	-3742	-0.97



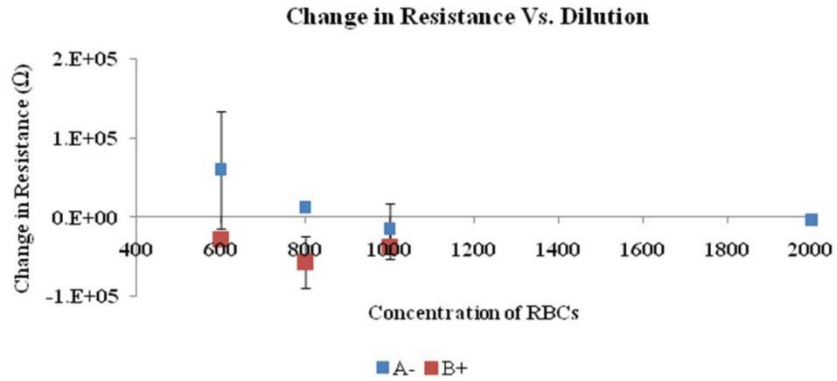


Figure 9.8 Average change in resistance with standard deviations at different concentrations of erythrocytes. Resistance change can be accurately observed at high concentration of erythrocytes compared to lower concentrations

### 9.5.3 Conductivity dependency

Red blood cells at 1:1000 concentrations were tested for medium conductivity dependencies at different D-glucose buffers (3-5%). Resistance measurements were more efficient at lower conductivities than at higher conductivities. In Figure 9.9, the conductivities varied between 100 and 700 mS/cm for 5-3% D-glucose buffers and a representative image for O+ blood type are shown.

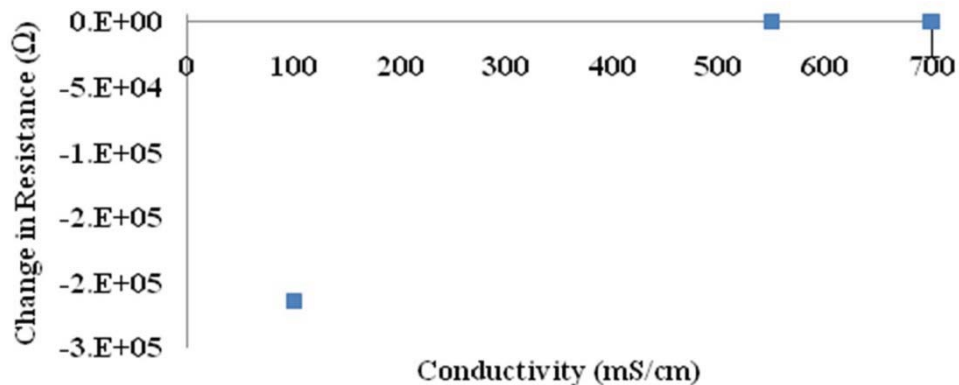


Figure 9.9 Representative image to show conductivity dependency on resistance measurement. O+ blood type at 1:1000 concentration and 100 V/cm DC electric field was employed at 3%, 4% and 5% D-glucose added buffers (100, 550, 700 mS/cm).

From Figure 9.9, it is apparent that in low conductivity buffers, an appreciable change in resistance is observed compared to high conductivity buffers. By keeping this as the standard, all the other experiments to detect resistance change were investigated with 5% D-glucose PBS buffer, corresponding to 100 mS/cm conductivity.

## 9.6 Conclusions

In this chapter, a proof of concept for a novel tool for quantification of erythrocytes by measuring DC resistance of a red blood cell suspension is demonstrated. This is a simple, non-optical method and can be integrated easily with a microfluidic platform as an analysis tool for quantifying cell concentrations in nanoliters of medium.

Three dependencies were explored to investigate the solution resistance of red blood cells. Blood type dependency showed that the resistance differed with blood type. This might be attributed to the different antigens variations present in each blood type. B- offered the most resistance to flow in the microchannel, followed by AB-. A+ and A- yielded the least resistance compared to all other blood types. Concentration dependency studies indicated that larger changes in resistance are observed for highly concentrated samples compared to dilute samples i.e. 1:600 concentrated red blood cell samples were very conductive compared to 1:2000 concentrated samples. From conductivity dependency studies, lower medium conductivities were necessary to detect resistance changes i.e. 5% D-glucose PBS buffers showed the largest percent changes in resistance compared to other buffers.

Overall, this preliminary investigation shows promise as a useful tool to quantify red blood cell suspension concentrations and avoid labor intensive optical methods. This

could be further applied to other types of cells such as white blood cells, diseased cells, bacteria, or even to blood-borne pathogens or large analytes.

## CHAPTER X

### CONCLUSIONS

#### 10.1 Summary and key conclusions

This dissertation is focused on developing a microfluidic platform or lab-on-a-chip device for sorting red blood cells via dielectrophoresis based on the ABO blood typing antigen expression. Sorting of red blood cells was achieved by applying both AC and DC electric fields in separate microdevices. The AC microdevices were custom fabricated from HybriWells and platinum wires while the DC microdevices were built with a soft photolithography technique adapted from the Whitesides *et al.* rapid prototyping method to yield poly(dimethylsiloxane) (PDMS) devices with features smaller than 30  $\mu\text{m}$ . The platform developed here could be improved into a point of care diagnostic tool for rapid and accurate blood typing in medical diagnostic applications especially in cases desiring portability such as trauma or emergency situations. Dielectrophoresis is a non-invasive and non-destructive electrokinetic technique suited for microparticle / biological cell manipulations to achieve focusing and separation. Biological cells remain viable after treatment and can be used for further analysis downstream in the microdevice.

Previous research by our group yielded blood typing of positive blood types by employing low amplitude, 1 MHz AC frequency electric fields. At this frequency, both negative and positive DEP were observed separately for different ABO - Rh positive blood typed cells; O+ could be distinguished with more than 95% confidence from all

other blood cells. All blood types could be distinguished from each other with 56% confidence. From these results, dielectrophoretic response of red blood cells are influenced by the ABO antigens expressed on the cell membrane. This was the first report on blood typing *via* dielectrophoresis in the literature. The findings were beneficial in that the device relied on low amplitude AC electric fields, which move closer to the desired portability of the devices. With this foundation, the hypothesis that continuous sorting of blood cell types could be achieved using DC-iDEP electric fields was tested.

Direct current insulator-based dielectrophoresis is a novel technique that has seen rapid growth over the last 10 years. It has yielded >40 journal publications and the literature lacks a comprehensive review article on this subject. Here, a comprehensive review on DC-iDEP state of the art technique is been presented.

In order to generate non-uniformities in the channel by applying DC electric fields, an insulating obstacle embedded in the channel is necessary. A microdevice platform was built with a rectangular insulating geometry in the channel. The inlet was split into four outlet ports which was a novel design not previously explored in DC-iDEP. As a preliminary study, the behaviors of fluorescent polystyrene particles of different sizes (diameters selected based on cells in the human blood system: platelets, red blood cells and white blood cells) was observed. Particle deflections were achieved by a combination of electrokinetic and dielectrophoretic forces in the DC-iDEP PDMS device. Electrokinetics is a combination of electrophoresis and electro-osmosis, and in this research work electrophoretic mobility was neglected due to the large cell size. Electro-osmotic mobility in the channel for plasma oxidation (and other) sealed devices at medium conductivities ranging from 100 mS/cm to 900 mS/cm is quantified. Three dependencies were studied: particle size, medium conductivity and electric field.

Simulations and experiments were conducted. Dielectrophoretic forces are greater on larger particles compared to smaller particles and those forces are maximized at lower medium conductivities. A comparison was made between our results and previous researchers who accomplished separation of size based particles in a rectangular insulating geometry with two outlet channels. Our system yielded comparable separations using much lower electric fields (17.12 V/cm) compared to other researchers (>200 V/cm). Further, our design was simpler and easier to operate due to the electric field being applied uniformly throughout the channel. Medium properties and electric field to divert the particles into one of the four outlet channels could be easily tuned. Results indicate that larger particles preferred channels 1 and 2 (side opposing the insulating obstacle) and smaller particles preferred channels 3 and 4 (side with the insulating obstacle). Simulations of the system in COMSOL Multiphysics® found the results agreeable with that of the experiments. This size dependency separation could be roughly compared to the manipulation of components of blood such as platelets, red blood cells and white blood cells by fine-tuning the applied DC electric field and medium conductivities. All experiments had a 5 min duration suggesting that separation could be accomplished within this time frame thus saving time, money and labor compared with conventional methods of separating blood components.

After completing the foundational exploration of AC dielectrophoresis of ABO-Rh positive blood cells and DC dielectrophoretic separation of polystyrene particles, designing a continuous flow microdevice to separate red blood cells based on the cells' ABO blood type antigen expressed on its surface was explored. In this work, donor dependency, blood type dependency, electric field dependency and conductivity dependency were studied. Results indicated that donor variability was minimal and

therefore was not considered when analyzing the other dependencies. Deflection of red blood cells into channels from the insulating obstacle was found to vary with blood type. Greater dielectrophoretic forces were imparted on A-, B+, AB+, AB-, O+, O-, A+ and B- in that order. A straightforward single dominant channel trend was not observed, but differing fractions of red blood cells deflected into the four outlet channels for each blood type were found. Ratio metric analysis of the cell fractions in channels revealed striking differences between the blood types. Positive blood types were recognizable from negative blood types in all A, B, AB and O blood samples. Further, all blood types could be distinguished from each other by examining a combination of channel fraction ratios. Red blood cells of different ABO-Rh types showed nearly consistent channel preferences by electric field, although 100 V (68.5 V/cm) showed slightly better separation fractions. These results are encouraging because they suggest that separations of comparable efficiencies could be achieved at lower electric fields. Medium conductivity studies indicated that lower conductivity buffers were optimal to achieve separations of all eight blood types. By fine-tuning these parameters, separation efficiencies could be optimized further. This is the first reported technique using DC insulator dielectrophoresis to manipulate red blood cells based on blood type; the approach utilized a multi-channel microdevice with rectangular insulating obstacle geometry for sorting.

Another small project involved quantifying erythrocyte presence and relative cell counts with a DC resistance measurement. Resistance, as expected, decreased when the concentration of the red blood cells in the sample was lowered. Additionally, different blood types exhibited different electrical resistances when flowing in a microchannel. This could be dependent on the antigen expression on the red blood cell membrane. Highest resistance was observed in B- blood type and lowest resistance was in A+ and A-

blood types. Medium conductivities were also explored and the best results were achieved at lower conductivities near 100 mS/cm.

To conclude, a novel platform that could be adapted for point of care purposes in medical diagnostic applications has been developed. This approach utilizes smaller sample volumes (1 to 2 drops of blood), less time (<5 min) and less money (estimated at \$ 3/ device). It is simple to design and not labor intensive to operate (it is labor intensive to analyze). Due to the use of low amplitude DC electric fields, it could be made portable, because fluid flow is achieved by electro-osmotic flow phenomena. Further, sample preparation is minimal and could be optimized to not require pre-processing (centrifugation). Lab-on-a-chip devices are steadily increasing in accuracy and/or false negative test results. Such point of care diagnostic tools could be more realistic to apply in remote geographical locations and developing countries where medical diagnostics is expensive and not reachable by the common population.

## **10.2 Recommendations for future work**

This section discusses some of the limitations of the current research study and provides very general recommendations for future research.

AC dielectrophoretic blood typing experiments in a custom built microdevice (inconsistent geometries without microfabrication capabilities) yielded sorting efficiencies of 56% among positive blood types (A+, B+, AB+, and O+). This confidence interval must be improved above 95% for this approach to be viable for medical diagnostics. The confidence interval could be further improved by optimizing the device fabrication such that the distance between the two perpendicular Pt electrodes in the HybriWell chamber is consistent between devices. Further, electrode shape and surface



chemistry could be carefully controlled using clean-room electrode deposition and microfabrication techniques. The dielectrophoretic forces experienced by the erythrocytes could also be improved by optimizing the AC electric field (amplitude and frequency) as well as by manipulating medium conductivities that influence red blood cell polarizations according to the Clausius-Mossotti factor. AC dielectrophoretic sorting also was a batch process whose accurate quantification was hindered by the migration of red blood cells out of the video microscope's field of view. This equipment / analysis limitation impacted red blood cell counts in the field of view with time. Larger observation area as well as other measurement tools to quantify cell counts as a function of position could improve this. Examination of an impedance strategy<sup>209,245,247</sup> to accomplish this led to the resistance sub-project presented in Chapter 9.

Additionally, the limitation of a finite observation window was overcome by switching to a continuous flow microdevice. This design utilized DC electric field to achieve dielectrophoresis of the red blood cells. This concept was first demonstrated on different sized fluorescent polystyrene particles in rectangular insulating obstacle geometry. Separation of different sized particles was achieved at low DC electric fields and by using a wide range of medium conductivity. To improve separation efficiency further, COMSOL modeling of different insulating obstacle geometries can be studied and employed to separate particles of interest. Through COMSOL modeling, DC electric field, medium conductivity properties and particle properties can be used to estimate the optimal conditions for achieving higher separation in a continuous flow system.

Separation of polystyrene particles was further extended to separate red blood cells by human ABO blood type. While preliminary ratio metric analysis demonstrates that positive and negative blood types can be quickly discerned, this concept could be

further extended to separate diseased cells like malaria, circulating tumor cells (CTCs) and breast cancer cells. The polarizability of diseased cells is different compared to normal healthy cells<sup>89,111,187</sup>. Normal or viable cells are more rigid and maintain shape integrity compared to diseased cells<sup>94</sup>. Researchers have demonstrated that viable and non-viable pathogenic bacteria could be sorted dielectrophoretically based on the polarizability<sup>112</sup>. Some blood diseases like malaria result in drastic physiological changes easily distinguished by dielectrophoresis or other methods<sup>140-141,188</sup>. Circulating tumor cells in the blood could be separated and targeted for further treatment<sup>249</sup>.

Insulating obstacle geometries that increase the spatial electric field gradient could be further adjusted to suit the separation of a particle of interest. The four-channel geometry could be further optimized by COMSOL modeling of the dominant forces in the system to explore sequential obstacle systems, non-symmetrical channel geometries, and altered channel wall charge. The particle velocity depends on electrokinetic and dielectrophoretic forces. In this research electrophoretic forces were neglected and only electro-osmotic forces were considered for simulation. By considering the neglected electrophoretic forces, separation of particles and cells could be further optimized.

Additionally, alternative biofluids could be adapted for analysis *via* dielectrophoretic fields. Large molecules, including globular proteins and long strands of DNA, can be manipulated via DEP<sup>127</sup>. Traditional gel-electrophoretic techniques are time consuming, not convenient for very long DNA strands, and generate significant biohazard waste. Size separation of DNA strands via DEP based on different migration velocities due to different length dependent polarizabilities has been explored by researchers employing AC electric fields<sup>127</sup>. Conventionally protein purifications are achieved by chromatography, membrane filtration, crystallization and precipitation which

involve high sample and reagent volumes. Protein separations by DEP can cut purification costs significantly in the biopharmaceutical industry<sup>126</sup>. This means that saliva samples might be analyzed using DEP, although this would likely require extra processing steps to concentrate and selectively separate target molecules in saliva samples.

Combinations of schemes to recognize differences in molecular expression on cell surfaces may be necessary. Molecular expression on cell surfaces can currently be probed using linear electrophoretic techniques as well as by gene expression profiles<sup>250</sup>, cDNA microarrays<sup>251</sup>, *in situ* hybridization<sup>250</sup> and tissue microarrays<sup>252</sup>. These gene dependent techniques have enabled measurement of the expression of thousands of genes in a single experiment, revealing many new, potentially important genes. In addition, there is only a small amount of abnormal cells present in a large amount of normal cell background in clinical samples. However, limitations of these are that linear electrophoretic techniques simply yield charge to size information (which is the reason this is so powerful for DNA fragments, but so limited for whole cell analysis).

The work explored in this research is a unique technique to probe whole cell characteristics. The important implications of this research into cell dielectrophoresis are that it suggests that molecular expression on cell surfaces can be differentiated. This is a powerful and important advance to the field of dielectrophoresis. Antibody / antigen binding kinetics (measurable by ELISA, fluorescence correlation spectroscopy, microarray, optical biosensor, surface plasmon resonance, atomic force microscopy) combined with non-linear electrokinetic characterizations may be required to achieve >99% confidence intervals in medical microdevices.

Analysis of hundreds of specimens from patients in different stages of disease is needed to establish the diagnostic, prognostic and therapeutic potential. These techniques rely on optical imaging like fluorescence detection or colorimetric analysis for quantifying the molecular expressions and often require tissue samples by biopsy which is invasive and painful for the patient. Conventionally, real time polymerase chain reaction (RT-PCR) technique is used to amplify the molecular expression from isolated total RNA, which may be difficult at times to detect the differences over the normal healthy cells due to low volume of target diseased cells. Bulkier components, large sample volume, labor intensive and more expensive due to the resources needed in developing these systems for quantifying molecular expression are some of the other limitations associated with it. These methods are also dependent on the availability of high affinity probes. Irreversible attachment of these probes to target cells also influences cell behavior. In the absence of a specific or unique marker or to avoid potential interactions of probes with cells, alternative methods are required to identify and manipulate target cells in heterogeneous cell populations.

Researchers have shown the separation of single diseased cells in a large volume of healthy cell samples by dielectrophoresis and subsequent positioning in a microchannel for further analysis<sup>151</sup>. On-chip library screening has been achieved in a continuous system that sorts antibody-binding target cells captured on microparticles through DEP<sup>151</sup>. DEP operates on the intrinsic dielectric properties of cells, and so is potentially capable of sorting cells without the need for engineered labels or tags. The effective membrane capacitance of a smooth cell will be less than that for a cell having a complex cell surface topography. This influences the cross-over frequency (transition from negative to positive DEP), which has important implications for applying DEP to

characterize and selectively sort target cells from other cells<sup>151</sup>. DEP can also be used as an alternative method to integrate large-scale purification and concentration of particles in a single step, with the potential to replace bulkier chromatographic purification methods, which has been a conventional approach employed to eliminate contaminants. Once a highly reproducible combination of methods is found, it would need to undergo clinical trials before introduction to the market. However, the findings obtained in this research are directly relevant to the field of dielectrophoresis because it provides strong evidence that a cell's polarizability is directly correlated to molecular expression on the red blood cell surface. Further experiments will reveal if this observation holds for other cell systems.

## REFERENCES

1. Srivastava, S. K.; Daggolu, P. R.; Burgess, S.; Minerick, A. R., Dielectrophoretic characterization of erythrocytes: Positive ABO blood types. *Electrophoresis* 2008, *29*, 5033-5046.
2. Gest, H., The discovery of microorganisms by Robert Hooke and Antoni Van Leeuwenhoek, fellows of the royal society. *Notes and records of The Royal Society* 2004, *58* (2), 187-201.
3. Ritchison, G. Human Physiology. <http://people.eku.edu/ritchisong/301notes1.htm> (accessed May 16 2010).
4. Kang, J. H.; Park, J.-K., Technical Paper on Microfluidic devices- Cell Separation Technology. *Asia-Pacific Biotech news* 2005, pp 1135-1146.
5. Krylov, S. N.; Dovichi, N. J., Single-cell analysis using capillary electrophoresis: influence of surface support properties on cell injection into the capillary. *Electrophoresis* 2000, *21*, 767-773.
6. Yi, C.; Li, C.-W.; Ji, S.; Yang, M., Microfluidics technology for manipulation and analysis of biological cells. *Analytica Chimica Acta* 2006, *560*, 1-23.
7. Toner, M.; Irimia, D., Blood-on-a-Chip. *Annu. Rev. Biomed. Eng.* 2005, *7*, 77-103.
8. Erickson, D.; Li, D., Integrated microfluidic devices. *Analytica Chimica Acta* 2004, *507*, 11-26.
9. Chiou, P. Y.; Ohta, A. T.; Wu, M. C., Massively parallel manipulation of single cells and microparticles using optical images. *Nature* 2005, *436*, 370-372.
10. Andersson, H.; Berg, A. v. d., Microtechnologies and nanotechnologies for single-cell analysis. *Current Opinion in Biotechnology* 2004, *15*, 44-49.
11. Yun, S.-S.; Yoon, S. Y.; Song, M.-K.; Im, S.-H.; Kim, S.; Lee, J.-H.; Yang, S., Handheld mechanical cell lysis chip with ultra-sharp silicon nano-blade arrays for rapid intracellular protein extraction. *Lab on a Chip* 2010, *10*, 1442-1446.
12. Anette, S.; Anders, K.; Frida, R.; Maximillan, D.; T, C. D.; Owe, O., Microfluidic device for combinatorial fusion of liposomes and cells. *Analytical Chemistry* 2001, *73*, 126-130.

13. Tresset, G.; Takeuchi, S., A Microfluidic Device for Electrofusion of Biological Vesicles *Biomed Microdevices* 2004, 6 (3), 213-218.
14. Manz, A.; Graber, N.; Widmer, H. M., Miniaturized total chemical analysis systems: A novel concept for chemical sensing *Sensors and Actuators B-Chemical* 1990, 1, 244-248.
15. Minerick, A. R., The Rapidly Growing Field of Micro and Nanotechnology to Measure Living Cells. *AIChE J.* 2008, 54 (9), 2230-2237.
16. Verpoorte, E.; Rooij, N. F. D., Microfluidics Meets MEMS. *Proc of IEEE* 2003, 91 (6), 930-953.
17. Tüdos, A. J.; Besselink, G. A. J.; Schasfoort, R. B. M., Trends in miniaturized total analysis systems for point-of-care testing in clinical chemistry. *Lab on a Chip* 2001, 1, 83-95.
18. Whitesides, G. M., The origins and the future of microfluidics. *Nature* 2006, pp 368-373.
19. Ohno, K.-i.; Tachikawa, K.; Manz, A., Microfluidics: Applications for analytical purposes in chemistry and biochemistry. *Electrophoresis* 2008, 29, 4443-4453.
20. Davidson, M. W. Molecular Expressions.  
<http://micro.magnet.fsu.edu/cells/images/cellsfigure1.jpg> (accessed May 16 2010).
21. Fan, Z. H.; Harrison, D. J., Electroosmotic Pumping and Valveless Control of Fluid Flow within a Manifold of Capillaries on a Glass Chip. *Analytical Chemistry* 1994, 66 (20), 3485-3491.
22. Li, P. C. H., *Microfluidic Lab-on-a-Chip for Chemical and Biological Analysis and Discovery*. CRC press: Boca Raton, FL, 2006; Vol. 94.
23. Dittrich, P. S.; Tachikawa, K.; Manz, A., Micro Total Analysis Systems. Latest Advancements and Trends. *Anal Chem* 2006, 78, 3887-3908.
24. Sassa, F.; Morimoto, K.; Satoh, W.; Suzuki, H., Electrochemical techniques for microfluidic applications. *Electrophoresis* 2008, 29, 1787-1800.
25. Beebe, D. J.; A.Mensing, G.; M.Walker, G., Physics and applications of microfluidics in biology. *Annu. Rev. Biomed. Eng.* 2002, 4, 261-286.
26. Sudarsan, A. P.; Ugaz, V. M., Fluid mixing in planar spiral microchannels. *Lab on a Chip* 2006, 6, 74-82.
27. Whitesides, G. M., The origins and the future of microfluidics. *Nature* 27 July, 2006, pp 368-373.
28. Sia, S. K.; Kricka, L. J., Microfluidics and point-of-care testing. *Lab Chip* 2008, 8, 1982-1983.

29. Kang, J. H.; Park, J.-K., Cell Separation Technology. *Asia Pacific Biotech News* 2005, 9 (21), 1135-1146.
30. Walt, D. R., Miniature Analytical Methods for Medical Diagnostics. *Science* 2005, 308, 217-219.
31. Chin, C. D. Biotechnology for Global Health: Solutions for the Developing World *Consilience: The Journal of Sustainable Development* [Online], 2008.
32. Focke, M.; Kosse, D.; Müller, C.; Reinecke, H.; Zengerle, R.; Stetten, F. v., Lab-on-a-Foil: microfluidics on thin and flexible films. *Lab on a Chip* 2010, 10, 1365-1386.
33. Li, C.; Shutter, L. A.; Wu, P.-M.; Ahn, C. H.; Narayan, R. K., Potential of a simple lab-on-a-tube for point-of-care measurements of multiple analytes. *Lab on a Chip* 2010, 10, 1476-1479.
34. Yu, L.; Huang, H.; Dong, X.; Wu, D.; Qin, J.; Lin, B., Simple, fast and high-throughput single-cell analysis on PDMS microfluidic chips. *Electrophoresis* 2008, 29, 5055-5060.
35. Ahn, C. H.; Choi, J.-W.; Beaucage, G.; Nevin, J. H.; Lee, J.-B.; Puntambekar, A.; Lee, J. Y., Disposable Smart Lab on a Chip for Point-of-Care Clinical Diagnostics. *Proc of IEEE* 2004, 92 (1).
36. Stone, H. A.; Kim, S., Microfluidics: Basic Issues, Applications, and Challenges. *AIChE Journal* 2001, 47 (6), 1250-1254.
37. Yager, P. Basic microfluidic concepts. <http://faculty.washington.edu/yagerp/microfluidicstutorial/basicconcepts/basicconcepts.htm> (accessed 16 May 2010).
38. Saliterman, S. S., *Fundamentals of BioMEMS and Medical Microdevices*. SPIE-The International Society for Optical Engineering: 2006.
39. Kirby, B. J., *Micro- and Nanoscale Fluid Mechanics: Transport in Microfluidic Devices*. Cambridge University Press: Cambridge, 2010.
40. Sia, S. K.; Whitesides, G. M., Microfluidic devices fabricated in poly(dimethylsiloxane) for biological studies. *Electrophoresis* 2003, 24, 3563-3576.
41. Pohl, H. A., *Dielectrophoresis the behavior of neutral matter in nonuniform electric fields*. Cambridge University Press: Cambridge, 1978.
42. Chin, C. D.; Linder, V.; Sia, S. K., Lab-on-a-chip devices for global health: Past studies and future opportunities. *Lab on a Chip* 2007, 7 (3), 3-10.
43. The Merck Manuals- Online Medical Library. 2 ed.; Porter, R. S., Ed. Merck Research Laboratories: 2003. <http://www.merck.com/mmhe/appendixes/ap2/ap2b.html>.
44. Senagore, A. J., Type and Screen. In *Gale Encyclopedia of Surgery*, 1 ed.; Gale: 2004; Vol. 1.



45. Zaouk, R.; Park, B. Y.; Madou, M. J., Introduction to fabrication techniques. In *Microfluidic Techniques*, 1 ed.; Minter, S. D., Ed. Humana Press: 2006; Vol. 321.
46. Duffy, D. C.; McDonald, J. C.; Schueller, O. J. A.; Whitesides, G. M., Rapid Prototyping of Microfluidic Systems in Poly(dimethylsiloxane). *Anal. Chem.* 1998, *70*, 4974-4984.
47. Pan, T. Towards early stage disease detection in microdevices: fabrication and testing of micro total analysis systems for bioanalytical applications. Brigham Young University, 2007.
48. McDonald, J. C.; Duffy, D. C.; Anderson, J. R.; Chiu, D. T.; Wu, H.; Schueller, O. J. A.; Whitesides, G. M., Fabrication of microfluidic systems in poly(dimethylsiloxane). *Electrophoresis* 2000, *21*, 27-40.
49. Becker, H.; Gartner, C., Polymer microfabrication methods for microfluidic analytical applications. *Electrophoresis* 2000, *21*, 12-26.
50. Becker, H.; Gärtner, C., Polymer microfabrication technologies for microfluidic systems. *Anal Bioanal Chem* 2008, *390*, 89-111.
51. Xia, Y.; Whitesides, G. M., Soft Lithography. *Annu. Rev. Mater. Sci.* 1998, *28*.
52. Kumar, A.; Whitesides, G. M., Features of gold having micrometer to centimeter dimensions can be formed through a combination of stamping with an elastomeric stamp and an alkanethiol ink followed by chemical etching. *Applied Physics Letters* 1993, *63*, 2002-2004.
53. Zhao, X.-M.; Xia, Y.; Whitesides, G. M., Fabrication of three-dimensional microstructures: Microtransfer molding. *Advance Materials* 2004, *8* (10), 837-840.
54. Zhao, X.-M.; Stoddart, A.; Smith, S. P.; Kim, E.; Xia, Y.; Prentiss, M.; Whitesides, G. M., Fabrication of Single-Mode Polymeric Waveguides Using Micromolding in Capillaries. *Advance Materials* 1996, *8* (5), 420-424.
55. Rhee, M.; Burns, M. A., Microfluidic assembly blocks. *Lab Chip* 2008, *8*, 1365-1373.
56. Martinez, A. W.; Phillips, S. T.; Wiley, B. J.; Gupta, M.; Whitesides, G. M., FLASH: A rapid method for prototyping paper-based microfluidic devices. *Lab on a Chip* 2008, *8*, 2146-2150.
57. Grimes, d.; Breslauer, D. N.; Long, M.; Pegan, J.; Leeb, L. P.; Khine, M., Shrinky-Dink microfluidics: rapid generation of deep and rounded patterns. *Lab on a Chip* 2008, *8*, 170-172.
58. Qin, D.; Xia, Y.; Whitesides, G. M., Soft lithography for micro- and nano scale patterning. *Nature Protocols* 2010, *5* (3), 491-502.
59. Ng, J. M. K.; Gitlin, I.; Stroock, A. D.; Whitesides, G. M., Components for integrated poly(dimethylsiloxane) microfluidic systems. *Electrophoresis* 2002, *23*, 3461-3473.

60. Frienda, J.; Yeo, L., Fabrication of microfluidic devices using polydimethylsiloxane. *Biomicrofluidics* 2010, 4 (026502), 1-5.
61. Individual Pictures. <http://www.brewerscience.com/research/processing-theory/spin-coater-theory/>; [http://www.rsc.org/images/chiptip38-fig5\\_tcm18-167830.jpg](http://www.rsc.org/images/chiptip38-fig5_tcm18-167830.jpg); <http://umech.mit.edu/6.07J/fabpics/27-developing.jpg>; <http://store.clarksonlab.com/images/products/detail/H3400HP07.1.gif>.
62. Sikanen, T.; Tuomikoski, S.; Ketola, R. A.; Kostianen, R.; Franssila, S.; Kotiaho, T., Characterization of SU-8 for electrokinetic microfluidic applications. *Lab on a Chip* 2005, 5, 888-896.
63. McKechnie, J. Fabrication of Microfluidic Devices with Application to Membraneless Fuel Cells Univeristy of Victoria, 2004.
64. Liu, J.; Pan, T.; Woolley, A. T.; Lee, M. L., Surface-Modified Poly(methyl methacrylate) Capillary Electrophoresis Microchips for Protein and Peptide Analysis. *Anal. Chem.* 2004, 76 (23), 6948-6955.
65. Kelly, R. T.; Pan, T.; Woolley, A. T., Phase-Changing Sacrificial Materials for Solvent Bonding of High-Performance Polymeric Capillary Electrophoresis Microchips. *Anal. Chem.* 2005, 77 (11), 3536-3541.
66. Wu, H.; Huang, B.; Zare, R. N., Construction of microfluidic chips using polydimethylsiloxane for adhesive bonding. *Lab on a Chip* 2005, 5, 1393-1398.
67. Bhattacharya, S.; Datta, A.; Berg, J. M.; Gangopadhyay, S., Studies on Surface Wettability of Poly(Dimethyl)Siloxane (PDMS) and Glass Under Oxygen-Plasma Treatment and Correlation With Bond Strength. *J. Microelectromech. S.* 2005, 14 (3), 590-597.
68. Wong, I.; Ho, C.-M., Surface molecular property modifications for poly(dimethylsiloxane) (PDMS) based microfluidic devices. *Microfluid Nanofluid* 2009, 7, 291-306.
69. Belder, D.; Ludwig, M., Surface modification in microchip electrophoresis. *Electrophoresis* 2003, 24, 3595-3606.
70. Hong, S. M.; Kim, S. H.; Kim, J. H.; Hwang, H. I., Hydrophilic Surface Modification of PDMS Using Atmospheric RF Plasma. *J. Phys.* 2006, 34, 656-661.
71. García, C. D.; Dressen, B. M.; Henderson, A.; Henry, C. S., Comparison of surfactants for dynamic surface modification of poly(dimethylsiloxane) microchips. *Electrophoresis* 2005, 26, 703-709.
72. Badal, M. Y.; Wong, M.; Chiem, N.; Salimi-Moosavi, H.; Harrison, D. J., Protein separation and surfactant control of electroosmotic flow in poly(dimethylsiloxane)-coated capillaries and microchips. *Journal of chromatography A* 2002, 947, 277-286.
73. Dou, Y.-H.; Bao, N.; Xu, J.-J.; Meng, F.; Chen, H.-Y., Separation of proteins on surface-modified poly(dimethylsiloxane) microfluidic devices. *Electrophoresis* 2004, 25, 3024-3031.

74. Wang, A.-J.; Xu, J.-J.; Chen, H.-Y., Nonionic surfactant dynamic coating of poly(dimethylsiloxane) channel surface for microchip electrophoresis of amino acids. *Anal. Chim. Acta* 2006, *569*, 188-194.
75. Huang, B.; Kim, S.; Wu, H.; Zare, R. N., Use of a Mixture of n-Dodecyl- $\alpha$ -D-maltoside and Sodium Dodecyl Sulfate in Poly(dimethylsiloxane) Microchips To Suppress Adhesion and Promote Separation of Proteins. *Anal Chem* 2007, *79*, 9145-9149.
76. Liu, Y.; Fanguy, J. C.; Bledsoe, J. M.; Henry, C. S., Dynamic Coating Using Polyelectrolyte Multilayers for Chemical Control of Electroosmotic Flow in Capillary Electrophoresis Microchips. *Analytical Chemistry* 2000, *72*, 5939-5944.
77. Kaneta, T.; Ueda, T.; Hata, K.; Imasaka, T., Suppression of electroosmotic flow and its application to determination of electrophoretic mobilities in a poly(vinylpyrrolidone)-coated capillary. *J. Chromatogr. A* 2006, *1106*, 52-55.
78. Chen, L.; Ren, J.; Bi, R.; Chen, D., Ultraviolet sealing and poly(dimethylacrylamide) modification for poly(dimethylsiloxane)/glass microchips. *Electrophoresis* 2004, *25*, 914-921.
79. Berdichevsky, Y.; Khandurina, J.; Guttman, A.; Lo, Y.-H., UV/ozone modification of poly(dimethylsiloxane) microfluidic channels. *Sensor Actuat. B-Chem.* 2004, *97*, 402-408.
80. Lapizco-Encinas, B. H.; Rito-Palomares, M., Dielectrophoresis for the manipulation of nanobioparticles. *Electrophoresis* 2007, *28*, 4521-4538.
81. Keshavamurthy, S. S.; Leonard, K. M.; Burgess, S. C.; Minerick, A. R. In *Direct current dielectrophoretic characterization of erythrocytes: Positive ABO blood types*, NSTI-Nanotech, Boston, MA, June 1-5; Boston, MA, 2008; pp 401-404.
82. Zhang, C.; Khoshmanesh, K.; Mitchell, A.; Kalantar-zadeh, K., Dielectrophoresis for manipulation of micro/nano particles in microfluidic systems. *Anal Bioanal Chem* 2010, *396*, 401-420.
83. Cheng, I.-F.; Chang, H.-C.; Hou, D.; Chang, H.-C., An integrated dielectrophoretic chip for continuous bioparticle filtering, focusing, sorting, trapping, and detecting. *Biomicrofluidics* 2007, *1* (021503), 1-15.
84. Hughes, M. P., Strategies for dielectrophoretic separation in laboratory-on-a-chip systems. *Electrophoresis* 2002, *23*, 2569-2582.
85. Kua, C. H.; Lam, Y. C.; Yang, C.; Youcef-Toumi, K. *Review of bio-particle manipulation using dielectrophoresis*; Singapore-MIT Alliance: 2005.
86. Li, Y.; Dalton, C.; Crabtree, H. J.; Nilsson, G.; Kaler, K. V. I. S., Continuous dielectrophoretic cell separation microfluidic device. *Lab on a Chip* 2007, *7*, 239-248.
87. Jones, T. B., Basic Theory of Dielectrophoresis and Electrorotation: Methods for Determining the Forces and Torques Exerted by Nonuniform Electric Fields on Biological Particles Suspended in Aqueous Media *Micro- and Nanoelectrokinetics* 2003, pp 33-42.

88. Minerick, A. R.; Zhou, R.; Takhistov, P.; Chang, H.-C., Manipulation and characterization of red blood cells with alternating current fields in microdevices. *Electrophoresis* 2003, 24, 3703-3717.
89. Pethig, R.; Markx, G. H., Applications of dielectrophoresis in biotechnology. *Trends in Biotechnology* 1997, 15, 426-432.
90. Gimsa, J.; Wachner, D., A Unified Resistor-Capacitor Model for Impedance, Dielectrophoresis, Electrorotation, and Induced Transmembrane Potential. *Biophysical Journal* 1998, 75, 1107-1116.
91. Arnold, W. M.; Zimmerman, U., Rotating-field-induced rotation and measurement of the membrane capacitance of single mesophyll cells of *Avena sativa*. *Zeitschrift fuer Naturforschung* 1982, 37c, 908-915.
92. Arnold, W. M.; Schwan, H. P.; Zimmermann, U., Surface conductance and other properties of latex particles measured by electrorotation. *Journal of Physical Chemistry* 1987, 91 (19), 5093-5098.
93. Sun, T.; Morgan, H.; Green, N. G. In *Analytical solutions of the dielectrophoretic and travelling wave forces generated by interdigitated electrode arrays*, Journal of Physics, IOP publishing: 2008; pp 1-4.
94. Yang, J.; Huang, Y.; Wang, X.-B.; Becker, F. F.; Gascoyne, P. R. C., Cell Separation on Microfabricated Electrodes Using Dielectrophoretic/Gravitational Field-Flow Fractionation. *Anal Chem* 1999, 71, 911-918.
95. Gascoyne, P. R. C.; Vykoukal, J., Particle separation by dielectrophoresis. *Electrophoresis* 2002, 23, 1973-1983.
96. Matsui, T.; Franzke, J.; Manz, A.; Dirk Janasek, D., Temperature gradient focusing in a PDMS/glass hybrid microfluidic chip. *Electrophoresis* 2007, 28 (24), 4606-4611.
97. Ivory, C. F., Several New Electrofocusing Techniques. *Electrophoresis* 2007, 28 (1-2), 15-25.
98. Meighan, M. M.; Staton, S. J. R.; Hayes, M. A., Bioanalytical separations using electric field gradient techniques. *Electrophoresis* 2009, 30, 852-865.
99. Danger, G.; Ross, D., Development of a temperature gradient focusing method for in situ extraterrestrial biomarker analysis. *Electrophoresis* 2008, 29, 3107-3114.
100. Tuñón, P. G.; Wang, Y.; Myers, P.; Bartle, K. D.; Bowhill, L.; Ivory, C. F.; Ansell, R. J., Electrophoretic field gradient focusing: An investigation of the experimental parameters. *Electrophoresis* 2008, 29, 457-465.
101. Tracy, N. I.; Ivory, C. F., Protein separation using preparative-scale dynamic field gradient focusing. *Electrophoresis* 2008, 29, 2820-2827.
102. Pysher, M. D.; Hayes, M. A., Electrophoretic and dielectrophoretic field gradient technique for separating bioparticles. *Anal. Chem.* 2007, 79 (12), 4552-4557.

103. Choi, S.; Park, J.-K., Microfluidic system for dielectrophoretic separation based on a trapezoidal electrode array. *Lab on a Chip* 2005, 5, 1161-1167.
104. Pethig, R.; Huang, Y.; Wang, X.-B.; Burt, J. P. H., Positive and negative dielectrophoretic collection of colloidal particles using interdigitated castellated microelectrodes. *Journal of Physics D: Applied Physics* 1992, 25, 881-888.
105. Pham, P.; Texier, I.; Larrea, A.-S.; Blanc, R.; Revol-Cavalier, F.; Grateau, H.; Perraut, F., Numerical design of a 3-D microsystem for bioparticle dielectrophoresis: The Pyramidal Microdevice *Journal of Electrostatics* 2007, 65 (8), 511-520.
106. Huang, Y.; Pethig, R., Electrode design for negative dielectrophoresis. *Measurement Science and Technology journal* 1991, 2, 1142-1146.
107. Martinsen, Ø. G.; Grimnes, S.; Schwan, H. P., Interface phenomena and dielectric properties of biological tissue. In *Encyclopedia of Surface and Colloid Science*, Marcel Dekker, Inc.: 2002; pp 2643-2652.
108. Pethig, R.; Kell, D. B., The passive electrical properties of biological systems: their significance in physiology, biophysics and biotechnology. *Physics in Medicine and Biology* 1987, 32 (8), 933-970.
109. Martinsen, Ø. G.; Grimnes, S.; Karlsen, J., Low Frequency Dielectric Dispersion of Microporous Membranes in Electrolyte Solution. *Journal of Colloid and Interface Science* 1998, 199, 107-110.
110. Gimsa, J.; Moller, T.; Schnelle, T.; Fuhr, G., Dielectric Spectroscopy of Single Human Erythrocytes at Physiological Ionic Strength: Dispersion of the Cytoplasm. *Biophysical Journal* 1996, 71, 495-506.
111. Yang, F.; Yang, X.; Jiang, H.; Bulkhauls, P.; Wood, P.; Hrushesky, W.; Wang, G., Dielectrophoretic separation of colorectal cancer cells. *Biomicrofluidics* 2010, 4 (013204), 1-13.
112. Lapizco-Encinas, B. H.; Simmons, B. A.; Cummings, E. B.; Fintschenko, Y., Dielectrophoretic Concentration and Separation of Live and Dead Bacteria in an Array of Insulators. *Anal. Chem.* 2004, 76 (6), 1571-1579.
113. Cummings, E. B.; Singh, A. K., Dielectrophoresis in Microchips Containing Arrays of Insulating Posts: Theoretical and Experimental Results. *Anal. Chem.* 2003, 75, 4724-4731.
114. Kang, K. H.; Kang, Y.; Xuan, X.; Li, D., Effects of dc-dielectrophoretic force on particle trajectories in microchannels. *J. Appl. Phys.* 2006, 99 (6), 064702-064708.
115. Zhu, J.; Xuan, X., Dielectrophoretic focusing of particles in a microchannel constriction using DC-biased AC electric fields. *Electrophoresis* 2009, 30, 2668-2675.
116. Lapizco-Encinas, B. H.; Simmons, B. A.; Cummings, E. B.; Fintschenko, Y. In *High throughput electrodeless dielectrophoresis of viruses in polymeric microdevices*, 7th International Conference on Miniaturized Chemical and Biochemical Analysis Systems, California, USA, California, USA, 2003; pp 607-610.

117. Kang, K. H.; Kang, Y.; Xuan, X.; Li, D., Continuous separation of microparticles by size with Direct current-dielectrophoresis. *Electrophoresis* 2006, 27, 694-702.
118. Kang, Y.; Li, D.; Kalams, S. A.; Eid, J. E., DC-Dielectrophoretic separation of biological cells by size. *Biomed. Microdevices* 2008, 10 (2), 243-249.
119. Zhu, J.; Tzeng, T.-R. J.; Xuan, X., Continuous dielectrophoretic separation of particles in a spiral microchannel. *Electrophoresis* 2010, 31, 1382-1388.
120. Barbulovic-Nad, I.; Xuan, X.; Lee, J. S. H.; Li, D., DC-dielectrophoretic separation of microparticles using an oil droplet obstacle. *Lab Chip* 2006, 6, 274-279.
121. Chen, K. P.; Pacheco, J. R.; Hayes, M. A.; Staton, S. J. R., Insulator-based dielectrophoretic separation of small particles in a sawtooth channel. *Electrophoresis* 2009, 30, 1441-1448.
122. Zhang, L.; Bastemeijer, J.; Mollinger, J.; Bossche, A., Continuous Dielectrophoretic Separation in the Iterative Curves Using dc-Biased ac Electric Fields. In *Proceedings of the 3rd IEEE Int. Conf. on Nano/Micro Engineered and Molecular Systems*, IEEE: Sanya, China, 2008; pp 864-868.
123. Zhu, J.; Tzeng, T.-R. J.; Hu, G.; Xuan, X., DC dielectrophoretic focusing of particles in a serpentine microchannel. *Microfluid. Nanofluid.* 2009, 7, 751-756.
124. Lapizco-Encinas, B. H.; Davalos, R. V.; Simmons, B. A.; Cummings, E. B.; Fintschenko, Y., An insulator-based (electrodeless) dielectrophoretic concentrator for microbes in water. *J. Microbiol. Meth.* 2005, 62, 317-326.
125. Cho, Y.-K.; Kim, S.; Lee, K.; Park, C.; Lee, J.-G.; Ko, C., Bacteria concentration using a membrane type insulator-based dielectrophoresis in a plastic chip. *Electrophoresis* 2009, 30, 3153-3159.
126. Lapizco-Encinas, B. H.; Ozuna-Chacon, S.; Rito-Palomares, M., Protein manipulation with insulator-based dielectrophoresis and direct current electric fields. *J. Chromatogr. A* 2008, 1206 (1), 45-51.
127. Gallo-Villanueva, R. C.; pez, C. E. R. g.-L.; Diaz-de-la-Garza, R. I.; Reyes-Betanzo, C.; Lapizco-Encinas, B. H., DNA manipulation by means of insulator based dielectrophoresis employing direct current electric fields. *Electrophoresis* 2009, 30, 4195-4205.
128. Chou, C.-F.; Tegenfeldt, J. O.; Bakajin, O.; Chan, S. S.; Cox, E. C.; Darnton, N.; Duke, T.; Austin, R. H., Electrodeless Dielectrophoresis of Single- and Double-Stranded DNA. *Biophys. J.* 2002, 83 (4), 2170-2179.
129. Green, N. G.; Morgan, H., Dielectrophoretic separation of nano-particles. *J of physics* 1997, 30, L41-L44.
130. Washizu, M.; Kurosawa, O., Electrostatic manipulation of DNA in microfabricated structures *IEEE Transactions on Industry Applications* 1990, 26 (6), 1165-1172.

131. Parikesit, G. O. F.; Markesteijn, A. P.; Piciu, O. M.; Bossche, A.; Westerweel, J.; Young, I. T.; Garini, Y., Size-dependent trajectories of DNA macromolecules due to insulative dielectrophoresis in submicrometer-deep fluidic channels. *Biomicrofluidics* 2008, 2 (024103), 1-14.
132. Lapizco-Encinas, B. H.; Simmons, B. A.; Cummings, E. B.; Fintschenko, Y., Insulator-based dielectrophoresis for the selective concentration and separation of live bacteria in water. *Electrophoresis* 2004, 25 (10-11), 1695-1704.
133. Shafiee, H.; Sano, M. B.; Henslee, E. A.; Caldwell, J. L.; Davalos, R. V., Selective isolation of live/dead cells using contactless dielectrophoresis (cDEP). *Lab Chip* 2010, 10, 438-445.
134. Huang, Y.; Yang, J. M.; Hopkins, P. J.; Kassegne, S.; Tirado, M.; Forster, A. H.; Reese, H., Separation of Simulants of biological Warfare Agents. *Biomed Microdevices* 2003, 5 (3), 217-225.
135. Fiedler, S.; Shirley, S. G.; Schnelle, T.; Fuhr, G., Dielectrophoretic Sorting of Particles and Cells in a Microsystem. *Analytical Chemistry* 1998, 70, 1909-1915.
136. Barrett, L. M.; Skulan, A. J.; Singh, A. K.; Cummings, E. B.; Fiechtner, G. J., Dielectrophoretic Manipulation of Particles and Cells Using Insulating Ridges in Faceted Prism Microchannels. *Anal. Chem.* 2005, 77 (21), 6798-6804.
137. Kang, Y.; Cetin, B.; Wu, Z.; Li, D., Continuous particle separation with localized AC-dielectrophoresis using embedded electrodes and an insulating hurdle. *Electrochimica Acta* 2009, 54, 1715-1720.
138. Chen, D.; Du, H.; Tay, C. Y., Rapid Concentration of Nanoparticles with DC Dielectrophoresis in Focused Electric Fields. *Nano. Res. Lett.* 2010, 5, 55-60.
139. Zhu, J.; Xuan, X., Particle electrophoresis and dielectrophoresis in curved microchannels. *J. Colloid Interface Sci.* 2009, 340, 285-290.
140. Gascoyne, P.; Mahidol, C.; Ruchirawat, M.; Satayavivad, J.; Watcharasit, P.; Becker, F. F., Microsample preparation by dielectrophoresis: isolation of malaria. *Lab on a Chip* 2002, 2, 70-75.
141. Gascoyne, P.; Satayavivad, J.; Ruchirawat, M., Microfluidic approaches to malaria detection. *Acta Tropica* 2004, 89 (3), 357-369.
142. Kim, K. B.; Chun, H.; Kim, H. C.; Chung, T. D., Red blood cell quantification microfluidic chip using polyelectrolytic gel electrodes. *Electrophoresis* 2009, 30, 1464-1469.
143. Das, C. M.; Becker, F.; Vernon, S.; Noshari, J.; Joyce, C.; Gascoyne, P. R. C., Dielectrophoretic Segregation of Different Human Cell Types on Microscope Slides. *Analytical Chemistry* 2005, 77 (2708-2719).
144. Jun Yang, Y. H.; Wang, X.-B.; Becker, F. F.; Gascoyne, P. R. C., Differential Analysis of Human Leukocytes by Dielectrophoretic Field-Flow-Fractionation. *Biophysical Journal* 2000, 78, 2680-2689.

145. Wang, X.-B.; Yang, J.; Huang, Y.; Vykoukal, J.; Becker, F. F.; Gascoyne, P. R. C., Cell Separation by Dielectrophoretic Field-flow-fractionation. *Analytical Chemistry* 2000, 72, 832-839.
146. Demierre, N.; Braschler, T.; Muller, R.; Renaud, P., Focusing and continuous separation of cells in a microfluidic device using lateral dielectrophoresis. *Sensors and Actuators B-Chemical* 2008, 132 (2), 388-396.
147. Pethig, R.; Menachery, A.; Pells, S.; Sousa, P. D., Dielectrophoresis: A Review of Applications for Stem Cell Research. *Journal of Biomedicine and Biotechnology* 2010, 2010, 1-7.
148. Talary, M. S.; Mills, K. I.; Hoy, T.; Burnett, A. K.; Pethig, R., Dielectrophoretic separation and enrichment of CD34+ cell subpopulation from bone marrow and peripheral blood stem cells. *Medical and Biological Engineering and Computing* 1995, 33 (2), 235-237.
149. Feldman, Y.; Ermolina, I.; Hayashi, Y., Time Domain Dielectric Spectroscopy Study of Biological Systems. *IEEE Transactions on Dielectrics and Electrical Insulation* 2003, 10 (5), 728-753.
150. Lisin, R.; Ginzburg, B. Z.; Schlesinger, M.; Feldman, Y., Time domain dielectric spectroscopy study of human cells. I. Erythrocytes and ghosts. *Biochimica et Biophysica Acta* 1996, 1280, 34-40.
151. Pethig, R., Dielectrophoresis: Status of the theory, technology, and applications. *Biomicrofluidics* 2010, 4 (022811), 1-35.
152. Gheorghiu, E., Measuring living cells using dielectric spectroscopy. *Bioelectrochemistry and Bioenergetics* 1996, 40 (2), 133-139.
153. Morgan, H.; Sun, T.; Holmes, D.; Gawad, S.; Green, N. G., Single cell dielectric spectroscopy. *Journal of Physics D: Applied Physics* 2007, 40, 61-70.
154. Livshits, L.; Caduff, A.; Talary, M. S.; Feldman, Y., Dielectric response of biconcave erythrocyte membranes to D- and L-glucose. *Journal of Physics D: Applied Physics* 2007, 40, 15-19.
155. Asami, K., Characterization of heterogeneous systems by dielectric spectroscopy. *Progress in Polymer Science* 2002, 27, 1617-1659.
156. Dean, L., Blood groups and red cell antigens. Beck, B., Ed. NCBI book Shelf: Bethesda, MD, 2005. <http://www.ncbi.nlm.nih.gov/bookshelf/br.fcgi?book=rbcantigen>.
157. 56 facts about blood. <http://www.americasblood.org/go.cfm?do=page.view&pid=12> (accessed June 3).
158. Potter, S. Whole Blood Components. <http://www.scottpotter.net/artsandsciences/health/chap19/sub1.htm> (accessed June 3).



159. Okazaki, N. Blood. [http://faculty.weber.edu/nokazaki/Human\\_Physiology/Human-phys-master.htm](http://faculty.weber.edu/nokazaki/Human_Physiology/Human-phys-master.htm) (accessed June 4 2010).
160. Kimball, J. W., General Biology. 6 ed.; 1994. <http://users.rcn.com/jkimball.ma.ultranet/BiologyPages/> (accessed June 11 2010).
161. Fredrick, N. What is this pic? <http://www.abc.net.au/science/photos/whatis/> (accessed June 3).
162. Coghlan, A., First red blood cells grown in the lab. *NewScientist* 2008.
163. Cell Membrane. <http://www.columbia.edu/cu/biology/courses/c2005/purves6/figure05-01.jpg> (accessed June 3).
164. Fukuda, S.; Schmid-Schonbein, G. W., Centrifugation attenuates the fluid shear response of circulating leukocytes. *Journal of Leukocyte Biology* 2002, 72 (1), 133-139.
165. Table of Blood Group Systems. <http://ibgri.blood.co.uk/isbt%20pages/isbt%20terminology%20pages/table%20of%20blood%20group%20systems.htm> (accessed June 4).
166. Watkins, W. M., The ABO blood group system: Historical background. *Transfusion Medicine* 2001, 11, 243-265.
167. Berg, J. M.; Tymoczko, J. L.; Stryer, L., Biochemistry. In *The molecular design of life* [Online] 5 ed.; NCBI Book Shelf: New York, 2002. <http://www.ncbi.nlm.nih.gov/bookshelf/br.fcgi?book=stryer>.
168. Racial and ethnic distribution of ABO blood types. <http://www.bloodbook.com/world-abo.html> (accessed June 11 2010).
169. Blood Types in U.S. <http://bloodcenter.stanford.edu/images/Various/bloodtypes.jpg> (accessed June 4).
170. Nishi, K.; Rand, S.; Nakagawa, T.; Yamamoto, A.; Yamasaki, S.; Yamamoto, Y.; Kobayashi, A.; Kane, M.; Morimoto, A.; Spalthoff, H.; Annuss, B. ABO Blood Typing from Forensic Materials - Merits and demerits of detection methods utilized in our laboratories, and biological significance of the antigens *Anil Aggrawal's Internet Journal of Forensic Medicine and Toxicology* [Online], 2005. [http://www.geradts.com/anil/ij/vol\\_006\\_no\\_002/papers/paper001.html](http://www.geradts.com/anil/ij/vol_006_no_002/papers/paper001.html) (accessed June 14 2010).
171. Narayanan, S.; Galloway, L.; Nonoyama, A.; Leparac, G. F.; Garcia-Rubio, L. H.; Potter, R. L., UV-visible spectrophotometric approach to blood typing II: phenotyping of subtype A2 and weak D and whole blood analysis. *Transfusion* 2002, 42 (5), 619-626.
172. Soper, S. A.; Hashimoto, M.; Situma, C.; Murphy, M. C.; McCarley, R. L.; Cheng, Y.-W.; Barany, F., Fabrication of DNA microarrays onto polymer substrates using UV modification protocols with integration into microfluidic platforms for the sensing of low-abundant DNA point mutations *Methods* 2005, 37 (1), 103-113.

173. Zborowski, M.; Ostera, G. R.; Moore, L. R.; Milliron, S.; Chalmers, J. J.; Schechter, A. N., Red Blood Cell Magnetophoresis. *Biophysical Journal* 2003, *84*, 2638-2645.
174. Cheng, J.; Sheldon, E. L.; Wu, L.; Uribe, A.; Gerrue, L. O.; Carrino, J.; Heller, M. J.; O'Connell, J. P., Preparation and hybridization analysis of DNA/RNA from *E. coli* on microfabricated bioelectronic chips. *Nature Biotechnology* 1998, *16*, 541-546.
175. Helmke, B. P.; Minerick, A. R., Designing a Nano-Interface in a Microfluidic Chip to Probe Living Cells: Challenges and Perspectives. *Proceedings of National Academy of Sciences* 2006, *103* (17), 6419-6424.
176. Brahmasandra, S. N.; Ugaz, V. M.; Burke, D. T.; Mastrangelo, C. H.; Burns, M. A., Electrophoresis in Microfabricated Devices Using Photopolymerized Polyacrylamide Gels and Electrode Defined Sample Injection. *Electrophoresis* 2001, *22*, 300-311.
177. Biomedical- Lab Equipment, Hematology. <http://websites.labx.com/rankin/listings.cfm?show=1&catid=1282> (accessed June 14 2010).
178. Cohen, J., Monitoring Treatment: At What Cost? *Science* 2004, p 1936.
179. How common is sickle cell anemia? [http://www.ascaa.org/How\\_Common\\_Is\\_Sickle\\_Cell\\_Anemia.asp](http://www.ascaa.org/How_Common_Is_Sickle_Cell_Anemia.asp) (accessed June 14 2010).
180. Genetically inherited disease detection kit. <http://www.edvotek.com/116.html> (accessed June 14 2010).
181. Pethig, R., Dielectrophoresis: using inhomogeneous AC electrical fields to separate and manipulate cells. *Critical Reviews in Biotechnology* 1996, *16* (4), 331-348.
182. Gheorghiu, E., On the limits of ellipsoidal models when analyzing dielectric behavior of living cells. *Annals of the New York Academy of Sciences* 2006, *873*, 262-268.
183. Vrinceanu, D.; Gheorghiu, E., Shape effects on the dielectric behaviour of arbitrarily shaped particles with particular reference to biological cells *Bioelectrochemistry and Bioenergetics* 1996, *40*, 167.
184. Gheorghiu, E.; Asami, K., Monitoring cell cycle by impedance spectroscopy: experimental and theoretical aspects *Bioelectrochemistry and Bioenergetics* 1998, *45* (2), 139-143.
185. Becker, F. F.; Wang, X.-B.; Huang, Y.; Pethig, R.; Vykoukal, J.; Gascoyne, P. R. C., The removal of human leukaemia cells from blood using interdigitated microelectrodes *Journal of Physics D: Applied Physics* 1995, *27* (12), 2659-2662.
186. Sancho, M.; Martínez, G.; Martín, C., Accurate dielectric modeling of shelled particles and cells. *Journal of Electrostatics* 2003, *57* (2), 143-156.

187. Becker, F. F.; Wang, X.-B.; Huang, Y.; Pethig, R.; Vykoukal, J.; Gascoyne, P. R. C., Separation of human breast cancer cells from blood by differential dielectric affinity. *Proc of National Academy of Sciences* 1995, 92 (Cell Biology), 860-864.
188. Gascoyne, P.; Pethig, R.; Satayavivad, J.; Becker, F. F.; Ruchirawat, M., Dielectrophoretic detection of changes in erythrocyte membranes following malarial infection *Biochimica et Biophysica Acta (BBA) - Biomembranes* 1997, 1323 (2), 240-252.
189. Borgatti, M.; Altomare, L.; Baruffa, M.; Fabbri, E.; Breveglieri, G.; Feriotto, G.; Maresi, N.; Medoro, G.; Romani, A.; Tartagni, M.; Gambari, R.; Guerrieri, R., Separation of white blood cells from erythrocytes on a dielectrophoresis (DEP) based 'Lab-on-a-chip' device. *International journal of molecular medicine* 2005, 15 (6), 913-920.
190. Daniels, G.; Bromilow, I., *Essential Guide to Blood Groups*. Wiley-Blackwell: 2006.
191. Sheffield, W. P.; Tinmouth, A.; Branch, D. R., Blood Group Biochemistry: A Canadian Blood Services Research and Development Symposium *Transfusion Medicine Reviews* 2005, 19 (4), 295-307.
192. Patenaude, S. I.; Seto, N. O. L.; Borisova, S. N.; Szpacenko, A.; Marcus, S. L.; Palcic, M. M.; Evans, S. V., The structural basis for specificity in human ABO(H) blood group biosynthesis. *Nature Structural and Molecular Biology* 2002, 9 (9), 685-690.
193. Godin, C.; Caprani, A., Effect of blood storage on erythrocyte/wall interactions: implications for surface charge and rigidity. *European Biophysics Journal* 1997, 26 (2), 175-182.
194. Draper, C. J.; Greenwalt, T. J.; Dumaswala, U. J., Biochemical and structural changes in RBCs stored with different plasticizers: the role of  $\alpha$ -hexanol *Transfusion* 2002, 42 (7), 830-836.
195. COMSOL- Multiphysics Modeling. <http://www.comsol.com/> (accessed June 14 2010).
196. SAS- Statistical analysis software; Ver 9.1. <http://www.sas.com/> (accessed June 14 2010).
197. Ott, R. L.; Longnecker, M. T., *An Introduction to Statistical Methods and Data Analysis*. 5 ed.; Duxbury Press: 2000.
198. Gawron, A. J.; Martin, R. S.; Lunte, S. M., Microchip electrophoretic separation systems for biomedical and pharmaceutical analysis *European Journal of Pharmaceutical Sciences* 2001, 14 (1), 1-12.
199. Minerick, A. R., DC Dielectrophoresis in Lab-on-a-Chip Devices. In *Encyclopedia of Micro- & Nanofluidics*, Li, D., Ed. Springer: Berlin Heidelberg New York, 2008.

200. Gencoglu, A.; Minerick, A. R., Chemical and morphological changes on platinum microelectrode surfaces in AC and DC fields with biological buffer solutions. *Lab on a Chip* 2009, 9, 1866-1873.
201. Masuda, S.; Washizu, M.; Nanba, T., Novel method of cell fusion in field constriction area in fluid integrated circuit. *IEEE Transactions on Industry Applications* 1989, 25, 732-737.
202. Lee, S. W.; Yang, S. D.; Kim, Y. W.; Kim, Y. K.; Lee, S. H. In *Micromachined cell handling devices*, Medicine and Biology Society-16th Annual International Conf. IEEE 1994; pp 1019-1020.
203. Golan, S.; Elata, D.; Orenstein, M.; Dinnar, U., Floating electrode dielectrophoresis. *Electrophoresis* 2006, 27, 4919-4926.
204. Ozuna-Chacón, S.; Lapizco-Encinas, B. H.; Rito-Palomares, M.; Martínez-Chapa, S. O.; Reyes-Betanzo, C., Performance characterization of an insulator-based dielectrophoretic microdevice. *Electrophoresis* 2008, 29, 3115-3122.
205. Hawkins, B. G.; Smith, A. E.; Syed, Y. A.; Kirby, B. J., Continuous-Flow Particle Separation by 3D Insulative Dielectrophoresis Using Coherently Shaped, dc-Biased, ac Electric Fields. *Anal. Chem.* 2007, 79 (19), 7291-7300.
206. Thwar, P. K.; Linderman, J. J.; Burns, M. A., Electrodeless direct current dielectrophoresis using reconfigurable field-shaping oil barriers. *Electrophoresis* 2007, 28, 4572-4581.
207. Chou, C.-F.; Zenhausern, F., Electrodeless Dielectrophoresis for Micro Total Analysis Systems. *IEEE Engineering in Medicine and Biology Magazine* 2003, pp 62-67.
208. Moncada-Hernández, H.; Lapizco-Encinas, B. H., Simultaneous concentration and separation of microorganisms: insulator-based dielectrophoretic approach. *Anal. Bioanal. Chem.* 2010, 396, 1805-1816.
209. Sabounchi, P.; Morales, A. M.; Ponce, P.; Lee, L. P.; Simmons, B. A.; Davalos, R. V., Sample concentration and impedance detection on a microfluidic polymer chip. *Biomed. Microdevices* 2008, 10 (5), 661-670.
210. Hsiao, F.-B.; Hsu, H.-J.; Chen, H.-Y.; Hsu, H.-L. In *The Simulation Study of Bio-particle Trapping with Electrodeless Dielectrophoresis*, Proceedings of the 2nd IEEE International Conference on Nano/Micro Engineered and Molecular Systems, Bangkok, Thailand, Bangkok, Thailand, 2007.
211. Hsiao, F.-B.; Jen, C.-P.; Chen, H.-Y.; Hsu, H.-L.; Lee, Y.-C.; Chuang, C.-H.; Wang, C.-H. In *The Experimental Studies of Bio-Particle Trapping Using Electrodeless Dielectrophoresis*, Proceedings of the 3rd IEEE Int. Conf. on Nano/Micro Engineered and Molecular Systems, Sanya, China, Sanya, China, 2008.
212. Lewpiriyawong, N.; Yang, C.; Lam, Y. C., Dielectrophoretic manipulation of particles in a modified microfluidic H filter with multi-insulating blocks. *Biomicrofluidics* 2008, 2 (034105).

213. Jen, C.-P.; Huang, Y.-H.; Chen, T.-W. In *Cell Trapping Utilizing Insulator-based Dielectrophoresis in The Open-Top Microchannels*, DTIP of MEMS & MOEMS, France April 9-11; EDA publishing: France 2008.
214. Jen, C.-P.; Chen, T.-W., Trapping of cells by insulator-based dielectrophoresis using open-top microstructures. *Microsys. Tech.* 2009, *15*, 1141-1148.
215. Zhang, L.; Tatar, F.; Turmezei, P.; Bastemeijer, J.; Mollinger, J. R.; Piciu, O.; Bossche, A., Continuous Electrodeless Dielectrophoretic Separation in a Circular Channel. *J. Phys.* 2006, *34*, 527-532.
216. Martínez-López, J. I.; Moncada-Hernández, H.; Baylon-Cardiel, J. L.; Martínez-Chapa, S. O.; Rito-Palomares, M.; Lapizco-Encinas, B. H., Characterization of electrokinetic mobility of microparticles in order to improve dielectrophoretic concentration. *Anal. Bioanal. Chem.* 2009, *394*, 293-302.
217. Baylon-Cardiel, J. L.; Lapizco-Encinas, B. H.; Reyes-Betanzo, C.; Chavez-Santoscoy, A. V.; Martinez-Chapa, S. O., Prediction of trapping zones in an insulator-based dielectrophoretic device. *Lab Chip* 2009, *9*, 2896-2901.
218. Sabouchi, P.; Huber, D. E.; Kanouff, M. P.; Harris, A. E.; Simmons, B. A. In *Joule heating effects on insulator based dielectrophoresis*, Twelfth International Conference on Miniaturized Systems for Chemistry and Life Sciences, San Diego, San Diego, 2008.
219. Ai, Y.; Joo, S. W.; Jiang, Y.; Xuan, X.; Qian, S., Transient electrophoretic motion of a charged particle through a converging-diverging microchannel: Effect of direct current-dielectrophoretic force. *Electrophoresis* 2009, *30*, 2499-2506.
220. Dhopeswarkar, R.; Hlushkou, D.; Nguyen, M.; Tallarek, U.; Crooks, R. M., Electrokinetics in Microfluidic Channels Containing a Floating Electrode. *Journal of American Chemical Society* 2008, *130*, 10480-10481.
221. Golan, S.; Elata, D.; Dinnar, U., Hybrid dielectrophoresis devices that employ electrically floating electrodes. *Sensors and Actuators A* 2008, *142*, 138-146.
222. Shafiee, H.; Caldwell, J. L.; Sano, M. B.; Davalos, R. V., Contactless dielectrophoresis: a new technique for cell manipulation. *Biomed. Microdevices* 2009, *11*, 997-1006.
223. Davalos, R. V.; McGraw, G. J.; Wallow, T. I.; Morales, A. M.; Krafcik, K. L.; Fintschenko, Y.; Cummings, E. B.; Simmons, B. A., Performance impact of dynamic surface coatings on polymeric insulator-based dielectrophoretic particle separators. *Anal. Bioanal. Chem.* 2008, *390* (3), 847-855.
224. Freeman, D.; Gray, M.; Aranyosi, A. Manufacturing a PDMS microfluidic device via a Silicon Wafer Master 2007.
225. Kirby, B. J.; Jr., E. F. H., Zeta potential of microfluidic substrates: 2. Data for polymers. *Electrophoresis* 2004, *25*, 203-213.
226. Abate, A. R.; Lee, D.; Do, T.; Holtze, C.; Weitz, D. A., Glass coating for PDMS microfluidic channels by sol-gel methods. *Lab on a Chip* 2008, *8*, 516-518.

227. Xuan, X.; Raghbizadeh, S.; Li, D., Wall effects on electrophoretic motion of spherical polystyrene particles in a rectangular poly(dimethylsiloxane) microchannel. *J. Colloid Interface Sci.* 2006, 296, 743-748.
228. Xuan, X.; Xu, B.; Sinton, D.; Li, D., Electroosmotic flow with Joule heating effects. *Lab on a Chip* 2004, 4, 230-236.
229. Ai, Y.; Qian, S.; Liu, S.; Joo, S. W., Dielectrophoretic choking phenomenon in a converging-diverging microchannel. *Biomicrofluidics* 2010, 4 (013201).
230. Gray, D. S.; Tan, J. L.; Voldman, J.; Chen, C. S., Dielectrophoretic registration of living cells to a microelectrode array. *Biosensors and Bioelectronics* 2004, 19, 1765-1774.
231. Voldman, J., Electrical forces for microscale cell manipulation. *Annual Review of Biomedical Engineering* 2006, 8 (1), 425-454.
232. Hořlzel, R.; Calander, N.; Chiragwandi, Z.; Willander, M.; Bier, F. F., Trapping Single Molecules by Dielectrophoresis. *Physical Review Letters* 2005, 95 (128102), 1-4.
233. Xu, C.; Wang, Y.; Cao, M.; Lu, Z., Dielectrophoresis of human red cells in microchips. *Electrophoresis* 1999, 20, 1829-1831.
234. Huang, Y.; Joo, S.; Duhon, M.; Heller, M.; Wallace, B.; Xu, X., Dielectrophoretic Cell Separation and Gene Expression Profiling on Microelectronic Chip Arrays. *Analytical Chemistry* 2002, 74, 3362-3371.
235. Pethig, R.; Lee, R. S.; Talary, M. S., Cell physiometry tools based on dielectrophoresis. *Journal of the association for laboratory automation* 2004, 9 (5), 324-330.
236. Ermolina, I.; Morgan, H., The electrokinetic properties of latex particles: comparison of electrophoresis and dielectrophoresis. *J. Colloid Interface Sc.* 2005, 285, 419-428.
237. Kwon, J.-S.; Maeng, J.-S.; Chun, M.-S.; Song, S., Improvement of microchannel geometry subject to electrokinesis and dielectrophoresis using numerical simulations *Microfluid. Nanofluid.* 2008, 5 (1), 23-31.
238. Huang, X.; Gordon, M. J.; Zare, R. N., Current monitoring method for measuring electroosmotic flow rate in capillary zone electrophoresis. *Anal. Chem.* 1988, 60, 1837-1838.
239. Ren, X.; Bachman, M.; Sims, C.; Li, G. P.; Allbritton, N., Electroosmotic properties of microfluidic channels composed of poly(dimethylsiloxane). *J Chromatogr B* 2001, 762, 117-125.
240. Dou, Y.-H.; Bao, N.; Xu, J.-J.; Chen, H.-Y., A dynamically modified microfluidic poly(dimethylsiloxane) chip with electrochemical detection for biological analysis. *Electrophoresis* 2002, 23, 3558-3566.

241. Coltro, W. K. T.; Lunte, S. M.; Carrilho, E., Comparison of the analytical performance of electrophoresis microchannels fabricated in PDMS, glass, and polyester-toner. *Electrophoresis* 2008, 29, 4928-4937.
242. Ross, D.; Johnson, T. J.; Locascio, L. E., Imaging of Electroosmotic Flow in Plastic Microchannels. *Anal. Chem.* 2001, 73 (11), 2509-2515.
243. Wakizaka, Y.; Hakoda, M.; Shiragami, N., Effect of electrode geometry on dielectrophoretic separation of cells. *Biochemical Engineering Journal* 2004, 20, 13-19.
244. Brown, D., Tonicity, pH, Buffer Capacity, and Stability Considerations for Technicians. *Journal of Pharmacy Society of Wisconsin* 2009, May/June, 17-22.
245. Segerink, L. I.; Sprenkels, A. J.; Braak, P. M. t.; Vermes, I.; Berg, A. v. d., On-chip determination of spermatozoa concentration using electrical impedance measurements. *Lab on a Chip* 2010, 10, 1018-1024.
246. Cheng, X.; Liu, Y.-s.; Irimia, D.; Demirci, U.; Yang, L.; Zamir, L.; Rodriguez, W. R.; Toner, M.; Bashir, R., Cell detection and counting through cell lysate impedance spectroscopy in microfluidic devices. *Lab on a Chip* 2007, 7, 746-755.
247. Sengupta, S.; Battigelli, D. A.; Chang, H.-C., A micro-scale multi-frequency reactance measurement technique to detect bacterial growth at low bio-particle concentrations. *Lab on a Chip* 2006, 6, 682-692.
248. Lima, R.; Wada, S.; Tanaka, S.; Takeda, M.; Ishikawa, T.; Tsubota, K.-i.; Imai, Y.; Yamaguchi, T., In vitro blood flow in a rectangular PDMS microchannel: experimental observations using a confocal micro-PIV system. *Biomedical Microdevices* 2008, 10 (2), 153-167.
249. Riethdorf, S.; Fritsche, H.; Müller, V.; Rau, T.; Schindlbeck, C.; Rack, B.; Janni, W.; Coith, C.; Beck, K.; Jänicke, F.; Jackson, S.; Gornet, T.; Cristofanilli, M.; Pantel, K., Detection of Circulating Tumor Cells in Peripheral Blood of Patients with Metastatic Breast Cancer: A Validation Study of the CellSearch System *Clinical Cancer Research* 2007, 13 (3), 920-928.
250. Peng, X.-H.; Cao, Z.-H.; Xia, J.-T.; Carlson, G. W.; Lewis, M. M.; Wood, W. C.; Yang, L., Real-time Detection of Gene Expression in Cancer Cells Using Molecular Beacon Imaging: New Strategies for Cancer Research. *Cancer Research* 2005, 65 (5), 1909-1917.
251. Chen, J. J. W.; Wu, R.; Yang, P.-C.; Huang, J.-Y.; Sher, Y.-P.; Han, M.-H.; Kao, W.-C.; Lee, P.-J.; Chiu, T. F.; Chang, F.; Chu, Y.-W.; Wue, C.-W.; Peck, K., Profiling Expression Patterns and Isolating Differentially Expressed Genes by cDNA Microarray System with Colorimetry Detection *Genomics* 1998, 51 (3), 313-324.
252. Kononen, J.; Bubendorf, L.; Kallionimeni, A.; Bärnlund, M.; Schraml, P.; Leighton, S.; Torhorst, J.; Mihatsch, M. J.; Sauter, G.; Kallionimeni, O.-P., Tissue microarrays for high-throughput molecular profiling of tumor specimens. *Nature Medicine* 1998, 4, 844-847.